

Self-assembled Functionalised Peptides for Small-diameter Vascular Graft Applications

Fatimah Basem Samman

Submitted in accordance with the requirements for the degree of
Doctor of Philosophy

The University of Leeds

School of Chemistry

October 2017

The candidate confirms that the work submitted is her own and that appropriate credit has been given where reference has been made to the work of others.

This copy has been supplied on the understanding that it is copyright material and that no quotation from this thesis may be published without proper acknowledgement.

The right of Fatimah Basem Samman to be identified as Author of this work has been asserted by her in accordance with the Copyright, Design and Patents Act 1988.

©2017 The University of Leeds and Fatimah Basem Samman

Acknowledgement

All praise is due to Allah for providing me with the strength and patience that kept me going through the tough times during my PhD journey and for surrounding me with kind, loving, helpful and supportive people.

First and foremost, I would like to express my deep and sincere thanks to my supervisors Dr Stuart Warriner, Professor Eileen Ingham and Dr Stacy-Paul Wilshaw. You provided me with guidance and direction when I was lost, continuous support, encouragement and knowledge throughout this project. Thank you for being there when I needed and for your endless patience!

Many thanks to everyone in the lab who has made my time in the lab enjoyable, particularly Normalina Sandora for her friendship and always offering help without even asking, Nicola Conway for her continuous emotional support and Dr Nagitha Wijayathunga for his patience and time spent in optimising the methods for the multiphoton work.

I have been fortunate to work with wonderful people, Dr Dan Thomas, Dr Steve Maude, Dr Pill Davies, Dr Danielle Mile, Dr Robert Guillatt, Dr Andrew Aldridge and James Warren. Thank you all for your expertise and willingness to teach.

Thanks to my friends who have been supportive and encouraging, particularly Ghadeer Albadrani. Special thanks to my family my father Basem, my mother Khadijah, my sisters Nosaibah and Linah and my brothers Abdullah, Sulaiman and Mohammad, who believed in me and without hesitation were always there to offer encouragement, support and prayers. To my family, you have been my inspiration during this time and I will always be grateful!

Finally, I would like to thank everyone who put their faith in me to finish my thesis!

And my success is not but through Allah. Upon him I have relied, and to Him I return.

Holy Quran: Chapter 11, Hud, Verse 88

Abstract

Current clinically used small-diameter vascular grafts have been shown to have poor patency rates mainly caused by thrombus formation due to the absence of the anti-thrombogenic endothelium. Studies of novel small-diameter decellularised porcine arteries in large animal models of vascular replacement have also shown poor patency rates. The aim of this study was to develop a series of bioactive self-assembled P₁₁ peptides as surface coatings to enhance re-endothelialisation of decellularised porcine external iliac arteries and potentially mitigate thrombus formation.

Porcine external iliac arteries were decellularised and validated for acellularity and *in vitro* biocompatibility. These acellular scaffolds lacked the natural anti-thrombogenic endothelium lining the arterial lumen. The peptides P₁₁₋₄, P₁₁₋₈ and P₁₁₋₁₂ were studied at different concentrations under physiological conditions using Fourier transform infrared spectroscopy and transmission electron microscopy as possible candidates for surface coatings. The peptides in their monomeric state were tested for anti-thrombogenic properties using a Chandler loop model. Self-assembly of peptides within acellular arteries was then assessed for the ability to form surface coatings by scanning electron microscopy, fluorescent microscopy and multiphoton laser scanning microscopy. P₁₁ peptides were functionalised with bioactive cell attachment motifs (GRGDS and YIGSR) using copper catalysed azide-alkyne click chemistry. These motifs are found in extracellular matrix proteins and can be recognised by endothelial cell integrins. The effect of functionalisation on cell attachment of isolated ovine femoral endothelial cells onto acellular artery was assessed by live/dead[®] assay for 72 hours.

The results showed that decellularisation of porcine external iliac arteries was reproducible with preserved extracellular matrix and DNA reduction of > 97 %. P₁₁₋₄, P₁₁₋₈ and P₁₁₋₁₂ at 20 mg.mL⁻¹, were shown to have high β -sheet proportions and the former two peptides were shown to form self-supporting gels almost instantaneously. P₁₁₋₄ and P₁₁₋₈ were shown to have anti-thrombogenic properties when present in blood potentially reducing thrombus formation. Moreover, the two peptides were shown to coat the extracellular matrix structures of the luminal surface of decellularised porcine external iliac arteries. *In vitro*, the bioactive peptides GRGDS-P₁₁₋₄ and YIGSR-P₁₁₋₄ were shown to enhance cell attachment and retention when compared to the

corresponding scrambled control coatings, non-functionalised P₁₁-4 coatings and uncoated acellular arteries. To conclude, the use of bioactive self-assembling peptides is a promising approach for improving the functionality of acellular arterial xenografts.

Table of Contents

Acknowledgement	ii
Abstract	iii
Table of Contents	v
List of Figures	xii
List of Schemes	xvii
List of Tables	xviii
List of Equations	xix
List of Abbreviations	xx
1 Introduction	1
1.1 Clinical Need.....	1
1.2 Blood Vessels – Structure and Function	1
1.3 Cardiovascular Disease and Treatment	5
1.4 Surgical Grafts	7
1.4.1 Autograft.....	7
1.4.2 Allografts.....	8
1.4.3 Synthetic Grafts	9
1.4.4 Xenografts.....	10
1.5 Decellularisation	11
1.5.1 Decellularisation Methods	12
1.5.2 Sterilisation Techniques.....	14
1.6 Haemostasis, Coagulation and Thrombosis.....	15
1.7 Approaches to Prevent Thrombus Formation	21
1.7.1 Cell Seeding.....	21
1.7.2 Anti-fouling Surfaces	23
1.7.3 Anticoagulant Agents	24
1.7.4 Bioactive Surface Coatings	27
1.8 Advantages and Limitations of Current Small-diameter Vascular Grafts..	30
1.9 Amino Acids and Peptides	32
1.9.1 α -helix	32
1.9.2 β -sheet.....	33
1.10 Self-assembly of Peptides	34
1.11 Responsiveness of Peptide Self-assembly	34

1.12	β -sheet Based Self-assembling Peptide Systems.....	35
1.12.1	β -hairpin Peptides	35
1.12.2	EAK and RAD Based Peptides	37
1.12.3	P ₁₁ Peptide Series	39
1.13	Peptide Hydrogels as Biomaterials	44
1.14	Advantages and Limitations of Peptides as Biomaterials in Tissue Engineering Applications	45
1.15	Aims and Objectives.....	47
2	Materials and Methods.....	48
2.1	Materials	48
2.1.1	Equipment	48
2.1.2	Glassware.....	49
2.1.3	Plastic Ware	49
2.1.4	Chemicals and Materials	49
2.1.5	Peptides	52
2.1.6	Mammalian Cells	53
2.1.7	Mammalian Tissue.....	53
2.1.8	Antibody-labelling and Antibodies	53
2.1.9	General Reagents.....	54
2.2	Experimental Methods.....	55
2.2.1	Sterilisation Methods	55
2.2.1.1	Sterilisation by Dry Heat	55
2.2.1.2	Sterilisation by Autoclaving.....	55
2.2.1.3	Sterilisation by Filtration	55
2.2.1.4	Sterilisation by Gamma Irradiation	56
2.2.2	Measurement of pH	56
2.2.3	Cell Biology	56
2.2.3.1	Resurrecting and Maintaining Cells	56
2.2.3.2	Passaging and Maintaining Cells	57
2.2.3.3	Counting Viable Cells Using Trypan Blue Exclusion Assay	57
2.2.3.4	Cryopreservation of Cells	58
2.2.4	Decellularisation of Porcine External Iliac Arteries	58
2.2.4.1	Isolation of Arteries.....	60
2.2.4.2	Decellularisation.....	61
2.2.5	Acellularity Validation.....	63

2.2.5.1	Sterility of Acellular Arteries	63
2.2.5.2	Histology.....	63
2.2.5.2.1	Fixation and Paraffin Wax Embedding	63
2.2.5.2.2	Sectioning	63
2.2.5.2.3	Dewaxing and Rehydration	64
2.2.5.2.4	Haematoxylin and Eosin (H & E) Staining	64
2.2.5.2.5	DAPI Staining	65
2.2.5.3	DNA Isolation and Quantification	65
2.2.6	Biocompatibility.....	67
2.2.6.1	Contact Cytotoxicity Assay	68
2.2.6.2	Extract Cytotoxicity Assay	69
2.2.7	Preparation of Peptide Samples.....	71
2.2.7.1	Preparation of Peptides at Physiological Conditions	71
2.2.7.2	Preparation of Functionalised Peptides at a Molar Ratio.....	72
2.2.7.3	Peptide Self-assembly within Acellular Tissue.....	73
2.2.8	Synthesis of Functionalised Peptides	74
2.2.8.1	FITC-labelled Peptides.....	74
2.2.8.2	Cell Attachment Motifs (Alkyne-functionalised Peptides).....	75
2.2.8.3	P ₁₁ Peptides Functionalised with Cell Attachment Motifs.....	76
2.2.8.4	Kaiser Colour Test	77
2.2.8.5	Peptide Purification.....	77
2.2.8.6	Analysis of Synthesised Peptides	78
2.2.9	Characterisation of Peptide Gels.....	78
2.2.9.1	Fourier Transform Infrared (FTIR) Spectroscopy	78
2.2.9.2	Transmission Electron Microscopy (TEM).....	80
2.2.10	Chandler Loop Model	81
2.2.11	Characterisation of Peptide Self-assembly within Acellular Arteries	82
2.2.11.1	Field Emission Gun Scanning Electron Microscopy (FEGSEM)	82
2.2.11.2	Fluorescent Microscopy	83
2.2.11.3	Multiphoton Laser Scanning Microscopy (MPLSM).....	84
2.2.12	Isolation, Maintenance and Characterisation of Ovine Femoral Endothelial Cells	84
2.2.12.1	Isolation.....	84
2.2.12.2	Maintenance and Passaging	86

2.2.12.3	Cryopreservation.....	86
2.2.12.4	Immunofluorescence	86
2.2.13	Attachment of Endothelial Cells.....	89
2.2.13.1	Peptide Coated Acellular Artery Samples and Tissue Preconditioning.....	89
2.2.13.2	Seeding Peptide Coated Acellular Artery Samples with Endothelial Cells.....	89
2.2.13.3	Live/dead® Staining	90
2.2.13.4	Imaging and Analysis.....	90
2.3	Statistical Analysis.....	92
3	Decellularisation of Porcine External Iliac Arteries.....	93
3.1	Introduction	93
3.1.1	University of Leeds Decellularisation Methods.....	93
3.2	Aims and Objectives.....	94
3.3	Methods.....	94
3.3.1	Acellular Artery Production	94
3.3.2	Acellularity and Biocompatibility Validation	94
3.4	Results.....	96
3.4.1	Sterility of Acellular Arteries.....	96
3.4.2	H & E Staining	96
3.4.3	DAPI Staining	97
3.4.4	DNA Content.....	98
3.4.5	Contact Cytotoxicity Assay	98
3.4.6	Extract Cytotoxicity Assay.....	100
3.5	Discussion.....	101
3.6	Summary of Acellularity and Biocompatibility of All Batches	105
4	Characterisation of Self-assembling P₁₁ Peptides Under Physiological Conditions	106
4.1	Introduction	106
4.2	Aims and Objectives.....	107
4.3	Methods.....	107
4.3.1	FTIR Spectroscopy for Peptide Secondary Structures	107
4.3.2	TEM Imaging for Peptide Morphology and Dimensions	108
4.4	Results.....	109
4.4.1	FTIR Spectra – β -sheet Proportion and Equilibrium.....	109

4.4.2	Peptide Gelation Over Time	117
4.4.3	TEM Images of Peptide Fibrillar Networks Forming Gels.....	119
4.5	Discussion.....	123
4.6	Summary of Peptide Self-assembly Characterisation.....	128
5	Synthesis of Functionalised Peptides	130
5.1	Introduction	130
5.2	Aims and Objectives.....	130
5.3	Solid Phase Peptide Synthesis (SPPS) – Fmoc Chemistry	131
5.3.1	FITC-labelled Peptides Synthesis	132
5.4	Click Chemistry.....	136
5.4.1	Copper Catalysed Azide-alkyne Click Chemistry	136
5.4.2	Peptides Functionalised with Cell Attachment Motifs Synthesis..	137
5.4.2.1	Linear Synthesis of Alkyne-functionalised Cell Motifs using SPPS	138
5.4.2.2	Modular Synthesis of Functionalised Peptides using Click Chemistry	141
5.5	Discussion.....	143
6	Peptide Self-assembly within Acellular Arteries.....	146
6.1	Introduction	146
6.1.1	The Extracellular Matrix (ECM) – Structural Proteins	146
6.1.1.1	Collagen.....	146
6.1.1.2	Elastin	147
6.1.2	Thrombogenicity Evaluation.....	148
6.2	Aims and Objectives.....	149
6.3	Methods.....	150
6.3.1	Effect of Peptides on Thrombus Formation in Blood Using a Chandler Loop Thrombosis Model.....	150
6.3.2	Visualisation of Peptide Coated Acellular Artery Tissue by FEGSEM (Dry Sample)	151
6.3.3	Fluorescent Microscopy Imaging of FITC-labelled Peptide Self-assembled within Acellular Artery Tissue (Cryosections)	151
6.3.4	MPLSM Imaging of FITC-labelled Peptide Coated Acellular Artery Tissue (Wet Sample).....	153
6.4	Results.....	155
6.4.1	Effect of Peptides on Thrombus Formation in Blood.....	155
6.4.2	FEGSEM Imaging of the Luminal (Internal) Surface of Coated and Uncoated Acellular Artery Tissue	157

6.4.3	Fluorescent Microscopy Imaging of FITC-labelled Peptide Self-assembled within Acellular Artery Tissue.....	158
6.4.4	MPLSM Imaging of FITC-labelled Peptide Coated Acellular Artery Tissue	162
6.5	Discussion.....	169
6.5.1	Anti-thrombogenic Properties of P ₁₁ Peptides.....	169
6.5.2	P ₁₁ Peptides as Surface Coatings for Vascular Grafts	171
6.6	Summary of Peptide Self-assembly within Acellular Tissue	174
7	Effect of Peptide Functionalisation on Cell Attachment to Peptide Coated Acellular Artery.....	175
7.1	Introduction	175
7.1.1	Cell Adhesion Molecules.....	175
7.1.2	Design of Synthetic Bioactive Peptides – Cell Attachment Motifs	177
7.1.3	Endothelial Cells – Identification and Isolation	180
7.2	Aims and Objectives.....	182
7.3	Methods.....	182
7.3.1	Isolation, Maintenance and Characterisation of Endothelial Cells	182
7.3.2	Biocompatibility – Contact Cytotoxicity Assay	183
7.3.3	Seeding Method Optimisation	183
7.3.3.1	Effect of Tissue Preconditioning on Cell Attachment to Uncoated Acellular Tissue	183
7.3.3.2	Cell Densities in Uncoated Acellular Tissue Over Time.....	183
7.3.3.3	Effect of Different P ₁₁₋₄ Peptides Coatings on Cell Attachment without Tissue Preconditioning	183
7.3.3.4	Effect of Tissue Preconditioning on Cell Attachment to Non-functionalised Peptide Coated Acellular Tissue.....	184
7.3.3.5	Imaging and Data Analysis	184
7.3.4	Effect of Functionalised Peptides on Attachment and Growth of Endothelial Cells to Acellular Arteries	184
7.4	Results.....	185
7.4.1	Endothelial Cells in Culture.....	185
7.4.2	Phenotype of Endothelial Cells - Immunofluorescence	188
7.4.3	Biocompatibility of Acellular Arteries with Endothelial Cells.....	192
7.4.4	Seeding Method Optimisation	193
7.4.4.1	Effect of Tissue Preconditioning on Cell Attachment to Uncoated Acellular Tissue	193
7.4.4.2	Cell Densities in Uncoated Acellular Tissue Over Time.....	193

7.4.4.3	Effect of Different P ₁₁ -4 Peptides Coatings on Cell Attachment without Tissue Preconditioning	194
7.4.4.4	Effect of Tissue Preconditioning on Cell Attachment to Non-Functionalised Peptide Coated Acellular Tissue	195
7.4.5	Effect of Functionalised Peptides on Attachment and Growth of Endothelial Cells to Acellular Arteries	197
7.5	Discussion.....	203
7.5.1	Isolation and Characterisation of Endothelial Cells.....	203
7.5.2	Seeding Method Optimisation	204
7.5.3	Peptide Functionalisation for Cell Attachment of Endothelial Cells to Acellular Arteries	205
8	Conclusions.....	212
8.1	Summary	212
8.2	Future Work	213
8.3	Significance of Work	219
A	Appendix.....	220
A.1	Amino Acids	220
A.2	P ₁₁ Peptides.....	221
A.3	FTIR Spectra – Other Concentrations	223
A.4	P ₁₁ Peptides Gelation Over time	226
A.5	FTIR – Effect of Temperature on Peptide Self-assembly	228
A.6	Peptide Synthesis Results	229
A.6.1	FITC-labelled Peptides	229
A.6.2	Alkyne-functionalised Cell Attachment Motifs	231
A.6.3	Bioactive (Cell Attachment Functionalised) P ₁₁ Peptides.....	235
A.7	FEGSEM Images of the Abluminal (External) Surface of Coated and Uncoated Acellular Artery Tissue.....	243
A.8	MPLSM Images of Cellular and Acellular Arteries at the Luminal Surface	244
A.9	MPLSM Images of Peptide Coated Acellular Arteries.....	247
	References	251

List of Figures

Figure 1.1: Schematic of blood vessel structure.	2
Figure 1.2: Schematic diagram showing the ECM cell adhesion molecules.	4
Figure 1.3: Schematic diagram showing the development of atherosclerosis.	6
Figure 1.4: Schematic of a bypass graft.	7
Figure 1.5: Schematic of the decellularisation process.	12
Figure 1.6: Coagulation Cascade Model.	18
Figure 1.7: Schematic of the development of cell seeded vascular graft.	22
Figure 1.8: Schematic of the action of heparin in the prevention of thrombus formation.	25
Figure 1.9: Functionalisation of biomaterial surface with bioactive motifs for enhancement of cell attachment <i>in vivo</i>	27
Figure 1.10: Schematic of β -sheet parallel and antiparallel arrangements of β -strands.	33
Figure 1.11: Structures and self-assembly of MAX peptides into β -hairpins.	36
Figure 1.12: Structures and self-assembly of ionic complementary RAD and EAK peptides.	38
Figure 1.13: Hierarchical self-assembly of P ₁₁ peptides into β -sheet structures. ...	40
Figure 1.14: Sequences and structures of P ₁₁₋₄ (P01), P ₁₁₋₈ (P02) and P ₁₁₋₁₂ (P03).	42
Figure 1.15: Effect of ionic strength on self-assembly – β -sheet percentages of peptides at 6.3 mM (approximately 10 mg.mL ⁻¹) in D ₂ O as a function of pD as determined by FTIR (circle) and NMR (triangle).	43
Figure 2.1: Trypan blue exclusion assay for counting cells in haemocytometer grids.	58
Figure 2.2: Porcine external iliac artery dissection.	60
Figure 2.3: Flow diagram summarising the decellularisation process for the porcine external iliac artery.	62
Figure 2.4: Schematic of sectioning of wax embedded arteries.	64
Figure 2.5: Flow diagram showing the process of DNA isolation from tissue.	67
Figure 2.6: Schematic diagram of contact cytotoxicity assay set-up in a six-well plate.	68
Figure 2.7: Schematic diagram showing streaking of extract onto an agar plate to test for sterility.	70
Figure 2.8: Schematic diagram showing the peptide gelation procedure by changing the ionic strength at physiological pH.	72

Figure 2.9: Schematic diagram showing inclusion of acellular artery tissue section (or segment as specified) within the peptide solution procedure at physiological pH.	73
Figure 2.10: N-terminal Fmoc-protected amino acid building blocks used for the synthesis of FITC-labelled peptides and cell attachment motifs.	74
Figure 2.11: Rink amide NovaGel™ resin used for the synthesis of FITC-labelled peptides.	75
Figure 2.12: NovaSyn®TG Sieber resin used for the synthesis of cell attachment motifs.	76
Figure 2.13: Schematic diagram showing the preparation of TEM grids.	81
Figure 2.14: Schematic diagram of Chandler loop model experimental set-up.	82
Figure 2.15: Schematic diagram showing the cell seeding set-up for immunofluorescence.	88
Figure 2.16: Schematic diagram showing tissue cell seeding set-up and positions of images taken from tissue for cell studies.	91
Figure 3.1: Positions of artery sections/segments used for decellularisation validation.	95
Figure 3.2: Sterility of acellular porcine external iliac arteries following decellularisation.	96
Figure 3.3: Cellular and acellular porcine external iliac arteries fixed in NBF and stained with H & E.	97
Figure 3.4: Cellular and acellular porcine external iliac arteries fixed in NBF and stained with DAPI.	98
Figure 3.5: Contact cytotoxicity of acellular porcine external iliac arteries with BHK cells.	99
Figure 3.6: Contact cytotoxicity of acellular porcine external iliac arteries with L929 cells.	100
Figure 3.7: Relative ATP content of BHK and L929 cells cultured with extracts of acellular porcine external iliac arteries.	101
Figure 4.1: P ₁₁₋₄ FTIR spectra at 20 mg.mL ⁻¹ over time after triggering self-assembly by addition of Ringer's solution.	109
Figure 4.2: Fitted P ₁₁₋₄ FTIR spectrum at 20 mg.mL ⁻¹ one day after triggering self-assembly.	110
Figure 4.3: P ₁₁₋₄ β-sheet percentages at different concentrations over time after triggering self-assembly by addition of Ringer's solution.	111
Figure 4.4: P ₁₁₋₈ FTIR spectra at 20 mg.mL ⁻¹ over time after triggering self-assembly by addition of Ringer's solution.	112
Figure 4.5: Fitted P ₁₁₋₈ FTIR spectrum at 20 mg.mL ⁻¹ one day after triggering self-assembly.	113

Figure 4.6: P ₁₁ -8 β -sheet percentages at different concentrations over time after triggering self-assembly by addition of Ringer's solution.....	114
Figure 4.7: P ₁₁ -12 FTIR spectra at 20 mg.mL ⁻¹ over time after triggering self-assembly by addition of Ringer's solution.	115
Figure 4.8: Fitted P ₁₁ -12 FTIR spectrum at 20 mg.mL ⁻¹ one day after triggering self-assembly.....	116
Figure 4.9: P ₁₁ -12 β -sheet percentages at different concentrations over time after triggering self-assembly by addition of Ringer's solution.....	117
Figure 4.10: P ₁₁ peptides gelation over time.	118
Figure 4.11: TEM images of P ₁₁ -4 at different concentrations.	120
Figure 4.12: TEM images of P ₁₁ -8 at different concentrations.	121
Figure 4.13: TEM images of P ₁₁ -12 at different concentrations.	122
Figure 4.14: P ₁₁ -4, P ₁₁ -8 and P ₁₁ -12 fibril widths as determined by TEM..	123
Figure 5.1: Structures of FITC-labelled P ₁₁ peptides and FITC control.....	133
Figure 5.2: Analytical HPLC trace for FITC-P ₁₁ -8 and its corresponding data.	135
Figure 5.3: General copper catalysed azide-alkyne click chemistry model.	137
Figure 5.4: Schematic diagram showing the peptide chains required for P ₁₁ peptides functionalisation with cell attachment motifs through copper catalysed azide-alkyne click chemistry.	138
Figure 5.5: Structures of alkyne-functionalised cell attachment motifs and the corresponding scrambled controls (for click chemistry).	139
Figure 6.1: Schematic diagram showing the formation of collagen fibres.	147
Figure 6.2: Schematic diagram showing the stretching and relaxation of elastic fibres.	148
Figure 6.3: Schematic of fluorescent microscopy imaging.	152
Figure 6.4: A schematic diagram comparing the fluorescent signals detected in fluorescent, confocal and multiphoton microscopes..	154
Figure 6.5: Schematic diagram showing MPLSM sample set-up and imaging.	155
Figure 6.6: Effect of peptides on thrombus weight (mg) using the Chandler loop model.	156
Figure 6.7: Appearance of blood treated with 3.0 mM self-assembled P ₁₁ -4.	156
Figure 6.8: FEGSEM images showing self-assembling peptides at 20 mg.mL ⁻¹ as surface coatings for the luminal surface of acellular arteries.	158
Figure 6.9: Fluorescent microscope cross-sectional images of controls for FITC-labelled peptides self-assembled within acellular artery.	159
Figure 6.10: Fluorescent microscope cross-sectional images of FITC-labelled peptides self-assembled within acellular artery.	161
Figure 6.11: Multiphoton images of uncoated acellular artery.	163

Figure 6.12: Multiphoton images of acellular arteries coated with 20 mg.mL ⁻¹ FITC-labelled P ₁₁ -4 at a molar ratio of 1:150 of the FITC-labelled to the non-labelled peptides.	164
Figure 6.13: Multiphoton images of acellular arteries coated with 20 mg.mL ⁻¹ FITC-labelled P ₁₁ -8 at a molar ratio of 1:150 of the FITC-labelled to the non-labelled peptides.	165
Figure 6.14: Multiphoton images of acellular arteries coated with 20 mg.mL ⁻¹ FITC-labelled P ₁₁ -12 at a molar ratio of 1:150 of the FITC-labelled to the non-labelled peptide..	166
Figure 6.15: Low magnification multiphoton z-stack images of acellular arteries coated with 20 mg.mL ⁻¹ FITC-labelled peptides at a molar ratio of 1:150 of the FITC to the non-labelled peptides.....	167
Figure 6.16: High magnification multiphoton z-stack images of acellular arteries coated with 20 mg.mL ⁻¹ FITC-labelled peptides at a molar ratio of 1:150 of the FITC-labelled to the non-labelled peptides.....	168
Figure 7.1: Schematic diagram of integrin cell adhesion receptor showing the main features of α and β subunits.....	177
Figure 7.2: Isolated ovine femoral endothelial cells in culture at early passages before purification through successive passaging with three-minute trypsin/EDTA treatments..	186
Figure 7.3: Isolated ovine femoral endothelial cells in culture at different passages after purification through successive passaging with three-minute trypsin/EDTA treatments.	187
Figure 7.4: Antibody-labelling of impure isolated ovine femoral endothelial cells at passage two.	189
Figure 7.5: Antibody-labelling of isolated ovine femoral endothelial cells at passage four (antibodies).	190
Figure 7.6: Antibody-labelling of isolated ovine femoral endothelial cells at passage four (antibody isotype controls).	191
Figure 7.7: Contact cytotoxicity of isolated ovine femoral endothelial cells with acellular arteries.	192
Figure 7.8: A) Viable cells counted (%) and B) number of live cells counted per mm ² in uncoated acellular artery samples without preconditioning, with 4 and 24 hours of preconditioning.	193
Figure 7.9: A) Viable cells counted (%) and B) number of live cells counted per mm ² in uncoated acellular artery sample without preconditioning over time.	194
Figure 7.10: A) Viable cells counted (%) and B) number of live cells counted per mm ² in acellular artery samples coated with different P ₁₁ -4 peptides without tissue preconditioning after 4 and 72 hours.	195
Figure 7.11: A) Viable cells counted (%) and B) number of live cells counted per mm ² in acellular artery samples coated with non-functionalised peptides with tissue preconditioning after 4 and 72 hours..	196

Figure 7.12: Live/dead stained images of non-functionalised and functionalised P ₁₁ -4 coated acellular artery samples.....	198
Figure 7.13: Viable cells counted (%) in preconditioned acellular artery samples coated with different P ₁₁ -4 peptides after 4 and 72 hours.	199
Figure 7.14: Number of live cells counted per mm ² in preconditioned acellular artery samples coated with different P ₁₁ -4 peptides after 4 and 72 hours.	199
Figure 7.15: Live/dead stained images of non-functionalised and functionalised P ₁₁ -8 coated acellular artery samples.....	201
Figure 7.16: Viable cells counted (%) in preconditioned acellular artery samples coated with different P ₁₁ -8 peptides after 4 and 72 hours.	202
Figure 7.17: Number of live cells counted per mm ² in preconditioned acellular artery samples coated with different P ₁₁ -8 peptides after 4 and 72 hours.	202
Figure A.1: Categorisation of the twenty naturally occurring amino acids into different groups depending on their side-chain group.	220
Figure A.2: P ₁₁ -4 FTIR spectra at 10 mg.mL ⁻¹ (A) and 30 mg.mL ⁻¹ (B) over time after triggering self-assembly by addition of Ringer's solution.....	223
Figure A.3: P ₁₁ -8 FTIR spectra at 10 mg.mL ⁻¹ (A) and 30 mg.mL ⁻¹ (B) over time after triggering self-assembly by addition of Ringer's solution.....	224
Figure A.4: P ₁₁ -12 FTIR spectra at 10 mg.mL ⁻¹ (A) and 30 mg.mL ⁻¹ (B) over time after triggering self-assembly by addition of Ringer's solution.....	225
Figure A.5: P ₁₁ -4, P ₁₁ -8 and P ₁₁ -12 β-sheet percentages at 30 mg.mL ⁻¹ over time at room temperature (RT) and 37 °C.	228
Figure A.6: FEGSEM images showing self-assembling peptides at 20 mg.mL ⁻¹ as surface coatings for the abluminal surface of acellular arteries..	243
Figure A.7: Multiphoton z-stack images of cellular (A) and acellular (B) arteries with 5 μm intervals near the luminal surface into tunica media.....	245
Figure A.8: Multiphoton z-stack images of cellular (A) and acellular (B) arteries with 4 μm intervals near the luminal surface into tunica media.....	246
Figure A.9: Multiphoton images of FITC-βA control within acellular artery.....	247
Figure A.10: Multiphoton images of 20 mg.mL ⁻¹ FITC-labelled P ₁₁ -4 at a molar ratio of 1:150 of the FITC-labelled to the non-labelled peptides within acellular artery.....	248
Figure A.11: Multiphoton images of 20 mg.mL ⁻¹ FITC-labelled P ₁₁ -8 at a molar ratio of 1:150 of the FITC-labelled to the non-labelled peptides within acellular artery.....	249
Figure A.12: Multiphoton images of 20 mg.mL ⁻¹ FITC-labelled P ₁₁ -12 at a molar ratio of 1:150 of the FITC-labelled to the non-labelled peptides within acellular artery.....	250

List of Schemes

Scheme 5.1: Linear synthesis of FITC-P ₁₁ -8 by Fmoc SPPS.....	134
Scheme 5.2: Linear synthesis of cell attachment motifs using Fmoc SPPS.	140
Scheme 5.3: Modular synthesis of P ₁₁ peptide functionalised with cell attachment motifs using copper catalysed azide-alkyne click chemistry.	142

List of Tables

Table 2.1: Equipment used throughout the study.....	48
Table 2.2: Chemicals and reagents used during the study.	49
Table 2.3: Peptides, amino acids and resins used throughout the study.....	52
Table 2.4: Primary antibodies, secondary antibodies and isotype controls.....	54
Table 2.5: Conditions used for purification of synthesised peptides including; solvent in which peptide was solubilised, gradient of water to acetonitrile (%) for purification, additives to solvent and wavelength at which UV detection occurred.	78
Table 2.6: Absorption ranges in the amide I' region and their corresponding secondary structure, <i>amino acid side chain</i> or impurities.....	79
Table 3.1: Acellularity and <i>in vitro</i> biocompatibility results of all decellularised batches of porcine external iliac arteries.	105
Table 4.1: Summary of P ₁₁₋₄ , P ₁₁₋₈ and P ₁₁₋₁₂ characterisation at 10, 20 and 30 mg.mL ⁻¹ 0, 1, 6, 14 and 28 days after triggering self-assembly.	128
Table 5.1: Protecting groups used in SPPS.....	131
Table 5.2: Table summarising the analysis results for synthesised FITC-labelled peptides showing the expected molecular mass, mass acquired by mass spectrometry and purity acquired by HPLC.....	136
Table 5.3: Table summarising the analysis results for synthesised cell attachment motifs showing the expected molecular mass, mass acquired by mass spectrometry and purity acquired by HPLC (Ac - acetyl group CH ₃ CO).....	141
Table 5.4: Different conditions used for the click chemistry reaction.....	141
Table 5.5: Table summarising the analysis results for bioactive (cell attachment functionalised) peptide showing the expected molecular mass, mass acquired by mass spectrometry and purity acquired by HPLC (Ac - acetyl group CH ₃ CO).	143
Table 6.1: Peptide self-assembly within acellular tissue for anti-thrombogenic surface coating.....	174
Table 7.1: Percentages of cells attached to non-functionalised peptide coated tissue with preconditioning after 4 and 72 hours.	196
Table 7.2: Percentages of cells attached to non-functionalised/functionalised P ₁₁₋₄ and P ₁₁₋₈ peptide coated tissue with preconditioning after 4 and 72 hours.	203
Table A.1: Sequences, molecular weights and net charges at pH 7.4 of peptides used throughout the study.	221
Table A.2: Conversion of peptides concentrations used throughout the study (mg.mL ⁻¹ to mM and vice versa).	222
Table A.3: Summary of physical state observations in P ₁₁₋₄ , P ₁₁₋₈ and P ₁₁₋₁₂ at different concentrations over time.....	226

List of Equations

Equation 2.1: Calculating viable cells using trypan blue exclusion assay.	58
Equation 2.2: Calculating the DNA concentration per weight of tissue.	66
Equation 2.3: An equation to calculate the volume of stock solution required (V_{stock}) to make the intended working concentration (C_{working}) using the final peptide volume (V_{working}) and the final concentration of stock (C_{stock}).	72
Equation 2.4: An equation to calculate the volume of water required.	72
Equation 2.5: An equation to calculate pD from uncorrected pH reading (pH^*).	79
Equation 2.6: An equation to calculate the percentage of secondary structures observed in an FTIR spectrum of peptides.	80
Equation 2.7: Viability of cells (%) seeded onto tissue.	92
Equation 2.8: Cell density (cell per mm^2) in tissue.	92
Equation 2.9: Cells attached (%) to tissue.	92

List of Abbreviations

Ac	Acetyl
Ahx	Aminohexanoic acid
ANOVA	Analysis of variance
ATP	Adenosine triphosphate
BHK	Baby hamster Syrian kidney
Boc	<i>tert</i> -Butoxycarbonyl
BSA	Bovine serum albumin
CABG	Coronary artery bypass graft
CD31	Platelet endothelial cell adhesion molecule
CPS	Counts per second
DAPI	4',6-diamidino-2-phenylindole
DCM	Dichloromethane
DIC	Diisopropylcarbodiimide
DIPEA	N,N-Diisopropylethylamine
DMEM	Dulbecco's minimal Eagle's medium
DMF	Dimethylformamide
DMSO	Dimethyl sulfoxide
DNA	Deoxyribonucleic acid
ECGS	Endothelial cell growth supplement
ECM	Extracellular matrix
EDTA	Ethylenediaminetetra-acetic acid
ePTFE	Expanded polytetrafluoroethylene
Equiv	Equivalents
FBS	Foetal bovine serum
FDA	Food and Drug Administration
FEGSEM	Field emission gun scanning electron microscopy
FITC	Fluorescein isothiocyanate
Fmoc	9-Fluorenylmethoxycarbonyl
FTIR	Fourier transform infrared

GAG	Glycosaminoglycan
GFP	Green fluorescent protein
GMEM	Glasgow's minimal essential medium
GRGDS	Glycine-arginine-glycine-aspartic acid-serine
H & E	Haematoxylin and Eosin
HBSS	Hank's balanced salt solution
HCTU	O-(1H-6-Chlorobenzotriazole-1-yl)-1,1,3,3-tetramethyluronium hexafluorophosphate
HPLC	High performance liquid chromatography
KIU	Kallikrein inhibitor unit
L929	Mouse C3H/An connective tissue
LC-MS	Liquid chromatography-mass spectroscopy
LMWH	Low molecular weight heparin
MeCN	Acetonitrile
MPLSM	Multiphoton laser scanning microscopy
NBF	Neutral buffered formalin
NMR	Nuclear magnetic resonance
P ₁₁	11 amino acid peptide chain
PAA	Peracetic acid
Pbf	2,2,4,6,7-Pentamethyldihydrobenzofuran-5-sulfonyl
PBSa	Phosphate buffered saline (autoclaved)
PEG	Polyethylene glycol
PERV	Porcine endogenous retrovirus
PVC	Polyvinyl chloride
qRT-PCR	Quantitative reverse transcription polymerase chain reaction
RNA	Ribonucleic acid
rpm	Revolutions per minute
SD	Significant difference
SDS	Sodium dodecyl sulphate
SPPS	Solid phase peptide synthesis
T-25	25 cm ² tissue culture flask

T-75	75 cm ² tissue culture flask
T-175	175 cm ² tissue culture flask
TBS	Tris buffered saline
TBTA	Tris(benzyltriazolylmethyl)amine
tBu	tert-Butyl
TCEP	Tris(2-carboxyethyl)phosphine
TEM	Transmission electron microscopy
TF	Tissue factor
TFA	Trifluoroacetic acid
TFPI	Tissue factor pathway inhibitor
TIPS	Triisopropylsilane
TPB	Tryptone phosphate broth
Trt	Trityl
UV	Ultraviolet
v/v	Volume/volume
vWF	Von Willebrand factor
w/v	Weight/volume
w/w	Weight/weight
YIGSR	Tyrosine-isoleucine-glycine-serine-arginine

1 Introduction

1.1 Clinical Need

In 2012, cardiovascular disease became the second major cause of mortality in the UK for the first time, causing 28 % of deaths after cancer with 29 %. Over 300 million medications for cardiovascular diseases were prescribed to patients in 2013 and millions of pounds are spent each year as the cost for these prescriptions (£6.8 billion for cardiovascular disease treatment in England 2012/2013) ¹. However, surgical interventions may be required, particularly for complex conditions. For instance, coronary artery bypass grafts (CABG) remain one of the main surgical treatments for complex conditions and around 25,000 CABG procedures are carried out annually in the UK; however these are not cost-effective ¹⁻³. Although cardiovascular disease is no longer the first cause of mortality in the UK, it is still the major cause of death for women and remains a burden to the UK in terms of health and cost ¹. The current medical interventions for medium and large-diameter vascular grafts (> 6 mm) have shown long-term satisfactory results, but there is still a demand for small-diameter vascular grafts (< 6 mm) due to the poor patency rates caused by thrombosis and occlusion ⁴.

1.2 Blood Vessels – Structure and Function

Arteries and veins but not capillaries with < 6 mm diameter are referred to as small-diameter blood vessels ⁵. Blood vessels are composed of three main layers, starting from the internal luminal surface into the external abluminal surface: the intima, the tunica media and the tunica adventitia. Each layer has a specific structure and function determined by the cellular and non-cellular extracellular matrix (ECM) components of that layer, which also contribute to the functional and mechanical properties of the blood vessel as a whole ⁵⁻⁸. This basic blood vessel structure is similar in arteries and veins with varying thicknesses. Arteries also contain elastin in their structure, while veins have valves in the luminal side ⁹ (Figure 1.1).

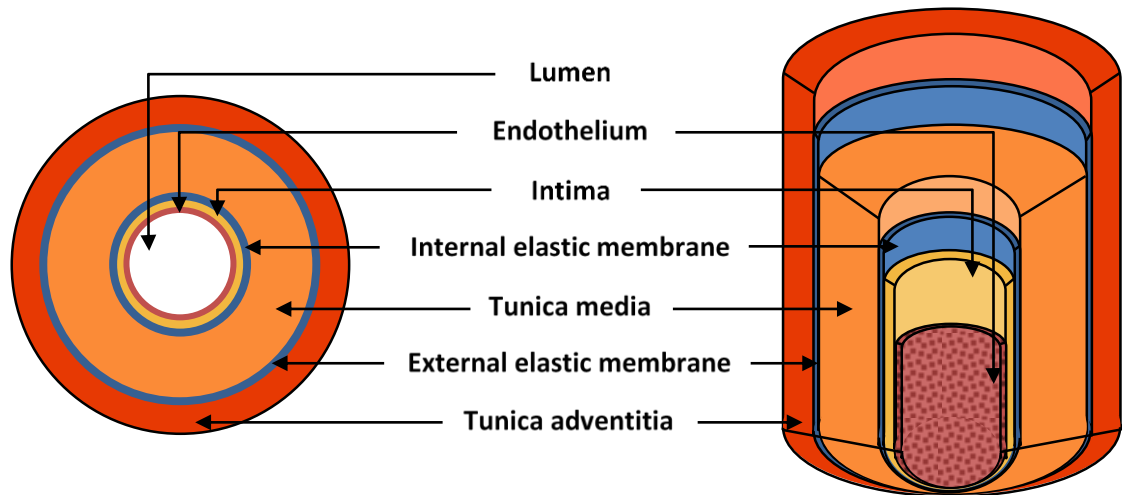


Figure 1.1: Schematic of blood vessel structure. *Blood vessels are composed of three main layers, the intima, tunica media and tunica adventitia. An endothelial layer forms the lining of the intima on the luminal surface. In arteries, internal and external elastic membranes separate the intima from the tunica media and the tunica media from the tunica adventitia, respectively.*

The intima comprises an endothelial layer and subendothelial basement membrane¹⁰. The endothelial cells are lined on the luminal surface as a monolayer⁵. The endothelium plays an important role in blood vessel functionality. It acts as an anti-thrombogenic surface and a selective permeable barrier facilitating a laminar blood flow through the vessel^{5,11}. It also acts as a sensor for blood flow, hence shear stress changes, by relaying the signal from the lumen throughout the vessel wall in order to regulate the vascular response to haemodynamic changes¹². This regulation is achieved by release of vasodilation and vasoconstriction factors. For instance, the endothelial cells produce nitric oxide, vasodilation molecules, in response to increased shear stress that diffuses into the vascular smooth muscle cells inducing relaxation¹².

The endothelium also regulates many other physiological functions including; adhesion, activation and aggregation of platelets, leucocyte adhesion and smooth muscle cell migration and proliferation, all of which are inhibited by nitric oxide in a healthy vessel^{5,11}. Endothelial cells have Weibel-Palade bodies that release von Willebrand factor (vWF) and other molecules that contribute to platelet binding, recruitment of leucocytes and modulate inflammation⁹. In a normal functioning blood vessel, platelets are repelled by the negatively charged glycosaminoglycans (GAGs) from the endothelium surface⁹. However, under certain vascular conditions, adhesion, activation and migration of these cells can be promoted. For example, during

haemostasis upon vascular injury, circulating platelets adhere to the exposed subendothelium, become activated and overcome the repulsion, aggregate promoting thrombin generation and then develop a stable fibrin clot. Leukocytes also adhere to endothelial cells during inflammation, spread, migrate to underlying tissue and are recruited to where they are needed^{9,11}.

Endothelial cells can also produce elastin, possibly contributing to the internal elastic membrane formation¹⁰. They are involved in the healing process after inflammation or wounding and tissue repair, hence needed for angiogenesis, which refers to the formation of a new blood vessel⁹.

Since endothelial cells are involved in many essential processes including regulation of thrombus formation and inflammation, dysfunction or injury of the endothelium results in early development of atherosclerosis plaque⁹ as will be discussed in Section 1.3.

The subendothelial basement membrane to which endothelial cells are anchored provides structural support to cells. The different components in the basement membrane such as collagen type IV, laminin, and fibronectin affect cell adhesion, proliferation, migration and differentiation. The cell-ECM interaction is mediated by integrin and non-integrin cell adhesion receptors (more detail on integrins is presented in Chapter 7, Section 7.1.1). Therefore, the basement membrane components are important for regulating normal and pathological blood vessel functionality^{7,8,13}.

Collagen type IV is an important component of the basement membrane in the intima because it contains ligands that have an affinity for endothelial cells, hence it plays a role in endothelial cell attachment and migration^{8,14}. It is also involved in many other processes as it limits smooth muscle cell growth, reduces low-density lipoprotein (involved in atherosclerosis) and inhibits calcification⁷. Collagen type IV contributes to the structural stability of the basement membrane¹².

Laminin is a heterodimeric glycoprotein composed of α , β and γ chains⁷. It can be produced by endothelial and smooth muscle cells¹³. Several cell attachment recognition sites have been identified in laminin including RGD (arginine-glycine-aspartic acid) in the α chain, YIGSR (tyrosine-isoleucine-glycine-serine-arginine) in the β chain and IKVAV (isoleucine-lysine-valine-alanine-valine) near the C-terminus of the α chains (Figure 1.2). These peptide sequences are involved in cell adhesion, migration,

growth and differentiation of various cell types, hence laminin is essential for the maintenance and organisation of the blood vessel structure^{8,14}. For example, the RGD binding sites mediate endothelial cell binding through $\alpha_5\beta_1$, $\alpha_v\beta_1$, $\alpha_v\beta_3$ and $\alpha_v\beta_5$ integrins, which are highly expressed on the endothelium¹³. Laminin also facilitates the adhesion of the other cell types within the ECM⁸. Laminin is the major biologically active component of the basement membrane and in addition to mediating cell-ECM attachment, it is involved in binding collagen IV and other ECM molecules¹³.

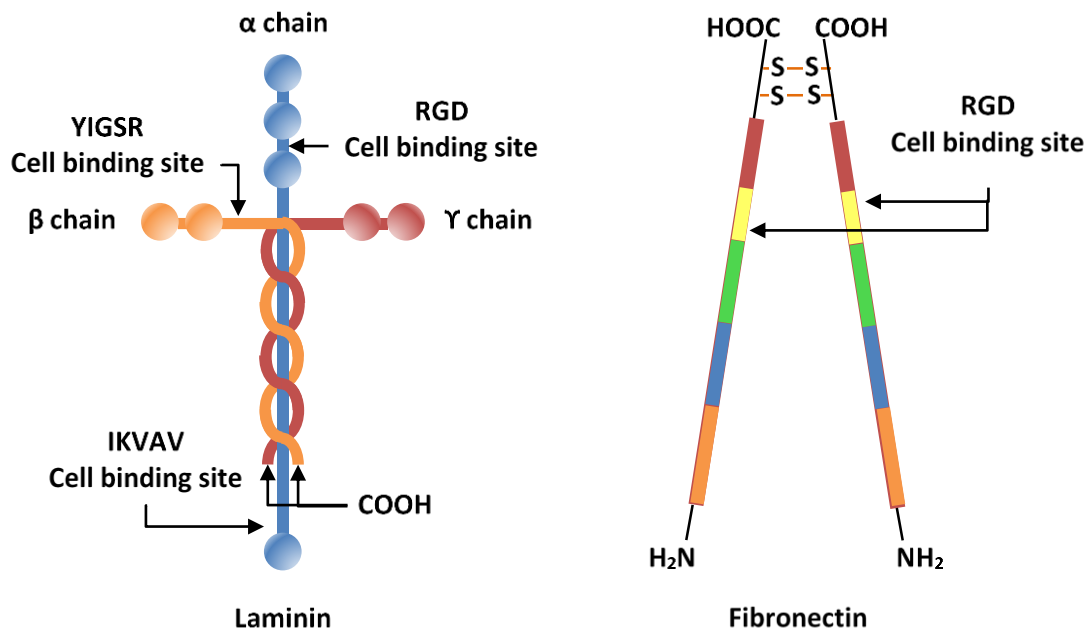


Figure 1.2: Schematic diagram showing the ECM cell adhesion molecules. Laminin (left) composing of three chains and having cell binding sites with the peptide sequences: RGD, YIGSR and IKVAV. Fibronectin (right) composing of several binding sites one of which is the cell binding site with the peptide sequence RGD.

Fibronectin is a dimeric multidomain glycoprotein that is widely distributed through the ECM and can be found on the basement membrane^{7,8,15}. It is composed of two subunits that are linked via a disulphide bond near the C-terminus¹⁵ (Figure 1.2). It can be produced by smooth muscle cells and fibroblasts⁷. Fibronectin is involved in the cell-ECM adhesion via various integrins through several peptide sequences (cell binding sites)¹⁵. For example, the $\alpha_5\beta_1$ integrin that is expressed by smooth muscle cells, endothelial cells and fibroblasts through RGD^{7,15}. The $\alpha_4\beta_1$ integrin also mediates cell adhesion through REDV (arginine-glutamic acid-aspartic acid-valine) and LDV (leucine-aspartic acid-valine)¹⁵. Fibronectin is also important for cell migration, growth and

differentiation of endothelial progenitor cells that are involved in vascular repair ⁷. Other adhesion domains on fibronectin bind and control the deposition and organisation of various important proteins such as heparin, collagen and fibrin ¹⁵.

An internal elastic membrane separates the intima from the tunica media ¹⁶. In the tunica media, collagen fibres (types I and III) and smooth muscle cells are circumferentially arranged and sandwiched between elastin fenestrated sheets that are interconnected throughout the layer by thin elastic fibres ^{5,7,10,16}. Collagen and elastin are primarily produced by smooth muscle cells ^{7,10}. Collagen contributes to the strength of the vascular wall and elastin distributes stress evenly throughout the vascular wall and onto the collagen fibres ¹⁰. Vessel elasticity is contributed to by proteoglycans secreted by smooth muscle cells, collagen and elastin fibres as well as elastic sheets ⁵. Elastic sheets also contribute to the mechanical integrity of arteries. Elastic fibres are degraded with ageing or disease, causing an increase in arterial wall stiffness ⁷.

An external elastic membrane separates the tunica media from the tunica adventitia ¹⁶. The tunica adventitia contains connective tissue composing of collagen types I and III mainly, elastin and fibroblasts ^{5,7}. Collagen, elastin and fibronectin in this layer are primarily produced by fibroblasts ⁷. The tunica adventitia collagen fibres prevent rupturing of the vessel at very high pressures ¹⁰. Nerves are also contained within this layer in large arteries but do not penetrate into the tunica media ¹⁶.

1.3 Cardiovascular Disease and Treatment

Cardiovascular disease is one of the major killers in the developing countries and can be caused by smoking, diabetes and obesity but reduced with healthier lifestyle ¹⁷. Atherosclerosis is an inflammatory disease that can lead to cardiovascular disease. Atherosclerosis is the formation of a lesion or a plaque within the lumen of arteries ^{18,19}. It is mainly caused by irregularities and dysfunction of endothelium in response to an injury increasing the endothelial permeability and adhesiveness to platelets and leukocytes ^{11,20}. Plaque formation is initiated by low-density lipoprotein cholesterol coagulating within the arterial wall, leading to fatty streaks. This incites an inflammatory response involving mononuclear phagocytes and lymphocytes. Migration and proliferation of smooth muscle cells is caused by the inflammatory response such as the release of cytokines and other mediators by monocytes, lymphocytes and macrophages

leading to arterial wall thickening. Therefore, continued inflammatory response results in progression of plaque formation leading to narrowing or even total blockage of arteries¹⁸⁻²⁰. Rupture of plaque in an advanced lesion occurring at the thinning fibrous tissue cap that covers the lesion of accumulated cells, macrophages, leucocytes and lipids causes haemorrhage, hence rapid thrombosis due to the release of tissue factor²⁰ (Figure 1.3).

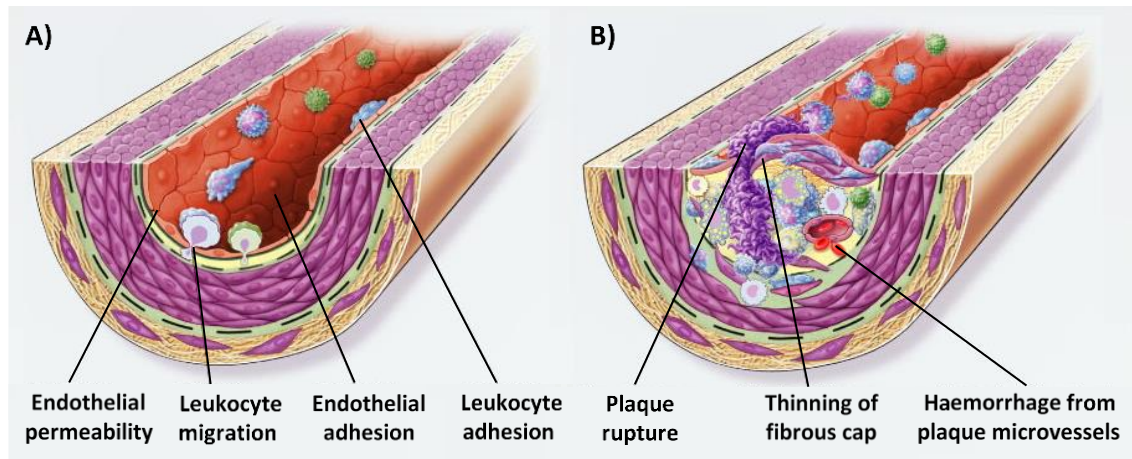


Figure 1.3: Schematic diagram showing the development of atherosclerosis. A) Endothelial dysfunction, that progresses to fatty-streak formation, advanced lesion formation and D) plaque rupture in atherosclerosis. Adapted with permission from Ross²⁰. Copyright Massachusetts Medical Society.

The primary treatment method for cardiovascular disease is the use of medication such as blood glucose control, lipid-lowering and anti-platelet therapies¹⁷. The use of stents may be required for the treatment of more advanced stages of cardiovascular diseases such as atherosclerosis. Stents are metallic tubes that are permanently inserted into the diseased artery, consequently patients with stents are required to take anti-thrombotic drugs for 6 - 12 months following the procedure and aspirin for their lifetime¹⁹. However, failure of medication or use of a stent may require surgical intervention using vascular grafts for replacement of the affected arteries. For example, in peripheral arterial disease and coronary heart disease, both require bypass grafting.

1.4 Surgical Grafts

1.4.1 Autograft

Bypass grafts provide an alternative route for blood flow in an occluded vessel (Figure 1.4). Autografts are tissues which are transplanted from one site in the patient to where it is required within the patient themselves. Autografts are the gold standard for bypass grafts including CABG or other small-diameter vascular grafts. Autografts should ideally display the biomechanical properties of the native vessel and contain autologous cells, minimising immunological responses. Examples of autografts include the saphenous vein and the internal thoracic artery (also known as the internal mammary artery) ²¹⁻²⁵.

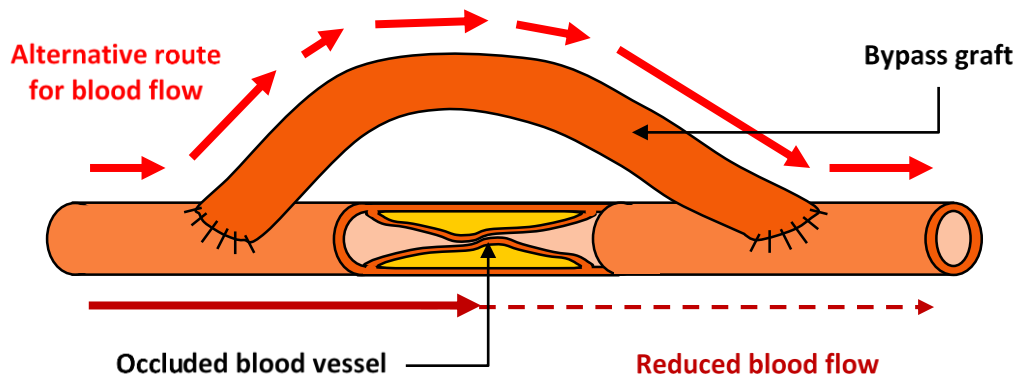


Figure 1.4: Schematic of a bypass graft. A bypass graft provides an alternative route for blood flow when the blood vessel is occluded.

For coronary artery bypass grafting (CABG), autologous veins were widely used, but these were not good substitutes for arteries as they differ in structure and biomechanical properties. They have short patency rates requiring surgery after a few years and patients may require more than one bypass graft ¹⁹. A follow-up study by Arima *et al.* over ten years reported that the patency rate of saphenous vein grafts for CABG was lower than left internal thoracic artery grafts ²². In general, arteries have higher patency rates than veins because arteries are stiffer, meaning that veins have higher extensibility which might hinder them from accommodating high blood pressures in arteries due to compliance mismatch, leading to thrombosis or intimal hyperplasia ^{19,22}. Therefore, the use of autologous arteries rather than veins for CABG is now favoured.

Autografts remain the gold standard for vascular bypass due to their higher patency rates when compared to allografts or synthetic grafts^{23,26}. However, surgical difficulties often lead to their failure²³. Additionally, a third of patients are unable to provide suitable vessels for grafting due to pre-existing vascular disease or previous surgeries^{21,24,25}.

1.4.2 Allografts

Allografts are transplants within the same species. Allografts are used as alternatives for autografts since they contain the human endothelial cells and have the appropriate biomechanical properties when using similar sized arteries²⁷.

Unlike autografts, allografts need to be harvested from the donor prior to requirement for surgery. Therefore, effective storage procedures and careful handling are needed, ensuring sterility and integrity of the endothelium to maintain patency of the graft²⁸. Fresh allografts are prone to rapid rejection due to an immune response and preserved allografts may not maintain normal endothelial cell function causing thrombosis and may still elicit an immune response. Early attempts of allograft preservation used freezing to cause lysis of the cellular elements, reducing antigenicity and facilitating storage²⁷. Histocompatibility, blood group matching between donor and recipient and treatment of allograft recipients with immunosuppressants may also improve the performance of allografts²⁷. In contrast to simple freezing storage methods, cryopreservation is used for controlled cooling of donor tissue such as blood vessels to prevent ice nucleation, preserving cell viability for long-term use and storage²⁷. Long-term storage has been shown to have no impact on structure, regeneration and patency of blood vessel allografts²⁹. However, the immune response of the recipient remains a major concern resulting in graft failure, requiring the use of immunosuppressants²⁷. It has, however been reported by Carpenter *et al.* that the use of low doses of the immunosuppressant azathioprine with cryopreserved saphenous venous allografts did not prevent graft rejection. Therefore, stronger immunosuppressants were suggested to reduce the host immune response and reduce the rate of allograft failure^{27,30}.

Although allografts have improved patency, their use can be associated with problems such as damage of endothelial cells, which can result in thrombosis²⁷. Moreover, there may be a shortage of human donor tissue to provide allografts³¹. Another concern is

the immunological response that can be caused due to the presence of viable cells in allografts, resulting in frequent failure at early stages following implantation ^{27,30}.

1.4.3 Synthetic Grafts

Over the years polymeric materials have been employed for vascular implantation. Polymeric materials have many advantages over natural materials: they are easily produced in large scales, readily available, their mechanical and biochemical properties can be controlled at the time of manufacture and their properties are easily manipulated ^{19,32}.

The use of synthetic grafts for replacement of large-diameter vessels when autografts are unavailable has been shown to be successful ²⁵. The most clinically used synthetic non-degradable polymers are expanded polytetrafluoroethylene (ePTFE), Dacron[®] (polyethylene terephthalate) and polyurethane ^{33,34}. In contrast to ePTFE and Dacron[®], polyurethane can be manufactured to match the compliance of native blood vessel ^{34,35}. For such materials to be used as vascular grafts, particularly small-diameter vessels, they must not introduce an infection to the vessel and they must allow endothelium formation on their luminal surface ³⁶. The use of synthetic grafts without any pre-treatment for small-diameter applications often leads to low patency and failure of the graft. This is caused by early thrombus formation because of platelet adhesion due to an absence of endothelium or other complications ^{35,36}. For example, intimal hyperplasia at the suture sites resulting from migration and proliferation of smooth muscle cells from the tunica media to the intima, hence ECM deposition, and compliance mismatch between the graft and the native vessel at the suture point ⁴. The patency rates of ePTFE used for CABG have been shown to be reduced from approximately 60 % after one year to < 30 % after two years, compared to autologous graft that remained > 90 % patent after two years ⁴.

Biodegradable polymers such as polycaprolactone and polyethylene glycol (PEG) have been reported to be used with other polymers for vascular grafts, and seeded with cells prior to use as vascular grafts. The advantage of using biodegradable polymers is the ability to support the release of various bioactive molecules such as growth factors and also support cell infiltration. However, their use is challenging due to cell sourcing and limited long-term patency caused by compliance mismatch ³⁴.

Synthetic polymers are readily available, but lack of spontaneous endothelialisation and cell signalling components that are crucial for cell adhesion, proliferation, differentiation and migration results in low patency and failure of synthetic grafts in small-diameter applications, though this does not affect the performance of large-diameter vascular grafts^{21,33,37,38}. Another limitation for synthetic grafts is that they are more prone to infection that can be life-threatening when compared to autografts and residues of degraded polymers may display cytotoxic effects^{32,39,40}. For improvement of patency of such grafts, seeding of the luminal surface with endothelial cells or using a combination of synthetic polymers and natural materials that enhances endothelialisation may potentially prevent thrombus formation^{34,35}.

1.4.4 Xenografts

An increasing demand for tissue implantation and the shortage of human donor tissue has led to the use of xenogeneic tissue, which is tissue that is transplanted from one species to another^{31,41,42}. Porcine tissue is very similar to human tissues hence commonly used for human implantation⁴¹.

The major limitation in using xenogeneic grafts is the hyperacute rejection of the implanted graft caused by the immune system of the host to xenoantigens. The action of pre-formed antibodies triggers the complement cascade leading to various complications including rapid thrombus formation hence causing loss of patency within a few minutes or hours of implantation^{31,42,43}. For example, the interaction of anti-Gal α (1,3)Gal antibodies that are present in humans, old world monkeys and apes with the Gal α (1,3)Gal antigens, which are found in all other mammals. This antigen results from the activity of the α 1,3 galactosyltransferase enzyme that is expressed by the α 1,3 galactosyltransferase gene. This gene is found in all non-primate mammals but found in an unexpressed form in humans, hence is inactivated. Such interaction causes lysis of xenograft cells leading to failure of the graft^{43,44}. One way to overcome this interaction is by inhibiting the activity of the gene that activates the Gal α (1,3)Gal in genetically modified donor pigs. The other way is to prevent hyperacute rejection, by inhibiting complement activation by expressing genes for human complement regulators in genetically modified donor pigs⁴³. In an attempt to prevent this response, Cozzi *et al.* expressed human regulators of complement activation on non-human cells *in vitro* and

the use of regulators was suggested to prevent cell lysis upon activation of human complement ⁴¹. Another concern of using xenografts is cross-species disease transmission such as porcine endogenous retrovirus (PERV) ³¹.

Although xenografts are promising candidates for the reconstruction of blood vessels in humans due to their availability, the hyperacute rejection caused by xenoantigens and cross-species disease transmission remain major issues ^{31,41-43}. Therefore, a more advanced approach to prevent the immune response to xenogeneic tissues is the removal of the immunogenic viable cells from the tissue to be grafted in a process called decellularisation.

1.5 Decellularisation

Allografts and xenografts contain antigens that are recognised as foreign by the host as well as viable cells, activating inflammatory and immunological responses upon implantation. This leads to graft rejection because allografts and xenografts are treated as foreign by the host ⁴⁵⁻⁴⁷. Decellularisation of tissues is the main approach to overcome the adverse immunological response to allografts and xenografts ³². In this process, DNA, cellular components and antigens are removed from the tissue prior to implantation in order to prevent rejection once implanted, whilst keeping the biomechanical properties, biological properties and composition of the native tissue ECM intact or with minimal modification ^{25,47-49}. In addition, decellularisation has the potential to overcome cross-species disease transmission when using xenografts as it has been reported that no PERV and no infection were observed in the host following implantation of acellular porcine pulmonary arteries into sheep models ⁵⁰.

Therefore, decellularisation is a promising approach for the creation of biological scaffolds composed of native ECM. Several studies have shown that acellular tissue scaffolds are biocompatible and support cell attachment, growth and proliferation in addition to being clinically applicable ^{48,51-55}. An *in vivo* study using acellular grafts for large-diameter blood vessel applications reported successful endothelialisation and deposition of collagen and elastin following implantation with no complications ⁵⁶. However, low patency rates have been reported *in vivo* for small-diameter acellular vascular grafts caused by thrombus formation and occlusion ^{54,57,58}. This is because the lack of the endothelial layer has been reported to contribute to the thrombogenicity of

the acellular tissue graft caused by platelet adhesion to exposed collagen fibres and the promotion of intimal hyperplasia and thickening of the vascular wall, resulting in graft occlusion^{54,57}. Therefore, the evidence indicates that formation of an endothelial layer is required *in vitro* prior to implantation or *in vivo* following implantation to prevent thrombus formation in small-diameter decellularised vascular grafts.

1.5.1 Decellularisation Methods

Decellularisation involves cell lysis, dissociation of cells from the ECM, solubilisation of cytoplasmic/nuclear components and removal of cellular residues⁵⁹ (Figure 1.5). This can be achieved by three main methods: physical; chemical and enzymatic.

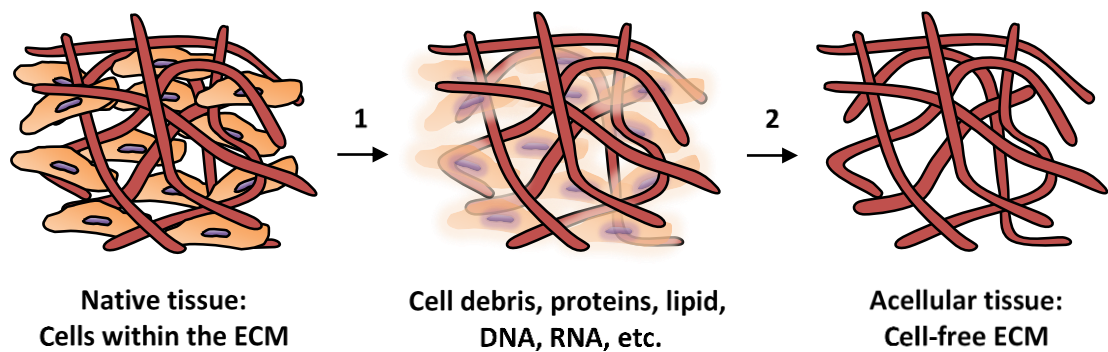


Figure 1.5: Schematic of the decellularisation process. 1) Cell lysis interspersed by use of protease inhibitors to prevent ECM degradation. 2) Removal of DNA and RNA using DNase and RNase and removal of cell debris, lipids and proteins by the use of detergents.

Physical methods cause direct cell lysis and include freezing, pressure, agitation and sonication. Freezing disrupts the cell membrane and causes cell lysis through the formation of ice crystals. However, this does not remove highly immunogenic cell fragments from tissue. Moreover, freezing can disrupt the ECM requiring exact control of the freezing rate to avoid excessive damage. Application of pressure to tissue results in cell lysis but may significantly damage the ECM⁴⁷. Some studies have shown that high pressure removed the cellular component more effectively than detergent-based decellularisation⁶⁰. Mechanical agitation or sonication can result in cell lysis but application of such methods may cause damage to the ECM when used aggressively and are commonly used with chemical/enzymatic immersion to improve effectiveness^{47,60}.

Chemical approaches are often used in combination with other treatments for optimal cell removal ⁴⁷. Acids/bases are used to solubilise the cytoplasmic component and nucleic acids. Bases are commonly used for dense tissue decellularisation such as the dermis and acids can be used for sterilisation. However, these can degrade and solubilise ECM proteins such as collagen, GAGs and growth factors. Therefore, the choice of the dose or exposure times of acid/base is important and is tissue-specific requiring the exact method optimised ^{47,60,61}.

Hypertonic and hypotonic solutions cause cell lysis by changing the osmotic pressure across the cell membrane with minimal structural/chemical changes to the ECM and are commonly used in early stages of decellularisation. However, cellular components are not removed requiring application over several cycles with other treatments. Therefore, detergents are often used alongside for maximised cellular removal ^{47,61}.

Detergents can remove proteins, lipids and DNA by disrupting the protein-protein, lipid-protein, lipid-lipid, and DNA-protein interactions but can cause some ECM disruption. Commonly used detergents are sodium dodecyl sulphate (SDS) and Triton X-100. SDS is an ionic detergent that solubilises cytoplasmic and nuclear membranes but denatures proteins by disrupting the protein-protein interactions ^{47,60,61}. SDS was reported to successfully decellularise several tissue types with sufficient removal of cellular and DNA content, but because it disrupts protein-protein interactions, SDS can be disruptive to the ECM ⁶². Low concentrations of SDS are required to minimise the effect on the ECM ideally using multiple washes with short exposure times or low temperatures. Moreover, residual SDS may be difficult to remove leading to a cytotoxic effect ⁶⁰, especially when used at high concentrations. Triton X-100 is a non-ionic detergent that disrupts lipid-lipid and lipid-protein interactions leaving protein-protein interactions intact, hence minimally affecting the ECM ^{47,60,61}. Residual Triton X-100 (1 %; w/v) was also reported to cause some cytotoxic effect ⁵³.

The effect of detergent use on the ECM and cytotoxicity may vary depending on tissue type, detergent concentration and exposure times. Different studies have shown different degrees of decellularisation possibly due to different cell densities within tissue and tissue thickness ⁶⁰. In *in vitro* studies, SDS (1 and 0.1 %; w/v) treated tissue was shown to have less confluent cells with atypical morphology when compared to other detergents such as Triton X-100. This was more evident at higher concentrations

of SDS and was attributed to residual SDS and loss of ECM structures including collagen, elastin, GAGs and growth factors⁶³. Triton X was also reported to cause less GAGs loss when compared to SDS and trypsin treated tissue, but again, the results varied for different tissue types^{60,64}. Tissue treated with 3 % Triton X-100 was also shown to be positive for collagen IV basement membrane when compared to 1 % SDS treatment⁶⁵. Accordingly, selection of the type of detergent and concentration can be determined by the tissue type and structure.

Chelating agents such as ethylenediaminetetra-acetic acid (EDTA) can bind and isolate divalent metal cations which are important for cell-adhesion, facilitating cellular removal from the ECM without causing cell lysis^{47,60}. EDTA may leave cell residues, hence is used in conjugation with other detergents retaining the ECM major components⁶⁰.

Removal of cellular residues can also be achieved by enzymatic treatment such as trypsin and nucleases. Trypsin causes cleavage of peptide bonds but prolonged exposure can cause disruption in collagen and elastin structures. Nucleases are used for the degradation of DNA and RNA by cleaving the nucleic acid sequences⁶¹.

It is important to preserve the ECM after decellularisation because it contains the structural proteins and composition required for cell attachment, migration and adhesion^{24,66,67}. The choice of methods used in the decellularisation process is therefore dependent on several factors including cellular population, tissue type, structure and thickness^{47,61}. For successful decellularisation, a balance between thorough removal of cellular components and minimal modification to the ECM component which is required to withstand biomechanical load should be considered. Consequently, an effective decellularisation technique uses a combination of these methods rationally to produce a clinically applicable non-immunogenic acellular scaffold^{8,59}.

1.5.2 Sterilisation Techniques

Sterility is a prerequisite of any medical device in order for it to be used safely. Sterilisation of the acellular scaffold is also required prior to use in *in vivo* studies or clinical application, ensuring removal of viable microbes⁶¹. Following decellularisation, tissue can be sterilised by incubation in solvents or acids/bases or by gamma and

electron beam irradiations to reduce the chances of infection or disease transmission⁶¹. An alteration in the ECM characteristics is one of the major concerns for sterilisation of acellular scaffolds⁵⁹.

Studies have shown that gamma and electron beam irradiations reduce the mechanical properties of tissue as they cause structural damage to the ECM^{61,68}. The ECM damage is caused by the crosslinking of major structural components including collagen and this effect is increased with increasing dosage of irradiation⁶⁰.

Ethylene oxide may cause structural damage to the ECM but may leave it unaltered. However, its use has been limited due to the possibilities of mutagenic effects caused by harmful residues resulting in adverse host immune responses^{60,61,69,70}.

Peracetic acid has antimicrobial and antiviral activities and is commonly used for the sterilisation of delicate instruments. It has a lower toxicity due to the harmless natural reaction products⁷⁰ and therefore preferred over other sterilisation methods. Peracetic acid however has been reported to have an effect on collagen IV within the basement membrane⁷¹.

For use as a medical device, the biological decellularised tissue is typically regulated by the Food and Drug Administration (FDA)^{59,60}. The ECM product requires being terminally sterilised following certain guidelines with regards to the bacterial load. It is crucial for the product to pass sterility tests in order to be used clinically but the structural/mechanical loss caused by the sterilisation method must be taken into consideration⁶⁰.

1.6 Haemostasis, Coagulation and Thrombosis

The blood has the ability to physically change by forming a clot in response to an injured or damaged vessel in order to prevent haemorrhage upon vascular injury in a process called haemostasis^{72,73}. In general, at the site of a vascular injury, the blood immediately contacts with the exposed vessel components in the subendothelium, platelet adhesion occurs to form a plug and this is then stabilised by formation of stable fibrin clots via the coagulation cascade⁷². The activated platelets release small molecules attracting more platelets to form a plug and allowing for tissue repair. The process of platelet adhesion is facilitated by vWF that binds to activated platelets and

bridges them to the subendothelium. The coagulation cascade is then facilitated triggering insoluble fibrin formation that strengthens the platelet plug ⁷⁴.

The coagulation cascade (Figure 1.6) is activated by two pathways; the extrinsic or tissue factor (TF) pathway which is initiated by release of TF from site of injury and the intrinsic or contact pathway which is initiated by contact with negatively charged surfaces such as phospholipids present on the surfaces of activated platelets or membranes of damaged cells ^{72,73}. The negatively charged phospholipids on platelets also provide a catalytic surface for the activation of several coagulation cascade factors by forming factor complexes ⁷⁵.

The extrinsic pathway initiates the coagulation cascade via contact of TF present in the subendothelium with blood following an injury ^{73,74,76}. TF forms a complex with factor VII that circulates in blood in presence of calcium ions allowing conversion of factor VII into serine protease factor VIIa. Factor X is then converted to factor Xa by the TF-VIIa complex once attached to cell membrane ^{73,74}.

The intrinsic pathway factors such as XI and XII are important for the propagation of thrombus. In this pathway, factor XII comes in contact with a negatively charged phospholipids surface and this activates the factor to XIIa. On the cell surface, XIIa activates XI to XIa which in turn activates IX to IXa that forms a complex with activated VIII (VIIIa). This complex with calcium ions activates X to Xa on the phospholipid surface. Because thrombus propagation occurs through this pathway, it is suggested that this pathway is possibly taking place in pathological thrombus formation ⁷³.

After activation of factor X, factor Xa forms a complex with factor Va in the presence of phospholipid and calcium ions forming a prothrombinase that converts prothrombin into thrombin ⁷⁴. Positive feedback from thrombin activates factors V, VIII, XI, XIII and inhibitor protein C. It also converts soluble fibrinogen to insoluble fibrin playing an essential role in haemostasis. The formed fibrin coagulates in the site of injury forming a mesh which is stabilised to a fibrin clot by the action of factor XIIIa.

It is important to regulate the coagulation cascade in order to prevent the formation of an insoluble fibrin deposit. In healthy individuals, this only occurs at the site of injury and for a certain duration which is sufficient to seal the site of injury by fibrin. This process is regulated by a number of factors to prevent the formation of massive fibrin

clots hence thrombus in the vessel. These include; tissue factor pathway inhibitor (TFPI) that targets the complex TF-VIIa, anti-thrombin that inhibits factors IXa, Xa, TF-VIIa complex and thrombin, protein C that inhibits activation of factors V and VIII preventing thrombin formation, and intrinsic pathway inhibitors that inactivates factor XIIa ⁷³. The final stage that controls the process is fibrinolysis, which produces fibrin degradation products from insoluble fibrins. This is achieved by the action of the enzyme plasmin which is converted from plasminogen by the action of plasminogen activators ⁷³.

Haemostasis must be regulated to prevent bleeding or thrombosis ⁷³ that can be caused by insufficient control over the activation and inhibition of factors, thrombin and fibrin. A thrombus is formed in circulating blood and it comprises of a platelet aggregate surrounded by leucocytes which are bound by fibrin strands that build up from the site of injured walls of blood vessels but it does not develop on the walls ⁷⁷.

Thrombus formation can be caused by various factors such as atherosclerosis due to artery narrowing or total blockage ¹⁸⁻²⁰. The levels of TF expressed by macrophages in patients with atherosclerosis is increased and since TF initiates the coagulation cascade, its presence in blood increases the risk of thrombosis ⁷⁸. Patients with coronary artery disease have a higher risk of thrombosis that is believed to be due to the abnormal formation of fibrin clots caused by increased platelet coagulation and thrombin generation that strengthens the clot making it more resistant to fibrinolysis ⁷⁹.

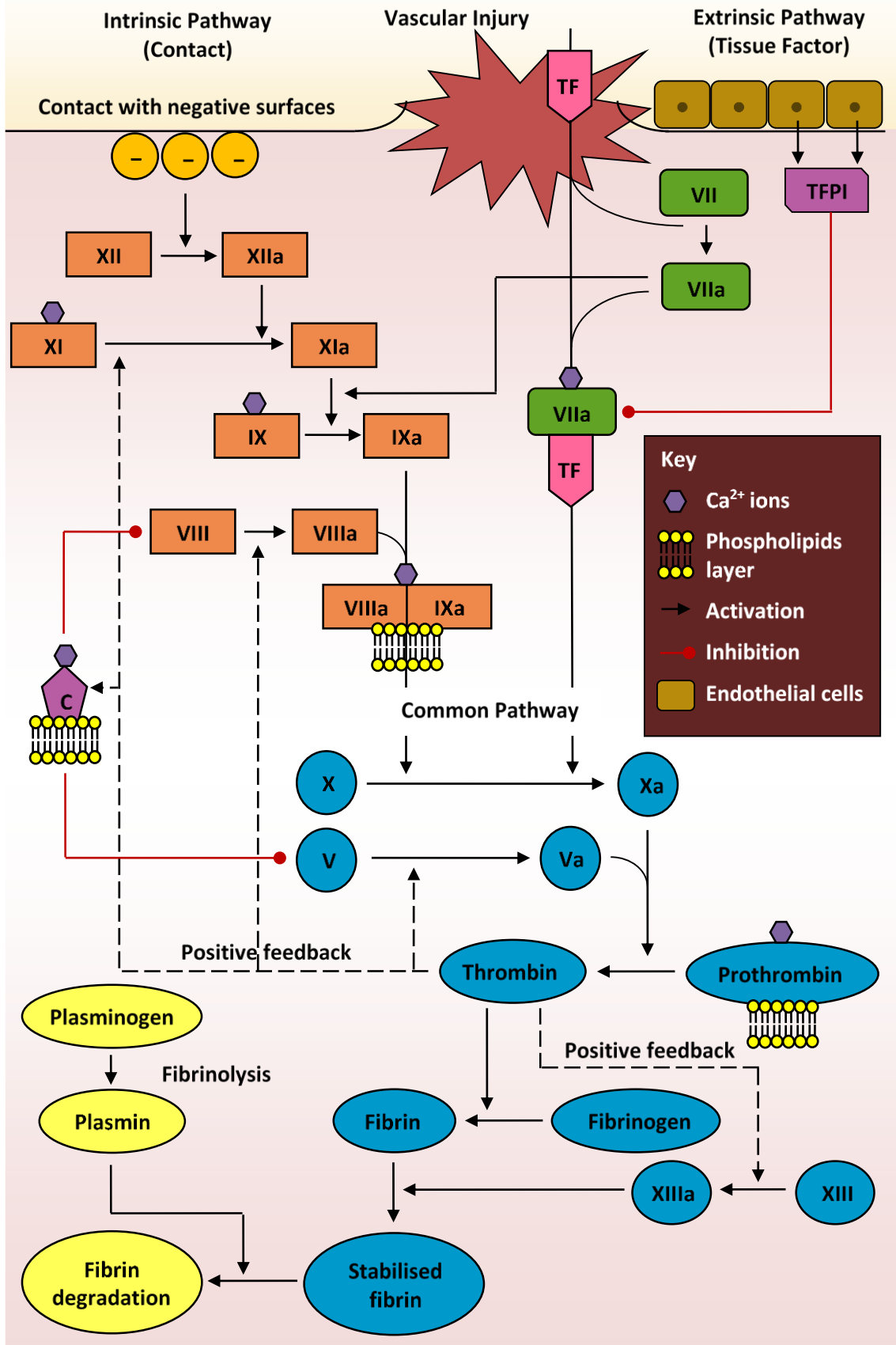


Figure 1.6: Coagulation Cascade Model. The cascade is initiated by the extrinsic/tissue factor pathway (orange) and propagated by the intrinsic/contact pathway (green) to the common pathway (blue) forming a stable fibrin that is degraded in the fibrinolysis process (yellow).

In vascular disease, when surgical grafts are required, thrombosis is one of the main reasons for unsuccessful grafts with low patency upon implantation²⁶, particularly small-diameter grafts. The endothelium is absent in biomaterials (synthetic or naturally-derived) used as vascular grafts introducing a foreign surface to circulating blood. Often this results in a thrombotic response by triggering several complex and interlinked events including protein adsorption, platelet and leukocyte activation/adhesion and activation of complement and coagulation cascades⁸⁰⁻⁸².

The first event that occurs almost immediately when the biomaterial is in contact with blood is protein adsorption^{80,82}. Other events are dependent on the interaction of blood with the adsorbed protein layer⁸³. For example, biomaterial-blood contact may initiate the intrinsic pathway through activation of factor XII. It can also trigger TF expression by monocytes and activate the extrinsic pathway⁸⁰. The amount and composition of the adsorbed protein is dependent on the biomaterial properties and this can preferentially activate complement or coagulation cascades⁸⁴. Adsorbed proteins including fibrinogen and vWF mediate platelet adhesion via integrin $\alpha_{IIb}\beta_3$ ^{82,85}.

Platelets play an important role in thrombus formation. They can be activated by contacting thrombogenic surfaces including: injured endothelium, subendothelium (e.g. collagen) and foreign surfaces; plasma proteins (thrombin and fibrinogen); or inflammatory molecules (leukocytes) resulting in physiological responses. The platelet adhesion receptor ($\alpha_{IIb}\beta_3$ integrin) mediates platelet aggregation and formation of platelet-leucocyte aggregates by binding to fibrinogen in activated platelets. In biomaterials, platelets will adhere to the adsorbed proteins on the surface and adhesion is mediated by $\alpha_{IIb}\beta_3$ integrin.⁸⁰ The intrinsic pathway activation also results in thrombin formation that induces fibrin formation on the biomaterial surface triggering platelet adhesion, activation and aggregation then stabilising thrombi on the surface^{82,83,85}. Platelet adhesion is also affected by shear rate and contact time⁸³.

The coagulation cascade can be activated through the intrinsic pathway by exposure of collagen in the subendothelium to blood following an injury⁸⁰, suggesting a similar response in acellular arteries where blood contacts the ECM structures. Tucker *et al.* tested thrombus formation in baboon and flow chamber models using ePTFE vascular graft coated with collagen. The study suggested the importance of factor XI in local thrombin generation, platelet activation and fibrin formation in thrombus propagation,

hence acute occlusion of small-diameter vascular grafts. Stability of formed thrombi was also dependent on factor XI activity ⁸⁶.

The complement system plays an important role in the inflammatory response and it consists of more than 20 plasma proteins that are involved in complex reactions. It can be activated by the classical pathway through an antigen-antibody complex or the alternative pathway that involves contact with a foreign surface ⁸⁰. In presence of a biomaterial vascular graft, the complement cascade is believed to be activated through the alternative pathway, playing a role in leukocyte response since the biomaterial lacks complement inhibition capacity ^{80,82,83}. The complement cascade is also associated with platelet activation and thrombus formation leading to inflammation and/or thrombosis ⁸⁴.

Leukocyte adhesion to the endothelium is important in the inflammatory response. In contact with biomaterials, leukocytes are activated and this promotes adhesion. The mechanism by which leukocytes adhere to biomaterials is not clear but is thought to be mediated by complement cascade products. Leukocytes also adhere to adherent platelets contributing to local thrombosis. TF expression on leukocytes following biomaterial-blood contact was shown to activate factor X and platelet-leukocyte aggregation ⁸⁰. Leukocytes contribute to thrombus formation, platelet adhesion, and fibrin formation ⁸³.

Other factors that can influence the biomaterial-induced thrombosis include surface properties, patient's condition and fluid dynamics ⁸⁷. For example, an instability in blood flow caused by compliance mismatch can lead to thrombosis ¹⁹. Flow conditions also play an important role in biomaterial-induced thrombosis. Fibrinogen is the main protein mediating platelet adhesion, forming platelet aggregates and stabilising thrombi under low shear stress, while vWF mediates the platelet adhesion to the site of injury under high shear stress ^{82,85}. Flow conditions can also affect the transport of blood components to the biomaterial, in which disturbed flow enhances the transport of components to the surface, resulting in accumulation of platelets and proteins at a critical concentration leading to thrombosis. If the shear force is large enough to overcome the thrombus adhesive forces, a thrombus can be detached and carried by circulating blood leading to other complications ⁸⁷.

The effect of biomaterial-induced thrombus formation can be mitigated by modification of the vascular graft, either by seeding with cells, use of anti-thrombogenic coatings or bioactive coatings that promote endothelialisation of the luminal surface.

1.7 Approaches to Prevent Thrombus Formation

For vascular grafts to be clinically successful; they are required to be non-thrombogenic, non-immunogenic, non-inflammatory, mimic the native blood vessel in the biomechanical properties and integrate with the surrounding environment ⁵. Improvements in small-diameter vascular grafts are still ongoing to produce a solution with long-term patency. Several *in vitro* or *in vivo* approaches have been investigated for such improvement. For example, seeding the surface of the graft with cells, the use of anti-thrombogenic surface coatings and enhancing the formation of a functioning endothelium using bioactive factors.

1.7.1 Cell Seeding

Cell seeding has been applied to various types of vascular grafts including, synthetic, naturally-derived and acellular tissue scaffolds. Endothelial cells, endothelial progenitor cells, smooth muscle cells and bone marrow-derived cells that can differentiate into the desired cell type under the correct conditions and factors have been used for vascular graft applications ^{5,54,58,88}.

Seeding of the luminal surface of synthetic grafts made from polyurethane and ePTFE with endothelial cells has been shown to enhance luminal coverage with minimal to no thrombus formation *in vivo* and high patency rates ^{89,90}.

Several studies in various animal models have reported non-thrombogenic small-diameter acellular allografts and xenografts with high patency rates when seeded with autologous endothelial cells or bone marrow-derived cells prior to implantation without complications such as aneurysm formation and minimal inflammatory response ^{54,58,88}.

Smooth muscle cells were shown to migrate into acellular allografts and xenografts during the implantation time with no evidence of platelet adhesion to the surface of cell seeded grafts ^{57,58,88}. Production of elastin and collagen have been reported in acellular allografts seeded with autologous bone marrow-derived cells in a dog model

Conventional two stage seeding of vascular grafts involves isolation/extraction of cells from source, prolonged culturing and expansion until an adequate number of cells is available followed by seeding into the vascular graft until confluency is achieved prior to implantation^{5,35}. This process is typically carried out in a suitable bioreactor system under a sterile and a closed environment³². To overcome this prolonged production period, a single stage process has been developed, in which the biomaterial is directly seeded for implantation³⁵. In an attempt to avoid the two stage seeding, Tiwari *et al.* have reported direct *in vitro* seeding of human umbilical vein endothelial cells onto a heparinised polyurethane graft containing a polymer with repeating RGD sequences. The graft showed improved retention of endothelial cells *in vitro* as well as having the anti-thrombogenic properties of heparin, which can be implanted back into patients directly reducing the time required for culturing⁹¹. The processes of cell seeding using the two and single stage seeding methods is illustrated in Figure 1.7. The use of anti-thrombogenic and bioactive surfaces will be discussed in the following sections.

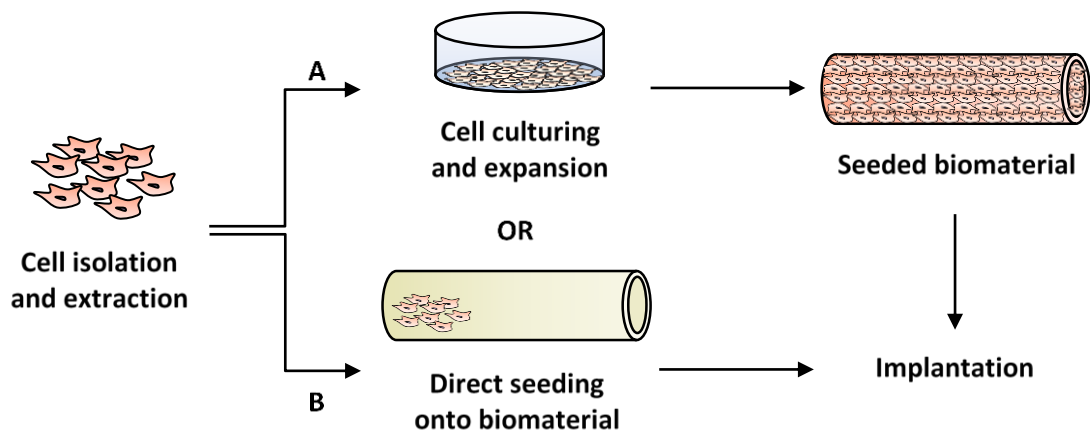


Figure 1.7: Schematic of the development of cell seeded vascular graft. *Isolation/extraction of cells from source. A) Two stage seeding: in vitro seeding until obtaining an adequate number of cells for seeding onto biomaterial prior to implantation. B) Single stage seeding: direct seeding onto biomaterial followed by implantation.*

Autologous cells isolated from patients such as endothelial cells, smooth muscle cells and bone marrow-derived cells are the first choice for vascular graft seeding, since these are non-immunogenic. Allogeneic cells can also be isolated but can induce an immunological response⁵. Cells can be obtained from small biopsy samples such as veins or skin^{5,57,92}. However, isolation and purification of cells is limited due to limited

adult tissue, infection of cells, difficulty of obtaining large numbers of cells from small biopsies leading to poor proliferation potential and possible loss of functionality during *in vitro* expansion^{5,35,57}. Bone marrow-derived cells have been reported to induce calcification when transplanted directly, requiring controlled cellular differentiation of adult stem cells in such applications⁹³. The invasive procedures to obtain cells may cause morbidity for donors⁵⁷. A non-invasive extraction procedure for endothelial progenitor cells from the peripheral blood has been reported, hence can be used as an alternative for endothelial cells⁸⁸. In summary, the main issue with this approach is the cell sourcing and prolonged time required for expansion and seeding of cells prior to implantation.

1.7.2 Anti-fouling Surfaces

Anti-fouling materials prevent or inhibit the covering of the surface with undesirable material from the surrounding environment⁹⁴. In the case of vascular graft applications, this undesirable process refers to the adsorption of proteins onto the biomaterial surface and subsequent events that lead to thrombus formation⁹⁵. In a normal functioning blood vessel, the luminal endothelium acts as a natural anti-fouling surface repelling proteins, platelets and leukocytes⁹⁴.

Chemical and physical features of the biomaterial play an important role in the surface anti-fouling properties⁹⁴. The surface chemistry of biomaterials can be altered by incorporation of groups that resist protein adsorption because this affects the hydration, attraction and repulsive forces of interaction⁹⁶. Ostuni *et al.* reported four different properties for surfaces to resist protein adsorption: hydrophilic, neutrally charged, contain hydrogen bond acceptors but not hydrogen bond donors⁹⁶. These are mainly synthetic polymers developed for biomedical applications. For example, self-assembled monolayers of oligo ethylene glycol that have shown resistance to adsorption of a variety of proteins and polyvinylamine that mimics the ECM anti-fouling glycoprotein suppressing platelet adhesion⁹⁵.

PEG is a hydrophilic polymer and one of the main anti-fouling materials that is being investigated with low protein adsorption due to steric repulsion that can be affected by the polymer density^{94,95,97}. It has been reported that PEG exhibited low protein adsorption when exposed to blood plasma^{98,99}. Platelet adhesion has also been

reported to decrease with increasing density and longer chains of PEG⁹⁹. Crosslinked polymer hydrogels such as PEG diacrylate have also been reported to have low protein adsorption^{94,100}. Hydrophobic polyethylene terephthalate surfaces have been modified with PEG to improve the surface hydrophobicity and it was reported to have less protein and platelet adsorption¹⁰¹. Coating the biomaterial surface with PEG can also improve its biocompatibility and blood compatibility^{84,85}.

The use of anti-fouling coatings may alter the mechanical and chemical properties of the biomaterial. In addition, the anti-fouling surface will potentially degrade during longer term use exposing the underlying biomaterial that promotes thrombus formation. This is more likely to occur in biomaterials that do not encourage formation of functional endothelial cells in an acceptable period following degradation of the coating.

1.7.3 Anticoagulant Agents

Anticoagulant agents including aspirin, heparin, low molecular weight heparin (LMWH) and Warfarin are typically used for the treatment of thrombotic disorders such as venous thrombosis, pulmonary embolism and coronary artery disease^{102,103}.

Heparin is a heavily sulphated glycosaminoglycan (GAG) that has a molecular weight of 3 kDa to 30 kDa. It is an anticoagulant that inhibits thrombin and factor Xa through anti-thrombin, a slow inhibitor in absence of heparin¹⁰²⁻¹⁰⁴. Heparin works by binding to anti-thrombin changing its conformation, stabilising the complex then accelerating the inhibition process. Therefore, it acts a catalyst during the reaction without being consumed as it is released from the complex once formed, efficiently preventing fibrin formation¹⁰⁴⁻¹⁰⁶. For acceleration of thrombin inhibition, heparin binds to both anti-thrombin and thrombin, while it is not required to bind to factor Xa for inhibition¹⁰² (Figure 1.8). Therefore, LMWH, a fragment derived from heparin having a molecular weight between 1 kDa and 10 kDa, can inhibit factor Xa but not thrombin^{102,105}. Heparin also inhibits other clotting enzymes including factors IXa and XIa through complex reactions and regulates the coagulation cascade, complement cascade and platelet adhesion^{80,84}.

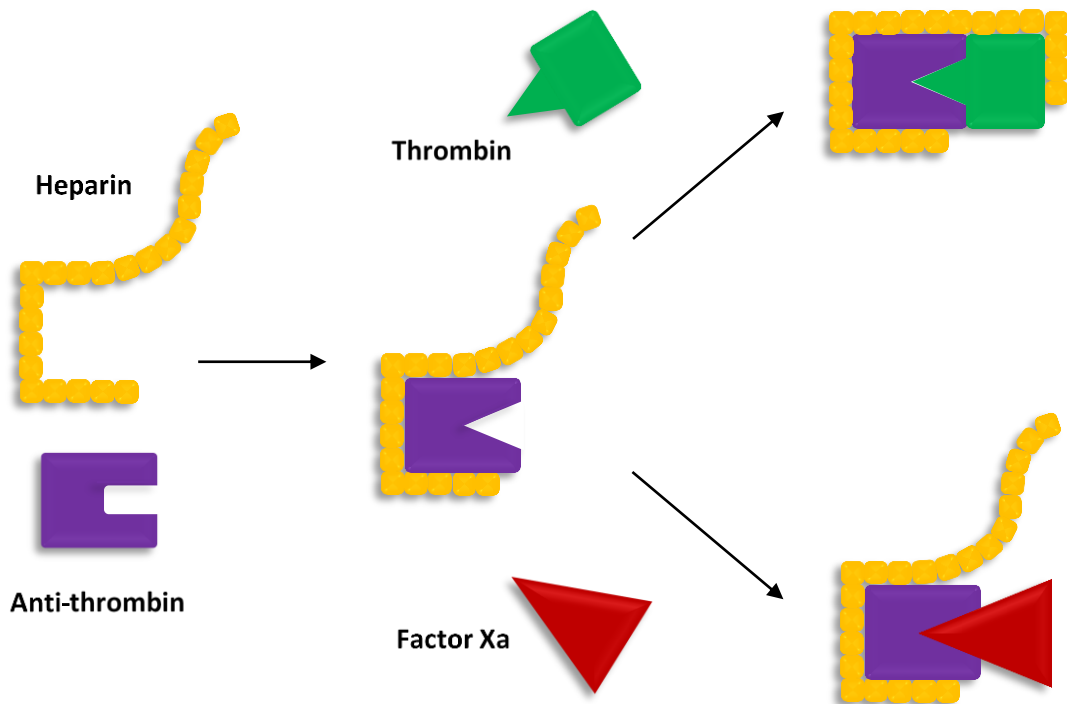


Figure 1.8: Schematic of the action of heparin in the prevention of thrombus formation. Heparin binds to anti-thrombin causing a conformational change and activating the enzyme inhibitor. The activated anti-thrombin inhibits thrombin (requiring the whole heparin length) and factor Xa (requiring a partial length of heparin).

Heparin is the main anticoagulant used with synthetic grafts such as ePTFE, Dacron®, and polycaprolactone as well as naturally-derived grafts such as decellularised scaffolds. Heparin treatment has been applied to small-diameter vascular grafts to improve patency and reduce thrombogenicity of the graft, having a similar mechanism of anti-thrombin action ^{36,107-111}.

Heparin has been reported to reduce platelet adhesion with non-activated morphologies and inhibit blood clotting with no change in its anticoagulation activity over the tested period *in vitro* ^{107,109}. Heparin treated acellular allografts and xenografts have been shown to have very high patency rates with no evidence of thrombosis or stenosis following implantation ^{109,111}. The mechanical properties of decellularised dog common carotid arteries have been shown to be unaffected by heparin treatment ¹¹¹.

In addition to the anti-thrombogenic effect, heparin coating has been reported to significantly increase endothelial cell density on wire coated copolymer coils *in vitro*. This could be due to direct stimulation of endothelial growth or through binding

circulating growth factors to enhance cell proliferation ¹¹². Heparin has also been demonstrated to support adhesion, spreading and proliferation of functional endothelial cells that expressed vWF and were capable of producing nitric oxide, while reducing or inhibiting smooth muscle cell proliferation which is a major cause for intimal hyperplasia ^{107,108,110}. However, it has also been reported that heparin use has no effect on cellular remodelling as populating the tunica media with smooth muscle cells and covering the lumen with endothelial cells has been demonstrated in non-heparinised and heparinised acellular grafts ¹¹¹.

The use of heparin with other methods such as incorporation of vascular endothelial growth factor has also shown improved patency of decellularised dog carotid arteries in dog models with sustained release of the growth factor within less than a month, forming a confluent organised endothelium. Presence of growth factors was shown to inhibit intimal hyperplasia ¹¹⁰.

It has been demonstrated that ionic bonding of heparin to the synthetic polymer polycaprolactone resulted in sustained release over a one month period, resulting in optimal anti-thrombogenic effect while maintaining patency of the synthetic graft following implantation in rat models with almost complete endothelial cell coverage ¹⁰⁸.

Therefore, the type of biomaterial used and conjugation of heparin with other factors such as growth factors have all been shown to affect the endothelial cell response and thrombogenicity of vascular grafts *in vivo*, requiring the careful consideration of these effects for the design of vascular grafts.

Heparin is a natural anticoagulant and long-term usage is limited as it may lead to haemorrhage ¹⁰⁵. Therefore, the use of anticoagulants is challenging and limited in patients with inherited bleeding disorders, requiring further monitoring of the condition or alternative approaches. In addition, despite the anti-thrombogenic effect of heparin that improves graft patency, loss of heparin from the surface of an acellular scaffold vascular graft may limit the maintenance of patency in the long-term, particularly if a complete endothelial layer is not formed, potentially resulting in thrombus formation ³⁶.

1.7.4 Bioactive Surface Coatings

Bioactive surface coatings for vascular grafts are thought to enhance the formation of an endothelial layer *in situ*, for example, by using cell attachment motifs. The cell attachment motifs are short peptide sequences that are derived from ECM adhesion proteins such as laminin, fibronectin and collagen, which usually mediate cell-ECM adhesion through integrins^{7,8,13-15} (Figure 1.9). Several cell attachment motifs have been reported in the literature for enhanced endothelial cell binding such as RGD, YIGSR and REDV and other sequences such as IKVAV and PHSRN are widely used with RGD or YIGSR for a synergistic effect¹¹³⁻¹¹⁶.

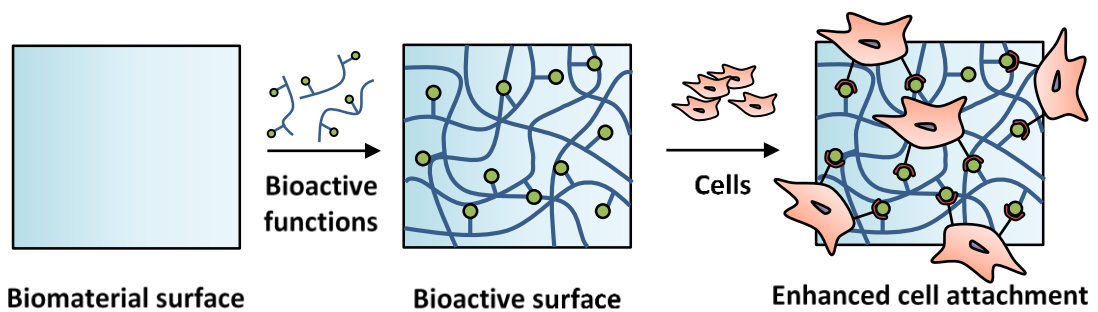


Figure 1.9: Functionalisation of biomaterial surface with bioactive motifs for enhancement of cell attachment *in vivo*.

RGD, found in most ECM proteins is the main focus of interest in the literature as it has been shown to enhance endothelial cell attachment, migration, proliferation and survival^{115,117}. It is often used in the forms RGD, PRGDS, YRGDS, GRGDY and GRGDSP¹¹⁷⁻¹²⁰. Coating the surface of electrospun polycaprolactone with RGD has been shown to improve the patency of these synthetic grafts in rabbit models, in which RGD was shown to support the infiltration and migration of endothelial and smooth muscle cells as well as inhibition of platelet adhesion and thrombus formation. The alignment of endothelial cells in an RGD modified synthetic polycaprolactone polymer has been reported to be similar to that of native blood vessel¹²¹. A cyclic form of RGD is more stable *in vivo* against proteolysis and enhances cell attachment better than linear forms^{119,122}. Modification of electrospun poly(L-lactic acid)/polycaprolactone surfaces with cyclic RGD (cGRGDdvc) using a PEG spacer has been shown to support attachment and proliferation of endothelial cells with no significant change in the expression of markers,

significantly improving surface coverage *in vitro*. The peptide was shown to have weaker affinity for platelets and monocytes when compared to GRGD sequence ¹²².

RGD is recognised by more than half of the known integrins, hence binds various cell types other than endothelial cells such as platelets ¹¹⁵. This requires using a different sequence of the peptide with lower affinity towards other unwanted cells as discussed earlier or using other cell adhesion motifs that are more endothelial cell-specific.

A bioactive polyurethane-urea has been synthesised by incorporation of a YIGSR into the polymer. It has been demonstrated that YISGR enhanced endothelial cell attachment, spreading and migration but not platelet adhesion, hence this peptide sequence has more affinity for endothelial cells without contributing to the thrombogenicity of graft ¹²³. Another peptide sequence REDV used to modify a PTFE surface through a PEG spacer has been demonstrated to enhance endothelial cell attachment, while reducing platelet and microbial attachment. This modification combined the bioactivity of REDV and anti-fouling properties of PEG ¹²⁴. However, REDV has also been reported to neither support endothelial cell attachment nor platelet adhesion on a polyethylene terephthalate modified surface. In the same study both YIGSR and RGD modified surfaces increased the attachment of endothelial cells. Moreover, RGD also increased platelet attachment ¹¹⁴. The use of a mixture of cell attachment motifs was shown to enhance cell attachment. For example, RGD and YIGSR enhanced endothelial cell migration, while RGD supported cell adhesion better than YIGSR when used separately ¹¹³.

Other peptide sequences have been reported to enhance endothelial cell attachment. For example, the peptide sequence RRETAWA that has high affinity towards endothelial cells through $\alpha_5\beta_1$ integrin ¹²⁵. Larsen *et al.* demonstrated the limited platelet adhesion of cyclic CRRETAWAC, which specifically targeted endothelial cells, enhancing attachment and proliferation in ePTFE graft *in vitro*. Attached cells have also been shown to be stable under shear stress ¹²⁵. Similar results have been reported by Meyers *et al.* with regards to platelet and endothelial cell attachment ¹²⁶. Li *et al.* reported the improved patency of ePTFE coated with collagen-derived P15 peptide (GTPGPQGIAGQGRVV) in a sheep model with a thick uniform endothelial cell coverage ¹²⁷.

It is clear that the affinity of bioactive peptide sequence towards endothelial cells and cellular response are dependent on many factors including the type and properties of the biomaterial being coated, sequence or form of peptide and use of spacer that affects integrin accessibility¹²⁸. Fibronectin bioactive peptide sequences cyclic RGD and REDV, but not LDV or PHSRN have been shown to play an important role in mediating the attachment of human microvascular endothelial cells to the porcine ECM. The biochemical composition of tissue is thought to be responsible for the different attachment behaviour of cells¹²⁹. The concentration of the bioactive peptide has also been reported to affect cell attachment that typically increased with increasing concentration¹²⁰. Therefore, careful design of the bioactive surface coating is required to tune the affinity for different cells as needed, achieving optimal endothelialisation but minimal or no protein, platelet or leukocyte adhesion. The criteria for synthesising bioactive peptides are discussed in more detail in Chapter 7, (Section 7.1.2), focusing on RGD and YIGSR motifs.

The use of a bioactive surface coating is an attractive approach for small-diameter vascular grafts mainly to promote *in situ* endothelialisation, in particular, cell attachment motifs. Many cell attachment motifs have been reported to enhance cell attachment, spreading and proliferation and these can be tailored to produce the most suited motif for vascular graft applications. Several studies have reported the use of PEG as a linker in order to improve the anti-fouling properties of the surface of biomaterials^{114,122,124}. However, since this approach encourages *in situ* cellularisation, attached cells must resist shear stresses by allowing cytoskeletal organisation to prevent detachment with blood flow for a more efficient graft performance¹³⁰. Treating ePTFE vascular grafts with an RGD containing peptide was shown to improve the shear resistance of endothelial cells¹³¹. Increasing the concentration of RGD was shown to increase cell retention under flow shear stress conditions¹²⁰. It is therefore important to study cell retention under shear stress, ensuring cells are not detached from the surface of the graft, which could lead to thrombus formation.

1.8 Advantages and Limitations of Current Small-diameter Vascular Grafts

Biomaterial scaffolds for tissue engineering must be biocompatible, have surface properties to facilitate cell adhesion, proliferation and differentiation, highly porous allowing for migration and infiltration of cells and diffusion of essential molecules such as growth factors and have mechanical properties to withstand the target load *in vivo*¹³². Subsequently, an ideal vascular graft should mimic the native blood vessel in structural and biomechanical properties as well as functional and biological activities and allow for guided cell repopulation^{32,38}. It must also be readily available and cost-effective^{35,58}. Thrombus formation is the main reason for poor patency rates in current clinically used small-diameter vascular grafts⁴. This is caused mainly by an absence of the natural anti-thrombogenic endothelium. Therefore, research and development of an ideal small-diameter vascular graft is still ongoing.

Autografts remain the gold standard, since these do not elicit an immunological response but have limited availability and can cause complications such as intimal hyperplasia^{23,26 25}, particularly when using veins for arterial bypass grafts. Therefore, allografts, having the appropriate biomechanical properties have been considered. However, because of the immunological response caused by alloantigens, associated cost and long waiting times, the use of allografts is limited^{27,30,31}. Xenografts, in addition to the hyperacute rejection caused by the immune response, can lead to cross-species disease transmission making them unfavourable for vascular graft applications^{31,42,43}. Synthetic grafts are readily available and are successfully used in large-diameter vascular grafts. However, the lack of an endothelial layer and inability to encourage luminal endothelialisation limits their use in small-diameter applications⁴. Acellular tissue scaffolds are of considerable promise for small-diameter applications, especially using the readily available xenografts. These have a reduced immunological response due to removal of immunogenic cellular content and the appropriate biomechanical and bioactive properties because they are derived from the native vessel^{32,67}. Decellularised tissue is also biocompatible and can be used as a scaffold for cell adhesion and proliferation⁴⁸ but, as with synthetic grafts, a lack of endothelial layer raises thrombosis and low patency issues.

Formation of an endothelial layer or use of anti-thrombogenic strategies are hypothesised to improve the performance of vascular grafts by preventing thrombus formation. Cell seeding using autologous cells is limited due to the inability to isolate adequate cells for expansion, which is time-consuming and requires expansion of cells *in vitro* prior to implantation^{5,35}. The use of anti-thrombogenic materials such as anti-fouling or anticoagulant coatings is important for the initial stages of implantation to maintain graft patency but is limited due to possible thrombus formation following degradation of material from the surface in the case of incomplete endothelialisation^{36,94}. Combining anti-thrombogenic treatments with endothelialisation enhancement methods is a possible approach to prevent long-term thrombus formation. The use of bioactive surface coatings such as cell attachment motifs enhances the graft cellularisation and may be tailored to act as an anti-thrombogenic coating, whilst binding cells to the surface^{119,124}. However, this requires extensive studies as some cell attachment motifs have shown strong affinities towards endothelial cells but also for platelet and leukocytes^{114,125}, which are involved in the thrombus formation process.

Self-assembly of peptides containing bioactive functions is an attractive method for coating vascular grafts in order to enhance luminal endothelialisation. These peptides are able to form nanofibers spontaneously that have similar dimensions to ECM collagen fibrils¹³². Previous studies have shown that peptides containing the cell attachment motif, RGD self-assembled into nanofibers on the biodegradable polycaprolactone and polyglycolic acid synthetic grafts under physiological conditions^{121,133}. The bioactive peptide coatings showed homogeneous distribution on the surface in addition to being stable since the self-assembled structures were retained under biological fluid conditions or in excess of cell culture medium^{121,133,134}. The mechanical properties, surface morphologies and the nanoporous structure of the synthetic polycaprolactone grafts have been reported to be unaffected by the coating as the peptide only coated the scaffold fibres^{134,135}. Coating the surface of synthetic vascular grafts has demonstrated improved cell attachment, spreading, proliferation, infiltration and migration^{121,133-135}. In addition, multiple bioactive functions can be introduced within the self-assembled peptides potentially enhancing the interaction of cells with the surface of the graft. Peptide self-assembly for tissue engineering applications is discussed in more detail in the subsequent sections.

The combined technology of a decellularised porcine artery scaffold and bioactive peptide surface coating have the potential for small-diameter vascular graft development because of the biocompatibility of both materials, appropriate tissue scaffold biomechanical properties and biological activities, availability of both materials and time effectiveness due to *in situ* endothelialisation. Nevertheless, screening of various cell attachment motifs used individually and in combination for synergetic effects is still required prior to any *in vivo* testing. The stability of attached endothelial cells under shear stress must be assessed to evaluate the effectiveness of bioactive peptides. Furthermore, long-term animal studies need to be carried out prior to any clinical applications.

1.9 Amino Acids and Peptides

There are 20 naturally occurring amino acids which are the building blocks of proteins and peptides. All amino acids share the same basic structure with a central carbon atom to which a hydrogen, an amino group (NH₂, N-terminus), a carboxyl group (COOH, C-terminus) and a side-chain group are attached. Glycine is the smallest amino acid having a hydrogen as the side-chain group. Amino acids are categorised into different groups depending on their side-chain group that determines their properties ^{136,137} (Appendix A.1).

Generally, peptides are short linear structures with two levels of structure, primary and secondary ¹³⁶. The primary structure is defined as the linear sequence of amino acids along the peptide chain. The spatial arrangement of the peptide backbone, determined by the local conformation of these peptide chains and often influenced by hydrogen bonding, is referred to as the secondary structure. Two common secondary structures are the α -helices and β -sheets ¹³⁶⁻¹⁴⁰.

1.9.1 α -helix

The α -helix is a rod-like structure with a right-handed coiling of the peptide chain. This helical structure arises from strong intramolecular hydrogen bonding within the peptide backbone between oxygen in the C=O bond of residue (n) and hydrogen in the N-H bond of residue (n + 4) along the helix axis with 3.6 amino acid residues per turn ^{136,137,139}. These hydrogen bonds are parallel to the axis of the helix and act to stabilise the

structure. The side-chains of the amino acid residues in the α -helix extend out of the rod-like structure, whereas the coiled backbone forms the core of the helix^{138,139}.

1.9.2 β -sheet

The β -sheet is formed by joining two or more β -strands via intermolecular hydrogen bonding between oxygen in the C=O bond on one β -strands and hydrogen in the N–H bond on the adjacent β -strands¹³⁶⁻¹³⁸. This results in a parallel or an antiparallel arrangement of β -strands in the β -sheet. The antiparallel arrangement is more stable than the parallel arrangement, hence it is more common because the hydrogen bonding in the parallel β -sheets is more distorted^{136,137} (Figure 1.10). The side-chain of alternating residues point in opposite directions and the length between two adjacent amino acid residues along the β -strand is 3.5 Å, while the distance between two β -strands in an antiparallel arrangement is 4.7 Å^{136,139,141}.

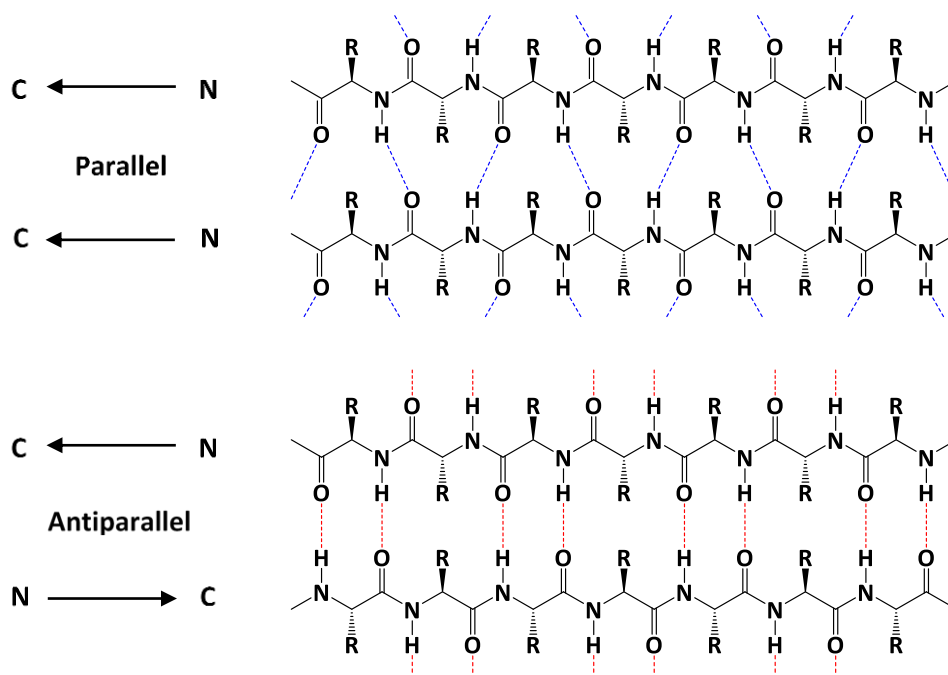


Figure 1.10: Schematic of β -sheet parallel and antiparallel arrangements of β -strands. The intermolecular hydrogen bonding is demonstrated by the dashed lines: parallel (blue) and antiparallel (red). Arrows represent the direction of a β -strand. Side-chain group (R).

1.10 Self-assembly of Peptides

The development of nanomaterials can be achieved via two main approaches, top-down or bottom-up. Molecular self-assembly is a bottom-up approach in many biological systems, in which molecules are organised spontaneously into more stable well-defined supramolecular structures held together via weak non-covalent interactions such as hydrogen bonding, electrostatic forces and hydrophobic interactions stabilising the structure ^{132,142-146}. Peptides are an example of these self-assembling bioinspired nanomaterials that can be developed using the bottom-up approach, in which the building blocks for the peptide chain are amino acids that can be arranged into secondary structures such as α -helices or β -sheets. This means there are various self-assembly systems that are mainly based on α -helix and β -sheet structures ¹⁴⁰. Self-assembly can either be non-nucleated or nucleated. In the non-nucleated self-assembly, monomers are added step-wise to the growing chain and increasing the concentration increases the number and length of a chain gradually and slowly. Therefore, the formation of elongated structures is only formed at high concentrations ¹⁴⁷. In a nucleated self-assembly, monomers and elongated structures are present within the system above a critical concentration, once a nucleus is formed, below which only monomers and unstable seeds are present ^{147,148}.

1.11 Responsiveness of Peptide Self-assembly

The process of self-assembly must be controlled carefully to enable formation of a monomeric solution or a self-assembled gel where required, especially in biological applications. Therefore, external triggers can be applied to control the self-assembly of peptides switching between the monomeric and self-assembled forms as required, including chemical triggers such as pH and ionic strength or physical triggers such as temperature, light and mechanical force application ^{142,149-153}. For use in biological applications, in which salt concentration and pH are regulated, mixing complementary peptides that form self-assembled aggregates at physiological pH 7.4 as well as the use of peptides that undergo self-assembly at physiological conditions are potential candidates. This property of self-assembling peptides allows for different methods of introduction either as monomeric peptides that self-assemble *in situ* or as self-assembled peptides that are placed *in vivo*, depending on the target application.

The response to external stimuli can be tuned by careful design of the primary structure. For example, the pH response can be achieved by incorporation of charged amino acids that can be protonated and deprotonated in response to pH changes leading to electrostatic attraction or repulsion, hence changing the macroscopic reversible state of the peptide^{149,152}. Changing the ionic strength/concentration can be achieved by salt addition to the peptide solution resulting in a shift in the critical concentration at which self-assembly occurs. Presence of salt ions causes screening of electrostatic repulsion between like charges on adjacent molecules, either shifting the pH at which transition between macroscopic states occurs or shortening the gelation time^{142,154,155}.

1.12 β -sheet Based Self-assembling Peptide Systems

1.12.1 β -hairpin Peptides

A number of peptides based on 20 amino acid residues have been developed by Schneider and co-workers. MAX1 is the parent β -hairpin peptide from which MAX8 was derived¹⁵⁵. MAX peptides consist of alternating hydrophobic and hydrophilic residues with a tetrapeptide (valine, D-proline, L-proline and threonine) in the middle of the sequence. The peptides remain unfolded adopting a random coil conformation at pH 7.4 under low ionic strength conditions due to the electrostatic repulsion between the positively charged lysine residues. However, in response to an external stimulus (i.e. DMEM cell culture medium), folding of the peptide occurs due to screening of the lysine residues. Folded peptides adopt β -hairpin conformations consisting of two antiparallel β -strands joined together by β -turns resulting from the flanking tetrapeptide^{152,154,155} (Figure 1.11 A).

The β -hairpins are amphiphilic molecules with a hydrophobic face and a hydrophilic face that can self-assemble into β -sheet rich fibrils and undergo gelation under physiological conditions^{154,155}. Self-assembly of β -hairpins is achieved laterally due to intermolecular hydrogen bonding as well as facially due to hydrophobic interactions between two hydrophobic faces i.e. burial of the hydrophobic face in aqueous solution^{152,155}. Fibrils are physically crosslinked non-covalently by hydrophobic interaction between entangled fibrils, allowing for recovery following shear application^{154,155} (Figure 1.11 B). In MAX8, one of the lysine residues was replaced with the negatively charged glutamic

acid lowering the overall positive charge of the peptide for screening by salt ions, resulting in faster self-assembly and gelation ¹⁵⁵.

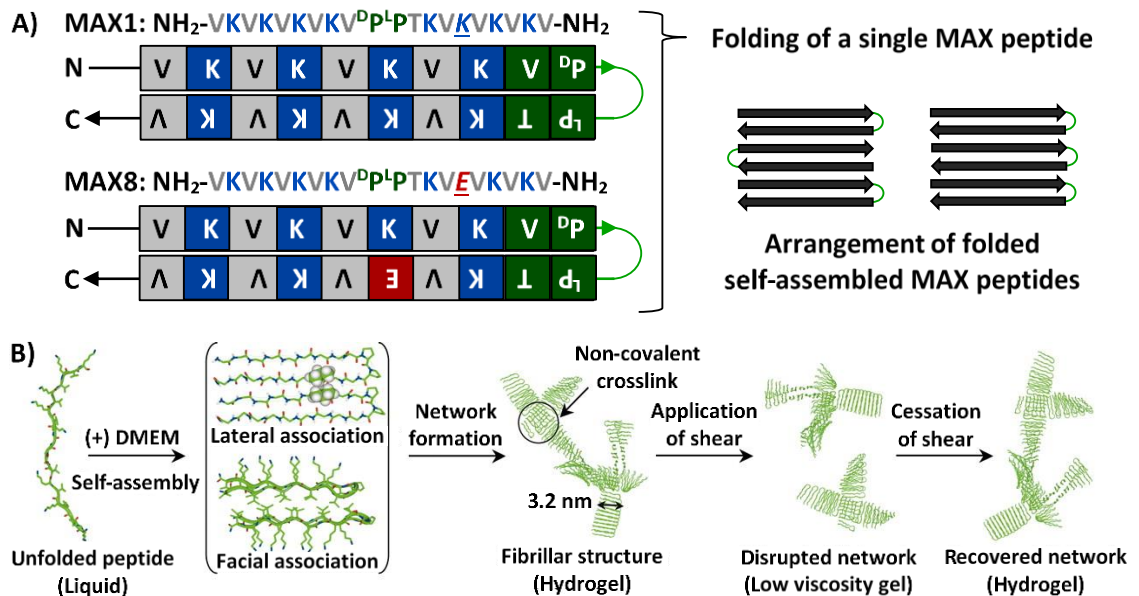


Figure 1.11: Structures and self-assembly of MAX peptides into β -hairpins. A) Peptide sequences and folding of MAX1 and MAX8 into β -hairpins and self-assembly into fibrillar arrangement consisting of β -turns. Positively charged (blue), negatively charged (red), hydrophobic (grey) and β -turns (green). B) Self-assembly of MAX peptides in presence of DMEM cell culture medium into fibrils forming hydrogels that can be disrupted and restored following injection due to non-covalent crosslinks. Adapted from Haines-Butterick et al. ¹⁵⁵. Copyright (2007) National Academy of Sciences.

MAX1 and MAX8 gel encapsulated cells have been reported to remain viable during the encapsulation and delivery processes, suggesting the potential of encapsulation in precise injectable cell delivery to a target site ¹⁵⁵. This ability of gel encapsulation also allowed for drug delivery applications such as in cancer therapies. MAX8 gel encapsulated vincristine has been shown to release the chemotherapeutic agent when injected without affecting the mechanical properties of the gel *in vitro*. The release was sustained over a period of one month with low, local and effective release of the chemotherapeutic to the target specifically ¹⁵⁶. MAX8 encapsulating gels have also been reported to deliver several neurotropic growth factors *in vitro* with a tuneable release time that was achieved by varying the peptide concentration ¹⁵⁷.

MAX1 has been shown to be non-cytotoxic to fibroblasts by supporting cell adhesion and proliferation even in the absence of serum proteins, whilst maintaining the mechanical properties of the gel. The study suggested the potential use of these peptides in tissue engineering applications ¹⁵⁴.

Assessment of the inflammatory response to MAX1 and MAX8 gels has been conducted by Haines-Butterick *et al.* prior to any *in vivo* animal model investigations. Both peptide gels have been reported to elicit no macrophage activation *in vitro* ¹⁵⁸. Moreover, MAX1 gels have been reported to exhibit antibacterial activities against Gram negative and positive bacteria, potentially reducing infection when used as a biomaterial for tissue engineering applications ¹⁵⁹.

1.12.2 EAK and RAD Based Peptides

Zhang and co-workers developed a 16 amino acid residues EAK16 peptide with alternating hydrophobic and hydrophilic residues based on the yeast protein Zuotin. EAK16 self-assembles into non-cytotoxic antiparallel β -sheets through the formation of ionic complementary bonding and intermolecular hydrogen bonding between the glutamic acid and lysine residues at pH 7.4. The self-assembled β -sheets have a hydrophobic face and a hydrophilic face, allowing for the formation of double-sheet nanofibers through hydrophobic interactions. The stability of these peptide structures arises from the ionic complementary bonding, hydrogen bonding and hydrophobic interactions ¹⁶⁰⁻¹⁶². Based on the EAK16 peptide, Zhang and co-workers developed RAD16 peptides, in which the arginine and aspartic acid replace the lysine and glutamic acid residues that self-assemble in a similar manner to EAK16 ^{153,161}. In water, the self-assembly of this class of peptides is spontaneous in the presence of salt and the formed nanofibers are stable across a wide range of pH, hence self-assembly can be controlled by changing the salt concentration at physiological pH ^{153,161,162} (Figure 1.12).

Out of these peptide series, RAD16-I and RAD16-II are the most investigated in the literature ¹⁶³. The RAD16-I peptide has been commercialised under the name PuraMatrix[®] and was investigated in various applications ¹⁶⁴.

RAD16-II has been reported to support the growth and organisation of endothelial and smooth muscle cells for myocardial regeneration. It was also demonstrated that the peptide promoted vascularisation better than Matrigel (usually used for vascularisation

studies) by supporting endothelial cell growth ¹⁶⁵. Cho *et al.* studied RAD16-II and it has been shown that the peptide promoted endothelial cell attachment and enhanced angiogenesis *in vitro* and *in vivo* ¹⁶⁶.

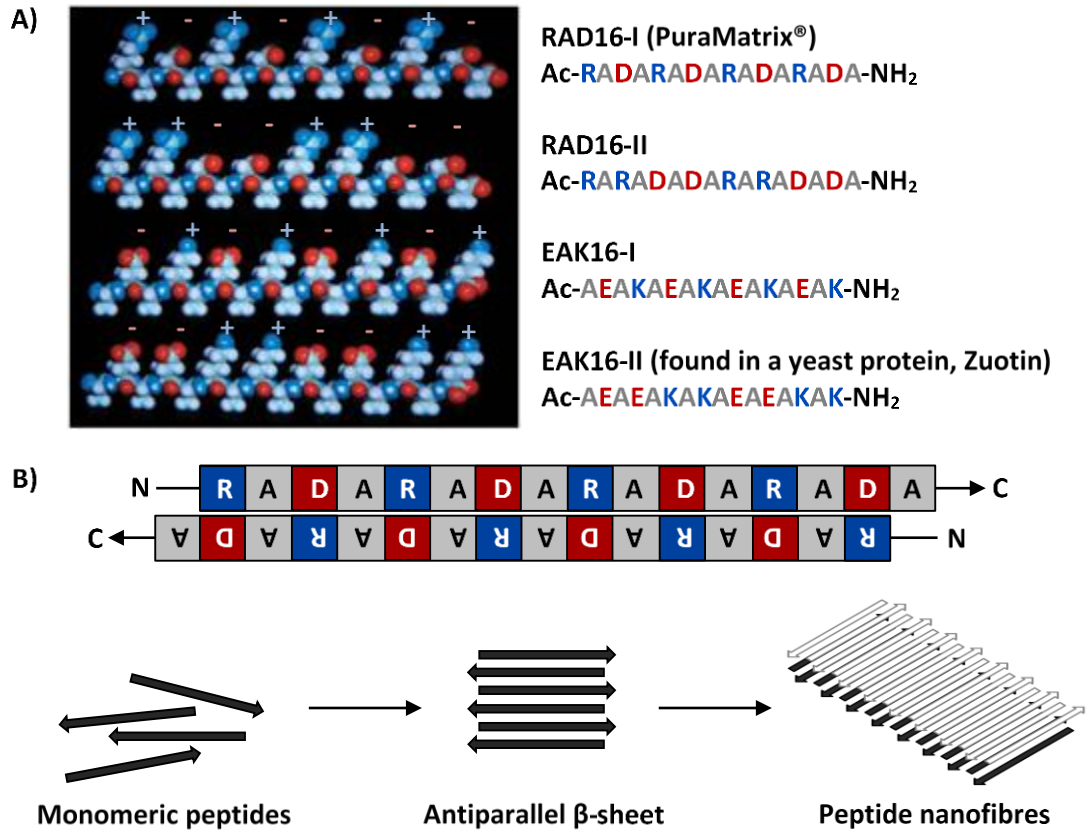


Figure 1.12: Structures and self-assembly of ionic complementary RAD and EAK peptides. A) Sequences of the peptides RAD16-I, RAD16-II, EAK16-I and EAK16-II. The top surface of the peptide is hydrophilic and charged, whilst the bottom is hydrophobic. Adapted from Hauser *et al.* ¹⁶⁷ with permission from The Royal Society of Chemistry (4195511000095). Positively charged (blue), negatively charged (red) and hydrophobic (grey). B) Self-assembly of two RAD16-I peptides into antiparallel β -sheets (shown by arrows) with hydrophilic (white) and hydrophobic (black) surfaces into long nanofibers.

The RAD16 peptides have been reported to be non-immunogenic and non-inflammatory in animal models ^{153,168}. RAD16-I, RAD16-II and EAK16-I have been shown to elicit no immunological or inflammatory responses when tested *in vivo* in rat, rabbit and goat models ¹⁶⁹.

The biological function of the RAD16 peptides has been enhanced by addition of cell attachment motifs such as RGD and YIGSR. Addition of RGD to RAD16-I peptide has

been shown to significantly promote cell proliferation in a murine model when compared to pure RAD16-I peptide ¹⁶⁸. Genove *et al.* functionalised RAD16-I with several ECM basement membrane proteins including the laminin-derived YIGSR. Functionalised RAD16-I peptides have been shown to increase the attachment and growth of endothelial cells ¹⁷⁰.

1.12.3 P₁₁ Peptide Series

The P₁₁ peptide series have been developed by Aggeli and co-workers at the University of Leeds with about 30 peptides all consisting of 11 amino acid residues with varying properties. The rationally designed P₁₁-2 peptide consisting of alternating hydrophobic and hydrophilic residues was the basis for most of P₁₁ peptides that followed ¹⁷¹. Maude *et al.* has reported a criterion for the development of these peptides for applications in tissue engineering and regenerative medicine. This criterion states that an individual peptide must have a net charge of at least ± 2 to allow for the formation of a self-supporting fibrillar gel network in physiological solutions at low concentrations of ≤ 2.0 % (w/v) with a variety of surface properties ¹⁷².

The P₁₁ peptides self-assemble into antiparallel β -sheet forming structures in a hierarchical one-dimensional nucleated manner and the process is concentration dependent, where the proportion of β -sheet increases with an increased concentration. The increase in β -sheet proportion is initially slow at low concentrations but at a particular concentration, a sudden increase is observed and this is referred to as the critical concentration at which self-assembly starts to occur (Figure 1.13) ¹⁷¹⁻¹⁷⁴. Gelation occurs with further increase in concentration (above the critical gelation concentration), where fibrillar networks form by entanglement of self-assembled peptide fibrils/fibres reducing solvent flow within the structure ¹⁷⁵.

Self-assembly occurs through recognition between complementary donor and acceptor groups and hydrogen bonding on adjacent β -strands that straighten from monomeric random coils ^{174,176}. These β -strands self-assemble into helical tapes that bend due to the chemically different surfaces, hydrophilic and hydrophobic, resulting from alternating polar and non-polar amino acids residues that are aligned on opposite sides of the peptide chain. Since the two surfaces have different affinities for water, they associate into ribbons (double tapes) through hydrophobic interactions with the

hydrophilic face contacting water. Stacks of ribbons associate into fibrils, and, finally, entwining of fibrils forms fibres by edge-to-edge interaction. These different self-assembly levels are all intrinsically twisted due to the chirality of the monomer^{173,174,176}.

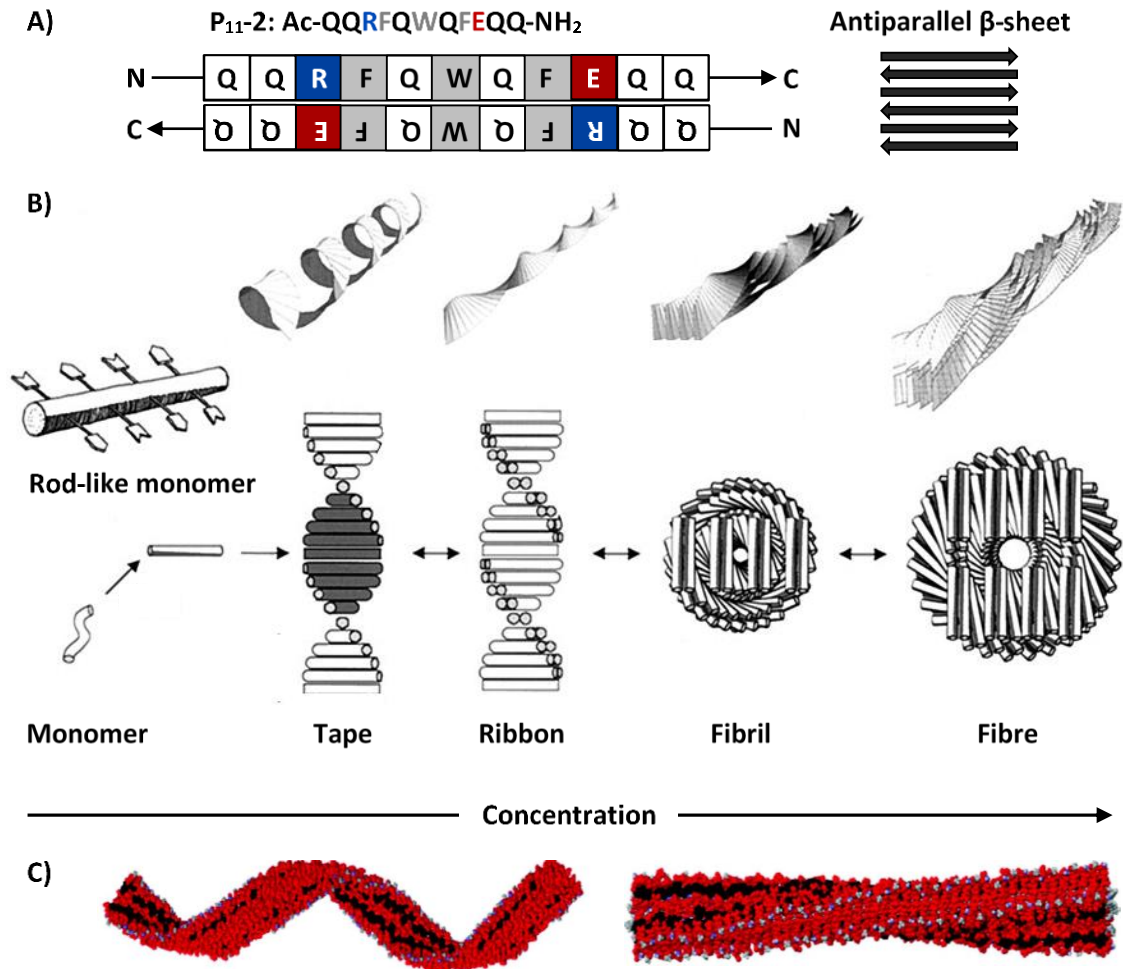


Figure 1.13: Hierarchical self-assembly of P_{11} peptides into β -sheet structures. A) P_{11-2} self-assembly into antiparallel β -sheet (shown by arrows). Positively charged (blue), negatively charged (red), hydrophilic (white, Q) and hydrophobic (grey). B) Self-assembly starts from monomeric random coils, to tapes with hydrophilic (white) and hydrophobic (black) surfaces, ribbons (interaction of hydrophobic surfaces of tapes), fibrils (stacks of ribbons) and finally fibres (edge-to-edge fibril interactions). Adapted with permission from Aggeli et al.¹⁷³. Copyright (2001) National Academy of Sciences. C) Molecular modelling (side-view) of self-assembled P_{11-1} (Ac-QQRQQQQEQQ-NH₂) tape (left) and P_{11-2} ribbon (right). Charged side-chain groups (black) and polar groups (red). Adapted with permission from Davies et al.¹⁷⁶ Copyright (2006) Taylor and Francis Group.

Fibrils and fibres have finite sizes determined by the number of stacked tapes and distinct morphologies depending on amino acid residues incorporated into the primary structure of the peptide and to a lesser extent on the presence of charged side-chains^{142,173}. Incorporation of amino acid residues of different sizes into the peptide sequence results in the formation of fibrils with different thicknesses because interaction between the side-chains of these residues within the fibril affects the molecular packing of the peptide, e.g. forming loose or tightly packed fibrils¹⁴².

Some P₁₁ peptides were designed to self-assemble in response to pH and ionic strength changes such as P₁₁₋₄, P₁₁₋₈ and P₁₁₋₁₂, while a few were designed to remain monomeric due to electrostatic repulsion but self-assemble and undergo gelation once mixed together by complementary self-assembly such as P₁₁₋₁₃/P₁₁₋₁₄.^{142,149-151}

P₁₁₋₄ and P₁₁₋₈ are based on the polar glutamine residue, whereas P₁₁₋₁₂ is based on the polar serine residue. The design of the negatively charged P₁₁₋₄ (net charge of - 2 at physiological pH) includes glutamic acid residues allowing it to be in its gel form at low pH and in its monomeric state at high pH. The opposite effect is seen with the positively charged P₁₁₋₈ and P₁₁₋₁₂ (net charge of + 2 at physiological pH) due to the incorporation of ornithine residues¹⁴². The sequences and structures of these three peptides can be found in Figure 1.14.

In a previous study (Figure 1.15), the effect of ionic strength on self-assembly of P₁₁₋₄, P₁₁₋₈ and P₁₁₋₁₂ in D₂O was investigated at 6.3 mM (approximately 10 mg.mL⁻¹) and self-assembly curves of the β -sheet percentage against pD (2 - 14) were obtained using Fourier transform infrared (FTIR) spectroscopy and nuclear magnetic resonance (NMR) spectroscopy data in absence and presence of salt (130 mM NaCl)¹⁴².

In the absence of salt, P₁₁₋₄ self-assembled into a gel at pD < 3 which flocculated at higher pD. Further increase in pD resulted in a weak viscous solution at physiological pD 7.7 then a monomeric solution at basic pD > 9. In the presence of salt, transition into a monomeric solution was shifted to a higher pD due to screening of negative repulsive charges. Moreover, the peptide self-assembled into a gel at physiological pD 7.7 and formed a monomeric solution with further pD increase (Figure 1.15 A)¹⁴². In the absence of salt, a monomeric solution was observed in P₁₁₋₈ at pD < 6, which formed a biphasic solution consisting of gel within solution at 6 < pD < ~10 and self-assembled

into a gel at higher pD. Addition of a salt, shifted all the macroscopic states to a lower pD forming the self-assembled gels at pD > ~ 8 (Figure 1.15 B)¹⁴². P₁₁₋₁₂ was shown to monomerise at low pD similar to P₁₁₋₈ but formed a weak viscous solution at pD < 9 then self-assembled into a weak gel at pD > ~ 9. In the presence of salt, transition between states was observed at lower pD ~ 8 (Figure 1.15 C)¹⁴².

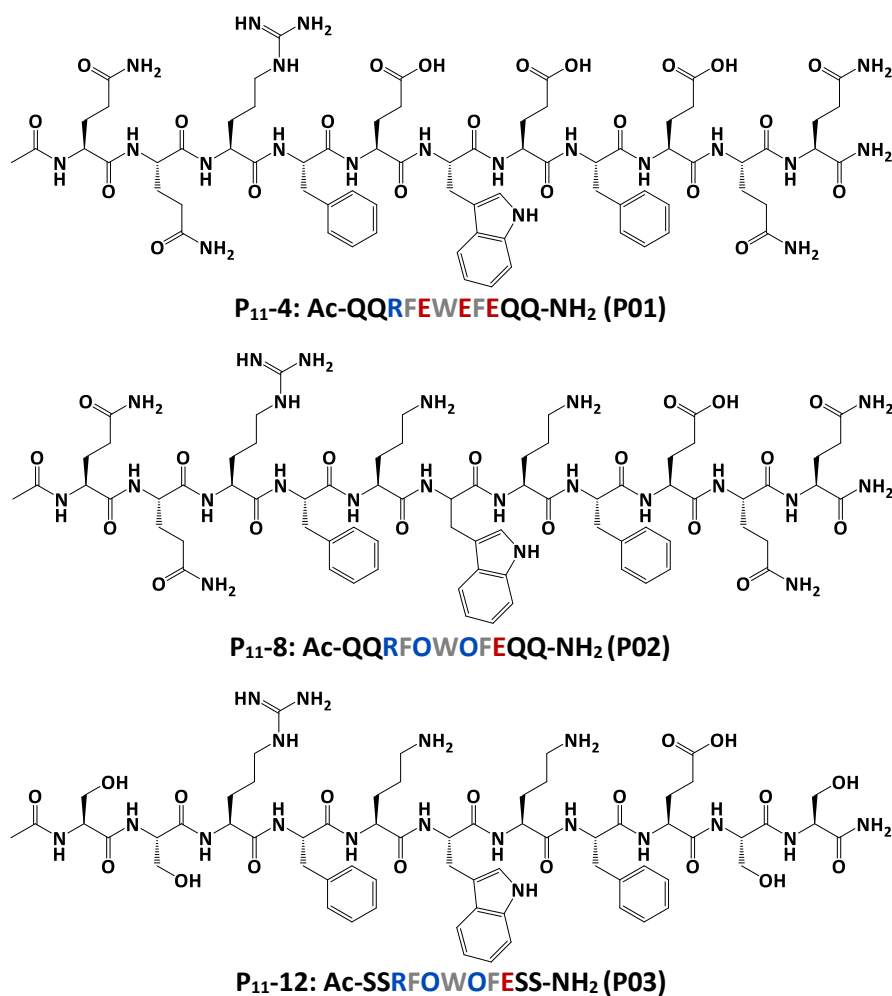


Figure 1.14: Sequences and structures of P₁₁₋₄ (P01), P₁₁₋₈ (P02) and P₁₁₋₁₂ (P03). At physiological pH 7.4, P₁₁₋₄ has a net charge of -2 due to glutamic acid residues, whilst P₁₁₋₈ and P₁₁₋₁₂ have a net charge of +2 due to ornithine residues. Positively charged (blue), negatively charged (red), hydrophilic (black) and hydrophobic (grey).

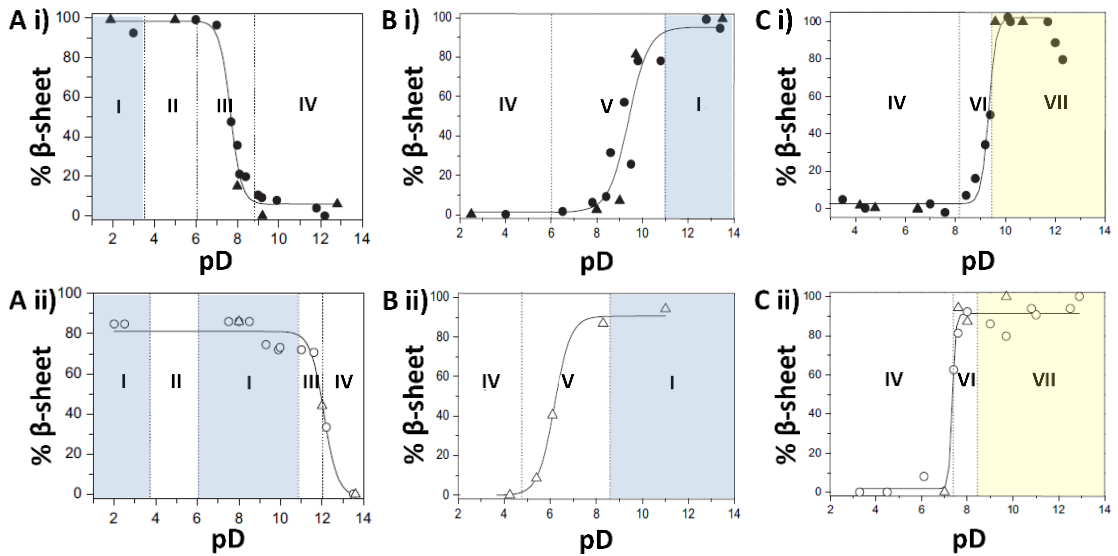


Figure 1.15: Effect of ionic strength on self-assembly – β -sheet percentages of peptides at 6.3 mM (approximately $10 \text{ mg}\cdot\text{mL}^{-1}$) in D_2O as a function of pD as determined by FTIR (circle) and NMR (triangle). Curves correspond to P_{11-4} (A), P_{11-8} (B) and P_{11-12} (C) in absence of salt (i) and presence of 130 mM NaCl (ii). I: nematic gel (blue shaded regions), II: flocculate, III: nematic fluid, IV: isotropic fluid, V: biphasic solution, VI: weakly nematic viscous fluid and VII: weakly nematic gel (yellow shaded regions). Adapted with permission from Carrick et al. ¹⁴² (4182681391766).

The P_{11} peptides have also been tested *in vitro* for cytotoxic effects. The positively charged peptides P_{11-8} , P_{11-12} , P_{11-16} and P_{11-18} have been reported to have no cytotoxic effect on L929 murine fibroblasts, but only P_{11-8} was found to support growth and proliferation of cells in a three-dimensional gel. This was thought to be caused by the peptide stability as all peptides (except for P_{11-8}) have shown gel degradation with time, resulting in poor encapsulation of cells within the degrading gel scaffold which were lost in solution during incubation ¹⁷².

In vitro, P_{11-4} and P_{11-8} have been shown to be biocompatible to human and murine fibroblasts. Lymphocytes from peptide immunised mice have shown no response to both peptides ^{119,177}. A library of P_{11} peptides have been screened in a previous study and the majority of peptides were shown to be non-cytotoxic and haemocompatible in addition to not having an effect on thrombus formation, suggesting the potential of using these peptides in biomedical applications requiring blood contact ¹⁷⁸.

P₁₁-4 has been commercialised under the name CUROLOX®TECHNOLOGY. The peptide has been applied non-invasively to patients and it has been reported to be safe for clinical use when tested for regeneration of enamel ^{179,180}.

1.13 Peptide Hydrogels as Biomaterials

Peptide gels consist of fibrillar networks formed by entanglement of the self-assembled peptide fibrils reducing solvent flow within the structure ¹⁷⁵. Consequently, for gel formation, two criteria must be satisfied. The interactions between peptide chains must be sufficiently strong in order for them to self-assemble and to form high hierarchical structures that give rise to the gel network, yet the solvent should be included within the network preventing the peptide from precipitating out of the solution ¹⁸¹.

The nature of peptide hydrogels and the reversible responsiveness to external stimuli make them interesting as biomaterial candidates for: delivery of various materials such as drugs, cells and growth factors by encapsulation within the gel; acting as scaffolds for cellular attachment and growth facilitated by the porosity of the gel to allow for cell penetration; inclusion of bioactivities within the peptide structure allowing for enhanced biological performance; and understating the behaviour of the peptide within the tested system by inclusion of dyes or labels as reporting molecules that can allow for visualisation or tracing of the peptide.

It has been reported by Maude *et al.* that cell attachment within the peptide gel matrix can be optimised by incorporation of bioactive sites into the peptide primary structure ¹⁷². The resultant matrix is capable of spontaneous reformation after it breaks, making P₁₁ peptides possible candidates to act as scaffolds for cells in tissue engineering applications ¹⁷². Since self-assembling peptides consist mostly of natural amino acid residues, they are more likely to be biocompatible. The biodegradability of such peptides is also beneficial, once the peptide serves its purpose by delivering the desired material or supporting cell attachment and growth, it can be removed from the system.

1.14 Advantages and Limitations of Peptides as Biomaterials in Tissue Engineering Applications

Recently, self-assembling peptides have been investigated intensively as novel biomaterials for many applications in regenerative medicine such as tissue engineering and drug delivery ¹⁸²⁻¹⁸⁷. This is because such peptides can be chemically diverse, versatile, manufactured easily with tuneable properties, cost-effective, biocompatible and biodegradable ^{145,185,188}. Peptides are also stable and robust structures that can form nanostructures and self-assemble into gels upon exposure to external stimuli ¹⁴⁵. The process of self-assembly and gelation is reversible ¹⁸⁹. Self-assembling peptides were reported to have the potential for use *in vivo* and clinically ¹⁹⁰.

MAX peptides were shown to be non-cytotoxic, non-inflammatory and inhibited infection *in vitro* ^{154,158,159}. Although these properties make MAX peptides good candidates for use in tissue engineering applications, the main focus of current studies from the literature have been oriented to delivery applications as an injectable encapsulating gel. In addition, more *in vitro* and *in vivo* studies are required for better understanding of the different peptide properties for various applications. The use of these peptides can also be limited due to the large size of this peptide and associated cost.

EKA16 and RAD16 based peptides were shown to be non-cytotoxic, non-inflammatory and non-immunogenic *in vitro* and *in vivo* ^{153,168,169}. Functionalisation of these peptides with bioactive motifs was shown to improve cellularisation ^{168,170}. The RAD16-I peptide has also been commercialised as PuraMatrix® ¹⁶⁴. However, several studies have shown the rapid haemostatic properties of these peptides ¹⁹¹⁻¹⁹³. The EKA16 peptide has been reported to have an agglutination effect *in vitro* that increased with increasing concentration as well as an effective rapid haemostasis in rabbit models ¹⁹¹. RAD16-I has been reported to have an effect on haemostasis by reducing bleeding in rat kidney models *in vivo* ¹⁹². The haemostatic properties of EKA and RAD peptides limit their use in vascular tissue engineering applications, in which thrombus formation is a major concern.

The P₁₁ peptide series have potential in various applications because of the wide range of peptides with different primary structures and properties ¹⁷². These peptides have

been employed in different applications at the University of Leeds. P₁₁ peptides were shown to be haemocompatible with no effect on thrombus formation¹⁷⁸. P₁₁-4 has been reported to be safe for clinical use and has been commercialised as CUROLOX®TECHNOLOGY. The small size of P₁₁ peptides makes them cost-effective when compared to MAX peptide and possibly more commercially desirable. Bioactive functionalised P₁₁-4 has been studied at the University of Leeds and was shown to have a potential for use in enhancing cell attachment and growth. However, more investigation is required on these peptides, especially the less studied ones to compare to currently investigated peptides in the literature. In addition, more *in vitro* and *in vivo* studies are needed for investigating the effect of functionalising these peptides with various bioactive motifs on cellular behaviour to assess their suitability for potential applications.

1.15 Aims and Objectives

The aim of this study was to develop a series of bioactive functionalised self-assembled P₁₁ peptides as surface coatings for decellularised porcine external iliac arteries and evaluate their ability to enhance the process of re-endothelialisation for applications in small-diameter vascular grafts.

The specific objectives were:

- To apply an established decellularisation process to porcine external iliac arteries and reproducibly produce biocompatible acellular arteries;
- To characterise the peptides P₁₁-4, P₁₁-8 and P₁₁-12 under physiological conditions at different concentrations for self-assembly behaviour and suitability for application in vascular grafts;
- To synthesise: FITC-labelled P₁₁ peptides using solid phase peptide synthesis (SPPS) to enable investigation of self-assembled peptides within acellular arteries, and bioactive (cell attachment functionalised) P₁₁ peptides using click chemistry to assess the effect of functionalisation on cell attachment onto acellular arteries;
- To assess the anti-thrombogenic properties of monomeric P₁₁-4, P₁₁-8 and P₁₁-12 and investigate their self-assembly within acellular arteries as suitable candidates for surface coatings;
- To investigate the effect of functionalised self-assembling peptides on cell attachment of ovine arterial endothelial cells to acellular arteries.

The potential outcome of this study was to reduce thrombus formation in acellular xenografts by combining a biological acellular scaffold which is free from cells and genetic material that can impose an adverse host reaction with a bioactive self-assembled peptide which supports cell attachment and retention for enhanced tissue re-endothelialisation.

2 Materials and Methods

2.1 Materials

2.1.1 Equipment

The laboratory equipment used throughout the study is listed in Table 2.1.

Table 2.1: Equipment used throughout the study.

Equipment	Model	Manufacturer
Automatic Pipettes	Various	Gilson
Balance	ABJ-NM/ABS-N	KERN
Bench top centrifuge	Harrier 15/80	SANYO Biomedical Europe BV
Centrifuge	5810	Eppendorf
Class II safety cabinet	Heraeus 85	Kendro
CO ₂ incubator	MCO-20AIC	SANYO Biomedical Europe BV
Cryostat	CM1860 UV	Leica
Dissection kit	N/A	Thackeray Instruments
Field emission gun scanning electron microscope (FEGSEM)	Quanta 200 FEGSEM	FEI
Fourier transform infrared (FTIR) spectrometer	Nicolet 6700	Thermo Electron Corporation
Freeze drier	VirTis BenchTop Pro	SP Scientific
Histology water bath	MH8515	Barnstead Electrothermal
Hotplate	E18/1	Raymond A Lamb
Hot wax dispenser	E66	Raymond A Lamb
Hot wax oven	E18/31	Raymond A Lamb
Incubator	MIR-554-PE	Panasonic
Inverted microscope	IX71 and CK40	Olympus
Magnetic stirrer	SB161	Stuart Scientific
Micro centrifuge	5415 R	Eppendorf
Microplate reader	Chameleon plate	Hidex
Microshaker	AM69	Cooke
Microtome	RM2255	Leica
Multiphoton laser scanning microscope (MPLSM)	LSM 710 Axio Examiner	Zeiss
NanoDrop spectrophotometer	ND-1000	Labtech

pH meter	3510 Docu-pHMETER	Jenway Sartorius
Pipette boy	Acu	Integra Biosciences
Rotator	SB3	Stuart
Sonicator	SONOREX SUPER RK52H	Bandelin
Table shaker	POS-300 and PSU-10i	Grant
Tissue processor	TP1020	Leica
Transmission electron microscope (TEM)	JEM-1400 Plus	JOEL
Upright microscope	Axio Imager M2	Zeiss
Vortexer	SA8	Stuart
Water bath	Grant	Jencons PLC

2.1.2 Glassware

All laboratory glassware was obtained from Fisher Scientific (Loughborough, UK) unless otherwise stated. Glassware was cleaned by immersion in a 1 % (v/v) solution of Neutracon® for one hour and was then rinsed with tap water and dried or sterilised using dry heat.

2.1.3 Plastic Ware

All sterile and non-sterile disposable plastic ware was purchased from Scientific Laboratory Supplies Ltd. (Nottingham, UK) unless otherwise stated.

2.1.4 Chemicals and Materials

The chemicals/reagents and materials used throughout the study are listed in Table 2.2.

Table 2.2: Chemicals and reagents used during the study.

Chemical/Material	Supplier
3M Steri-Strip Skin Closure 3 mm x 75 mm	Medisave
Acetic acid glacial	Fisher Scientific
Acetic anhydride	Sigma-Aldrich
Acetone	Sigma-Aldrich
Acetonitrile	Fisher Scientific
Ammonia (NH ₃) solution (35 %; w/w)	Fisher Scientific

Aprotinin (10000 KIU.mL ⁻¹)	Nordic Pharma
ATPlite™ assay	Perkin-Elmer
Benzonase (> 90 % purity)	Merck Millipore
Biopsy punch	Schuco International
Bovine serum albumin (BSA)	Sigma-Aldrich
Calcium chloride dihydrate	Sigma-Aldrich
Collagenase type II (215 U.mg ⁻¹)	Life Technologies
Copper(II) sulphate pentahydrate	Sigma-Aldrich
Cryoembed medium	VWR
Dako fluorescent mounting medium	Dako
DAPI stain (4',6-diamidino-2-phenylindole dihydrochloride)	Sigma-Aldrich
Deuterium chloride (DCI; 35 %; w/w)	Sigma-Aldrich
Deuterium oxide (D ₂ O)	Sigma-Aldrich
Dichloromethane (DCM)	Fisher Scientific
Diethyl ether	VWR Chemicals
Diisopropylcarbodiimide (DIC)	Merck Chemical Ltd.
Dimethylformamide (DMF)	Sigma-Aldrich
Dimethyl sulphoxide (DMSO)	Sigma-Aldrich
DNeasy Blood and Tissue Kit	Qiagen
DPX mountant	Atom Scientific
Dulbecco's modified Eagle's medium (DMEM)	Sigma
Dulbecco's phosphate buffered saline (PBS) tablets	Oxoid
Endothelial cell growth supplement from bovine tissue (ECGS)	Sigma-Aldrich
Eosin Y	Merck Millipore
Ethanol (100 %; v/v)	Thermo Fisher Scientific Ltd.
Ethylenediaminetetra-acetic acid (EDTA)	Thermo Fisher Scientific Ltd.
Fluorescein isothiocyanate isomer I (FITC)	Sigma-Aldrich
Foetal bovine serum (FBS)	Sera Lab
Fresh blood agar plates	Oxoid
Gentamycin sulphate	Merck Chemicals Ltd.
Giemsa solution	VWR International
Glasgow's minimal essential medium (GMEM)	Sigma
Hank's balanced salt solution (HBSS) with and without calcium and magnesium	Sigma
Heparin sodium (1000 U.mL ⁻¹)	Fannin

Human α -thrombin	Cambridge Bioscience
Hydrochloric acid (HCl; 37 %; w/w))	Fisher Scientific Ltd.
Hydrochloric acid (HCl; 5 M)	Thermo Fisher Scientific Ltd.
L-glutamine (200 mM)	Sigma
LIVE/DEAD [®] Viability/Cytotoxicity Kit	Life Technologies
M-199	Sigma
Magnesium chloride hexahydrate	VWR International
Mayer's haematoxylin	Atom Scientific
Mersilk Suture Cutting Needle 16 mm, 38 cm 4-0	Medisave
Mersilk Suture Taper Point 36 mm, 75 cm 3-0	Medisave
Methanol (100 %; v/v)	Atom Scientific
N,N-diisopropylethylamine (DIPEA)	Sigma-Aldrich
Neutral buffered formalin (NBF) 10 % (w/v)	Atom Scientific
Nutrient agar plates	Oxoid
Nutrient broth	Oxoid
O-(1H-6-chlorobenzotriazole-1-yl)-1,1,3,3-tetramethyluronium hexafluorophosphate (HCTU)	Merck Chemical Ltd.
Oxyma Pure [®]	Merck Chemical Ltd.
Paraffin wax pellets	Bios Europe Ltd.
PBS with and without calcium and magnesium	Sigma
Penicillin (5000 U.mL ⁻¹) / streptomycin (5 mg.mL ⁻¹) solution	Sigma
Peracetic acid	Sigma-Aldrich
Piperidine	Sigma-Aldrich
Plastic histology cassettes	VWR International
Polymyxin B sulphate salt	Merck Chemicals Ltd.
Polyvinyl chloride (PVC) tubing 180 metric medical grade	Techmate Ltd.
Sabouraud Dextrose agar plates	Oxoid
Scott's tap water substitute 10 x concentration	Atom Scientific
Sodium azide 1 % (w/v) solution	G Biosciences
Sodium chloride	Thermo Fisher Scientific Ltd.
Sodium deuterioxide (NaOD; 40 %; w/w)	Sigma-Aldrich
Sodium hydroxide pellets	Fisher Scientific Ltd.
Sodium L-ascorbate	Sigma-Aldrich
Sodium phosphate dibasic anhydrous (Na ₂ HPO ₄)	Acros organics
Sodium phosphate monobasic monohydrate (NaH ₂ PO ₄ .H ₂ O)	Acros organics

Sterile citrated sheep blood (sodium citrate as the standard 4 %; w/v anticoagulant)	V H Bio
Superglue (cyanoacrylate contact adhesive)	Any
Trifluoroacetic acid (TFA)	Fisher Scientific
Triisopropylsilane (TIPS)	Sigma-Aldrich
Tris(2-carboxyethyl)phosphine (TCEP) hydrochloride	Acros organics
Tris(benzyltriazolylmethyl)amine (TBTA)	Sigma-Aldrich
Trizma [®] base	Sigma-Aldrich
Trypan blue solution (0.4 %; v/v)	Sigma-Aldrich
Trypsin (17000 U.L ⁻¹) / EDTA (200 mg.L ⁻¹)	Sigma
Tryptone phosphate broth (TPB)	Sigma
Tween 20	Sigma-Aldrich
UltraPure [™] 10 % (w/v) sodium dodecyl sulphate solution (SDS)	Invitrogen Life Technologies
Vancomycin hydrochloride hydrate	Merck Chemicals Ltd.
Virkon	Scientific Laboratory Supplies
Water for HPLC	VWR Chemicals
Xylene	Atom Scientific

2.1.5 Peptides

All peptides and Fmoc-protected amino acids were purchased from commercial suppliers (unless otherwise stated) and lyophilised peptides were stored at - 20 °C, listed in Table 2.3. Each peptide and Fmoc-protected amino acid was thawed at room temperature before use.

Table 2.3: Peptides, amino acids and resins used throughout the study.

Amino Acids and Peptides	Supplier
Azide-functionalised P ₁₁ -4	Cambridge Research Biochemicals
Azide-functionalised P ₁₁ -8	Cambridge Research Biochemicals
FITC-labelled P ₁₁ -4	PolyPeptide Group
Fmoc-Arg(Pbf)-OH	Merck Chemical Ltd.
Fmoc-Asp(OtBu)-OH	Merck Chemical Ltd.
Fmoc-β-Ala-OH	Merck Chemical Ltd.
Fmoc-Gln(Trt)-OH	Merck Chemical Ltd.

Fmoc-Glu(OtBu)-OH	Merck Chemical Ltd.
Fmoc-Gly-OH	Merck Chemical Ltd.
Fmoc-Ile-OH	Merck Chemical Ltd.
Fmoc-L-propargylglycine	Fluorochem
Fmoc-NH-(PEG) ₂ -COOH	Merck Chemical Ltd.
Fmoc-Orn(Boc)-OH	Merck Chemical Ltd.
Fmoc-Phe-OH	Merck Chemical Ltd.
Fmoc-Ser(tBu)-OH	Merck Chemical Ltd.
Fmoc-Trp(Boc)-OH	Merck Chemical Ltd.
Fmoc-Tyr(tBu)-OH	Merck Chemical Ltd.
NovaSyn TG Sieber resin	Merck Chemical Ltd.
P ₁₁ -4	Credentis
P ₁₁ -8	C S Bio
P ₁₁ -12	C S Bio
Rink Amide NovaGel™ resin	Merck Chemical Ltd.

2.1.6 Mammalian Cells

Cell lines, BHK-21 strain 31 (baby hamster kidney epithelial cells) and L929 (mouse fibroblast cells), used in the *in vitro* biocompatibility testing were obtained from the Health Protection Agency. These were resurrected from liquid nitrogen storage.

2.1.7 Mammalian Tissue

Porcine legs were obtained from a local abattoir, JC Penny (Leeds). All legs were dissected within less than 24 hours of slaughter. Porcine external iliac arteries were isolated from the legs and stored at - 80 °C until use.

Ovine legs were obtained from a local abattoir, M & C Meats (Leeds). All legs arrived fresh within less than 24 hours of slaughter. All procedures involving the ovine legs were carried out on the day of arrival aseptically inside a class II safety cabinet.

2.1.8 Antibody-labelling and Antibodies

Primary antibodies, secondary antibodies and corresponding isotype controls used for immunofluorescence studies are listed in Table 2.4.

Table 2.4: Primary antibodies, secondary antibodies and isotype controls. Concentrations displayed correspond to the working protein concentration and isotype controls were diluted at the same concentration as their primary antibody in antibody diluent.

Primary Antibodies				
Antigen	Type	Isotype Control	Concentration	Supplier
Fibroblast, 5B5	Mouse anti-human	IgG1	3.1 mg.L ⁻¹	Dako
Smooth muscle myosin heavy chain, N1/5	Mouse anti-human	IgG1	20 mg.L ⁻¹	Merck Millipore
Smooth muscle α -actin, 1A4	Mouse anti-human	IgG2a	4 mg.L ⁻¹	Sigma-Aldrich
Von Willebrand Factor (vWF)	Rabbit anti-human	Polyclonal	15.5 mg.L ⁻¹	Dako
Secondary Antibodies				
Antigen	Type	Conjugate	Concentration	Supplier
Mouse F(ab') ₂ fragment	Goat anti-mouse	Alexa Fluor 488	0.5 mg.L ⁻¹	Invitrogen
Rabbit F(ab') ₂ fragment	Goat anti-rabbit	Alexa Fluor 488	0.5 mg.L ⁻¹	Invitrogen
Isotype Controls				
Antigen	Host	Isotype	Concentration	Supplier
<i>Aspergillus niger</i> glucose oxidase	Mouse	IgG2a	As primary	Dako
<i>Aspergillus niger</i> glucose oxidase	Mouse	IgG1	As primary	Dako
-	Rabbit	Immunoglobulin fraction	As primary	Dako

2.1.9 General Reagents

Dulbecco's phosphate buffered saline (PBSa): Ten Oxoid PBS tablets were dissolved in distilled water (1 L) and the pH was adjusted to 7.2 - 7.4. The solution was sterilised by autoclaving and stored for up to one month at room temperature.

Dye buffer (10 mM tris, 1 mM Na₂EDTA, 1 mM NaCl): Trizma base (1.211 g), EDTA (0.3724 g) and sodium chloride (0.058 g) were dissolved in distilled water (1 L) and the pH was adjusted to 7.4 immediately before use.

4',6-diamidino-2-phenylindole (DAPI) dye stock solution (1 mg.mL⁻¹): DAPI (10 mg) was added to nuclease free water (10 mL) and stored in aliquots of 20 µL at - 20 °C for up to six months.

Working DAPI solution (0.1 µg.mL⁻¹): DAPI dye stock solution (20 µL) was added to dye buffer (200 mL) in a dark bottle and the solution was used immediately.

Ringer's solution (10X strength): Four Oxoid Ringer's solution tablets, were dissolved in distilled water (50 mL) and the pH was adjusted to 7.4 - 7.6. The solution was sterilised by autoclaving and stored for up to one month at room temperature.

Tris buffered saline (TBS) (0.05 M Tris buffer, 0.15 M NaCl): Trizma base (6.05 g) and sodium chloride (8.76 g) were dissolved in distilled water (1 L) and the pH was adjusted to 7.6. The solution was sterilised by autoclaving and was stored at room temperature for up to one month.

Nutrient broth: Nutrient broth powder (25 g) was dissolved in 1 L of distilled water. This was sterilised by autoclaving and stored at 4 °C.

2.2 Experimental Methods

2.2.1 Sterilisation Methods

2.2.1.1 Sterilisation by Dry Heat

Items were placed in suitable containers or wrapped with tinfoil and placed into a hot air oven at a temperature of 190 °C for four hours.

2.2.1.2 Sterilisation by Autoclaving

Solutions/items not suitable for sterilisation by dry heat were sterilised by autoclaving. Solutions/items were placed into suitable containers or autoclave bags. Solutions/items were autoclaved at 15 psi at 120 °C for 20 minutes.

2.2.1.3 Sterilisation by Filtration

Solutions not suitable for autoclaving were filtered using 0.2 µm pore size filters using disposable syringes inside a class II safety cabinet.

2.2.1.4 Sterilisation by Gamma Irradiation

Peptides were not suitable for sterilisation by dry heat, autoclaving or filtration. Peptides used in biological experiments were weighed out into glass vials and sterilised as a dry powder by gamma sterilisation with 25 kGy using a Tcell Elite Irradiator (Xiros, Leeds, UK).

2.2.2 Measurement of pH

The pH meter was calibrated using purchased solutions of pH 4, 7 and 10. The pH of solutions was measured at room temperature using temperature compensation. Adjustment of pH was carried out by drop-wise addition of 6 M hydrochloric acid (HCl) or 6 M sodium hydroxide (NaOH) whilst stirring unless otherwise stated.

2.2.3 Cell Biology

Tryptone phosphate broth stock solution (TPB; 29.5 g.L⁻¹): TPB (7.38 g) was dissolved in distilled water (250 mL) then sterilised by filtration and stored in aliquots of 20 mL at - 20 °C for up to six months.

Dulbecco's modified Eagle's medium (DMEM), L929 cell culture medium, (2 mM L-glutamine, 100 U.mL⁻¹ penicillin / 0.1 mg.mL⁻¹ streptomycin, 10 %; v/v FBS): L-glutamine (1 mL, 200 mM), penicillin (5000 U.mL⁻¹) / streptomycin (5 mg.mL⁻¹; 2 mL) and foetal bovine serum (FBS; 10 mL) were added to DMEM (87 mL). The solution was mixed by inversion and stored at 4 °C for up to one week. Cell culture medium was pre-warmed at 37 °C before use.

Glasgow's minimal essential medium (GMEM), BHK cell culture medium, (2 mM L-glutamine, 100 U.mL⁻¹ penicillin / 0.1 mg.mL⁻¹ streptomycin 10 %; v/v TPB and 5 %; v/v FBS): L-glutamine (1 mL, 200 mM), penicillin (5000 U.mL⁻¹) / streptomycin (5 mg.mL⁻¹; 2 mL), TPB (10 mL) and FBS (5mL) were added to GMEM (82 mL). The solution was mixed by inversion and stored at 4 °C for up to one week. Cell culture medium was pre-warmed at 37 °C before use.

2.2.3.1 Resurrecting and Maintaining Cells

Cells were removed from liquid nitrogen storage using the appropriate personal protective equipment and defrosted in a water bath at 37 °C. All cells were handled

within a class II environment. Supplemented cell culture medium (10 mL) was added drop-wise to cells in a sterile universal tube. Cells were centrifuged at 150 x g for ten minutes, the supernatant was discarded in 1 % (w/v) Virkon and the cell pellet was suspended in 5 mL of supplemented cell culture medium. The cell suspension was transferred into a T-25 tissue culture flask and cells were incubated at 37 °C with 5 % (v/v) CO₂ in air. The medium was replaced with 5 mL of supplemented cell culture medium every 48 hours until cells reached approximately 80 % confluency.

2.2.3.2 Passaging and Maintaining Cells

Upon reaching approximately 80 % confluency, the medium was removed from the cells within a tissue culture flask. The cell surface was washed with PBS without calcium and magnesium (5 mL for T-25, 10 mL for T-75 and 15 mL for T-175 flasks) for five minutes. This was subsequently removed and replaced with trypsin/EDTA solution (1 mL for T-25, 2.5 mL for T-75 and 5 mL for T-175 flasks) and was incubated at 37 °C with 5 % (v/v) CO₂ in air for no longer than five minutes. Following trypsin/EDTA treatment, the tissue culture flask was tapped gently to facilitate cell detachment from the surface of the flask, which was ensured by examination under an inverted phase contrast light microscope. The trypsin was neutralised by adding supplemented cell culture medium (5 mL for T-25, 10 mL for T-75 and 15 mL for T-175 flasks), transferred into a sterile universal tube and centrifuged at 150 x g for ten minutes. The supernatant was discarded in 1 % (w/v) Virkon and the cell pellet was suspended in supplemented cell culture medium (5 mL for T-25, 10 mL for T-75 and 15 mL for T-175 flasks). Cells were incubated at 37 °C with 5 % (v/v) CO₂ in air and medium was replaced every 48 hours until cells reached approximately 80 % confluency.

2.2.3.3 Counting Viable Cells Using Trypan Blue Exclusion Assay

Cell pellets were obtained as described in Section 2.2.3.2 and suspended in supplemented cell culture medium. The cell suspension was mixed with 0.4 % (v/v) trypan blue dye with 1:1 volume ratio. Stained cell suspension, 10 µL, was transferred into Neubauer haemocytometer chamber. Under an inverted phase contrast light microscope, the number of unstained viable cells was counted in a 1 mm² square etched onto the Neubauer haemocytometer (Figure 2.1). For accurate counting, the cell

suspension was diluted so that the number of viable cells counted was between 30 and 300 cells. The total number of viable cells per mL was calculated (Equation 2.1).

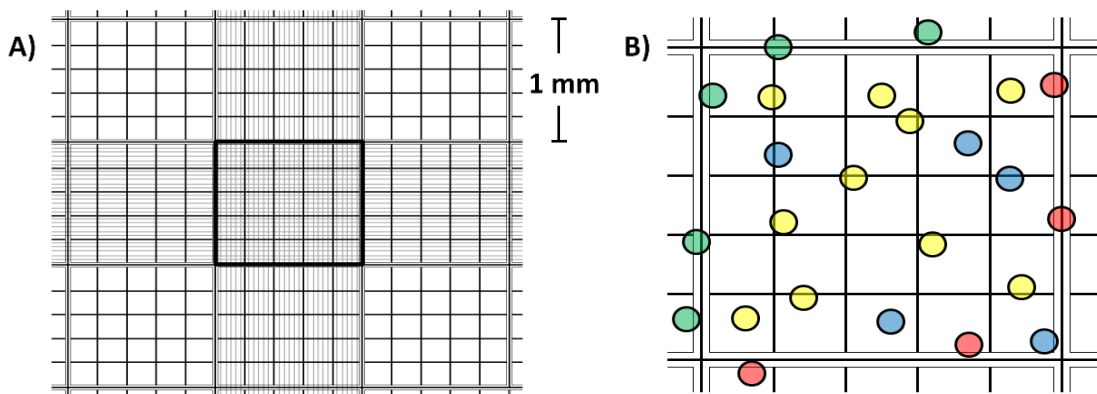


Figure 2.1: Trypan blue exclusion assay for counting cells in haemocytometer grids. A) Full haemocytometer grid consisting of nine 1 mm² squares, each square consists of 25 smaller squares. B) Individual 1 mm² square, where viable cells lying inside the square (yellow) and on the left and top lines of the square (green) are counted but dead cells lying inside the square (blue) and viable ones on the right and bottom lines (red) are not counted in an individual square.

Equation 2.1: Calculating viable cells using trypan blue exclusion assay.

$$\text{No. of cells/mL} = \frac{\text{Total no. of viable cells}}{\text{No. of 1 mm}^2 \text{ squares counted}} \times \text{dilution factor} \times 10^4$$

2.2.3.4 Cryopreservation of Cells

Cell pellets were obtained as described in Section 2.2.3.2 and suspended in supplemented cell culture medium containing 10 % (v/v) DMSO. The suspension was immediately aliquoted into 1 mL cryovials and placed in a container containing isopropanol, stored at - 80 °C overnight then transferred to liquid nitrogen until the cells were required.

2.2.4 Decellularisation of Porcine External Iliac Arteries

PBSa containing 2.7 mM Na₂EDTA and 10 KIU.mL⁻¹ aprotinin: Ten PBS tablets and EDTA (1 g) were dissolved in distilled water (1 L) and the pH was adjusted to 7.2 - 7.4. The solution was sterilised by autoclaving and stored for up to one month at room temperature. Prior to use, aprotinin (200 µL) was added aseptically to 200 mL of solution (1 mL of aprotinin per of 1 L solution).

Disinfection solution (0.05 mg.mL⁻¹ vancomycin hydrochloride, 0.5 mg.mL⁻¹ gentamycin sulphate and 0.2 mg.mL⁻¹ Polymyxin B): Vancomycin hydrochloride (2.5 mL, 10 mg.mL⁻¹), gentamycin sulphate (2.5 mL, 100 mg.mL⁻¹) and Polymyxin B (2 mL, 50 mg.mL⁻¹) were prepared then added to sterile PBSa (100 mL) and the pH was adjusted to 7.2 - 7.4. The solution was made up to 500 mL using sterile PBSa to achieve the final required working concentration of antibiotics.

EDTA solution (200 mM): EDTA (74.4 g) was dissolved in distilled water (1 L) and the pH was adjusted to 7.2 - 7.4. The solution was sterilised by autoclaving and stored for up to one month at room temperature.

Hypotonic buffer (10 mM Tris buffer, 2.7 mM Na₂EDTA and 10 KIU.mL⁻¹ aprotinin): Trizma base (1.21 g) and EDTA (1 g) were dissolved in distilled water (900 mL) and the pH was adjusted to 8.0 - 8.2. The volume was made up to 1 L using distilled water. The solution was sterilised by autoclaving and stored at room temperature for up to one month. Prior to use, aprotinin (200 µL) was added aseptically to 200 mL of hypotonic buffer.

SDS hypotonic buffer (0.1 % (w/v) SDS, 10 mM Tris buffer, 2.7 mM Na₂EDTA and 10 KIU.mL⁻¹ aprotinin): SDS (10 mL, 10 %; w/v) was added aseptically to autoclaved hypotonic buffer (990 mL) and the solution was inverted to mix. Prior to use, aprotinin (200 µL) was added to 200 mL of SDS buffer aseptically. This was stored at 4 °C for up to one week if opened aseptically.

Nuclease solution (50 mM Tris buffer, 1 mM MgCl₂.6H₂O, 1 U.mL⁻¹ Benzonase): Trizma base (6.1 g) and magnesium chloride hexahydrate (0.203 g) were dissolved in distilled water (100 mL) and the pH was adjusted to 7.5 - 7.7. The volume was made up to 1 L using distilled water. The solution was sterilised by autoclaving and stored at room temperature for up to one month. Before using, the nuclease solution, Benzonase (4 µL, 250 U.µL⁻¹) was added and the solution was used within ten minutes of preparation.

Hypertonic buffer (50 mM Tris buffer, 1.5 M NaCl): Trizma base (6.06 g) and sodium chloride (87.66 g) were dissolved in distilled water (900 mL) and the pH was adjusted to 7.5 - 7.7. The volume was then made up to 1 L using distilled water. The solution was sterilised by autoclaving and stored for up to one month at room temperature.

Peracetic acid solution (0.1 %; v/v): Peracetic acid (3.14 mL) was added to autoclaved PBS (1 L) and the pH was adjusted to 7.2 - 7.5. The solution was used within one hour of production.

2.2.4.1 Isolation of Arteries

The external iliac arteries were dissected from porcine legs within 24 hours of slaughter. The external iliac artery was located (Figure 2.2 A) and dissected from the surrounding tissue, 0.5 - 1.0 cm of arterial branches were retained and arteries between 9 - 19 cm were obtained with internal diameters ranging between 5 - 9 mm (large end) and 3 - 6 mm (small end; Figure 2.2 B - C). Following isolation connective tissue was removed using blunt dissection (Figure 2.2 D). Each artery was washed three times for 30 minutes at 4 °C using PBSa containing EDTA and aprotinin to remove excess blood. Arteries were stored at - 80 °C on PBS moistened filter paper until needed.

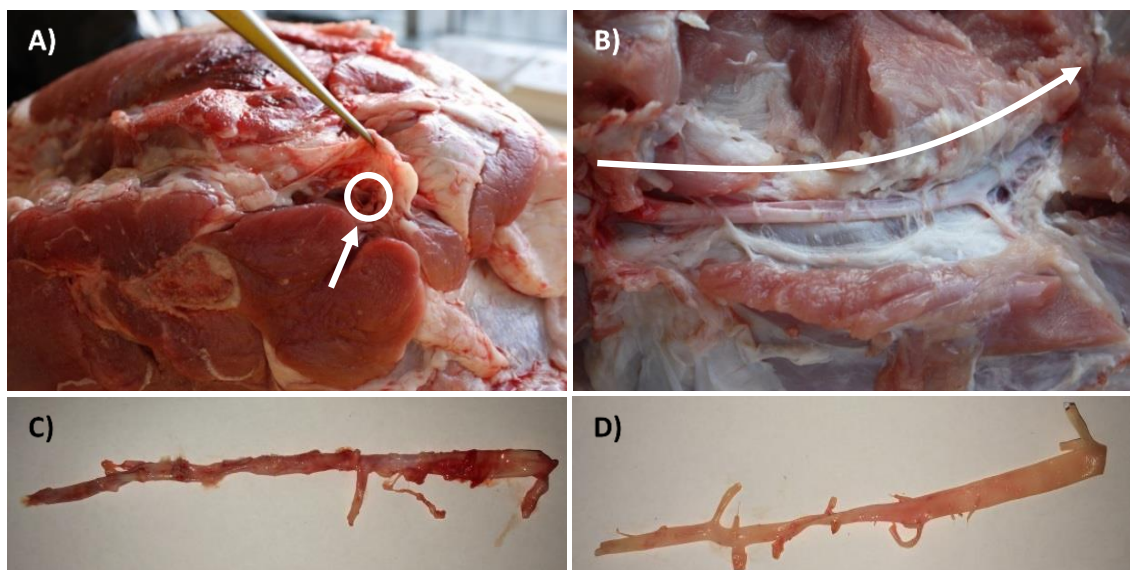


Figure 2.2: Porcine external iliac artery dissection. A) Identification of the iliac artery end shown by an arrow. B) dissection of the artery from surrounding tissue following the arrow direction. C) isolation of the artery and D) following blunt dissection to remove connective tissues.

2.2.4.2 Decellularisation

All washes were carried out with agitation on a table shaker at 120 rpm, except for the nuclease wash which was carried out at 50 rpm. The solutions were incubated at the required temperature before use and 200 mL of each solution was used to wash a single artery in an individual sterile 250 mL plastic container.

Porcine iliac arteries were thawed at 37 °C for 20 minutes. Each artery was washed for 30 minutes in a disinfection solution at 37 °C then washed in EDTA for 24 hours at 4 °C. Each artery was incubated in a hypotonic buffer for 24 hours at 4 °C, subsequently washed in SDS hypotonic buffer for 24 hours at 37 °C, incubated again in a hypotonic buffer for 24 hours at 4 °C then washed in PBSa containing EDTA and 10 KIU.mL⁻¹ aprotinin over the weekend (48 - 56 hours) at 4 °C. Once more, arteries were washed in SDS hypotonic buffer for 24 hours at 37 °C followed by three PBSa washes at 37 °C each for 30 minutes then a 24 hour PBSa wash at 37 °C. Each artery was incubated twice in nuclease solution with slower agitation at 37 °C for three hours each followed by three PBSa washes 37 °C each for 30 minutes then washed in PBSa overnight (16 hours) at 37 °C. Each artery was subsequently washed using hypertonic solution for 24 hours at 37 °C followed by three washes in PBSa at 37 °C each for 30 minutes. Peracetic acid was used to disinfect the arteries, each artery was incubated in peracetic acid for four hours at room temperature. The following steps were carried out aseptically inside a class II environment. Each artery was washed three times in PBSa at 37 °C each for 30 minutes then washed in PBSa over the weekend (48 - 56 hours) at 4 °C. Following that, each artery was washed five times in PBSa at 4 °C each for 24 hours. Finally, arteries were stored in PBSa at 4 °C until needed for up to three months. An overview of the decellularisation process may be found in Figure 2.3.

Following decellularisation of arteries, assessment of acellularity and *in vitro* biocompatibility of each batch was carried out as described in Section 2.2.5 and Section 2.2.6, respectively.

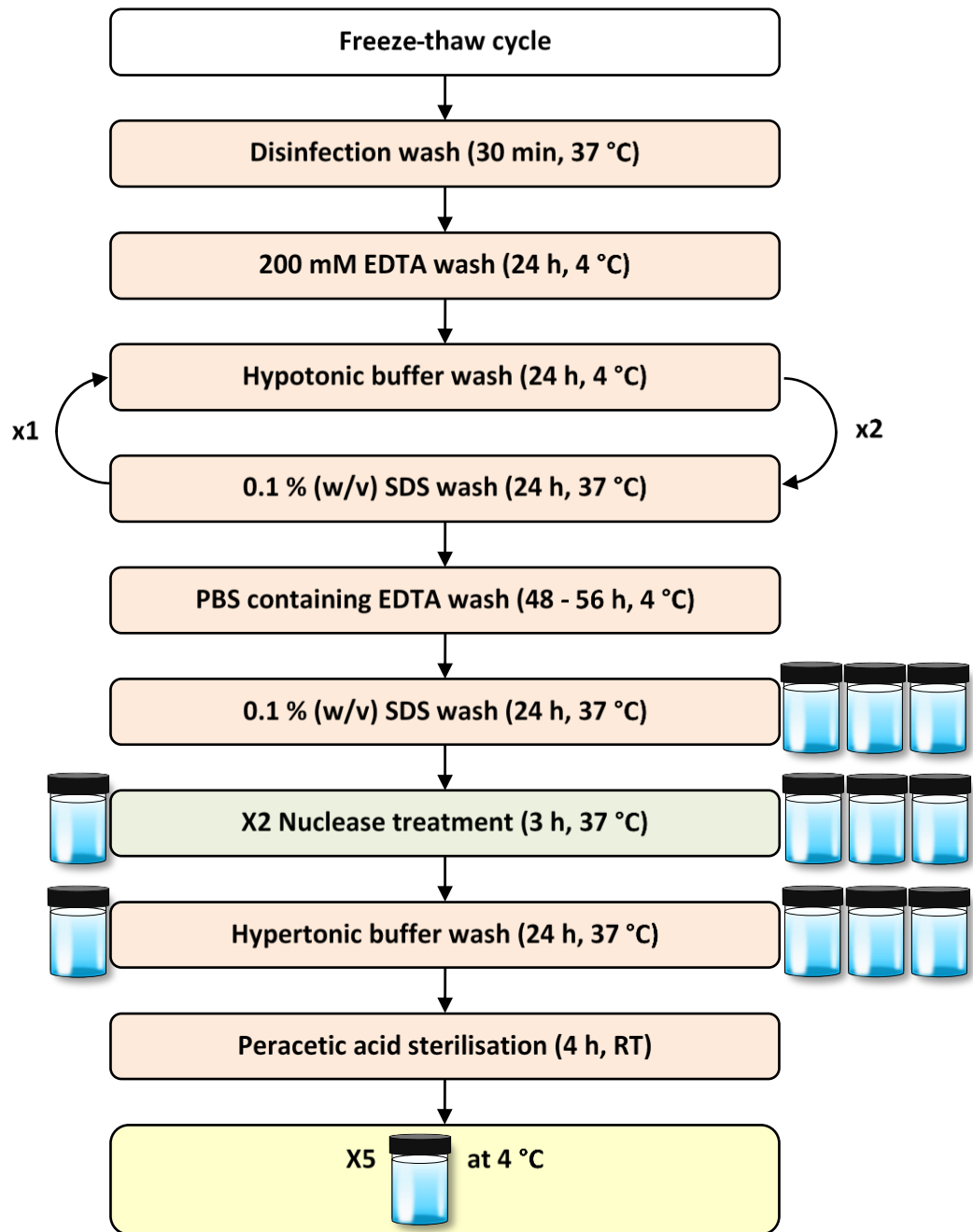


Figure 2.3: Flow diagram summarising the decellularisation process for the porcine external iliac artery. Washes in red and yellow boxes were carried out at 120 rpm whereas those in green boxes at 50 rpm. Following the final peracetic acid wash, all washes were carried out inside a class II safety cabinet. Three times PBSa 30 minutes washes are represented by three pots after each wash, while the overnight and 24 hour PBSa washes are represented by one pot before each wash.

2.2.5 Acellularity Validation

The following assessments were carried out after the decellularisation of a batch of arteries to ensure each artery was sterile and acellular before carrying out any further tests using a batch.

2.2.5.1 Sterility of Acellular Arteries

Acellular porcine iliac arteries were tested for sterility after the decellularisation process by incubating 1 cm segments individually in a microbial growth medium (nutrient broth). Arterial segments were placed in nutrient broth inside a class II safety cabinet to prevent any contamination then incubated at 37 °C for 72 hours. These were compared with a positive control (nutrient broth that was left in open air) and a negative control (nutrient broth that was in a sealed container). Following incubation, a clear medium was indicative of a sterile acellular artery, while a cloudy medium was indicative of a non-sterile acellular artery.

2.2.5.2 Histology

2.2.5.2.1 Fixation and Paraffin Wax Embedding

Artery segments (0.5 cm) from cellular and acellular tissue were fixed using 10 % (w/v) neutral buffered formalin (NBF) for 24 hours. Fixed samples were then dehydrated in an automated tissue processor, where the samples were immersed in a series of solutions: 70 % (v/v) ethanol for one hour, 90 % (v/v) ethanol for one hour, two changes of 100 % (v/v) ethanol for 30 minutes each, two changes of 100 % (v/v) ethanol for one hour each, three changes of xylene for one hour each and finally two changes of molten paraffin wax for two hours then one hour. Once the tissue processing was finished, samples were removed and kept in molten paraffin wax in an oven. Histology moulds were filled with molten paraffin wax and samples were immediately oriented in moulds using heated forceps. These were allowed to cool and harden before removing the wax blocks from moulds and trimming excess wax.

2.2.5.2.2 Sectioning

Paraffin wax blocks were cooled on ice to facilitate sectioning. These were then sectioned to 6 µm using a microtome. Sections were removed and carefully floated in a

histology water bath at 40 °C and collected onto SuperFrost glass slides each with two to four sections (Figure 2.4). Slides were placed on a hot plate for 30 minutes to aid adherence to the slide then placed on a rack to dry overnight.

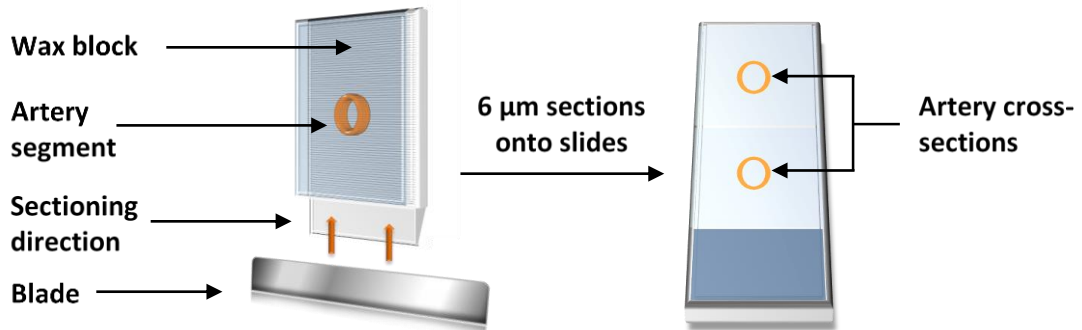


Figure 2.4: Schematic of sectioning of wax embedded arteries. *Wax embedded arteries were sectioned to 6 μm then collected onto SuperFrost glass slides.*

2.2.5.2.3 Dewaxing and Rehydration

Slides containing sections were placed in a metal slide holder and immersed in two changes of xylene, each for ten minutes to remove the paraffin wax. Slides were rehydrated by immersing in four changes of ethanol: 100 % (v/v) for three minutes, 100 % (v/v) for two minutes, 100 % (v/v) for two minutes and 70 % (v/v) for two minutes. They were then washed with running tap water for three minutes.

2.2.5.2.4 Haematoxylin and Eosin (H & E) Staining

Samples were dewaxed and rehydrated as described in Section 2.2.5.2.3, immersed in haematoxylin for one minute then rinsed under running tap water until the water ran clear. These were then immersed in Scott's tap water that was used for blueing the haematoxylin stain for three minutes then rinsed with running tap water for another three minutes. Samples were then immersed in eosin stain for three minutes then dehydrated by immersing in four changes of ethanol: 70 % (v/v) for five seconds, 100 % (v/v) for one minute, 100 % (v/v) for two minutes and 100 % (v/v) for three minutes. Finally, samples were immersed in xylene twice each for 10 minutes. To mount the slides, a drop of DPX mountant was added to each section on the slide inside a fume cupboard and a coverslip was placed on slides ensuring absence of bubbles then left

overnight to dry. Images were acquired digitally using a Zeiss upright microscope under normal Kohler illumination.

2.2.5.2.5 DAPI Staining

Samples were dewaxed and rehydrated as described in Section 2.2.5.2.3 then immersed in DAPI working solution (prepared as in Section 2.1.9) in the dark for ten minutes. Samples were then washed three times using PBS in the dark, each for ten minutes. Two drops of Dako fluorescence mounting medium were added to each slide and a coverslip was placed on the slide. These were stored in the dark overnight until the mounting medium was set. Slides were stored at 4 °C in the dark for short-term storage or at - 20 °C for long-term storage. Images were acquired using a Zeiss upright fluorescent microscope with a DAPI filter (excitation: 353 nm, emission/detection: 465 nm) to view the double-stranded DNA and a green fluorescent protein (GFP) filter (excitation: 488 nm, emission/detection: 509 nm) to view the extracellular matrix (ECM) structure due its auto-fluorescence.

2.2.5.3 DNA Isolation and Quantification

DNA isolation was carried out as per the Qiagen DNeasy Blood and Tissue Kit manufacturer's instructions. Tissue was macerated and placed in a 2 mL Eppendorf (wet weight; 25 - 50 mg of cellular tissue and 100 - 250 mg of acellular tissue). Buffer ATL (tissue lysis buffer, 180 µL for cellular and 360 µL for acellular tissue) and proteinase K (20 µL for cellular and 40 µL for acellular tissue) were added to tissue and the solutions were mixed thoroughly by vortexing. The samples were digested overnight at 56 °C with shaking at 900 rpm, after which they were vortexed for 15 seconds. Buffer AL (lysis buffer, 200 µL for cellular and 400 µL for acellular tissue) and 100 % (v/v) ethanol (200 µL for cellular and 400 µL for acellular tissue) were premixed thoroughly using a vortexer then added to digested samples and vortexed. Solutions of 600 µL were then transferred into DNeasy Mini Spin Column in a 2 mL collection tube and centrifuged for one minute at 6,000 x g, after which the solution was discarded. This step was repeated with the remaining 600 µL of acellular tissue solution. Following that, 500 µL of buffer AW1 (wash buffer 1) was added and samples were centrifuged for one minute at 6,000 x g, after which the solution was discarded. Buffer AW2 (wash buffer 2, 500 µL) was added, then samples were centrifuged for five minutes at 16,100 x g then the

solution and collection tube were discarded. The DNeasy Mini Spin Column was then transferred into a 2 mL Eppendorf and 200 μL of Buffer AE (elution buffer) was added directly to the DNeasy membrane. This was incubated at room temperature for one minute then centrifuged for one minute at 6,000 $\times g$ to elute. The final step was repeated to maximise DNA yield. The elute (400 μL) was stored at 4 $^{\circ}\text{C}$ for short-term use and at - 20 $^{\circ}\text{C}$ for long-term use. This process is summarised in Figure 2.5.

The DNA concentration was determined at an absorbance of 260 nm using a NanoDrop spectrophotometer ND-1000 with the associated software ND-1000 V3.7.1. The instrument was blanked against buffer AE before taking the reading of each sample (2 μL of sample/buffer was used) and the total DNA concentration was recorded in three replicates of each sample. The DNA concentration was measured in $\text{ng}\cdot\mu\text{L}^{-1}$, which was normalised to ng of DNA per mg of digested wet tissue taking the volumes used into account as in Equation 2.2.

Equation 2.2: Calculating the DNA concentration per weight of tissue.

$$\text{DNA concentration (ng/mg)} = \frac{\text{Concentration (ng/}\mu\text{L)}}{\text{Tissue wet weight (mg)}} \times \text{Elute volume (}\mu\text{L)}$$

Data were analysed for significant difference between cellular controls and acellular tissue using one-way ANOVA and post-hoc Tukey's test ($p < 0.05$; Section 2.3)

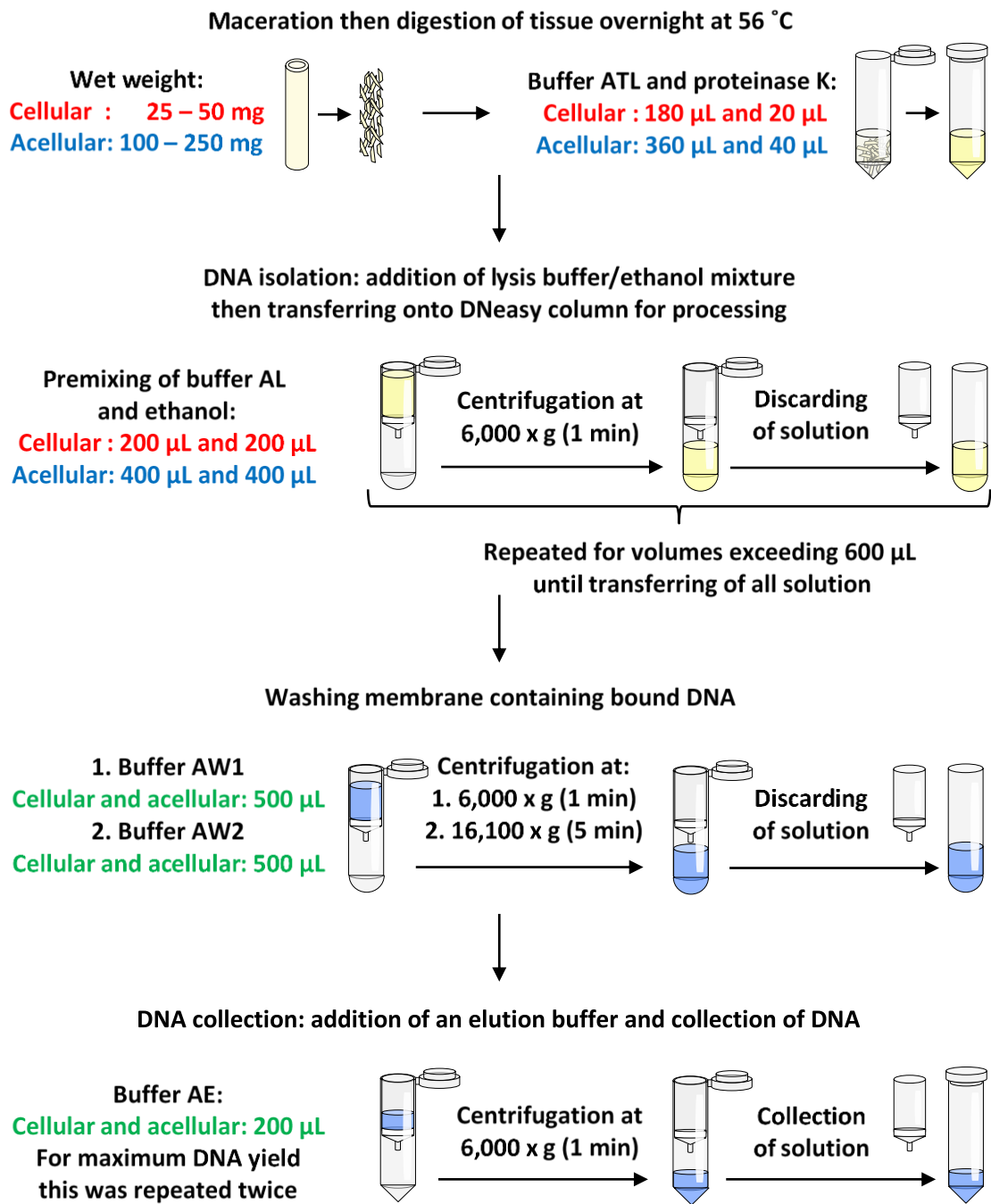


Figure 2.5: Flow diagram showing the process of DNA isolation from tissue. *Font colour represents different samples; red for cellular tissue, blue for acellular tissue and green for both cellular and acellular tissues.*

2.2.6 Biocompatibility

The initial *in vitro* biocompatibility of acellular arteries was tested for each batch using two different cytotoxicity assays and two distinct cell lines; BHK and L929. This was assessed by growing cells in contact with the acellular tissue (contact cytotoxicity assay)

or with the tissue extract (extract cytotoxicity assay) and comparing the results of the test to a negative control and a positive control to establish the biocompatibility of acellular arteries prior to any *in vivo* studies. Therefore, in this thesis, the term 'biocompatibility' refers to a reduced cytotoxicity of acellular tissue.

For the following assays, BHK and L929 cells were resurrected (Section 2.2.3.1), passaged (Section 2.2.3.2) then cells were counted as described in Section 2.2.3.3. The appropriate number of cells was suspended in the appropriate supplemented cell culture medium.

2.2.6.1 Contact Cytotoxicity Assay

Sections of 0.5 mm² were obtained from the end regions of acellular arteries. Sections of each sample were fixed in the middle of wells in a six-well plate with steri-strips using sterile forceps ensuring it was stuck properly to the bottom of the well. Steri-strips were fixed into one of the wells and treated as a negative control. A drop of cyanoacrylate contact adhesive (superglue) was added to the centre of another well and treated as a positive cytotoxic control. Cells were added to one of the wells and this was used for observing cell behaviour (Figure 2.6).

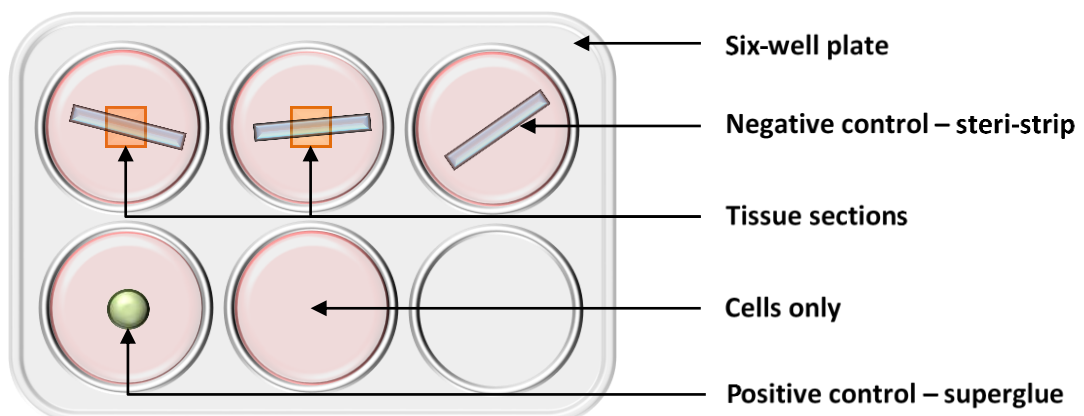


Figure 2.6: Schematic diagram of contact cytotoxicity assay set-up in a six-well plate. *In wells: superglue was the positive control displaying a cytotoxic effect to cells; steri-strip was the negative control, which is non-cytotoxic to cells; cells alone to serve as a cell control for observing their behaviour; and acellular tissue sections fixed in place with non-cytotoxic steri-strips to assess their cytotoxicity to cells.*

Wells were washed three times each for ten minutes using 2 mL of PBS without calcium and magnesium. Cell suspensions of BHK and L929 were prepared at a concentration of 250,000 cells.mL⁻¹ (cells were counted as in Section 2.2.3.3) and 2 mL of the cell suspension was added to each well (500,000 cells per well). These were incubated at 37 °C with 5 % (v/v) CO₂ in air for 48 hours. The medium was aspirated after incubation and wells were washed with PBS with calcium and magnesium. This was aspirated and 2 mL of 10 % (w/v) NBF was then added to wells to fix cells for ten minutes. NBF was aspirated and Giemsa stain was added to wells covering the cellular layer and plates were incubated for five minutes. Finally, wells were rinsed with running tap water until it ran clear and the plates were left to air dry before imaging. Cells were viewed under an inverted optical microscope before staining using the phase contrast mode and after staining using the bright field mode under normal Kohler illumination.

2.2.6.2 Extract Cytotoxicity Assay

Reagents

Double strength L929 cell culture medium (DMEM) (4 mM L-glutamine, 200 U.mL⁻¹ penicillin / 0.2 mg.mL⁻¹ streptomycin and 20 %; v/v FBS): L-glutamine (0.4 mL, 200 mM), penicillin (5000 U.mL⁻¹) / streptomycin (5 mg.mL⁻¹; 0.8 mL) and FBS (4 mL) were added to DMEM (14.8 mL). This was mixed by inversion and stored at 4 °C for up to one week. Cell culture medium was pre-warmed at 37 °C before use.

Double strength BHK cell culture medium (GMEM) (4 mM L-glutamine, 200 U.mL⁻¹ penicillin / 0.2 mg.mL⁻¹ streptomycin, 20 %; v/v TPB and 10 %; v/v FBS): L-glutamine (0.4 mL, 200 mM), penicillin (5000 U.mL⁻¹) / streptomycin (5 mg.mL⁻¹; 0.8 mL), TPB (4 mL) and FBS (4 mL) were added to GMEM (12.8 mL). This was mixed by inversion and stored at 4 °C for up to one week. Cell culture medium was pre-warmed at 37 °C before use.

Positive cytotoxic control (40 %; v/v DMSO): DMSO (8 mL) was added to non-supplemented DMEM (12 mL) aseptically.

Negative control: Non-supplemented DMEM.

ATPlite substrate: Substrate buffer (25 mL) was added to one bottle of lyophilised substrate and stored in aliquots of 5 mL at - 20 °C in the dark.

Procedure

The following procedure was carried out inside a class II safety cabinet to ensure sterility of tissue. Acellular tissue, 300 mg, was macerated, to which 3 mL of DMEM was added (the ratio was kept to 1 mL per 100 mg tissue depending on the amount of tissue). The solutions were incubated for 72 hours with 240 rpm agitation at 37 °C to obtain extracts. Following incubation, the sterility of extracts was ensured by streaking the extract onto nutrient agar and fresh blood agar plates, which were incubated at 37 °C for 48 hours and Sabouraud Dextrose agar, which was incubated at 30 °C for 48 hours. The extracts were stored at - 20 °C until sterility was assured by absence of contamination in agar plates following incubation (Figure 2.7).

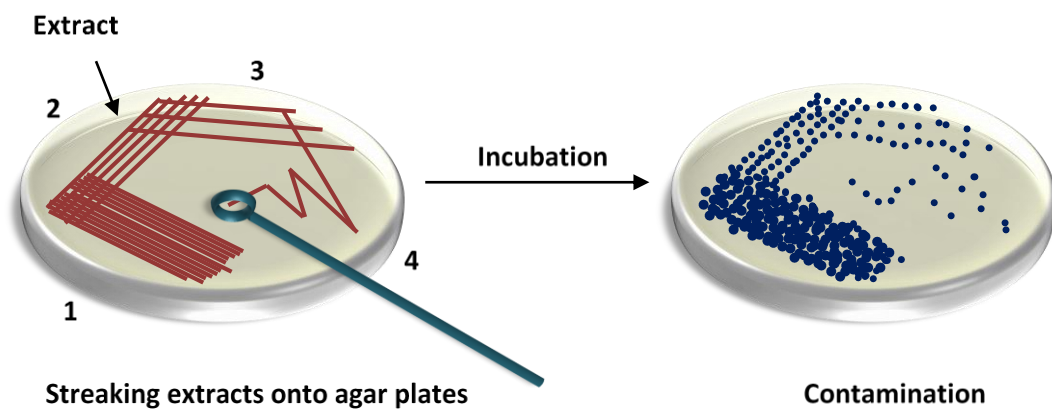


Figure 2.7: Schematic diagram showing streaking of extract onto an agar plate to test for sterility. Extracts are streaked onto agar plates following the lines in the order: 1, 2, 3 and 4 (left). If the extract was contaminated then bacterial growth should be observed in areas of streaking (right), otherwise extracts were sterile and ready for use.

Once sterility was confirmed, cell suspensions containing 50,000 cells.mL⁻¹ for BHK and 125,000 cells.mL⁻¹ for L929 were prepared (cells were counted as described in Section 2.2.3.3). Cell suspension, 200 µL, was added to flat-bottomed wells in a 96-well plate in three replicates for each sample and control (BHK 10,000 cells per well and L929 25,000 cells per well). These were incubated for 24 hours at 37 °C with 5 % (v/v) CO₂ in air. Medium was aspirated from wells after incubation, 100 µL of the appropriate double strength cell culture media were added immediately to appropriate wells. After thawing extracts at 37 °C, 100 µL was added to wells containing 100 µL of double strength medium in three replicates. Positive control containing DMSO in non-

supplemented DMEM, 100 μ L, was added to wells containing 100 μ L of double strength medium (20 %; v/v DMSO). For the negative control, 100 μ L of non-supplemented DMEM was transferred into wells. These were incubated at 37 °C with 5 % (v/v) CO₂ in air for 24 hours. Following incubation, 200 μ L medium was aspirated from each well and 50 μ L of the appropriate cell culture medium as well as 50 μ L of mammalian cell lysis solution (incubated at room temperature prior use) were added to the appropriate wells. Plates were incubated at room temperature for five minutes while shaking in a microshaker. Mammalian cell lysis solution released the ATP content into solution due to lysis of cells, which was measured using ATPlite™ assay. Solutions were then transferred into 96-well OptiPlates, following which 50 μ L of substrate solution was added to all wells and OptiPlates were sealed, covered with foil and incubated at room temperature while shaking using a microshaker for five minutes. Absence of bubbles in wells was ensured by briefly sweeping the blue flame from a Bunsen over the wells if bubbles were present to avoid melting the OptiPlate. OptiPlates were covered with a TopSeal cover and the luminescence from each well was determined using the Chameleon microplate reader and ATP2007 software. The determined relative ATP content (CPS) was plotted for all samples and controls in BHK and L929 using GraphPad Prism. Data were analysed for significant difference using one-way ANOVA and post-hoc Tukey's test ($p < 0.05$; Section 2.3).

2.2.7 Preparation of Peptide Samples

2.2.7.1 Preparation of Peptides at Physiological Conditions

Peptides were weighed out at the required mass and deionised water was added to the peptide to make 9/10 of the final volume. This was vortexed and subsequently sonicated for ten minutes at room temperature. The peptide was then monomerised ensuring homogeneous distribution of peptide in solution for a more uniform gel formation upon self-assembly. This was carried out by pH adjustment ($pH > 8$ for P₁₁₋₄ and $pH < 4$ for P₁₁₋₈ and P₁₁₋₁₂) using 2.5, 1, 0.5, 0.1, 0.05 and 0.01 M of HCl/NaOH (unless otherwise stated). The pH was then brought to physiological pH 7.4 by using HCl/NaOH and the mixture was left overnight. Ionic strength was chosen as a trigger for self-assembly. Therefore, Ringer's solution, 10X strength, was added to the peptide at 1/10 of the final volume and left overnight to allow self-assembly to occur. Peptide gels

were characterised after one day of triggering self-assembly unless otherwise stated. The procedure of peptide monomerisation and self-assembly triggering by changing the ionic strength of solution is described in Figure 2.8.

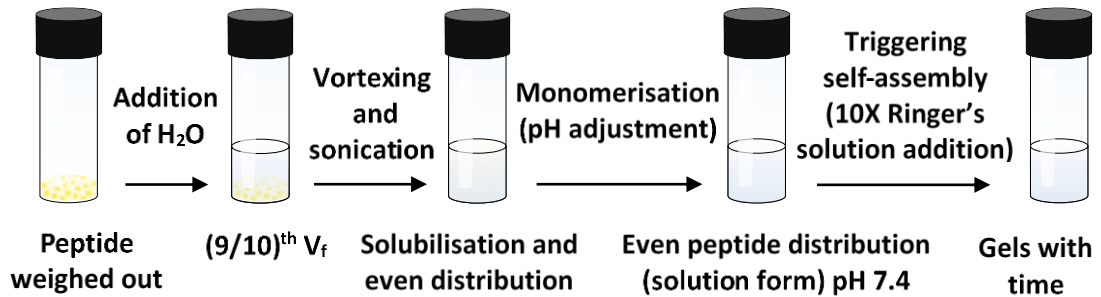


Figure 2.8: Schematic diagram showing the peptide gelation procedure by changing the ionic strength at physiological pH. Ionic strength was changed by addition of 10X strength Ringer's solution. V_f is the final volume of peptide.

2.2.7.2 Preparation of Functionalised Peptides at a Molar Ratio

For studies in which a functionalised peptide was required to be incorporated into the gel, a stock solution of the functionalised peptide was prepared at a higher molar ratio than that required. This was then diluted in the peptide solution to achieve the required final concentration (Equation 2.3). The appropriate amount of non-functionalised peptide was weighed out taking into consideration the required weight of functionalised peptide. Deionised water was then added at a certain volume calculated as shown in Equation 2.4. this was followed by monomerisation then triggering self-assembly of peptide as described in Section 2.2.7.1.

Equation 2.3: An equation to calculate the volume of stock solution required (V_{stock}) to make the intended working concentration ($C_{working}$) using the final peptide volume ($V_{working}$) and the final concentration of stock (C_{stock}).

$$V_{stock} = \frac{V_{working} \times C_{working}}{C_{stock}}$$

Equation 2.4: An equation to calculate the volume of water required.

$$V_{water} = \left(\frac{9}{10} \times V_{working}\right) - V_{stock}$$

2.2.7.3 Peptide Self-assembly within Acellular Tissue

To self-assemble peptides within acellular tissue, procedures described in Section 2.2.7.1 or Section 2.2.7.2 if a functionalised peptide was to be used were followed. The acellular tissue section (unless otherwise stated) was added after the monomerisation and change of pH to 7.4 steps and left overnight in peptide solution as before, allowing penetration of the peptide through the tissue ECM. After leaving overnight, peptide self-assembly was triggered by changing the ionic strength of solution by addition of 10X strength Ringer's solution. Again, this mixture was left overnight to allow for self-assembly within the acellular tissue. The procedure of triggering peptide self-assembly within acellular tissue by changing the ionic strength of solution is described in Figure 2.9.

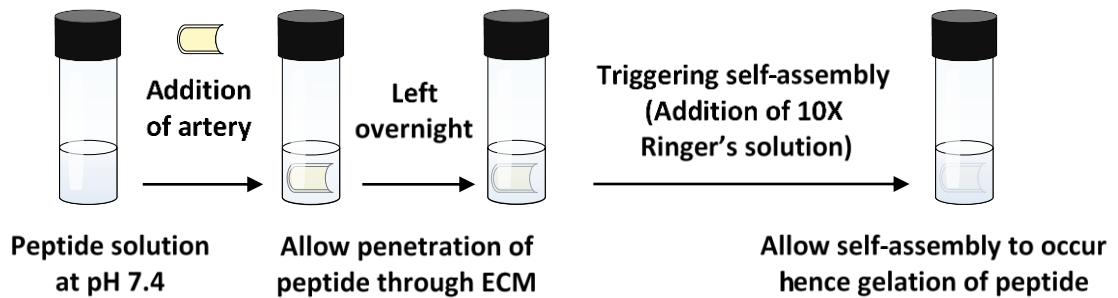


Figure 2.9: Schematic diagram showing inclusion of acellular artery tissue section (or segment as specified) within the peptide solution procedure at physiological pH.

2.2.8 Synthesis of Functionalised Peptides

FITC-labelled peptides and cell attachment motifs were synthesised by solid phase peptide synthesis (SPPS) using Fmoc (9-fluorenylmethoxycarbonyl) chemistry. The Fmoc-protected amino acid building blocks used in the synthesis are listed in Figure 2.10. Peptides functionalised with cell attachment motifs were synthesised by click chemistry between the azide-functionalised P₁₁ peptides and alkyne-functionalised cell attachment motifs.

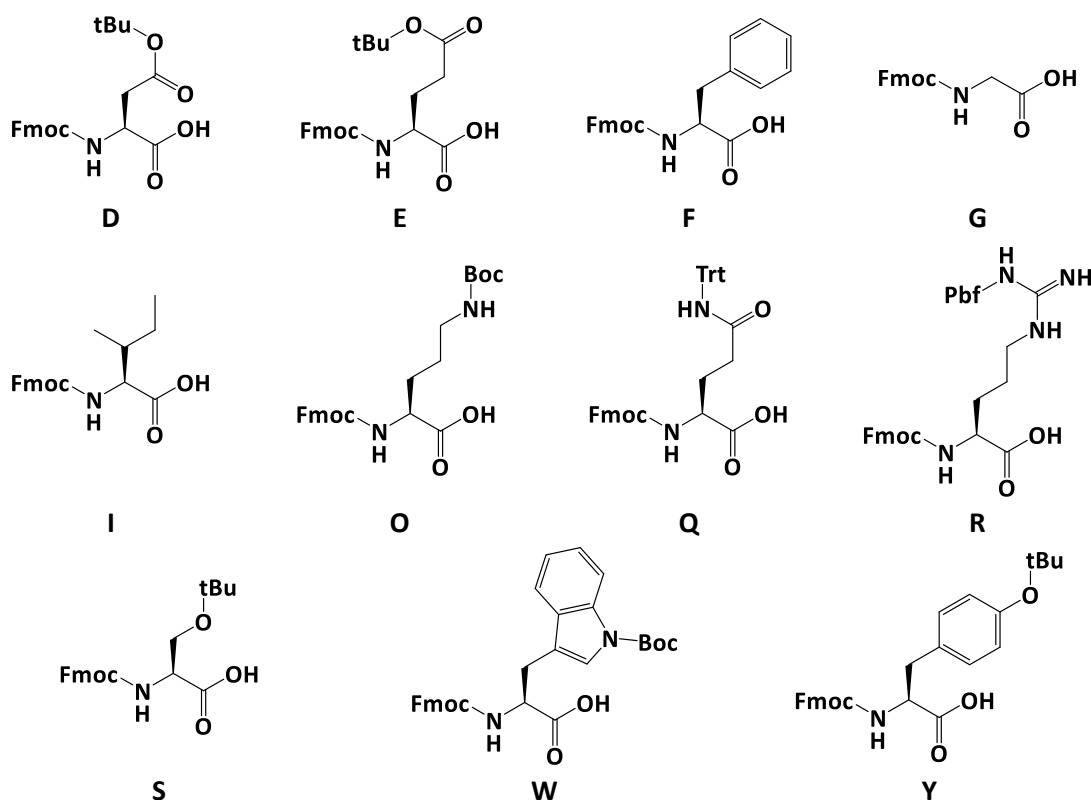


Figure 2.10: N-terminal Fmoc-protected amino acid building blocks used for the synthesis of FITC-labelled peptides and cell attachment motifs. *Letters under structures represent the one letter code for amino acid.*

2.2.8.1 FITC-labelled Peptides

FITC-labelled peptides were synthesised using Rink amide NovaGel™ resin with a loading capacity of 0.5 - 0.7 mmol.g⁻¹ (Figure 2.11). The resin, was swelled in DMF in a reaction vessel for one hour before loading. The first Fmoc-protected amino acid was coupled to the resin using Oxyma Pure® and DIC (all at 5 equivalents). This was repeated out until the resin was fully loaded. Complete resin loading was checked by performing

the Kaiser test (Section 2.2.8.4), a yellow colour was observed when all the resin sites were occupied.

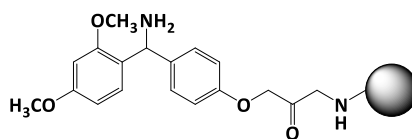


Figure 2.11: Rink amide NovaGel™ resin used for the synthesis of FITC-labelled peptides.

The next Fmoc-protected amino acids in the chain were coupled using DIPEA and HCTU (all at 5 equiv) in excess of DMF for one hour each. Fmoc group deprotection was carried out after each coupling of Fmoc-protected amino acid in order to allow the next residue to be coupled by exposing the N-terminus. This was achieved by three washes of 20 % (v/v) piperidine in DMF for five minutes each and two minutes DMF washes in between followed by final five two minutes DMF washes to ensure removal of any residual piperidine before the following coupling. FITC was then coupled to the peptide using DIPEA (all at 2 equiv) in excess of DMF for two hours in the dark.

Finally, peptides were cleaved from the resin and side-chain protecting groups were removed simultaneously by treatment with TFA mixture (5 mL per 1 g of resin; 95 % (v/v) TFA, 2.5 % (v/v) TIPS and 2.5 % (v/v) DCM) for six hours then peptide containing cleavage cocktail was separated from resin by filtration. TFA was then removed by evaporation and the resulting crude peptide was precipitated in diethyl ether then isolated by centrifugation in three changes of diethyl ether at - 20 °C for ten minutes each. The precipitated peptide was left overnight to remove the diethyl ether. Once dried, crude peptide was dissolved in water, lyophilised then redissolved in water before purification as described in Section 2.2.8.5.

2.2.8.2 Cell Attachment Motifs (Alkyne-functionalised Peptides)

Cell attachment motifs were synthesised using NovaSyn®TG Sieber resin with a loading capacity 0.1 - 0.25 mmol.g⁻¹ (Figure 2.12). The resin was first swelled in DMF in a reaction vessel for 30 minutes. This resin is Fmoc-protected therefore, deprotection was carried out using a 15 minute wash in 20 % (v/v) piperidine in DMF followed by three DMF washes before loading the resin. The first Fmoc-protected amino acid in the chain (propargylglycine) was coupled using Oxyma Pure® and DIC (all at 2.5 equiv) in

excess of DMF for one hour. This was repeated with 0.5 equiv of reagents until the resin was fully loaded. Full loading of the resin was confirmed by performing the Kaiser test (Section 2.2.8.4).

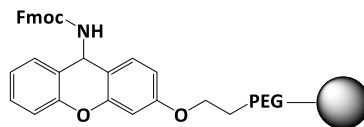


Figure 2.12: NovaSyn®TG Sieber resin used for the synthesis of cell attachment motifs.

The peptide chain was then assembled by stepwise coupling and Fmoc deprotection as described for FITC-labelled peptides (Section 2.2.8.1). The Fmoc-protected amino acids were coupled using Oxyma Pure® and DIC (all at 2.5 equiv for the (PEG)₂ spacer and 5 equiv for the amino acids in the chain). The N-terminus of the peptide chain was then acetylated to prevent a charge at the N-terminus using acetic anhydride (5 equiv) and DIPEA (10 equiv) in excess of DMF for one hour. The resin was then washed several times with DMF to remove any residues then isolated as described for FITC-labelled peptides (Section 2.2.8.1) with the TFA treatment carried out for four hours then purified as described in Section 2.2.8.5.

2.2.8.3 P₁₁ Peptides Functionalised with Cell Attachment Motifs

P₁₁ peptides were functionalised with cell attachment motifs (synthesised as described in Section 2.2.8.2) using copper catalysed click chemistry between an azide group on the N-terminus of the P₁₁ peptide (purchased from Cambridge Research Biochemicals) and an alkyne group on the C-terminus of the cell attachment motif.

Click reactions were carried out in a 3 mL scale mixture of azide and alkyne functionalised peptides, reducing reagent, stabilising ligand and a catalyst all at a final concentration of 1 mM in 50 mM sodium phosphate at pH 7.4. Sodium phosphate buffer (1.5 mL, 100 mM at pH 7.4) was added to a reaction vessel and degassed in nitrogen gas for five minutes, to which; azide-functionalised peptide (300 µL, 10 mM in DMSO), alkyne-functionalised peptide (300 µL, 10 mM in DMSO), sodium ascorbate (300 µL, 10 mM in water), TBTA (300 µL, 10 mM in DMSO) and copper (II) sulphate (300 µL, 10 mM in water) were added to phosphate buffer respectively to give a molar ratio of 1:1:1:1:1 of the components. The mixture was stirred using a magnetic stirrer during each addition then reaction left for 48 hours at 40 °C in the dark while stirring.

This procedure was carried out for each of the P₁₁ peptides functionalised with cell attachment motifs (eight reactions). The mixture was dissolved in water containing 10 % (v/v) DMSO, lyophilised and then redissolved in water before purification as described in Section 2.2.8.5.

2.2.8.4 Kaiser Colour Test

In order to ensure complete coupling in SPPS, the Kaiser test was carried out before adding the next amino acid in the chain preventing formation of peptide chains with missing residues hence having incorrect structures. In this test, two drops of the Kaiser test reagents (5 %; w/v ninhydrin in ethanol, 80 %; w/v phenol in ethanol and 2 %; v/v 1 mM KCN in pyridine) were added to a small amount of resin to be tested, then heated and left to develop for five minutes. A colour change determines the outcome, where a negative test indicative of a complete coupling reaction is observed by a yellow solution. However, a positive test is indicated by development into a blue colour requiring a further coupling.

2.2.8.5 Peptide Purification

Peptides were dissolved in water containing DMSO and ammonia for P₁₁₋₄ peptides or DMSO and acetic acid for P₁₁₋₈ and P₁₁₋₁₂ peptides. All peptides were purified using Biotage® Isolera™ One instrument using a RediSep Rf Gold® Reversed-phase C18 high performance column. The eluents used for purification were water (H₂O, HPLC grade) and acetonitrile (MeCN, HPLC grade) both with either 0.1 % (v/v) TFA or ammonia over an increasing gradient of acetonitrile. Different purification conditions were used for different peptides (Table 2.5). Acetonitrile was removed using Genevac EZ-2 personal evaporator followed by lyophilisation of peptide. The lyophilised peptides were stored at - 20 °C until use.

Table 2.5: Conditions used for purification of synthesised peptides including: solvent in which peptide was solubilised, gradient of water to acetonitrile (%) for purification, additives to solvent and wavelength at which UV detection occurred.

Peptide	Solvent	Water to Acetonitrile Gradient (%)	Additives 0.1 % (v/v)	UV Detection (nm)
FITC-labelled Peptides				
FITC-P ₁₁ -8	Acetic acid and DMSO in water	Initial: 90 - 10 Final: 10 - 90	TFA	242 495
FITC-P ₁₁ -12				
FITC control				
Cell Attachment Motifs and Their Scrambled Controls				
GRGDS GRDGS	DMSO in water	Initial: 95 - 5 Final: 5 - 95	TFA	220
YIGSR YIRSG				220 275
Peptides Functionalised with Cell Attachment Motifs				
GRGDS-P ₁₁ -4 GRDGS-P ₁₁ -4	Ammonia and DMSO in water	Initial: 95 - 5 Final: 5 - 95	Ammonia	220 254
YIGSR-P ₁₁ -4 YIRSG-P ₁₁ -4				254 275
GRGDS-P ₁₁ -8 GRDGS-P ₁₁ -8	Acetic acid and DMSO in water	Initial: 95 - 5 Final: 5 - 95	TFA	220 254
YIGSR-P ₁₁ -8 YIRSG-P ₁₁ -8				254 275

2.2.8.6 Analysis of Synthesised Peptides

Following synthesis, peptides (0.1 - 0.5 mg.mL⁻¹) were analysed using liquid chromatography-mass spectrometry (LC-MS) and accurate mass spectrometry to confirm their structures by comparing the determined molecular weights with the calculated ones. Their purity (%) was assessed using an analytical high performance liquid chromatography (HPLC) as described in Appendix A.6 (carried out by Martin Huscroft, School of Chemistry, University of Leeds).

2.2.9 Characterisation of Peptide Gels

2.2.9.1 Fourier Transform Infrared (FTIR) Spectroscopy

Peptide samples were prepared as described in Section 2.2.7.1, in which deuterium oxide (D₂O) was added to the lyophilised peptide (instead of water), peptide was monomerised then pD adjusted to 7.4 (Equation 2.5) using 2, 1, 0.5 and 0.1 M DCl/NaOD and finally, self-assembly was triggered by addition of 10X strength Ringer's

solution in D₂O and incubated at 37 °C until each FTIR spectrum was recorded. Control solutions were taken through the same pD adjustment as samples.

Equation 2.5: An equation to calculate pD from uncorrected pH reading (pH*).

$$\text{pD} = \text{pH}^* + 0.4$$

At each time point, peptide samples and controls (35 - 45 μL) were transferred to a cell with two calcium fluoride windows separated by a 0.025 mm copper spacer. All FTIR cell components were cleaned with methanol before/after each FTIR reading. FTIR spectra were recorded using a Nicolet 6700 FTIR spectrometer and were processed using the associated OMNIC software. Individual peptide FTIR spectra were obtained by subtraction of the control spectrum from that of peptide. Spectra were analysed by fitting the peaks in the amide I' region (1580 - 1720 cm^{-1}) using the peak analysis tool. Fitted peaks were used for determination of the secondary structures present in peptide samples (Table 2.6).

Table 2.6: Absorption ranges in the amide I' region and their corresponding secondary structure, amino acid side chain or impurities. Highlighted wavenumbers correspond to β -sheets¹⁹⁴⁻¹⁹⁶.

Wavenumber (cm^{-1})	Secondary Structure, Amino Acid or <u>Impurity</u>
1586 1608	<i>Arginine</i>
1613 - 1630	β-sheet
1635 - 1654	<i>Glutamine</i>
1642 - 1649	Unordered
1649 - 1655	α -helix
1658 - 1674	Turn
1673	<u>TFA</u>
1682 - 1690	β-sheet
1694 - 1697	Turn

The presence of TFA counterions gives a strong absorption at 1673 cm^{-1} and should be taken into account when fitting and assigning peaks¹⁹⁷, especially in peptides having positively charged residues in the chain. This is because TFA is used in the peptide purification process by the reversed-phase HPLC and is often bound to positively

charged residues as a counterion, hence can be present as an impurity^{198,199}. The proportion of TFA present in a peptide is therefore dependent on the number of positively charged residues in the peptide chain such as arginine and ornithine.

The percentage of β -sheet secondary structures present in the peptide sample was then calculated using Equation 2.6.

Equation 2.6: An equation to calculate the percentage of secondary structures observed in an FTIR spectrum of peptides.

$$\% \text{ Secondary structure} = \frac{\text{Area under secondary structure peaks} \times 100}{\text{Total area under peaks of all secondary structures}}$$

Spectra were collected at 0, 1, 7, 14 and 28 days following triggering self-assembly in three replicates for each peptide at each concentration tested (unless otherwise stated). Data were analysed for significant difference using two-way ANOVA (Section 2.3).

2.2.9.2 Transmission Electron Microscopy (TEM)

TEM grids were prepared by Martin Fuller (Faculty of Biological Sciences, University of Leeds), where Hexagon 400 mesh 3 mm diameter copper grids (3.05 mm) were coated with a 10 nm layer of carbon.

Peptide samples prepared for FTIR (Section 2.2.9.1) were also used for TEM investigation. These were tested at 10-fold dilution and 100-fold dilution in deuterium oxide (unless otherwise stated) because they formed gels consisting of a dense fibrillar network that were difficult to investigate under the TEM in their gel form. A drop of the undiluted/diluted peptide (7 μ L) was immediately placed on a piece of Parafilm[®] alongside a drop of the negative stain (1 %; w/v uranyl acetate, 7 μ L). After placing the drops of peptide and negative stain on the Parafilm[®], the grids were floated on the peptide drop first for 30 seconds then on the uranyl acetate drop for another 30 seconds. Following staining, a filter paper was used to absorb any remaining solution from the grids ensuring they were dry before imaging (Figure 2.13)

Images of the negatively stained peptide samples were acquired using a JEOL JEM-1400 Plus TEM at 120 KeV with the associated software AMT Image Capture Engine V602. Images were processed using ImageJ software for determination of fibril widths. Data were analysed for significant difference using two-way ANOVA (Section 2.3).

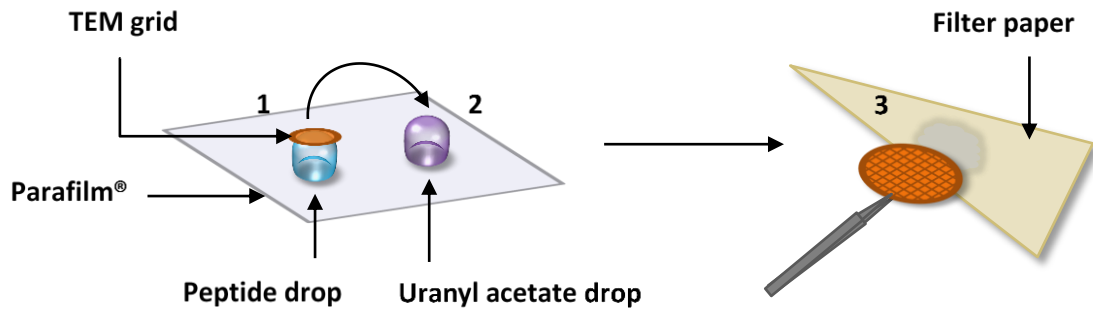


Figure 2.13: Schematic diagram showing the preparation of TEM grids. 1) The TEM grid floated on peptide drop for 30 seconds, then 2) floated on the uranyl acetate drop for another 30 seconds and finally 3) the remaining solution absorbed on filter paper ensuring the TEM grid was dry before imaging.

2.2.10 Chandler Loop Model

Reagents

Calcium chloride solution (250 mM): Calcium chloride dihydrate (3.68 g) was dissolved in distilled water (100 mL) and the pH was adjusted to 7.4. The solution was sterilised by autoclaving and was stored at room temperature for up to one month.

Dilute α -thrombin solution: Human α -thrombin (2 μ L) was added to distilled water (98 μ L) and mixed by inversion.

Procedure

Medical grade polyvinyl chloride (PVC) tubing with an internal diameter of 4 mm and an outer diameter of 5 mm was cut into 35 cm lengths using a sterile scalpel to get straight ends avoiding presence of gaps when the two ends were connected. The two ends of tubing were connected using 1 cm medical grade PVC with an internal diameter of 5 mm and an outer diameter of 8 mm. Peptides were prepared at concentrations of 4.95 mM and 49.5 mM to achieve final concentrations of 0.3 mM (monomeric form) and 3 mM (self-assembled form) in blood, respectively. Peptides were prepared by addition of 1 mL of distilled water to the lyophilised peptides. These were mixed by pipetting up and down then vortexing before carrying out the test. TBS, 0.6 mL, 50 μ L of 250 mM calcium chloride, 100 μ L of peptides or controls (dilute α -thrombin solution as the positive control and distilled water as the negative control) and 0.9 mL of citrated sheep blood were mixed together. Blood mixture was prepared in six replicates for each

sample/control then immediately transferred to the tubing by a syringe, using a large needle gauge to avoid damaging red blood cells, at a steady speed to avoid formation of air bubbles. The tubing was placed on a rotator and was spun at room temperature at 30 rpm for 90 minutes (Figure 2.14).

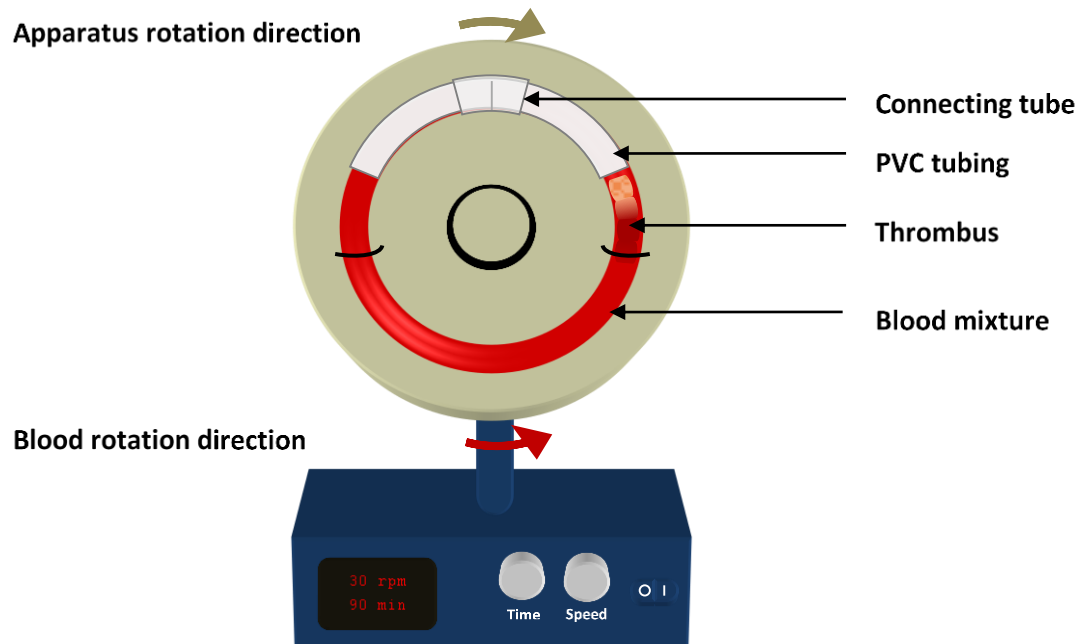


Figure 2.14: Schematic diagram of Chandler loop model experimental set-up. *The apparatus was rotated clockwise hence blood in tubing rotated anti-clockwise and thrombus was formed at the interface between blood mixture and air in tubing at the leading end.*

The loops were then emptied immediately and thrombi were removed using forceps and weighed (wet weight). Data were analysed for significant difference using one-way ANOVA test (Section 2.3).

2.2.11 Characterisation of Peptide Self-assembly within Acellular Arteries

2.2.11.1 Field Emission Gun Scanning Electron Microscopy (FEGSEM)

Acellular arteries were produced as described in Section 2.2.4 and were assessed for their acellularity (Section 2.2.5) and *in vitro* biocompatibility (Section 2.2.6). The acellular artery was washed in three changes of deionised water then cut into sections. The sections were then fixed in 10 % (v/v) NBF at room temperature for four hours and washed in three changes of deionised water to remove any NBF residues. Peptides were self-assembled within acellular arteries as in Section 2.2.7.3 by adding water to the

lyophilised peptide, monomerising the solution and changing the pH to 7.4 then triggering self-assembly using Ringer's solution. One day after triggering self-assembly, excess peptide was gently scraped off the surfaces of acellular artery sections which were then flattened on tinfoil in a petri-dish with the surface to be imaged facing upwards and they were left to dry in air for three days ensuring all water was removed before imaging. After ensuring that samples were fully dry, they were mounted on SEM stubs by placing carbon discs with double adhesive surfaces on the stub. The surface and the edges of the sample were coated with carbon paste and dried then samples were coated with a thin layer of 5 nm platinum. Samples were imaged using FEI Quanta 200 FEGSEM at 5 KeV using the secondary electron imaging.

2.2.11.2 Fluorescent Microscopy

Stock FITC-labelled peptide solution was made at 1:10 molar ratio of the FITC-labelled to the non-FITC-labelled peptides, which was then diluted to 1:150 molar ratio when added to non-FITC-labelled peptide solutions (unless otherwise stated). FITC-labelled peptide solutions were prepared in water, monomerised and the pH was adjusted to pH 7.4 as described in Section 2.2.7.2. Adjustment of pH was achieved using 2.5, 1, 0.5, 0.1, 0.05 and 0.01 M NaOH/HCl. Control samples were taken through the same pH adjustment as peptide samples. Before triggering self-assembly, unfixed acellular artery samples were placed in peptide solutions/controls, left overnight then 10X strength Ringer's solution was added as described in Section 2.2.7.3. Following triggering self-assembly, samples to be imaged were immersed in water using forceps to remove excess peptide on the surface then excess water was absorbed onto paper tissue by placing the edge of the sample on paper tissue. Samples were then embedded in a cryostat embedding solution (OCT compound mounting medium for cryotomy) inside plastic moulds. These were left inside the cryostat on a cold stage until they were solidified. After solidification, the blocks were removed from moulds and oriented on a cryostat stage at the desired direction and cryosectioning was carried out at 6 μm thickness sections at - 23 °C. Four sections were collected on a SuperFrost slide and stored at - 20 °C in the dark until use.

Images were acquired within 24 hours of sectioning using a Zeiss fluorescent upright microscope with a FITC filter (detection at 519 nm) using Zen software that was also used for image processing.

2.2.11.3 Multiphoton Laser Scanning Microscopy (MPLSM)

Stock FITC-labelled peptide solution was made at 1:10 molar ratio of the FITC-labelled to the non-FITC-labelled peptides, which was then diluted to 1:150 molar ratio when added to non-FITC-labelled peptide solutions (unless otherwise stated). FITC-labelled peptide solutions were prepared in water, monomerised and the pH was adjusted to pH 7.4 as described in Section 2.2.7.2. Adjustment of pH was achieved using 2.5, 1, 0.5, 0.1, 0.05 and 0.01 M NaOH/HCl. Control samples were taken through the same pH adjustment as peptide samples. Before triggering self-assembly, unfixed acellular artery samples were placed in peptide solutions/controls, left overnight then 10X strength Ringer's solution was added as described in Section 2.2.7.3. Following triggering self-assembly, the acellular tissue section was placed on a petri-dish with the surface to be investigated facing upwards and the sample was flattened by placing a coverslip on top and secured with steri-strips.

Images were acquired using MPLSM 710 Axio Examiner assisted by Dr Nagitha Wijayathunga, University of Leeds, using the second harmonic generation signal to visualise collagen and the two-photon excitation to visualise elastin that is auto-fluorescent. The peptide was imaged using the FITC signal. Images were processed in Zen software.

2.2.12 Isolation, Maintenance and Characterisation of Ovine Femoral Endothelial Cells

2.2.12.1 Isolation

Reagents

Antibiotic solution (300 U.mL⁻¹ penicillin / 0.3 mg.mL⁻¹ streptomycin): Penicillin (5000 U.mL⁻¹) / streptomycin (5 mg.mL⁻¹; 12 mL) was added to PBS with calcium and magnesium (188 mL). The solution was produced aseptically and used within 24 hours of production.

Collagenase type II stock (10 U.μL⁻¹): This was prepared as per the supplier's instructions. Collagenase type II (1 g, 215 U.mg⁻¹) was dissolved in Hank's balanced salt solution (HBSS) with calcium and magnesium (10 mL) and vortexed. HBSS with calcium

and magnesium (11.5 mL) was then added to the mixture. The solution was sterilised by filtration and aliquots of 500 μL were stored at $-20\text{ }^{\circ}\text{C}$ in the dark until use.

Working collagenase type II (0.5 %; w/v, 0.2 U. μL^{-1}): HBSS with calcium and magnesium (19.6 mL) was added to stock collagenase type II (400 μL , 10 U. μL^{-1}) and used immediately.

Endothelial cells growth supplement (ECGS; 3 mg. mL^{-1}): M-199 (5 mL) was added to 15 mg ECGS. This was stored at $-20\text{ }^{\circ}\text{C}$ until use.

M-199, endothelial cells culture medium (0.7 mM L-glutamine, 100 U. mL^{-1} penicillin / 0.1 mg. mL^{-1} streptomycin, and 20 %; v/v FBS, 75 $\mu\text{g}.\text{mL}^{-1}$ ECGS unless otherwise stated and 30 U. mL^{-1} heparin sodium): L-glutamine (0.7 mL, 200 mM), penicillin (5000 U. mL^{-1}) / streptomycin (5 mg. mL^{-1} ; 4 mL), FBS (40 mL), ECGS (5 mL, 3 mg. mL^{-1} , unless otherwise stated) and heparin sodium (6 mL, 1000 U. mL^{-1}) were added to M-199 (144.3 mL). This solution was mixed by inversion and stored at $4\text{ }^{\circ}\text{C}$ for up to one week. Cell culture medium was pre-warmed at $37\text{ }^{\circ}\text{C}$ before use.

Procedure

In a class II safety cabinet, femoral ovine arteries were aseptically dissected from ovine legs that were slaughtered the same morning. The ends of the artery were tied off with silk sutures and branches were also tied off along the dissection process to reduce any chances of contamination. Once dissected, the ties were removed from the ends of the artery which was placed in an antibiotic solution and incubated at $37\text{ }^{\circ}\text{C}$ for an hour. Following incubation, the inside of artery was washed thoroughly using a syringe filled with the antibiotic solution to remove blood or blood clots. Once cleaned from blood, one end of the artery was closed with a silk suture, a blunt needle was secured to the other end by a silk suture and a syringe was inserted to the needle to fill the artery with working collagenase solution then this was incubated for 30 minutes at $37\text{ }^{\circ}\text{C}$. The artery content was then emptied into a sterile universal tube followed by washing the inside of the artery with 10 mL PBS without calcium and magnesium. The content was centrifuged at $250 \times g$ for ten minutes, the supernatant was discarded in 1 % (w/v) Virkon and the cell pellet was suspended in 5 mL of M-199 endothelial cell culture medium then incubated in one T-25 tissue culture flask that was incubated at $37\text{ }^{\circ}\text{C}$ with

5 % (v/v) CO₂ in air. The medium was replaced every 48 hours with 5 mL of supplemented cell culture medium until cells reached approximately 80 % confluency.

2.2.12.2 Maintenance and Passaging

Upon reaching approximately 80 % confluency, the medium was removed from the flask and the cell layer was washed with 5 mL HBSS without calcium and magnesium for five minutes. This was subsequently removed and replaced with 1 mL trypsin/EDTA solution and was incubated at 37 °C with 5 % (v/v) CO₂ in air for no longer than three minutes. Trypsin was then neutralised by adding 5 mL supplemented cell culture medium, transferred into a sterile universal tube and centrifuged at 180 x g for ten minutes. The supernatant was discarded in 1 % (w/v) Virkon and the cell pellet was suspended in 5 mL supplemented cell culture medium. These were seeded into three flasks of the same size or one larger flask (5 mL for T-25, 10 mL for T-75 and 15 mL for T-175). Cells were incubated at 37 °C with 5 % (v/v) CO₂ in air and the medium was replaced every 48 hours for optimal growth until cells became 80 % confluent.

2.2.12.3 Cryopreservation

Endothelial cells were cryopreserved as described in Section 2.2.3.4 after passaging cells as described in Section 2.2.12.2.

2.2.12.4 Immunofluorescence

Reagents

Acetone and methanol mixture (1:1 volume ratio): Acetone (150 mL) was mixed with methanol (150 mL) and was used immediately.

Bovine serum albumin (BSA) solution (5 %; w/v): BSA (2.5 g) was dissolved in PBSa (50 mL). Solution was sterilised by filtration and aliquots of 5 mL were stored at - 20 °C for up to six months.

TBS containing 0.05 %; w/v Tween 20: Tween 20 (500 µL) was mixed with TBS (1 L) and the pH adjusted to 7.6. Solution was stored at room temperature for up to three months.

Antibody diluent TBS, (0.1 %; w/v sodium azide, 0.1 %; w/v BSA): Sodium azide (6 mL, 1 %; w/v) was mixed with BSA (300 µL, 5 %; w/v) and TBS (40 mL) and the pH was

adjusted to 7.6. Volume was made up to 60 mL with TBS and solution was stored at 4°C for up to three months.

Procedure

Multi-spot slides were cleaned with 70 % (v/v) ethanol, wrapped with tinfoil and sterilised by dry heat before cell seeding.

Endothelial cells were resurrected, passaged (Section 2.2.12.2) and cells were counted (Section 2.2.3.3) then suspended in M-199 endothelial cell culture medium at $17,500 \text{ cells.mL}^{-1}$. Cell suspension, 40 μL , was added to the spots of a multi-spot slide (700 cells per spot) in three replicates for each antibody/control, slides were then placed in a four-well plate and incubated for 24 hours at 37 °C with 5 % (v/v) CO₂ in air (Figure 2.15 A-B). M-199 endothelial cell culture medium, 7 mL, was added to each well containing a multi-spot slide and incubated for another 48 hours at 37 °C with 5 % (v/v) CO₂ in air (Figure 2.15 C). Following incubation, medium was aspirated (Figure 2.15 D) and cells were fixed by placing slides in a metallic slide holder and immersing in acetone and methanol mixture (1:1 volume ratio) for one minute. The slides were then allowed to dry in air for five minutes then washed in running tap water for ten minutes followed by a five minutes TBS wash.

Primary antibody solutions against von Willebrand factor (vWF), smooth muscle cell α -actin, smooth muscle cell myosin heavy chain and fibroblast 5B5 were diluted in antibody diluent at the manufacturer's recommended dilutions; anti-vWF 1:200, anti- α -actin 1:500, anti-myosin 1:50 and anti-5B5 1:50. Their isotype controls were also diluted in antibody diluent at the same primary antibody concentration (Table 2.4). Primary antibody, 20 μL , was added to each seeded spot and incubated in a moist environment for one hour at room temperature. Slides were washed twice in TBS-Tween 20 for ten minutes each then for ten minutes in TBS on an orbital shaker at 40 rpm. Secondary fluorescently-labelled antibody solutions were made against the primary antibody host species. Alexa Fluor 488-labelled (F(ab')₂ fragment) goat anti-rabbit diluted at 1:200 against anti-vWF antibody and Alexa Fluor 488-labelled (F(ab')₂ fragment) goat anti-mouse diluted at 1:200 against anti- α -actin, anti-myosin and anti-5B5 antibodies. Secondary antibody, 20 μL , was then added to the appropriate spots and incubated in a moist environment for 30 minutes in the dark. Slides were washed

twice in TBS-Tween 20 for ten minutes each then for ten minutes in TBS on an orbital shaker at 40 rpm. Slides were immersed in DAPI working solution for ten minutes in the dark. Then slides were immersed in three changes of PBS each for ten minutes in the dark. Slides were finally mounted with a coverslip using Dako fluorescent mount and stored for a maximum of 24 hours in the dark.

Images were acquired using a Zeiss fluorescent upright microscope with DAPI (detection at 465 nm) and FITC (detection at 519 nm) filters. Three images were randomly taken from each replicate and images were processed using Zen software.

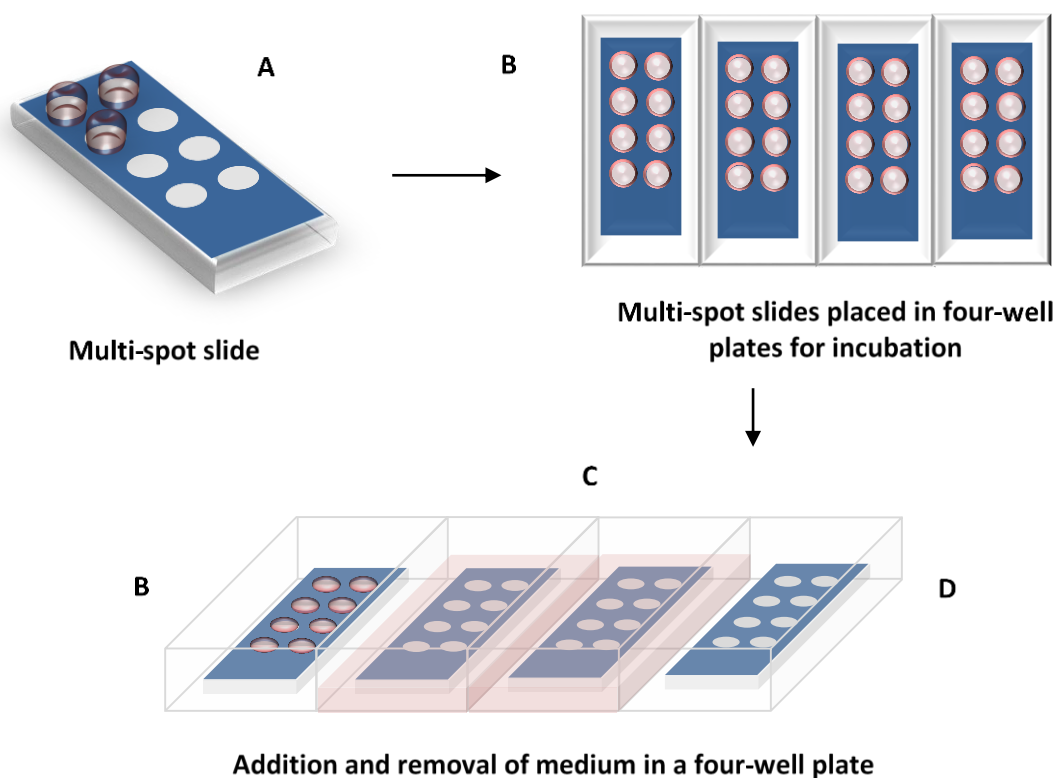


Figure 2.15: Schematic diagram showing the cell seeding set-up for immunofluorescence. A) Spots in a multi-spot slide were seeded with cells in three replicates for each antibody and control. B) Slides were placed in a four-well plate and incubated for seeding. C) Following seeding, medium was added to slides in wells and incubated. D) Finally, medium was removed and cells were ready for fixation then antibody labelling.

2.2.13 Attachment of Endothelial Cells

The following procedures were carried out inside a class II safety cabinet.

2.2.13.1 Peptide Coated Acellular Artery Samples and Tissue Preconditioning

After production of acellular arteries (Sections 2.2.4), they were assessed for their acellularity (Section 2.2.5) and *in vitro* biocompatibility (Section 2.2.6) then they were cut open and several sections with a diameter of 12 mm were cut using sterile 12 mm biopsy punches. Non-functionalised peptides, 20 mg, were sterilised by gamma irradiation (Section 2.2.1.4) before use for cell studies. Stock functionalised peptide solutions were made at 1:20 molar ratio of the functionalised to non-functionalised peptides, which were then diluted to 1:50 molar ratio when added to the non-functionalised peptide solutions. Non-functionalised and functionalised peptide solutions were made at 20 mg.mL⁻¹ in sterile water, monomerised and the pH was adjusted to pH 7.4 as described in Section 2.2.7.1 and Section 2.2.7.2, respectively. Monitoring of pH was achieved using pH test paper and adjustment carried out using 1, 0.5 and 0.05 M NaOH/HCl. Control samples were taken through the same pH adjustment as peptide samples. Before triggering self-assembly, tissue samples (three replicates per peptide solution/control for each tested time point) were placed in peptide solutions and controls, left overnight then 10X strength Ringer's solution was added as described in Section 2.2.7.3. Following triggering self-assembly, tissue samples were placed in the middle of wells in a 12-well plate with the luminal surface facing upwards (Figure 2.16 A). Preconditioning medium (M-199 endothelial cell culture medium without the ECGS), 1 mL, was used to gently wash the luminal surface removing any excess peptide then aspirated. Stainless steel seeding rings were then pressed firmly on the tissue creating a seal and 300 µL of the preconditioning medium was added to each sample and incubated overnight at 37 °C and 5 % (v/v) CO₂ in air to precondition the tissue (Figure 2.16 B).

2.2.13.2 Seeding Peptide Coated Acellular Artery Samples with Endothelial Cells

Endothelial cells were resurrected, passaged (Section 2.2.12.2) and cells were counted (Section 2.2.3.3) then suspended in M-199 endothelial cell culture medium at 25,000 cells.mL⁻¹. Cell suspension, 200 µL, was added to each seeding ring (5,000 cells per seeding ring) after aspirating the preconditioning medium then incubated at 37 °C

and 5 % (v/v) CO₂ in air for four hours. Following incubation, medium was aspirated, seeding rings were removed and tissue samples were gently washed with 1 mL of PBS for one minute then aspirated to remove any remaining unattached cells. In-house manufactured polytetrafluoroethylene (PTFE) support rings were then added to tissue replacing the seeding rings to keep the tissue flat during the experiment as removing the seeding ring and addition of medium resulted in folding or curling up of tissue. M-199 endothelial cell culture medium, 200 µL, was added to each well and incubated at 37 °C and 5 % (v/v) CO₂ in air and the medium was replaced every 48 hours (Figure 2.16 C).

2.2.13.3 Live/dead® Staining

Live/dead® staining solution of 1 µM calcein AM and 2 µM ethidium homodimer-1 was prepared in sterile PBS by addition of 5 µL of calcein AM and 20 µL of ethidium homodimer-1 in 20 mL of PBS with calcium and magnesium. At the intended time points, four hours and 72 hours, medium was aspirated, PTFE rings were removed and tissue samples were gently washed with PBS for one minute then aspirated. Staining solution, 1 mL, was added to each sample and incubated in the dark at 37 °C and 5 % (v/v) CO₂ in air for one hour. Staining solution was aspirated and tissue samples were washed with 1 mL of PBS for one minute then aspirated (Figure 2.16 D).

2.2.13.4 Imaging and Analysis

Images were acquired immediately after staining using a Zeiss fluorescent upright microscope with calcein AM (detection at 514 nm) and ethidium homodimer-1 (detection at 617 nm) filters and processed using Zen software. Five images were taken from each test/control sample and each replicate (n = 3) as described in Figure 2.16 E. Live and dead cells were counted in each image and averages were taken from the five images for each replicate (n = 3) for data analysis to determine the cell viability (%) cell density (cells.mL⁻¹) and cell attachment (%).

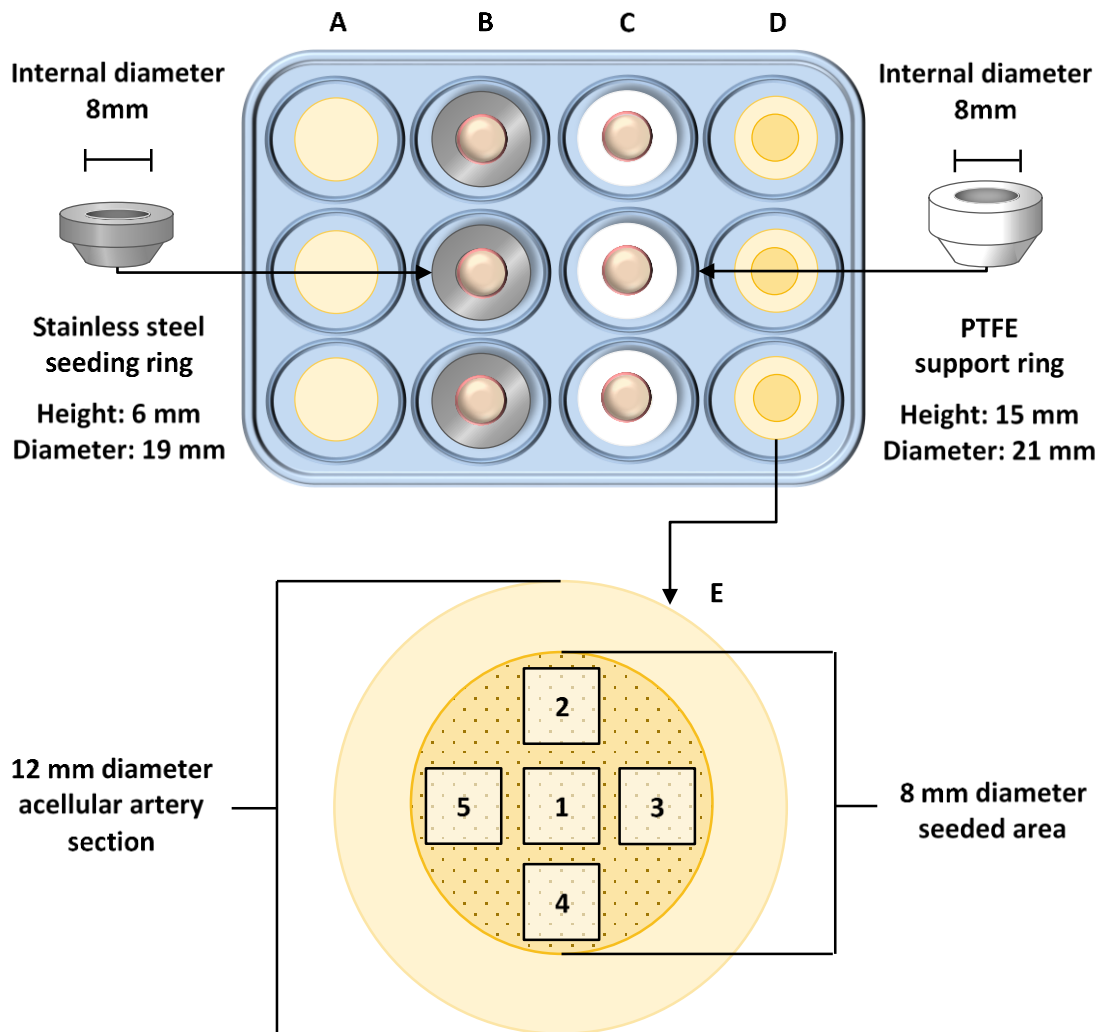


Figure 2.16: Schematic diagram showing tissue cell seeding set-up and positions of images taken from tissue for cell studies. A) Tissue sections were placed in the middle of the well of a 12-well plate then washed with the preconditioning medium, B) a seeding ring was pressed firmly creating a seal and tissue was preconditioned with medium overnight then seeded with endothelial cells in the area defined by the seeding ring for cell attachment, C) seeding rings removed, tissue washed with PBS and PTFE support rings were added for the remaining of the study then medium was added and finally D) PTFE rings were removed, tissue was washed with PBS then stained with Live/dead® staining and taken for imaging (E). E) Positions of images taken from seeded part of tissue.

The viability of cells in each image taken of each sample replicate was calculated as a percentage using Equation 2.7.

Equation 2.7: Viability of cells (%) seeded onto tissue.

$$\text{Cell viability (\%)} = \frac{\text{No. of live cells (cells)}}{\text{Total no. of cells (cells)}} \times 100$$

The density of cells (cells.mm⁻²) in each image taken of each sample replicate was calculated using Equation 2.8.

Equation 2.8: Cell density (cell per mm²) in tissue.

$$\text{Cell density (cells/mm}^2\text{)} = \frac{\text{No. of live cells (cells)}}{\text{Area of image used for cell counting (mm}^2\text{)}}$$

The Percentage of cells attached in each image taken of each sample replicate was calculated using Equation 2.9, where the number of cells seeded per a defined seeding area is equivalent to the initial number of cells seeded (5000 cells) divided by the defined seeded area (50.27 mm²).

Equation 2.9: Cells attached (%) to tissue.

$$\text{Cell Attachment (\%)} = \frac{\text{Cell density (cells/mm}^2\text{)}}{\text{No. of cells seeded per defined seeding area (cells)}} \times 100$$

Data were analysed for significant difference using two-way ANOVA (Section 2.3).

2.3 Statistical Analysis

Throughout this thesis, all numerical values represent means \pm 95 % confidence limits represented by the data and error bars respectively, unless otherwise stated.

Graphs were processed in GraphPad Prism software. Data were analysed using; one-way analysis of variance (ANOVA) for data with one test condition and more than two tested groups and two-way ANOVA for data with two test conditions and more than two tested groups. Following analysis of variance, individual differences between group means were determined using post-hoc Tukey's test ($p < 0.05$).

3 Decellularisation of Porcine External Iliac Arteries

3.1 Introduction

Decellularisation is one of the extensively investigated processes for vascular tissue engineering. This is because decellularised tissues have the advantage of being composed solely of the extracellular matrix (ECM), whilst lacking the cellular component⁶². It is therefore hypothesised that an acellular scaffold minimises the adverse host reaction to the graft²⁰⁰, hence minimising graft rejection. Decellularisation protocols developed at the University of Leeds have been applied to tissues from humans (allografts) and animals (xenografts) for many clinical applications such as blood vessel, heart valve and nerve regeneration^{25,201-205}. Porcine tissue is commonly used due to having similar anatomy and physiology to humans as well as its availability^{206,207}. However, the use of tissue from animal donors raises some concerns such as the immunological response and cross-species disease transmission²⁰⁶, which should be mitigated in decellularised scaffolds due to absence of donor cells or genetic material. The aim of this chapter was to decellularise porcine external iliac arteries using low concentrations of sodium dodecyl sulphate (SDS) for the development of small-diameter vascular grafts.

3.1.1 University of Leeds Decellularisation Methods

The decellularisation method developed at the University of Leeds has been applied to a range of different soft tissues, utilising a combination of the decellularisation techniques discussed in Chapter 1 (Section 1.5). For vascular tissue, the process is started with a freeze-thaw cycle that causes cell lysis by disrupting the cell membrane and finalised with peracetic acid disinfection²⁵. A series of chemical washes are applied in between with mechanical agitation that aids reagent diffusion through the tissue structure^{25,47}. A mixture of antibiotics is used to reduce the initial bioburden of the tissue. Ethylenediaminetetra-acetic acid (EDTA) treatment is used to aid in the dissociation of cells from the ECM (endothelial cells in the case of arteries). Hypotonic and hypertonic buffers are used for cell lysis. Treatment with low concentration of SDS solubilises proteins and lipid membranes. Aprotinin is a protease inhibitor and EDTA, a chelating agent used in low concentrations, is a matrix metalloprotease inhibitor.

Therefore, both are used in conjugation with other chemical treatments to prevent ECM degradation by protease or metal ions (required for the matrix metalloprotease) released from lysed cells. Lysed cells also release DNA and RNA and these are degraded by incubation with nuclease enzymes that digest nucleic acids. The chemical washes are interspersed with PBS washes to remove cell debris and residual reagents in order to avoid host immunogenic response and cytotoxic effects, respectively ²⁵.

3.2 Aims and Objectives

The aim of this chapter was to apply an established decellularisation process to porcine external iliac arteries and reproducibly produce biocompatible acellular arteries.

The specific objectives were:

- To isolate and decellularise porcine external iliac arteries using established methods;
- To assess the histoarchitecture and cellular content of treated arteries;
- To quantify total DNA within treated arteries;
- To assess the *in vitro* biocompatibility of acellular arteries using contact and extract cytotoxicity assays.

3.3 Methods

3.3.1 Acellular Artery Production

External iliac arteries were dissected from porcine legs and stored at - 80 °C (Section 2.2.4.1). All arteries were decellularised as batches (n = 3 - 30) in individual 200 mL solutions with agitation as described in Section 2.2.4.2. Following decellularisation, acellular arteries were stored at 4 °C for up to three months.

3.3.2 Acellularity and Biocompatibility Validation

All acellular arteries were validated for sterility (Section 2.2.5.1), histology (Section 2.2.5.2), DNA content (wet weight; Section 2.2.5.3) and *in vitro* biocompatibility for the initial assessment of medical devices using two different cell lines (Section 2.2.6).

In batches one to four, sections were validated from the end and middle regions of artery, while only sections from the end region were validated in batches five to ten (Figure 3.1). This was because in the first batches, all validated middle region sections were shown to be acellular and non-cytotoxic.

These quality control tests were crucial following decellularisation to ensure all acellular arteries were acceptable for use as vascular grafts by: being sterile to allow for use clinically; having a preserved ECM to act as a natural replacement of artery with the native mechanical/structural properties; being free of cells with reduced DNA content (> 90 % reduction) for lower chances of immunological response or disease transmission; and being non-cytotoxic in order to allow for re-cellularisation. If any artery failed any of these tests it would have been excluded from further studies.

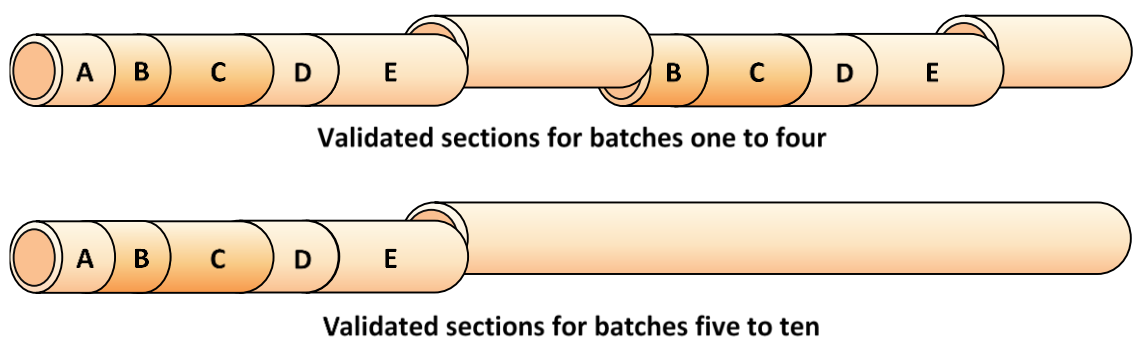


Figure 3.1: Positions of artery sections/segments used for decellularisation validation. Sections/segments were taken from the following positions for: A) sterility, B) histology, C) DNA content, D) contact cytotoxicity assay and E) extract cytotoxicity assay. Sections from the end and middle regions were validated in batches one to four, while sections from the end region only were validated in batches five to ten. B and C sections were taken from both cellular and acellular arteries, while sections A to E were only taken from acellular arteries. Unlabelled segments were used for further studies.

3.4 Results

The results presented here are representative of all decellularised batches and the data are summarised in Table 3.1.

3.4.1 Sterility of Acellular Arteries

Acellular arteries (n = 6) were found to be sterile following decellularisation. Sterility was confirmed by having a clear nutrient broth following incubation when compared to the cloudy positive control that was left in open air (Figure 3.2).

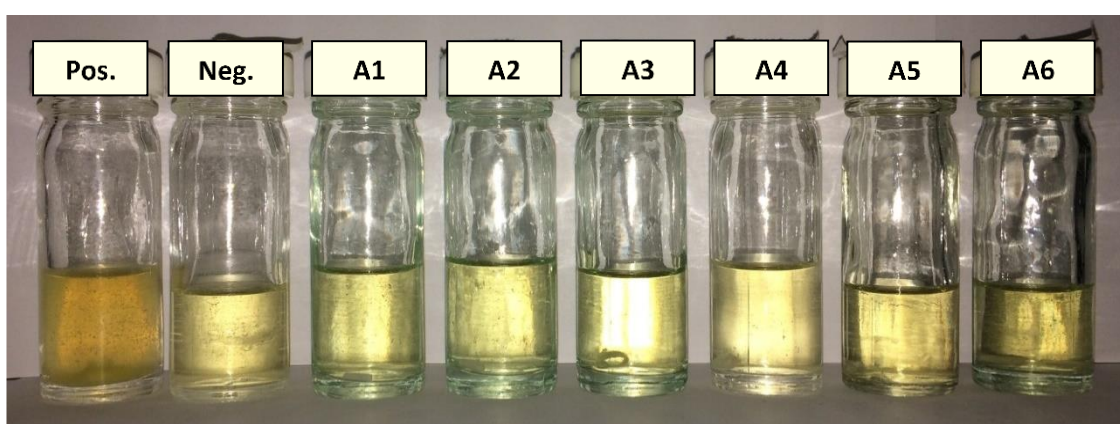


Figure 3.2: Sterility of acellular porcine external iliac arteries following decellularisation. Positive control (*pos.*): container incubated in open air and resulted in a cloudy medium. Negative control (*neg.*): incubated in a sealed container and resulted in a clear medium. Acellular artery samples (A1 - A6): incubated in sealed containers and resulted in a clear medium. All acellular arteries were shown to be sterile.

3.4.2 H & E Staining

H & E staining was used to visualise the histoarchitecture of cellular and acellular arteries (n = 6), in which the cell nuclei are stained with haematoxylin and appear blue/purple, while collagen and cytoplasm are stained with eosin and appear pink. In cellular tissue (Figure 3.3 A), H & E staining showed the presence of purple nuclei in all three artery layers 1) the intima, where circular endothelial cells were present 2) the tunica media was observed under the internal elastic membrane that separates the two layers, where elongated smooth muscle cells were present and collagen fibres were densely packed 3) the tunica adventitia consisted of randomly oriented collagen fibres with circular cells, which were less in population compared to the medial layer.

Decellularisation of arteries successfully removed cells and this was evident following H & E staining (Figure 3.3 B), in which the purple nuclei and cell structures were absent in all layers of acellular artery samples. However, there was some loss of the ECM structure, mainly in the tunica adventitia layer and part of the tunica media because the collagen fibres were loosely packed following decellularisation and the intima was observed less often than in cellular tissue, but the overall ECM structure was retained.

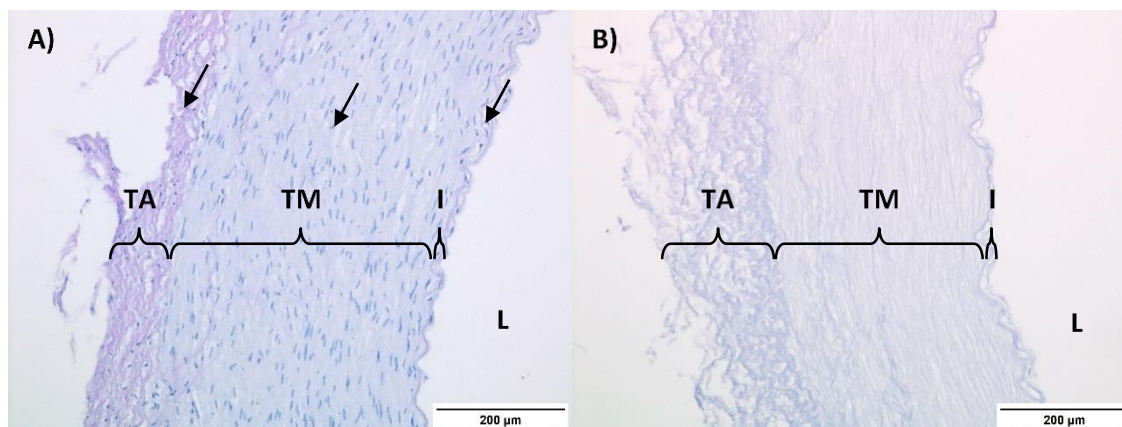


Figure 3.3: Cellular and acellular porcine external iliac arteries fixed in NBF and stained with H & E. A) Cellular artery showing presence of nuclei in all three layers. B) Acellular artery showing absence of nuclei in all three layers and preservation of the ECM structure. Cellular nuclei (blue), ECM (pink), lumen (L), intima (I), tunica media (TM), tunica adventitia (TA) and arrows point to nuclei. Images acquired with the bright field mode using x 10 objective and scale bars represent 200 µm.

3.4.3 DAPI Staining

DAPI (4',6-diamidino-2-phenylindole) is a fluorescent dye that binds to the minor grooves of double-stranded DNA, which is found in cellular nuclei. Therefore, the presence of double-stranded DNA hence cell nuclei in cellular and acellular arteries (n = 6) was examined by staining artery sections with DAPI. In DAPI stained section of cellular tissue (Figure 3.4 A), the double-stranded DNA was observed as blue fluorescence throughout all three artery layers. This was absent in acellular tissue sections (Figure 3.4 B) confirming the elimination of double-stranded DNA (cell nuclei).

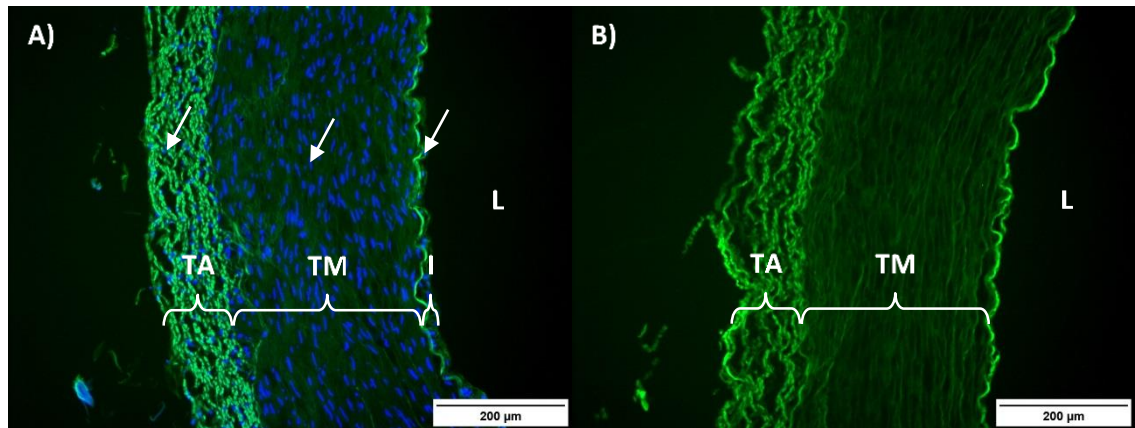


Figure 3.4: Cellular and acellular porcine external iliac arteries fixed in NBF and stained with DAPI. A) Cellular artery with double-stranded DNA present. B) Acellular artery with no double-stranded DNA present and preserved ECM structure. Double-stranded DNA (blue with DAPI filter), auto-fluorescence of ECM (green with GFP filter), lumen (L), intima (I), tunica media (TM), tunica adventitia (TA) and arrows point to double-stranded DNA. Images acquired with DAPI and GFP filters using $\times 10$ objective and scale bars represent $200\ \mu\text{m}$.

3.4.4 DNA Content

Total DNA was extracted from cellular and acellular arteries in order to determine the DNA content in each tissue and the success of the decellularisation process. It was determined that the average DNA concentration of acellular tissue was $3.3 \pm 0.9\ \text{ng}\cdot\text{mg}^{-1}$ ($n = 6$) compared to cellular tissue that contained $386.5 \pm 127.2\ \text{ng}\cdot\text{mg}^{-1}$ ($n = 6$) of DNA (wet weight, batch nine). These results showed a significant DNA reduction of $99.1 \pm 0.4\ %$ following decellularisation (ANOVA; $p < 0.05$).

3.4.5 Contact Cytotoxicity Assay

In this assay, lack of cytotoxic effect was indicated by growth of BHK and L929 cells up to and in contact with acellular tissue as displayed by the negative control (steri-strips), whereas a cytotoxic effect was indicated by cell lysis as displayed by the positive control (superglue). Following culturing of cells, there was no growth of both cell types in presence of the superglue positive control. However, in the negative control, cellular growth was observed up to and under the steri-strips. Both cell types also grew up to and in contact with the acellular artery samples indicating that acellular arteries were non-cytotoxic to these cells (BHK: Figure 3.5 and L929: Figure 3.6; $n = 6$).

Cells displayed normal morphologies when cultured with acellular artery samples compared to confluent cells cultured alone. BHK having the elongated spindle-shaped appearance (Figure 3.5) and L929 having the fibroblastic appearance (Figure 3.6).

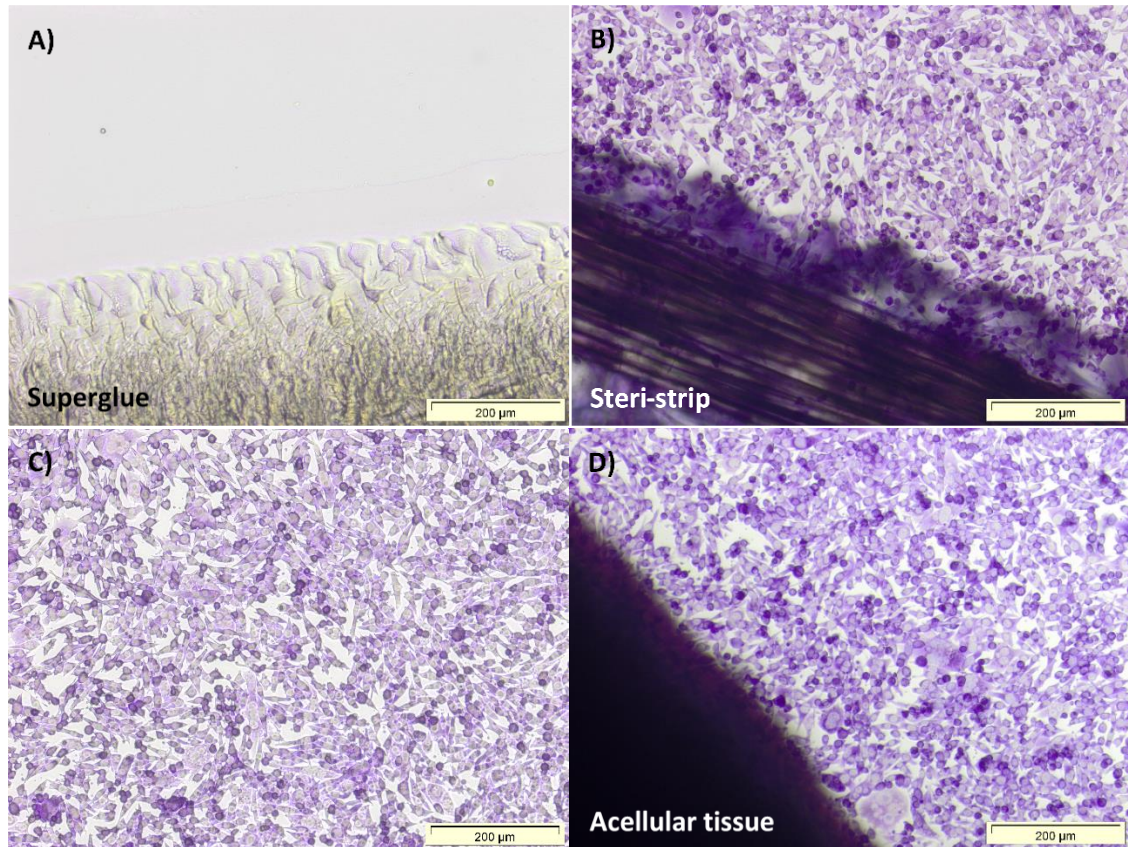


Figure 3.5: Contact cytotoxicity of acellular porcine external iliac arteries with BHK cells. A) *Superglue positive control, B) steri-strip negative control, C) cells only control and D) acellular artery sample. Cells grew up to and in contact with the acellular tissue and steri-strips with normal morphologies (as observed in cells cultured alone) indicating no cytotoxicity when compared to positive controls where no cells were present due to the cytotoxic effect of superglue. Images were acquired using x 10 objective and scale bars represent 200 µm.*

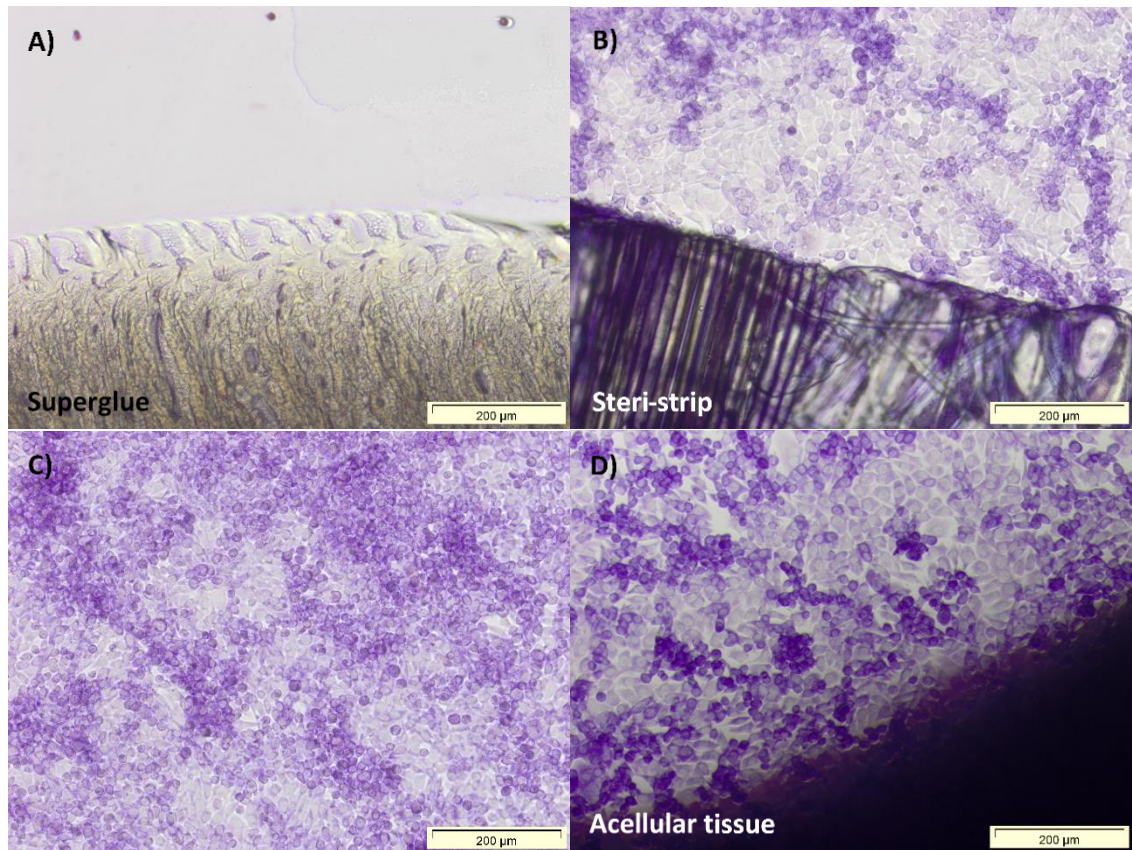


Figure 3.6: Contact cytotoxicity of acellular porcine external iliac arteries with L929 cells. A) *Superglue positive control*, B) *steri-strip negative control*, C) *cells only control* and D) *acellular artery sample*. Cells grew up to and in contact with the acellular tissue and steri-strips with normal morphologies (as observed in cells cultured alone) indicating no cytotoxicity when compared to positive controls where no cells were present due to the cytotoxic effect of superglue. Images were acquired using $\times 10$ objective and scale bars represent $200\ \mu\text{m}$.

3.4.6 Extract Cytotoxicity Assay

Adenosine triphosphate (ATP) is found in living cells and its concentration drops dramatically in dying or dead cells, so it can be used as an indicator of cell viability or metabolic function. Therefore, ATPlite™ assay was used to determine the viability of cells cultured with acellular tissue extracts in order to establish *in vitro* biocompatibility. In this assay, the cytotoxicity of extracts of acellular arteries was assessed ($n = 6$), the amount of ATP of cells in the extract was measured and compared to a positive control of cells cultured with 20 % (v/v) DMSO and negative control consisting of cell culture medium only. The ATP content of BHK and L929 cells in extracts of acellular arteries was not significantly different when compared to the negative control (ANOVA; $p < 0.05$).

These results indicated that acellular arteries were non-cytotoxic to both cell types (Figure 3.7).

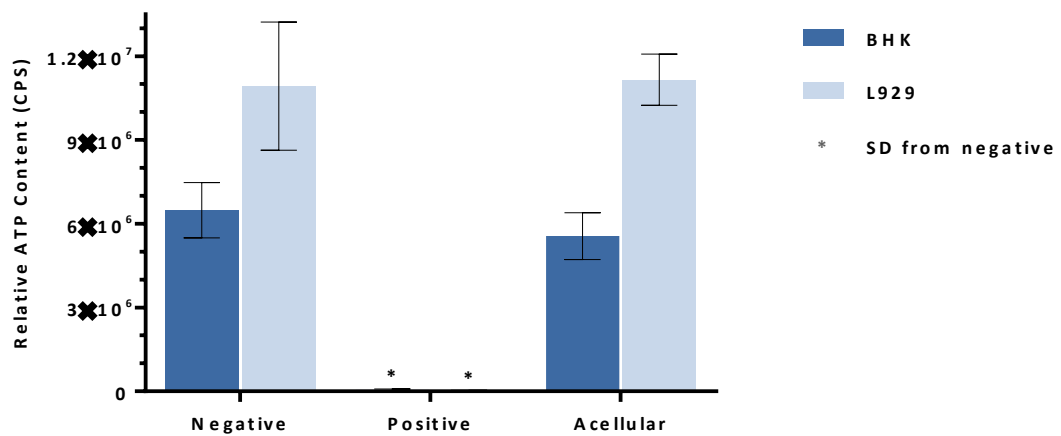


Figure 3.7: Relative ATP content of BHK and L929 cells cultured with extracts of acellular porcine external iliac arteries. Data represent the means ($n = 6$) \pm 95 % confidence limits. Positive control (40 %; v/v DMSO) and negative control (cell culture medium alone). There was no significant difference between ATP content of cells cultured with extracts and negative control. Significant difference (SD) was determined by one-way ANOVA and post-hoc Tukey's test ($p < 0.05$).

3.5 Discussion

The aim of this chapter was to produce an acellular biological scaffold by decellularisation of porcine external iliac arteries using a combination of chemical, enzymatic and physical methods. Following decellularisation, a number of factors were required for evaluation of the acellular ECM scaffold.

Firstly, maximised DNA removal (< 50 ng double-stranded DNA per dry weight tissue and < 200 base pair DNA fragment lengths), lack of visible nuclear cells in H & E/DAPI stained tissue sections and minimal remnant cellular components to avoid adverse host reaction^{59,61}. Residual DNA for example was reported to cause calcification in acellular porcine aortic roots *in vivo*²⁰⁸. Residual phospholipids can also have an effect on calcification because they are important for the formation of the phospholipid-calcium-phosphate complex, which acts as a nucleation site for calcification^{61,209}. Moreover, presence of cellular residues and longer length DNA fragments may possibly cause inflammatory responses as it was reported that tissue with less DNA content and

shorter DNA fragment length was shown to have less swelling of surrounding tissue and better host tissue response *in vivo* due to the reduced pro-inflammatory response that can be triggered by cellular mitochondria ²¹⁰. The nuclear material can be evaluated quantitatively by assays providing key information about remaining cell residues within the ECM or qualitatively by routine histological and immunohistochemical studies ^{61,200}. It is important to note that complete removal of the cellular residues is unlikely to be achieved by decellularisation and the degree of decellularisation contributes greatly to the host response to the acellular scaffold causing inflammatory response ^{60,210}.

Secondly, preservation of the major components of the ECM for optimal structural and functional tissue ^{200,211}. Collagen and elastin fibrous structural components of the ECM contribute greatly to the biomechanical properties of tissue ²¹² and preservation of such components is important to retain properties of the native tissue. Bioactive peptides and growth factors found in collagen, laminin and fibronectin also play an important role in the bioactivity of tissue and cell attachment ²¹¹. GAGs) are complex polysaccharides that play an important role in physiological behaviour of tissue including water retention. Presence of heparin-rich GAGs is desired in scaffolds for tissue repair due to its binding properties of cell surface receptors and growth factors ⁴⁹. Therefore, maintenance of the ECM component plays a key role in re-cellularisation of the acellular scaffold. However, decellularisation is known to have some effect on the ECM structure and the extent of disturbance of these components may vary in different tissue types and depending on decellularisation and sterilisation techniques used. Furthermore, removal or reduction of certain components may possibly have minimal effect on the properties required for the clinical application, especially if the acellular tissue is to be used in conjugation with other technologies to make up for the affected components. It is therefore important to carry out the required assessment for the intended application to ensure minimal losses in the ECM components.

Thirdly, lack of cytotoxic effect in the acellular scaffold ²⁰⁰ as it is important for any medical device to be biocompatible prior to animal studies or clinical trials. Presence of residual chemical detergents used during decellularisation can cause a cytotoxic effect and this can be minimised by mechanical agitation during treatments to facilitate their removal ⁶¹. Residual cytotoxic chemicals such as SDS were shown to discourage cellular growth, hence re-cellularisation of scaffold was affected. SDS can be quantified by

carrying out a colourimetric assay and the lower cytotoxic threshold for SDS was reported to be $10 \mu\text{g}.\text{mg}^{-1}$ ⁶⁰. Assessment of *in vitro* biocompatibility of acellular scaffolds can be carried out by cytotoxic assays with cells ²⁰⁰.

Although evaluation of the previous factors is crucial for the assessment of the extent of decellularisation, other tissue-specific and application-specific factors may need to be assessed.

In this work, histological studies of acellular porcine external iliac arteries have shown absence of cells and preservation of the ECM. Preservation of the ECM near the luminal surface was also noted in multiphoton images (Appendix A.8, more detail in Chapter 6). The DNA content was reduced by approximately 97.7 % (wet weight, $n = 116$) with an average DNA of $7.8 \pm 1.2 \text{ ng}.\text{mg}^{-1}$ ($n = 116$) in acellular tissue compared to cellular tissue that contained $337.6 \pm 56.1 \text{ ng}.\text{mg}^{-1}$ ($n = 32$). Initial biocompatibility of acellular arteries was assessed *in vitro* according to the cytotoxicity ISO standard 10993-5 for medical devices with BHK and L929 cells. Acellular arteries were shown to be non-cytotoxic to both cells lines.

Several studies within the University of Leeds produced acellular scaffolds following similar decellularisation methods that are tissue-specific have shown similar results ^{25,71,204,205,208}. Wilshaw *et al.* investigated decellularisation of human common femoral arteries following methods developed at the University of Leeds. Histological studies confirmed the absence of visible whole cells and cellular nuclei. DNA reduction of > 97 % was achieved with concentrations of $7 \pm 1 \text{ ng}.\text{mg}^{-1}$ and $273 \pm 72 \text{ ng}.\text{mg}^{-1}$ in wet weight acellular and cellular tissue, respectively. The acellular arteries were shown to be biocompatible *in vitro* with preserved biomechanical properties which were insignificantly different from native cellular arteries ²⁵.

Acellular scaffolds have been applied to animal models for pre-clinical trials in various tissue engineering applications. In one study using small animal models for small-diameter vascular grafts, acellular rabbit carotid arteries were implanted into rats for 56 days. Arteries were decellularised by initial freeze/thaw cycles followed by chemical treatments including enzymatic digestions, EDTA treatment, double-distilled water washing with agitation and finalised by an ultraviolet irradiation. Histological studies have shown no visible nuclear material and mechanical properties were retained.

Acellular scaffolds were shown to be biocompatible for *in vivo* applications with low cytotoxicity and reduced immune response⁵³. Jose *et al.* investigated implantation of acellular porcine aortic valves in sheep models as acellular xenografts for 6 months. The decellularisation process involved chemical treatments with agitation in hypotonic buffer, EDTA containing aprotinin, low concentration of SDS (0.1 %; w/v) and nuclease solution then sterilised in peracetic acid (0.1 %; w/v). Histological studies have shown no evidence of cells or cell remnants following decellularisation in the tested samples. The study demonstrated the regenerative potential and biocompatibility of the acellular xenograft. However, the decellularisation was not efficient for all decellularised tissue causing mild calcification in regions with residual nuclear material²⁰⁸. Another study investigated acellular porcine common carotid arteries for use in small-diameter vascular grafts using dogs as the animal model. These were decellularised using a combination of hypotonic and detergent treatments in addition to enzymatic digestions with mechanical means. Histological studies have shown complete cell removal with intact ECM structures and retained mechanical properties. Following decellularisation, acellular arteries were coated with heparin to reduce the graft thrombogenicity then implanted into dogs as a xenograft. It was reported that the grafts were patent at 67 days with smooth muscle cells densely populating the tunica media and endothelial cells covering the lumen²¹³.

Although small animal models are not ideal for translation to humans, and larger animal populations with long-term studies are preferable, the initial studies are crucial to understand the host reaction to the acellular xenograft. Moreover, the previous studies, have shown the potential for acellular scaffolds to be used clinically, but optimisation of decellularisation methods are required. In fact, there are several acellular products that are clinically available for vascular repair. For examples, CroMatrix[®] ECM[®] (USA) derived from small intestinal submucosa and PhotoFix[®] (CryoLife Inc., USA) derived from bovine pericardium⁵⁵.

In this chapter, acellular artery scaffolds were produced consistently with a preserved ECM. However, lack of the natural anti-thrombogenic endothelium may increase the probability of thrombus formation^{54,57,58,88}. Therefore, for a higher success rate in vascular grafts, it is proposed that a surface coating is required to enhance the re-endothelialisation of acellular scaffolds as will be discussed in subsequent chapters.

3.6 Summary of Acellularity and Biocompatibility of All Batches

All batches of acellular arteries produced were found to be sterile. Histologically, there was found to be an absence of cells and preservation of the histoarchitecture. The absence of cells was also confirmed by the significant DNA reduction in acellular tissue. All acellular arteries were non-cytotoxic to both BHK and L929 cells when tested in contact and extract cytotoxicity assays. Table 3.1 summarises the quality assurance data for all batches of acellular arteries produced throughout this thesis.

Table 3.1: Acellularity and *in vitro* biocompatibility results of all decellularised batches of porcine external iliac arteries.

Batch No.	Artery No.	Histology (H & E and DAPI)	DNA Quantification (ng.mg ⁻¹)	Biocompatibility (Contact and Extract)
Average Control (n = 32)	1 - 32	Cells	337.6 ± 56.1	-
1 (n = 3)	1 - 3	No cells	30.8 ± 10.1	Non-cytotoxic
2 (n = 6)	4 - 9	No cells	20.4 ± 6.0	Non-cytotoxic
3 (n = 10)	10 - 19	No cells	8.4 ± 1.4	Non-cytotoxic
4 (n = 10)	20 - 29	No cells	6.4 ± 2.1	Non-cytotoxic
5 (n = 20)	30 - 49	No cells	4.7 ± 1.0	Non-cytotoxic
6 (n = 10)	50 - 59	No cells	12.5 ± 3.6	Non-cytotoxic
7 (n = 30)	60 - 89	No cells	4.8 ± 1.5	Non-cytotoxic
8 (n = 15)	90 - 104	No cells	8.9 ± 1.5	Non-cytotoxic
9 (n = 6)	105 - 110	No cells	3.3 ± 0.9	Non-cytotoxic
10 (n = 6)	111 - 116	No cells	3.6 ± 1.4	Non-cytotoxic
Average Acellular (n = 116)	1 - 116	-	7.8 ± 1.2	-

4 Characterisation of Self-assembling P₁₁ Peptides Under Physiological Conditions

4.1 Introduction

Self-assembling peptides consisting of natural amino acids can be designed to have different physical properties depending on the required application. Since these sequences consist of natural building blocks, they have the potential to be biocompatible and degradable. This allows the use of such peptides in various biological applications for example as scaffolds for tissue engineering applications potentially without triggering an immune response ^{119,214}.

In Chapter 3, an acellular porcine arterial biological scaffold was produced but it lacked the natural anti-thrombogenic endothelial layer. The aim of this work was to enhance the re-endothelialisation of acellular artery tissue using functionalised self-assembled peptides. For this purpose, the P₁₁ peptide series was selected for investigation under physiological conditions. P₁₁ peptides are known to self-assemble into β -sheet structures and form gels consisting of fibrillar networks ^{173,176}. Different triggers including pH and ionic strength have been shown to switch the peptides from the self-assembled state to the monomeric state and vice versa ^{142,149}. Because of this property, these peptides can be used in applications in which *in vivo* self-assembly is required. P₁₁-4, P₁₁-8 and P₁₁-12 had previously been shown to be non-cytotoxic and form self-supporting gels at high concentrations under physiological conditions ^{172,177}, hence were selected for this study. The resultant gel matrix was proposed to act as a scaffold for re-cellularisation of the acellular artery tissue as will be discussed in subsequent chapters.

Here, the self-assembly behaviour of P₁₁-4, P₁₁-8 and P₁₁-12 was investigated under physiological conditions using Fourier transform infrared (FTIR) spectroscopy and transmission electron microscopy (TEM). Secondary structure, gelation behaviour and morphology were studied at different concentrations. Different concentrations were tested to determine the optimal concentration at which a gel was formed with high proportion of β -sheet structures to use for further studies within acellular tissue as will be discussed in Chapter 6.

4.2 Aims and Objectives

The aim of this chapter was to characterise P₁₁₋₄, P₁₁₋₈ and P₁₁₋₁₂ under physiological conditions at different concentrations for self-assembly behaviour and suitability for application in vascular grafts.

The specific objectives were:

- To determine the proportion of β -sheet secondary structure in peptide gels using Fourier transform infrared (FTIR) spectroscopy, hence the time taken for each peptide to reach equilibrium;
- To investigate peptide gelation over time;
- To investigate the morphology and width of peptide structures using transmission electron microscopy (TEM);
- To determine the peptide concentration to be used for future studies.

4.3 Methods

Further details of sequences, molecular weights, net charges at physiological pH 7.4 as well as the conversion of peptide concentrations used in this chapter from mg.mL⁻¹ to mM for P₁₁₋₄, P₁₁₋₈ and P₁₁₋₁₂ can be found in Appendix A.2.

4.3.1 FTIR Spectroscopy for Peptide Secondary Structures

Background

FTIR spectroscopy is a technique that allows determination of the secondary structure (intermolecular and intramolecular interactions) of proteins and peptides by observing the frequency at which absorption occurs^{197,215,216}. Most FTIR instruments measure absorptions in the mid-IR region between 400 cm⁻¹ and 4000 cm⁻¹, where proteins absorb vibrational energies²¹⁷. The FTIR spectrum results from the absorption of energy due to the vibrating chemical bonds and it is composed of three absorption band regions that are of interest in determining the secondary structure of proteins; amide I band absorbs in the region 1600 - 1700 cm⁻¹ (mainly due to the stretching of C=O), amide II band absorbs in the region 1500 - 1600 cm⁻¹ (due to N-H bending and C-N stretching) and the amide III band that absorbs in the region 1200 - 1350 cm⁻¹ (due to C-N stretching and N-H bending vibrations)^{215,217}.

Self-assembly of peptides involves intermolecular and intramolecular interactions, hence the most useful region in the FTIR spectrum of such peptides for the determination of their secondary structure is amide I region.

Method

P₁₁₋₄, P₁₁₋₈ and P₁₁₋₁₂ were prepared at concentrations of 10, 20 and 30 mg.mL⁻¹ in D₂O as described in Section 2.2.7.1 and incubated at 37 °C throughout the study. Peptide FTIR spectra were obtained in three replicates at different time points then processed individually and analysed by fitting the peaks as described in Section 2.2.9.1. Processed Spectra were averaged and plotted using OriginPro software. From the fitted spectra, percentages of β -sheet were calculated, plotted as means (n = 3) against time at each peptide concentration for all three peptides and then analysed using two-way ANOVA and post-hoc Tukey's test (p < 0.05; Section 2.3).

4.3.2 TEM Imaging for Peptide Morphology and Dimensions

Background

TEM is a high resolution imaging technique that works on the same principle as the light microscope but in TEM, electrons instead of light are transmitted through a thin sample to produce an image. This image shows fine details of the sample at magnifications higher than that of a light microscope because the wavelength of electrons is smaller than that of light.

The morphology as well as the dimensions of self-assembled β -sheet tape forming peptides were investigated using TEM due to the high resolution of images obtained using this technique.

Methods

P₁₁₋₄, P₁₁₋₈ and P₁₁₋₁₂ samples prepared for FTIR (Section 4.3.1) at 10, 20 and 30 mg.mL⁻¹ were also used for TEM imaging. Samples were prepared on TEM grids, imaged and processed as described in Section 2.2.9.2. Fibril widths were measured at the widest point away from the twists and measurements were taken from images at magnifications of x 30,000 and higher. Mean fibril widths (n = 40) were plotted against peptide concentration for each of the peptides then analysed using two-way ANOVA and post-hoc Tukey's test (p < 0.05; Section 2.3).

4.4 Results

4.4.1 FTIR Spectra – β -sheet Proportion and Equilibrium

P₁₁ peptides were investigated using FTIR over a period of 28 days to determine the time taken for each peptide at all tested concentrations (10, 20 and 30 mg.mL⁻¹) to reach equilibrium by comparing the β -sheet percentages between the different time points. Equilibrium was assumed to have been reached when there was no/insignificant change in the β -sheet percentages.

The data presented in this section and the data comparisons mainly correspond to one day following triggering self-assembly. This is because most of the data from studies within acellular artery tissue presented in Chapter 6 were acquired one day after triggering self-assembly.

P₁₁₋₄ FTIR spectra over time at 20 mg.mL⁻¹ are presented in Figure 4.1. Spectra at 10 and 30 mg.mL⁻¹ are presented in Appendix A.3.

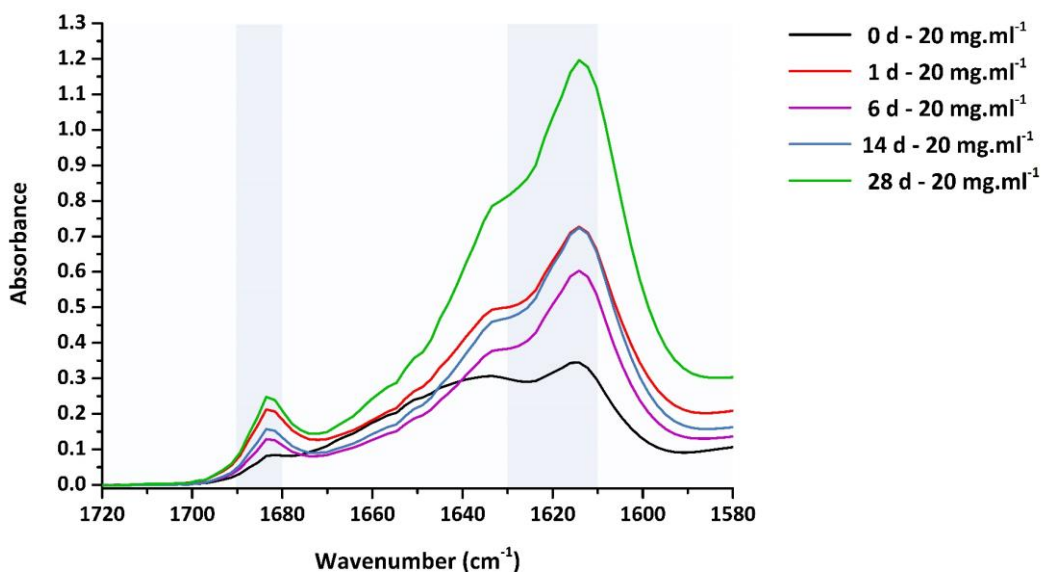
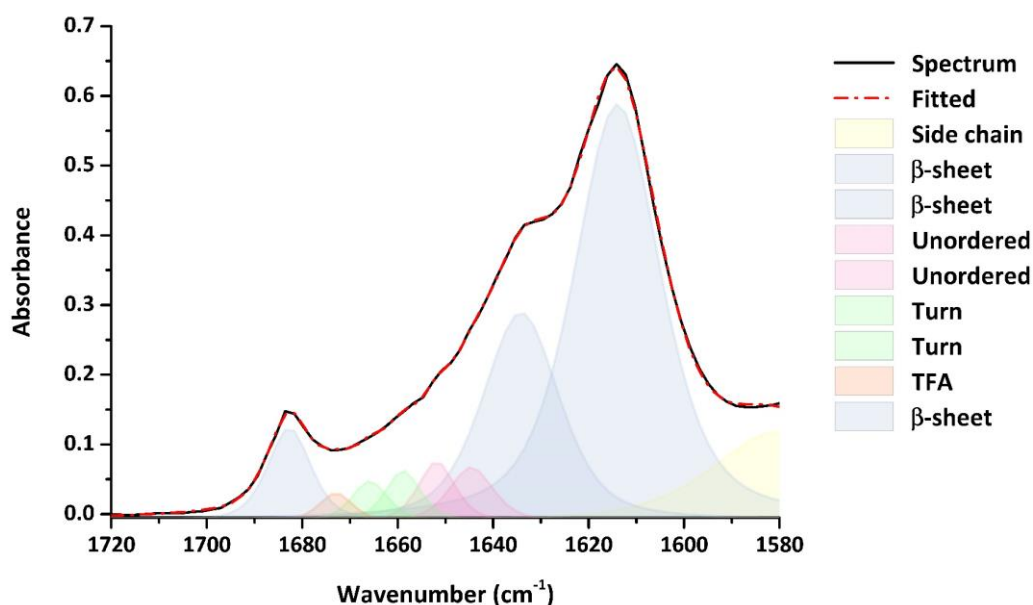


Figure 4.1: P₁₁₋₄ FTIR spectra at 20 mg.mL⁻¹ over time after triggering self-assembly by addition of Ringer's solution. Time: 0 (black), 1 (red), 6 (purple), 14 (blue) and 28 (green) days of incubation at 37 °C. Shaded areas correspond to β -sheet absorptions.

All the acquired spectra for P₁₁₋₄ were processed individually by fitting the spectrum then determining the proportion of secondary structures in the peptide sample as

shown in Figure 4.2 for 20 mg.mL⁻¹ of P₁₁₋₄ one day after triggering self-assembly by addition of Ringer's solution.



Wavenumber at Peak Centre (cm ⁻¹)	Area Under Peak	Peak Assignment	Secondary Structure (%)
1580.002	5.7063	Side chain	-
1613.953	17.2779	β-sheet	56.9
1634.145	7.4977	β-sheet	24.7
1644.588	1.1193	Unordered	3.7
1651.815	1.0332	Unordered	3.4
1658.858	0.8379	Turn	2.8
1665.842	0.6881	Turn	2.3
1672.946	0.4487	TFA	-
1682.703	1.8979	β-sheet	6.3

Figure 4.2: Fitted P₁₁₋₄ FTIR spectrum at 20 mg.mL⁻¹ one day after triggering self-assembly. Data in the Table correspond to each side chain or secondary structure absorption and the percentage of β-sheet deduced from this spectrum was 87.9 %. All other P₁₁₋₄ spectra at the different concentrations, time points and replicates were processed in the same way to determine the percentage of β-sheet in sample.

From the fitted data (Figure 4.2), the main peak for β-sheet conformation was observed centred at 1614 cm⁻¹ and a smaller peak at 1634 cm⁻¹. A weaker absorption band was observed centred at 1683 cm⁻¹ suggesting an antiparallel arrangement of the β-sheet

structure. The other peaks centred at 1645 cm^{-1} and 1652 cm^{-1} corresponded to the unordered random coil state. The total β -sheet secondary structure percentage in P₁₁₋₄ at 20 mg.mL^{-1} one day after triggering self-assembly by changing the ionic strength was 87.9 %, while the unordered random coil state was 7.1 %. In addition, a very small peak centred at 1673 cm^{-1} was assigned to TFA, which was possibly present from peptide synthesis.

The fitted spectra for the remaining replicates and time points at 20 mg.mL^{-1} of P₁₁₋₄ as well as those for 10 and 30 mg.mL^{-1} of P₁₁₋₄, showed similar absorption peaks with slight variations at which peaks were centred (data not shown).

The β -sheet percentages in P₁₁₋₄ samples were calculated from the fitted data and plotted for all tested concentrations at each time point as shown in Figure 4.3.

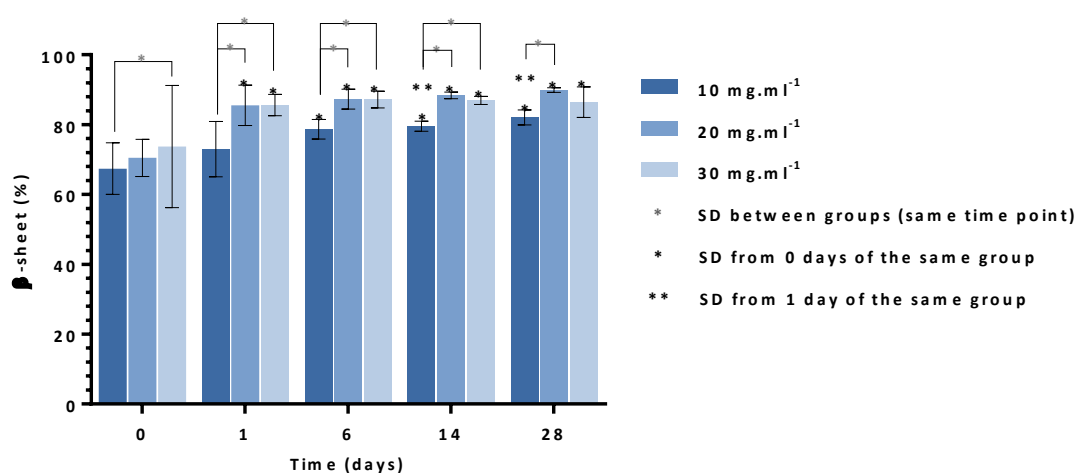


Figure 4.3: P₁₁₋₄ β -sheet percentages at different concentrations over time after triggering self-assembly by addition of Ringer's solution. Data represent the means ($n = 3$) \pm 95 % confidence limits. Equilibrium was reached between 6 and 14 days at 10 mg.mL^{-1} and within one day at 20 and 30 mg.mL^{-1} . The β -sheet percentage at 10 mg.mL^{-1} was significantly lower than at 20 and 30 mg.mL^{-1} at different time points. Significant differences (SD) were determined by two-way ANOVA and post-hoc Tukey's test ($p < 0.05$).

At 10 mg.mL^{-1} of P₁₁₋₄, the percentage of β -sheet was significantly different at days 14 and 28 from day 1 (ANOVA; $p < 0.05$) after triggering self-assembly but not from day 6 suggesting that equilibrium was reached sometime between 6 and 14 days. In 20 and 30 mg.mL^{-1} P₁₁₋₄ samples, equilibrium was reached within one day of triggering self-

assembly because the percentages of β -sheet were only significantly different from day zero (ANOVA; $p < 0.05$).

The percentage of β -sheet in 10 mg.mL⁻¹ of P₁₁₋₄ was significantly lower than in 20 mg.mL⁻¹ of P₁₁₋₄ (ANOVA; $p < 0.05$) at 1, 6, 14 and 28 days after triggering self-assembly, while it was significantly lower than in 30 mg.mL⁻¹ of P₁₁₋₄ at 0, 1, 6 and 14 days. At all time points, there was no significant difference between these values in 20 and 30 mg.mL⁻¹ of P₁₁₋₄.

Therefore, P₁₁₋₄ reached equilibrium within one day after triggering self-assembly and displayed similar β -sheet percentages at 20 and 30 mg.mL⁻¹.

P₁₁₋₈ FTIR spectra over time at 20 mg.mL⁻¹ are presented in Figure 4.4. Spectra at 10 and 30 mg.mL⁻¹ are presented in Appendix A.3.

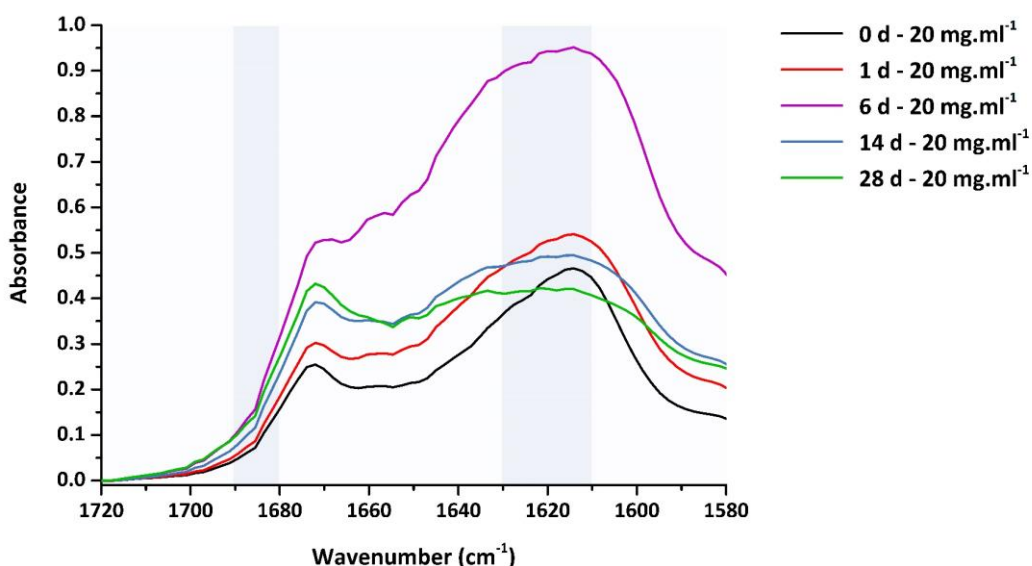
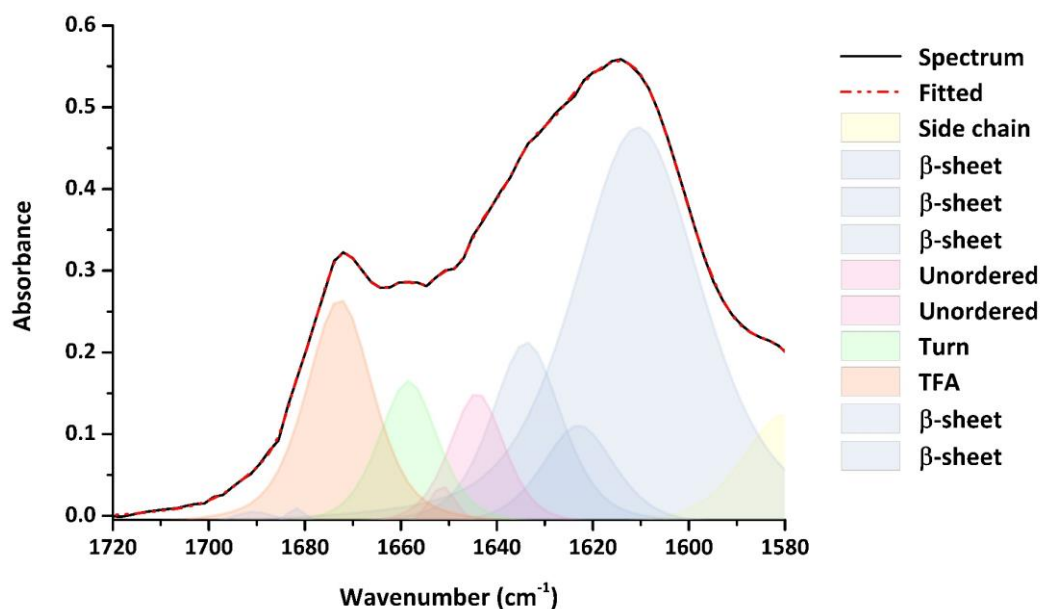


Figure 4.4: P₁₁₋₈ FTIR spectra at 20 mg.mL⁻¹ over time after triggering self-assembly by addition of Ringer's solution. Time: 0 (black), 1 (red), 6 (purple), 14 (blue) and 28 (green) days of incubation at 37 °C. Shaded areas correspond to β -sheet absorptions.

All the acquired spectra for P₁₁₋₈ were processed in a similar manner to P₁₁₋₄ as shown in Figure 4.5 for 20mg.mL⁻¹ of P₁₁₋₈ one day after triggering self-assembly by addition of Ringer's solution. The fitted data for P₁₁₋₈ (Figure 4.5) showed similar results to P₁₁₋₄ with an additional absorption band centred at 1621 cm⁻¹ and a weaker absorption band centred at 1691 cm⁻¹. The total β -sheet secondary structure percentage in P₁₁₋₈ at 20 mg.mL⁻¹ one day after triggering self-assembly by changing the ionic strength was

80.8 %, while the unordered random coil state was 9.6 %. Unlike P₁₁₋₄, an intense peak centred at 1673 cm⁻¹ for TFA was observed, which was introduced during the purification of the peptide by reversed-phase high performance liquid chromatography (HPLC) as a counterion and was possibly bound to positively charged arginine and ornithine residues in the chain.



Wavenumber at Peak Centre (cm ⁻¹)	Area Under Peak	Peak Assignment	Secondary Structure (%)
1580	3.8368	Side chain	-
1610.605	20.2524	β-sheet	56.8
1622.972	2.9518	β-sheet	8.3
1633.816	5.1688	β-sheet	14.5
1644.11	2.9498	Unordered	8.3
1651.341	0.4466	Unordered	1.3
1658.411	3.4561	Turn	9.7
1672.722	6.0998	TFA	-
1681.783	0.1527	β-sheet	0.4
1690.577	0.2908	β-sheet	0.8

Figure 4.5: Fitted P₁₁₋₈ FTIR spectrum at 20 mg.mL⁻¹ one day after triggering self-assembly. Data in the Table correspond to each side chain or secondary structure absorption and the percentage of β-sheet deduced from this spectrum was 80.8 %. All other P₁₁₋₈ spectra at the different concentrations, time points and replicates were processed in the same way to determine the percentage of β-sheet in sample.

The fitted spectra for the remaining replicates and time points at 20 mg.mL⁻¹ of P₁₁₋₈ as well as those for 10 and 30 mg.mL⁻¹ of P₁₁₋₈, showed similar absorption peaks with slight variations at which peaks were centred (data not shown).

The β -sheet percentages in P₁₁₋₈ samples were calculated from the fitted data and plotted for all tested concentrations at each time point as shown in Figure 4.6.

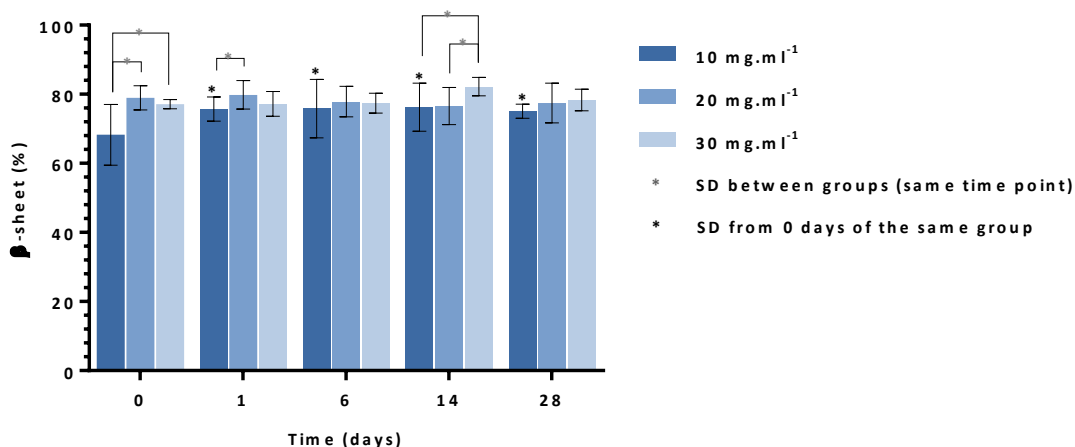


Figure 4.6: P₁₁₋₈ β -sheet percentages at different concentrations over time after triggering self-assembly by addition of Ringer's solution. Data represent the means ($n = 3$) \pm 95 % confidence limits. Equilibrium was reached within 1 day at 10 mg.mL⁻¹ and instantaneously at 20 and 30 mg.mL⁻¹. The β -sheet percentage at 10 mg.mL⁻¹ was significantly lower than at 20 and 30 mg.mL⁻¹ at different time points. Significant differences (SD) were determined by two-way ANOVA and post-hoc Tukey's test ($p < 0.05$).

At 10 mg.mL⁻¹ of P₁₁₋₈, the percentage of β -sheet was significantly different at day 1 from day 0 (ANOVA; $p < 0.05$) suggesting that equilibrium was reached within one day of triggering self-assembly. Equilibrium was reached almost instantly after triggering self-assembly in 20 and 30 mg.mL⁻¹ P₁₁₋₈ samples because the percentages of β -sheet were not significantly different between all tested time points.

The percentage of β -sheet in 10 mg.mL⁻¹ of P₁₁₋₈ was significantly lower than in 20 mg.mL⁻¹ of P₁₁₋₈ (ANOVA; $p < 0.05$) at 0 and 1 days after triggering self-assembly, while these were significantly lower than in 30 mg.mL⁻¹ of P₁₁₋₈ (ANOVA; $p < 0.05$) at 14 days. At all time points, there was no significant difference between these values in 20 and 30 mg.mL⁻¹ of P₁₁₋₈ (except at day 14).

Therefore, P₁₁₋₈ reached equilibrium immediately after triggering self-assembly and displayed similar β -sheet percentages at 20 and 30 mg.mL⁻¹.

P₁₁₋₁₂ FTIR spectra over time at 20 mg.mL⁻¹ are presented in Figure 4.7. Spectra at 10 and 30 mg.mL⁻¹ are presented in Appendix A.3.

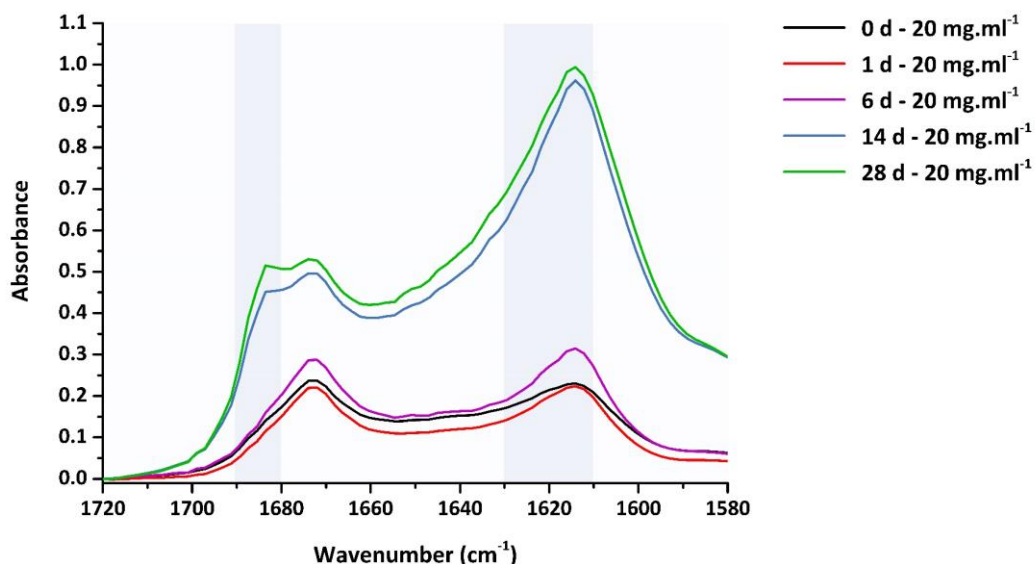
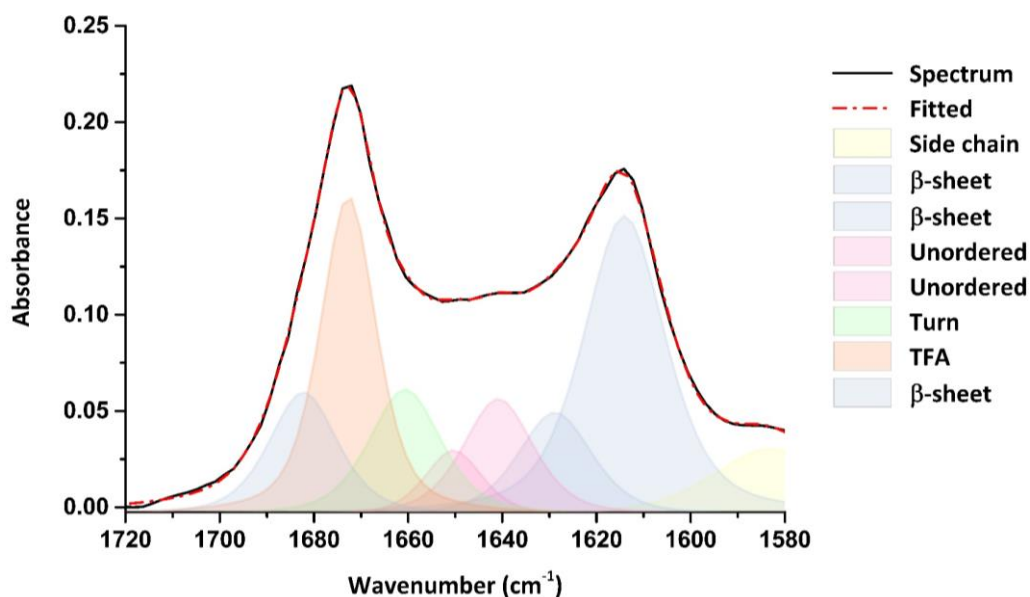


Figure 4.7: P₁₁₋₁₂ FTIR spectra at 20 mg.mL⁻¹ over time after triggering self-assembly by addition of Ringer's solution. Time: 0 (black), 1 (red), 6 (purple), 14 (blue) and 28 (green) days of incubation at 37 °C. Shaded areas correspond to β -sheet absorptions.

All the acquired spectra for P₁₁₋₁₂ were processed in a similar manner to P₁₁₋₄ as shown as shown in Figure 4.8 for 20mg.mL⁻¹ of P₁₁₋₁₂ one day after triggering self-assembly by addition of Ringer's solution. The fitted data in Figure 4.8 showed similar results to P₁₁₋₄. The total β -sheet secondary structure percentage in P₁₁₋₁₂ at 20 mg.mL⁻¹ one day after triggering self-assembly by changing the ionic strength was 66.1 %, while the unordered random coil state was 19.3 %. Similar to P₁₁₋₈ an intense peak for TFA was observed, which was introduced during the purification of the peptide.

The fitted spectra for the remaining replicates and time points at 20 mg.mL⁻¹ of P₁₁₋₁₂ as well as those for 10 and 30 mg.mL⁻¹ of P₁₁₋₁₂, showed similar absorption peaks with slight variations at which peaks where centred (data not shown).



Wavenumber at Peak Centre (cm ⁻¹)	Area Under Peak	Peak Assignment	Secondary Structure (%)
1583.014	1.3518	Side chain	-
1614.056	4.307	β-sheet	40.1
1628.776	1.3232	β-sheet	12.3
1640.825	1.4173	Unordered	13.2
1650.332	0.6536	Unordered	6.1
1660.614	1.5685	Turn	14.6
1672.691	3.1136	TFA	-
1682.227	1.4793	β-sheet	13.8

Figure 4.8: Fitted P₁₁₋₁₂ FTIR spectrum at 20 mg.mL⁻¹ one day after triggering self-assembly. Data in the Table correspond to each side chain or secondary structure absorption and the percentage of β-sheet deduced from this spectrum was 66.1 %. All other P₁₁₋₁₂ spectra at the different concentrations, time points and replicates were processed in the same way to determine the percentage of β-sheet in sample.

The β-sheet percentages in P₁₁₋₁₂ samples were calculated from the fitted data and plotted for all tested concentrations at each time point as shown in Figure 4.9.

At all tested concentrations of P₁₁₋₁₂, the percentage of β-sheet was not significantly different between all time points suggesting either that equilibrium was reached instantly or was yet to be reached. The latter suggestion was more likely due to the large variation in the calculated β-sheet percentages at the same concentration and time point.

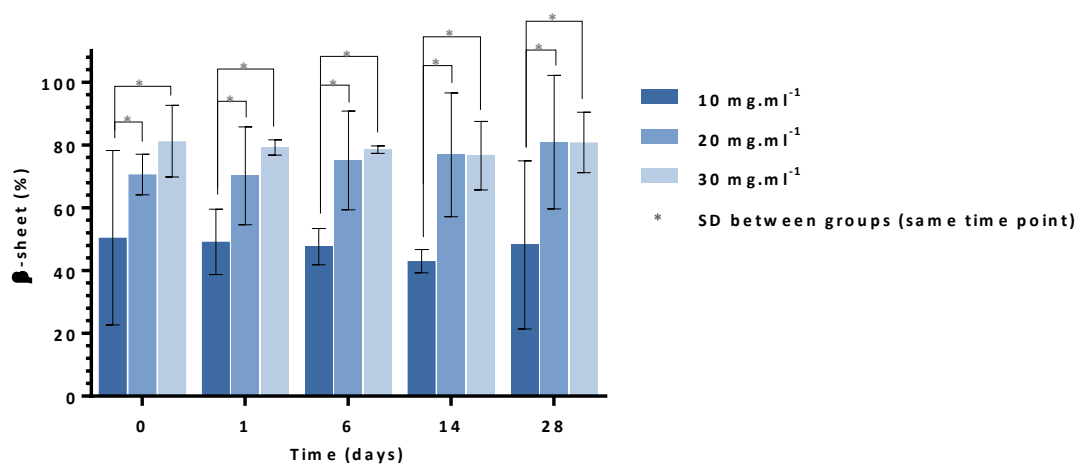


Figure 4.9: P₁₁₋₁₂ β -sheet percentages at different concentrations over time after triggering self-assembly by addition of Ringer's solution. Data represent the means ($n = 3$) \pm 95 % confidence limits. Equilibrium was possibly reached after 28 days at 10, 20 and 30 mg.mL⁻¹. The β -sheet percentage at 10 mg.mL⁻¹ was significantly lower than at 20 and 30 mg.mL⁻¹ at all time points. Significant differences (SD) were determined by two-way ANOVA and post-hoc Tukey's test ($p < 0.05$).

The percentage of β -sheet in 10 mg.mL⁻¹ of P₁₁₋₁₂ was significantly lower than in 20 and 30 mg.mL⁻¹ of P₁₁₋₁₂ (ANOVA; $p < 0.05$) at all tested time points after triggering self-assembly. At all time points, there was no significant difference between these values in 20 and 30 mg.mL⁻¹ of P₁₁₋₁₂.

Therefore, P₁₁₋₁₂ possibly reached equilibrium after 28 days of triggering self-assembly and displayed similar β -sheet percentages at 20 and 30 mg.mL⁻¹.

4.4.2 Peptide Gelation Over Time

The physical state of peptides processed for FTIR was observed at different time points over 91 days. The peptides were imaged before triggering self-assembly by addition of Ringer's solution, immediately after, and at 0, 1, 6, 14, 28 and 91 days after triggering self-assembly. Gelation was observed over time for all peptides at all concentrations as shown in Figure 4.10. In the following observations, the strength of a gel was decided by how easily the gel was disrupted by pipetting or vortexing.

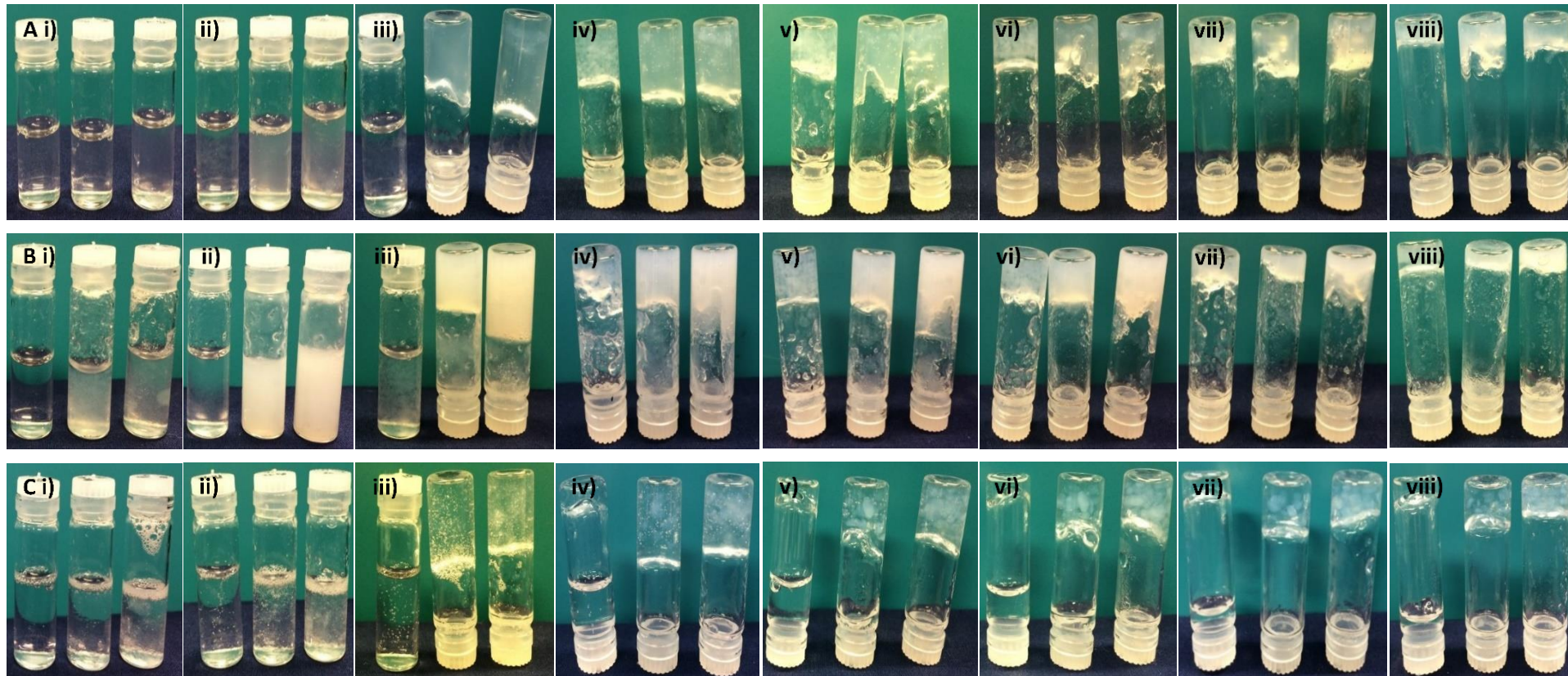


Figure 4.10: P₁₁ peptides gelation over time. A) P₁₁-4, B) P₁₁-8 and C) P₁₁-12 at pH 7.4 i) with no Ringer's solution (day 0), ii) immediately after addition of Ringer's solution (day 0) then following triggering self-assembly after: iii) 0 days, iv) 1 days, v) 6 days, vi) 14 days, vii) 28 days and viii) 91 days. Concentrations: 10, 20 and 30 mg.mL⁻¹ (left to right in each image).

In P₁₁₋₄ samples at 10, 20 and 30 mg.mL⁻¹, clear solutions were observed before triggering self-assembly. After triggering self-assembly, a cloudy solution was observed at 10 mg.mL⁻¹ of P₁₁₋₄ forming a viscous solution over time. While at 20 and 30 mg.mL⁻¹ of P₁₁₋₄, cloudy viscous solutions were observed forming cloudy gels over time. After one day, cloudy gels were observed which slightly increased in strength over the 28 day period and were stronger at 20 and 30 mg.mL⁻¹ of P₁₁₋₄. Very strong milky gels were observed after 91 days (Figure 4.10 A).

In P₁₁₋₈ samples a clear solution was observed at 10 mg.mL⁻¹, while cloudy viscous solutions were observed at 20 and 30 mg.mL⁻¹ of P₁₁₋₈ before triggering self-assembly. After triggering self-assembly, a cloudy solution was observed at 10 mg.mL⁻¹ of P₁₁₋₈ forming a viscous solution over time. While at 20 and 30 mg.mL⁻¹ of P₁₁₋₈ cloudy viscous solutions were observed forming milky gels over time. After one day, gels were observed which slightly increased in strength over the 28 day period and were stronger and milky at 20 and 30 mg.mL⁻¹ of P₁₁₋₈. Very strong milky gels were observed after 91 days (Figure 4.10 B).

In P₁₁₋₁₂ at 10, 20 and 30 mg.mL⁻¹, clear solutions were observed before triggering self-assembly. After triggering self-assembly, clear viscous solutions were observed forming a viscous solution over time at 10 mg.mL⁻¹ of P₁₁₋₁₂ then forming very weak gels at 20 and 30 mg.mL⁻¹ of P₁₁₋₁₂. After one day, clear weak gels were observed with small gel globules within, which increased in size with increasing concentrations and over time. These gels were stronger at 20 and 30 mg.mL⁻¹ yet easily or slightly disrupted. A strong clear gel with gel globules within, a slightly disrupted clear gel with gel globules within and a very weak clear gel were observed at 30, 20 and 10 mg.mL⁻¹ of P₁₁₋₁₂ respectively after 91 days (Figure 4.10 C).

Detailed observations of the physical state of each peptide at each concentration shown in Figure 4.10 can be found in Appendix A.4.

4.4.3 TEM Images of Peptide Fibrillar Networks Forming Gels

Images of peptide gel networks were obtained using TEM to investigate the morphology of P₁₁₋₄, P₁₁₋₈ and P₁₁₋₁₂ and are shown in Figure 4.11, Figure 4.12 and Figure 4.13, respectively.

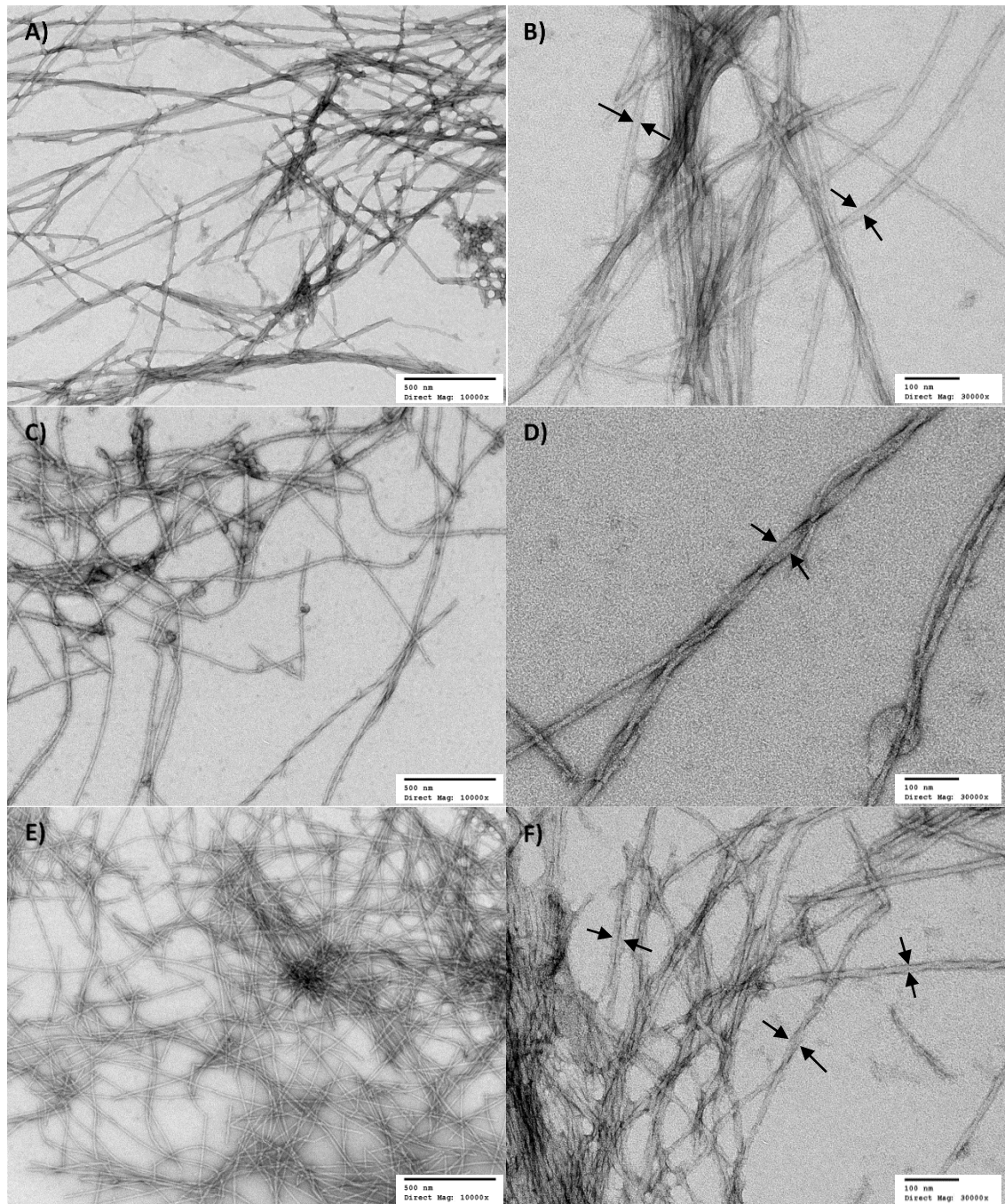


Figure 4.11: TEM images of P₁₁₋₄ at different concentrations. P₁₁₋₄ at: A - B) 10 mg.mL⁻¹, C - D) 20 mg.mL⁻¹ and E - F) 30 mg.mL⁻¹. Arrows represent the measured fibrillar widths. Images acquired at: x 10,000 magnification and scale bars represent 500 nm (left) and x 30,000 magnification and scale bars represent 100 nm (right).

P₁₁₋₄ formed long fibrils that extended beyond the field of view in the acquired images at all tested concentrations with average widths of 24.8 ± 4.9 nm, 24.1 ± 3.8 nm and 24.4 ± 5.2 nm ($n = 40$) at 10, 20 and 30 mg.mL⁻¹, respectively. Fibres consisting of entwining fibrils were more often observed in 20 and 30 mg.mL⁻¹ P₁₁₋₄ samples. These

fibrils/fibres formed dense networks that were slightly denser with increasing concentration (Figure 4.11).

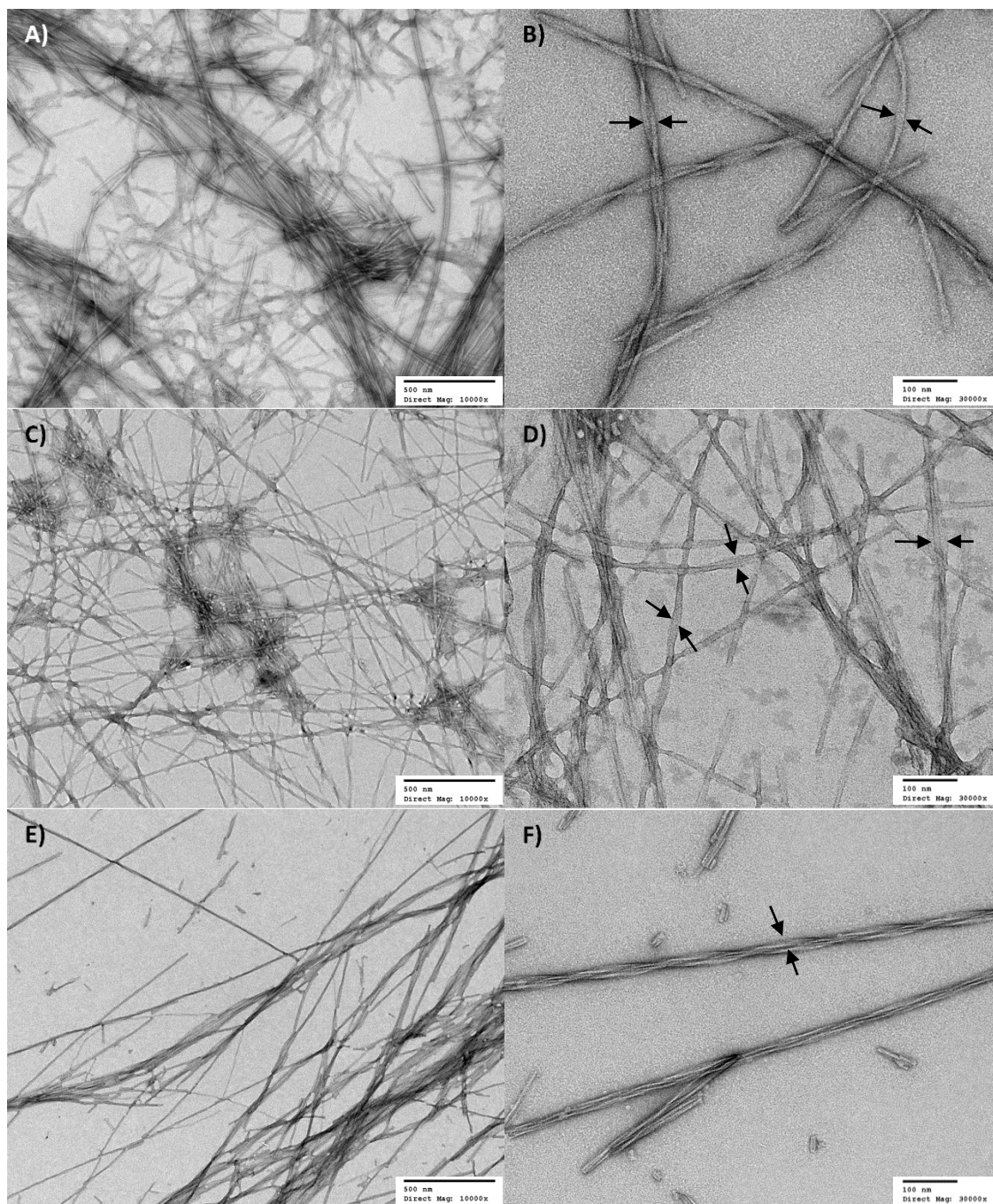


Figure 4.12: TEM images of P₁₁₋₈ at different concentrations. P₁₁₋₈ at: A - B) 10 mg.mL⁻¹, C - D) 20 mg.mL⁻¹ and E - F) 30 mg.mL⁻¹. Arrows represent the measured fibrillar widths. Images acquired at: x 10,000 magnification and scale bars represent 500 nm (left) and x 30,000 magnification and scale bars represent 100 nm (right).

P₁₁₋₈ formed long fibrils that extended beyond the field of view in the acquired images at all tested concentrations with average widths of 31.9 ± 21.3 nm, 29.1 ± 4.5 nm and

30.7 ± 4.5 nm ($n = 40$) at 10, 20 and 30 $\text{mg}\cdot\text{mL}^{-1}$, respectively. Fibres consisting of entwining fibrils were observed at all concentrations. These fibrils/fibres formed dense networks (Figure 4.12).

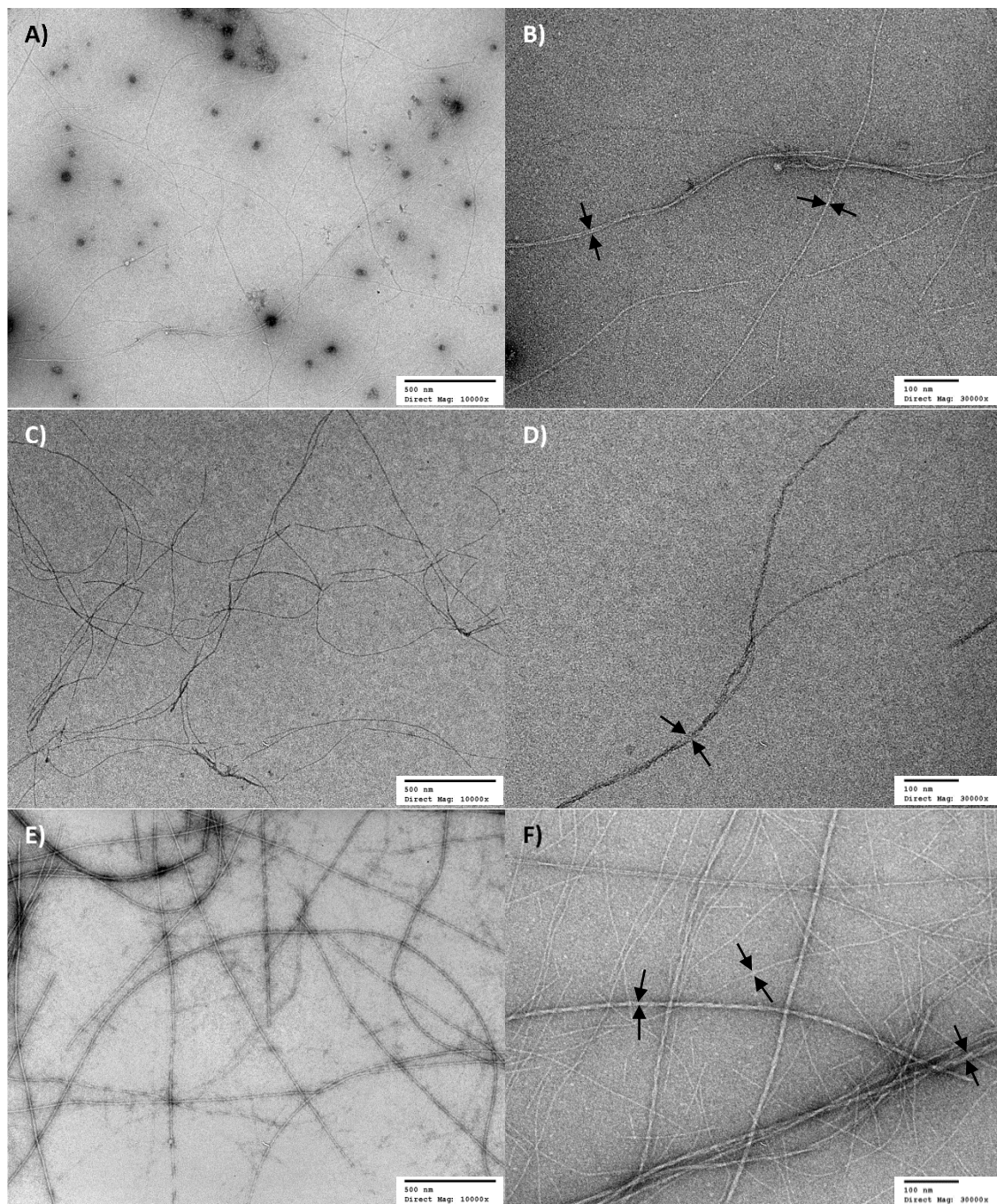


Figure 4.13: TEM images of P₁₁₋₁₂ at different concentrations. P₁₁₋₁₂ at: A - B) 10 $\text{mg}\cdot\text{mL}^{-1}$, C - D) 20 $\text{mg}\cdot\text{mL}^{-1}$ and E - F) 30 $\text{mg}\cdot\text{mL}^{-1}$. Arrows represent the measured fibrillar widths. Images acquired at: $\times 10,000$ magnification and scale bars represent 500 nm (left) and $\times 30,000$ magnification and scale bars represent 100 nm (right).

P₁₁₋₁₂ formed very thin long fibrils at all tested concentrations with average widths of 13.9 ± 2.6 nm, 13.1 ± 1.5 nm and 15.4 ± 2.2 nm ($n = 40$) at 10, 20 and 30 mg.mL⁻¹, respectively. Almost no fibres were observed at 10 and 20 mg.mL⁻¹, but possibly a few at 30 mg.mL⁻¹ of P₁₁₋₁₂. Fibrils formed networks that were denser in the 30 mg.mL⁻¹ P₁₁₋₁₂ sample (Figure 4.13).

There was no significant difference between fibril widths at different concentrations of the same peptide and between the same concentrations of P₁₁₋₄ and P₁₁₋₈. However, P₁₁₋₁₂ displayed the smallest fibril widths which were significantly smaller than that of P₁₁₋₈ at the same concentration (Figure 4.14, ANOVA; $p < 0.05$).

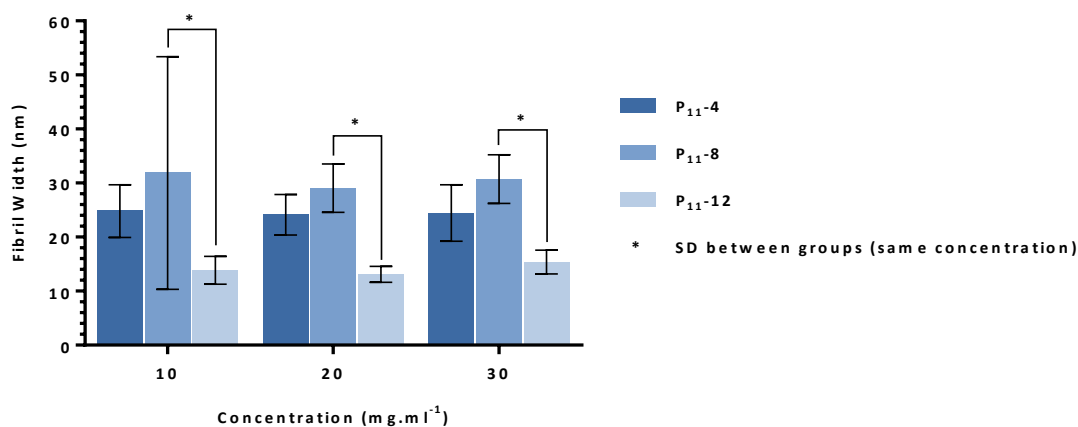


Figure 4.14: P₁₁₋₄, P₁₁₋₈ and P₁₁₋₁₂ fibril widths as determined by TEM. Data represent the means ($n = 3$) \pm 95 % confidence limits. P₁₁₋₁₂ was shown to have significantly smaller fibril widths compared to P₁₁₋₈ at 10, 20 and 30 mg.mL⁻¹. Significant differences (SD) were determined by two-way ANOVA and post-hoc Tukey's test ($p < 0.05$).

4.5 Discussion

Self-assembly and gelation behaviour of P₁₁₋₄, P₁₁₋₈ and P₁₁₋₁₂ was observed over 28 days. The secondary structures in these peptides at 10, 20 and 30 mg.mL⁻¹ were determined using FTIR, from which the β -sheet proportion was deduced and used to determine the time taken to reach equilibrium. Equilibrium was suggested to be when the proportion of β -sheet within a sample was unchanged or changed insignificantly between the tested time points. In P₁₁₋₄, equilibrium was reached between 6 and 14 days after triggering self-assembly at 10 mg.mL⁻¹, while it was reached within 1 day at 20 and 30 mg.mL⁻¹. In P₁₁₋₈, equilibrium was reached within 1 day after triggering self-

assembly at 10 mg.mL⁻¹, while it was reached almost instantly at 20 and 30 mg.mL⁻¹. However, it was possible that equilibrium was not reached within the tested time period of one month in P₁₁₋₁₂ at all tested concentrations because no significant difference was found in β -sheet percentage between all tested time points. Also because of the significant changes in the gelation behaviour observed over the tested period. Investigation over a longer period of time may be required for confirmation of these findings, especially for P₁₁₋₁₂.

In FTIR amide region I/I', the β -sheet conformation with antiparallel arrangement has been reported to have a high frequency absorption above 1680 cm⁻¹ and low frequency absorption below 1640 cm⁻¹ when compared to the parallel arrangement having low frequency absorptions but lacking the high frequency absorption^{218,219}. Here, high intensity absorption peaks between 1611 cm⁻¹ and 1634 cm⁻¹ alongside weaker absorptions > 1680 cm⁻¹ were observed in P₁₁₋₄, P₁₁₋₈ and P₁₁₋₁₂ at 10, 20 and 30 mg.mL⁻¹ and at all tested time points (0, 1, 6, 14 and 28 days) implying the antiparallel arrangement of the β -sheet structure. For the unordered random coil state, peaks were observed around 1640 cm⁻¹ and 1652 cm⁻¹. Similar results have been reported in previous studies using the P₁₁ peptides, where in general an intense and a weaker absorption peak was reported around similar frequencies corresponding to antiparallel β -sheet^{142,149,172}. In one study of peptides at approximately 10 mg.mL⁻¹, these absorption peaks were: at 1618 and 1682 cm⁻¹, respectively in P₁₁₋₄; and at 1614 and 1684 cm⁻¹, respectively in P₁₁₋₈. In P₁₁₋₁₂, the main peaks were observed at 1614 and 1625 cm⁻¹ and the weaker peaks at 1685 and 1695 cm⁻¹. In addition, an absorption peak for the unordered random coil state was reported at 1645 cm⁻¹ and another at 1672 cm⁻¹ for residual TFA counterions¹⁴².

The proportion of β -sheet and unordered random coil state were also determined by FTIR spectra. At 10 mg.mL⁻¹, both P₁₁₋₄ and P₁₁₋₈ were shown to have significantly higher percentages of β -sheet than P₁₁₋₁₂ over the 28 days. At 20 mg.mL⁻¹, P₁₁₋₄ was shown to have significantly higher percentages of β -sheet than P₁₁₋₈ and P₁₁₋₁₂ following triggering self-assembly after 1, 6, 14 and 28 days. At 30 mg.mL⁻¹, P₁₁₋₄ was also shown to have significantly higher β -sheet percentages than the other two peptides but at varying time points (data not shown). From the fitted data, one day after triggering self-assembly by changing the ionic strength at 20 mg.mL⁻¹, it was shown

that 85.5 % of secondary structures in P₁₁₋₄ were self-assembled into antiparallel β -sheet structures and 8.6 % were in the monomeric unordered random coil form. The percentages of self-assembled β -sheet structures and the monomeric unordered random coil form were 79.8 % and 11.3 %, respectively in P₁₁₋₈. In P₁₁₋₁₂, these were found to be 70.2 % and 18.0 %, respectively.

The degradability of these peptides can be facilitated *in vivo* due to the coexistence of the random coil monomeric state with the self-assembled state potentially allowing peptides to be used as biodegradable materials for biological applications. For tissue engineering applications requiring the presence of peptide gels for a certain period of time, for example when used with acellular arteries as a scaffold to enhance the re-endothelialisation of tissue, it is important for peptides to be stable *in vivo* for as long as possible to support cell attachment and growth. P₁₁₋₄ (0.31 ± 0.072 mM) and P₁₁₋₈ (0.4 ± 0.1 mM) have been reported to have lower critical self-assembly concentrations than P₁₁₋₁₂ (2.3 ± 0.75 mM) under physiological conditions, meaning they have a lower monomeric proportion because their structures are based on glutamine residues rather than the smaller serine residues in P₁₁₋₁₂ that result in weaker intermolecular interactions^{172,220,221}. It was therefore concluded that *in vivo*, the monomeric proportion of these peptides will diffuse out of gel when in contact with excess solution, hence these peptides will de-assemble to establish equilibrium by having the same proportion of the monomeric state (i.e. critical self-assembly concentration) until all peptide is removed from the system¹⁷². Because P₁₁₋₄ and P₁₁₋₈ have been shown to have a lower proportion of monomers than P₁₁₋₁₂, they may possibly have a longer lifetime *in vivo* as P₁₁₋₁₂ will be removed faster from the site of application to establish equilibrium. Here, P₁₁₋₄ generally exhibited the highest proportion of β -sheet at 20 mg.mL^{-1} and the lowest monomeric proportion (significantly lower than P₁₁₋₁₂; data not shown), hence would possibly be the most stable peptide with the potential to last for a longer period of time but this requires further studies. At the same concentration, P₁₁₋₈ also exhibited a lower monomeric proportion than P₁₁₋₁₂ and higher than P₁₁₋₄ but this was not significantly different (data not shown).

The gelation of peptides was noted before triggering self-assembly and at each time following triggering self-assembly, FTIR was carried out. All peptides were shown to form gels with varying concentrations at different rates with the exception of P₁₁₋₁₂ at

10 mg.mL⁻¹ that consisted of both a weak gel and a viscous solution. It has been reported that in the presence of 130 mM NaCl at 10 mg.mL⁻¹, P₁₁₋₄ formed a gel around 6 < pD < 11, P₁₁₋₈ formed a biphasic solution consisting of gel within a clear solution around physiological pD > ~ 7.4 while it formed a gel at pD > 8.5 and P₁₁₋₁₂ formed a viscous solution which formed gels with increasing pD > 8.5¹⁴². Another study reported formation of gels at 20 mg.mL⁻¹ in P₁₁₋₄, P₁₁₋₈ and P₁₁₋₁₂, whilst at 10 mg.mL⁻¹ these formed fluids, biphasic solutions and fluids, respectively at pH 7.4 in PBS²²². Different factors can contribute to self-assembly such as temperature and ionic strength²²³, which could potentially change the pH at which gelation occurs. An increase in ionic strength of a peptide with the same concentration has been reported to promote self-assembly by enhancing hydrophobic interactions and hydrogen bonding that interconnect forming fibrillar networks of stiffer gels at a faster rate than in the absence of salt²²⁴. In this study, it is possible that at 10 mg.mL⁻¹ P₁₁₋₈ formed a gel, whilst P₁₁₋₁₂ formed a gel that partially formed a viscous solution when inverted in a vial around physiological pD 7.4 because of the stronger charge screening effect caused by Ringer's solution containing components other than NaCl. Gels were also suggested to form at lower pH at higher concentrations¹⁴² and here, more stable and stronger gels were formed with increasing concentrations around physiological pD 7.4 in all peptides.

Ozbaz *et al.* reported a faster β -sheet self-assembly and gelation rate of samples (MAX1 peptide) at 37 °C when compared to 20 °C²²⁴. However, this should not have a significant effect in studies within acellular tissue because assessments will be carried out following at least one day after triggering self-assembly by ionic strength. Furthermore, the effect of temperature on self-assembly of P₁₁₋₄, P₁₁₋₈ and P₁₁₋₁₂ was investigated at 30 mg.mL⁻¹ over 28 days showing slight variations in the percentages of β -sheets as determined by FTIR (data can be found in Appendix A.5) with almost no visible changes in the physical state and gelation times.

P₁₁ peptides are known to self-assemble into β -sheet structures from tapes and ribbons to fibrils then fibres and the entanglement of these at high concentrations above the critical gelation concentrations forms gels^{172,173,176}. TEM was used to investigate the structures formed in these peptides at different concentrations. P₁₁₋₄ and P₁₁₋₈ formed both fibrils and fibres but only fibrils were formed in P₁₁₋₁₂ with the exception of 30 mg.mL⁻¹ samples. These were significantly thinner and less dense in P₁₁₋₁₂, however

all peptides formed fibrillar networks forming gels with varying densities and appearances at all concentrations. A previous study reported that a change in ionic strength did not have an effect on the morphology of fibrils formed in P₁₁₋₄, P₁₁₋₈ and P₁₁₋₁₂. These peptides were also shown to form fibrils with varying widths at pH 7.4 in presence of 130 mM NaCl ¹⁴².

The different properties exhibited by self-assembling peptides can be controlled by carefully designing the primary structure of the peptide chain with certain amino acid residues that would allow for different self-assembling behaviour as a response to external stimuli including pH, ionic strength and temperature with different mechanical properties depending on the type of application. For example, P₁₁₋₄ has been investigated as a scaffold for the regeneration of enamel in early caries lesions and was applied non-invasively as a treatment called 'filling without drilling'. In this application, the peptide was applied to the affected site and self-assembly was triggered *in vivo* by physiological changes of pH and ionic strength. These studies showed that P₁₁₋₄, in addition to supporting the regeneration of enamel, was safe to use clinically ¹⁷⁹.

The characterisation of peptides under physiological conditions presented in this chapter suggested the use of 20 mg.mL⁻¹ peptides for future investigations. This was because at this concentration, all peptides formed gels with high β -sheet percentages (> 70 %) within an acceptable period of time and results were not significantly different from those at the higher concentration of 30 mg.mL⁻¹. In addition, the data primarily suggested the use of P₁₁₋₄ and P₁₁₋₈ which formed more stable self-supporting gels compared to P₁₁₋₁₂, in addition to the inconsistent results and large variations found in P₁₁₋₁₂ which produced gels that were generally weaker with higher proportion of monomer present. However, studying self-assembly of these peptides within the acellular artery tissue may show better properties for applications in vascular grafts such as anti-thrombogenic properties and sufficient coating of the tissue ECM structures at the luminal surface. As a result, all three peptides were taken for further investigation of the effect on thrombus formation and self-assembly within tissue as will be discussed in Chapter 6.

4.6 Summary of Peptide Self-assembly Characterisation

The results in this chapter have shown that at 20 mg.mL⁻¹, both P₁₁₋₄ and P₁₁₋₈ reached equilibrium almost instantaneously following triggering self-assembly forming strong self-supporting gels. In contrast, equilibrium was possibly not reached within 28 days in P₁₁₋₁₂ forming weaker gels at the same concentration. P₁₁₋₁₂ was shown to form thinner fibrils than P₁₁₋₄ and P₁₁₋₈ with slower gelation times. A summary of the physical state of these peptides and characterisation results from FTIR and TEM studies are displayed in Table 4.1.

Table 4.1: Summary of P₁₁₋₄, P₁₁₋₈ and P₁₁₋₁₂ characterisation at 10, 20 and 30 mg.mL⁻¹ 0, 1, 6, 14 and 28 days after triggering self-assembly. *G* (gel), *S* (solution) and *VS* (viscous solution).

Peptides	Concentration (mg.mL ⁻¹)	Observation	FTIR		TEM
		State	β -sheet (%)	Equilibrium	Fibril Width (nm)
P ₁₁₋₄	10	0 days – cloudy (S) 1 day – cloudy (VS) 6 days – cloudy (G) 14 days – cloudy (G) 28 days – cloudy (G)	67.4 ± 7.4 73.0 ± 7.9 78.7 ± 2.8 79.5 ± 1.4 82.1 ± 2.1	Between 6 and 14 days following triggering self-assembly	24.8 ± 4.9
	20	0 days – cloudy (G) 1 day – cloudy (G) 6 days – cloudy (G) 14 days – cloudy (G) 28 days – cloudy (G)	70.5 ± 5.3 85.5 ± 5.8 87.3 ± 2.7 88.4 ± 1.6 89.9 ± 0.6	Within 1 day of triggering self-assembly	24.1 ± 3.8
	30	0 days – cloudy (G) 1 day – cloudy (G) 6 days – cloudy (G) 14 days – cloudy (G) 28 days – cloudy (G)	73.7 ± 7.5 85.6 ± 3.1 87.2 ± 2.4 86.9 ± 1.1 86.4 ± 4.4	Within 1 day of triggering self-assembly	24.4 ± 5.2
P ₁₁₋₈	10	0 days – cloudy (S) 1 day – cloudy (G) 6 days – cloudy (G) 14 days – cloudy (G) 28 days – cloudy (G)	68.3 ± 8.8 75.7 ± 3.5 73.8 ± 8.5 79.4 ± 7.0 75.1 ± 2.0	Within 1 day of triggering self-assembly	31.9 ± 21.3
	20	0 days – milky (G) 1 day – milky (G) 6 days – milky (G) 14 days – milky (G) 28 days – milky (G)	79.0 ± 3.5 79.8 ± 4.1 77.9 ± 4.4 76.7 ± 5.4 77.4 ± 5.8	Instantaneous	29.1 ± 4.5

Peptides	Concentration (mg.ml ⁻¹)	Observation	FTIR		TEM
		State	β -sheet (%)	Equilibrium	Fibril Width (nm)
	30	0 days – milky (G) 1 day – milky (G) 6 days – milky (G) 14 days – milky (G) 28 days – milky (G)	77.1 ± 1.3 77.2 ± 3.6 77.4 ± 2.9 82.2 ± 2.7 78.3 ± 3.1	Instantaneous	30.7 ± 4.5
P ₁₁₋₁₂	10	0 days – clear (VS) 1 day – clear (G/VS) 6 days – clear (G/VS) 14 days – clear (G/VS) 28 days – clear (G/VS)	50.5 ± 27.8 49.1 ± 10.4 47.6 ± 5.8 43.0 ± 3.7 48.2 ± 27.6	> 28 days (?) following triggering self- assembly due to the large variation within gel sample	13.9 ± 2.6 Significantly lower than P ₁₁₋₈ at the same concentration
	20	0 days – clear (G) 1 day – clear (G) 6 days – clear (G) 14 days – clear (G) 28 days – clear (G)	70.6 ± 13.5 70.2 ± 15.6 75.1 ± 18.7 76.9 ± 19.7 80.9 ± 21.3	> 28 days (?) following triggering self- assembly due to the large variation within gel sample	13.1 ± 1.5 Significantly lower than P ₁₁₋₈ at the same concentration
	30	0 days – clear (G) 1 day – clear (G) 6 days – clear (G) 14 days – clear (G) 28 days – clear (G)	81.2 ± 11.4 79.2 ± 2.4 78.4 ± 1.1 76.6 ± 14.0 80.8 ± 9.7	> 28 days (?) following triggering self- assembly due to the large variation within gel sample	15.4 ± 2.2 Significantly lower than P ₁₁₋₈ at the same concentration

5 Synthesis of Functionalised Peptides

5.1 Introduction

In this chapter, the synthesis of fluorescently-labelled peptides as well as cell attachment motifs is described using fluorenylmethoxycarbonyl (Fmoc) solid phase peptide synthesis (SPPS). Fluorescently-labelled peptides were synthesised to enable investigation of self-assembled peptides within acellular arteries under fluorescent and multiphoton microscopes allowing visualisation of these peptides within the tissue as will be discussed in Chapter 6. RGD and YIGSR are naturally binding motifs that are recognised by many cells including endothelial cells and found in native proteins of the extracellular matrix (ECM) which are known to enhance cell attachment to the ECM¹¹³. GRGDS and YIGSR cell attachment motifs and their scrambled controls (*GRDGS* and *YIRSG*) were synthesised to functionalise the P₁₁ peptides allowing investigation of the effect of functionalisation on cell attachment onto acellular arteries coated with these peptides as will be discussed in Chapter 7. The scrambled controls have the same amino acids as the corresponding cell attachment motifs but in a different order (shown in *italic*). These sequences were not reported to promote cell attachment and do not mimic the binding sites in nature, allowing for validation of the activity of the selected cell attachment motifs. The bioactive (cell attachment functionalised) peptides were synthesised by copper catalysed click chemistry between the cell attachment motifs GRGDS and YIGSR (and scrambled controls), which were synthesised with an alkyne group at the C-terminus and the P₁₁ self-assembling peptides, which have an azide group at the N-terminus.

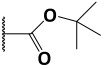
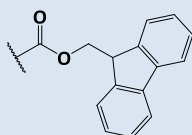
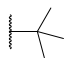
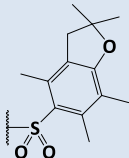
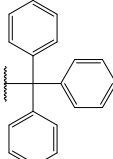
5.2 Aims and Objectives

- To synthesise and purify FITC-labelled P₁₁-8 and P₁₁-12 to mimic the previously synthesised FITC-labelled P₁₁-4 through Fmoc SPPS;
- To synthesise and purify P₁₁-4 and P₁₁-8 functionalised with the cell attachment motifs (GRGDS and YIGSR) and corresponding scrambled controls (*GRDGS* and *YIRSG*).

5.3 Solid Phase Peptide Synthesis (SPPS) – Fmoc Chemistry

SPPS is an efficient technique that is commonly used for linear peptide assembly. It was first developed by Merrifield in 1963²²⁵ and has since been significantly optimised. Peptides are assembled from the C-terminus to the N-terminus. The basis of this technique involves attaching the C-terminus of the first amino acid covalently to a solid polymer resin followed by stepwise addition of amino acid building blocks to make the desired peptide chain followed by cleavage of the peptide from the solid support^{225,226}. Fmoc protection of the N-termini of amino acids in SPPS is one of the two main protecting groups used in this procedure. Fmoc can be removed under basic conditions. Therefore, the side-chain protecting groups used in Fmoc chemistry can be removed simultaneously with the final peptide cleavage from the solid support under acidic conditions^{227,228}. The side-chain and N-terminal protecting groups used in the synthesis are listed in Table 5.1.

Table 5.1: Protecting groups used in SPPS.

Amino acid	Protecting Group	Abbreviation
Ornithine Tryptophan		Boc (<i>tert</i> -butoxycarbonyl)
All amino acids (N-terminus)		Fmoc (9-fluorenylmethoxycarbonyl)
Aspartic acid Glutamic acid Serine Tyrosine		OtBu (<i>tert</i> -butyl)
Arginine		Pbf (2,2,4,6,7-pentamethyl-2H-benzofuran-5-sulfonyl)
Glutamine		Trt (trityl)

5.3.1 FITC-labelled Peptides Synthesis

Labelling peptides with fluorescent dyes provides a way of studying them using fluorescent microscopy. In this study, peptides were labelled with FITC, a fluorescein derivative label widely used in biological studies, to allow for investigation of self-assembly within acellular tissue. FITC-labelled P₁₁₋₄ was previously synthesised by Fmoc SPPS. FITC-labelled P₁₁₋₈, P₁₁₋₁₂ and FITC- β -alanine (FITC- β A) control were synthesised (Figure 5.1) as described in Section 2.2.8.1.

For FITC-labelled P₁₁₋₈, the amino acids Q, Q, E, F, O, W, O, F, R, Q then Q were assembled onto the resin followed by β A to act as a spacer separating the bulky FITC label from the peptide chain. FITC was then coupled with DIPEA to the peptide chain and no activation was required as FITC is an amine reactive derivative. Finally, the peptide was cleaved from the resin. The process of coupling FITC to a peptide chain through a β A linker was previously reported by Jullian and co-workers²²⁹. The peptide assembly and cleavage is summarised in Scheme 5.1. Peptides were purified using a reversed-phase high performance liquid chromatography (HPLC) column with UV detection as described in Section 2.2.8.5.

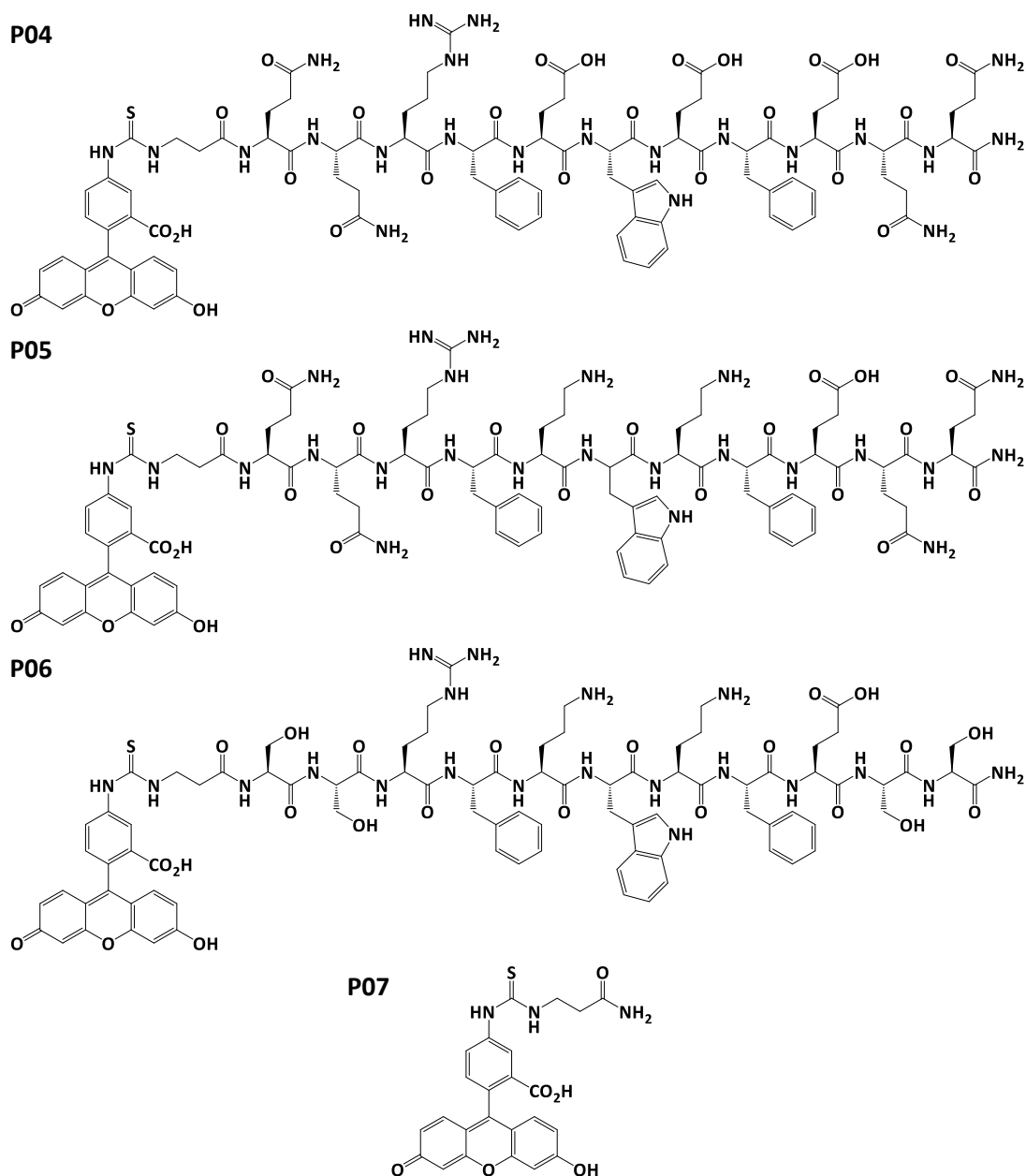
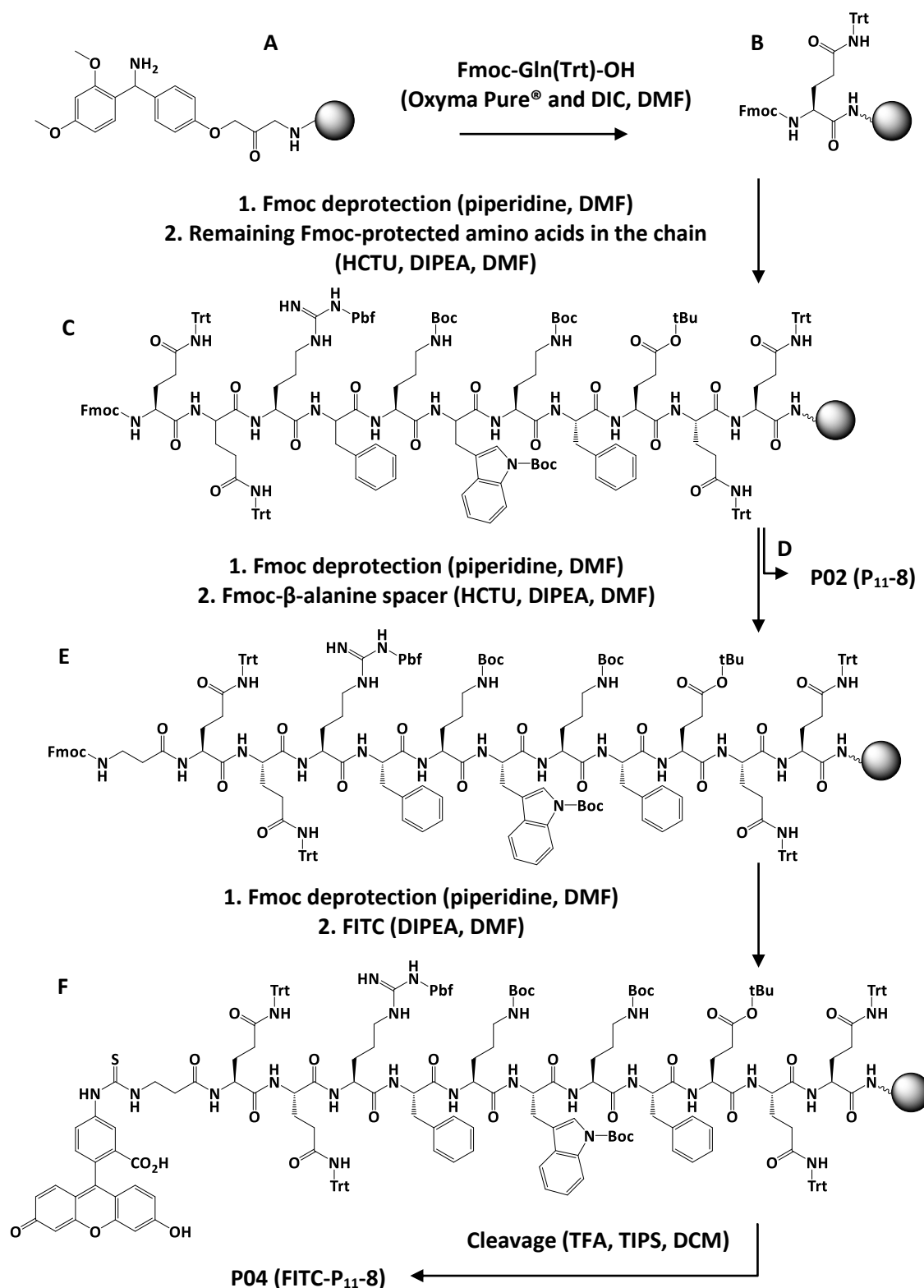


Figure 5.1: Structures of FITC-labelled P₁₁ peptides and FITC control. *FITC-P₁₁-4 (P04), FITC-P₁₁-8 (P05), FITC-P₁₁-12 (P06) and FITC-BA (control, P07).* In the chain, the β -alanine (β A) was used as a spacer between the FITC and the peptide chain. For control, the spacer and FITC were synthesised.



Scheme 5.1: Linear synthesis of FITC-P₁₁₋₈ by Fmoc SPPS. A) Rink amide NovaGelTM resin. B) Loading of first amino acid. C) Coupling of remaining amino acids in the chain. D) P₁₁₋₈ (P02) is synthesised by acetylation of the N-terminus following the assembly of amino acids in the chain then cleaved with the TFA cocktail. E) Coupling of β-alanine spacer. F) FITC coupling to the N-terminus of the peptide chain. Cleavage of E from resin producing peptide P04.

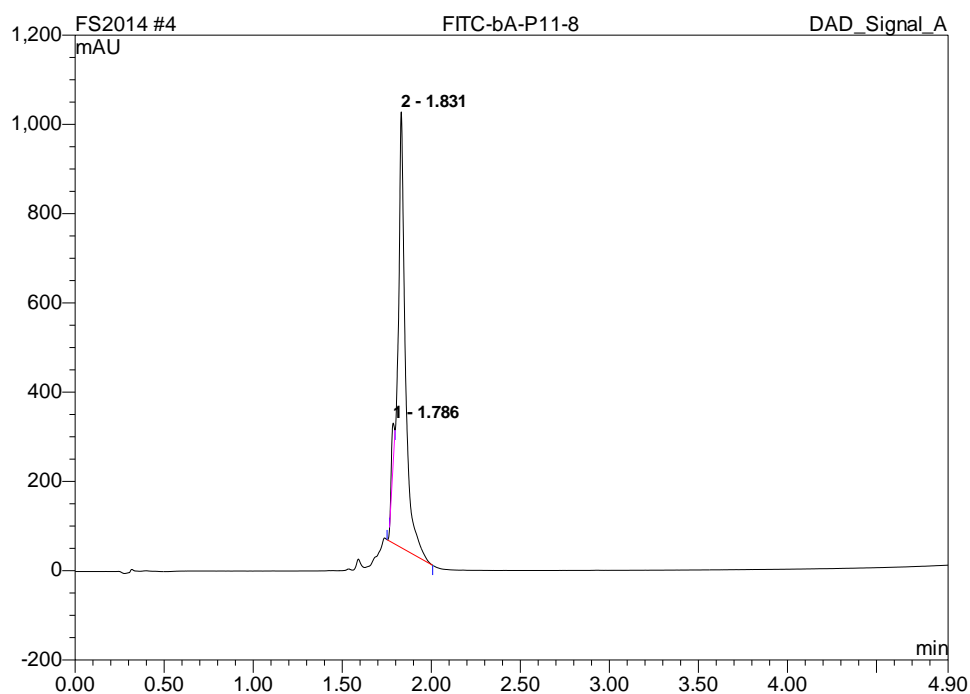
Following synthesis, analysis was carried out as described in Section 2.2.8.6. The synthesised peptide identity was confirmed by liquid chromatography-mass spectrometry (LC-MS) and accurate mass spectrometry. The purity was determined by analytical HPLC.

The results for FITC-P₁₁-8 (M_w 1984.2; Figure 5.2) were as follows:

Analytical HPLC trace: 96.67 %;

Accurate MS (ES⁺): m/z found $[M+3H]^{3+}$ 662.2930; C₉₄H₁₁₈N₂₄O₂₃S requires 662.2923;

LC-MS (ES⁺): m/z found $[M+2H]^{2+}$ 993.4, $[M+3H]^{3+}$ 662.3.



Peak No.	Ret.Time (min)	Height (mAU)	Area (mAU*min)	Rel.Area (%)
1	1.79	89.309	1.720	3.33
2	1.83	976.463	50.007	96.67
Total	-	1065.773	51.727	100.00

Figure 5.2: Analytical HPLC trace for FITC-P₁₁-8 and its corresponding data. The purity was found to be 96.7 %.

FITC-labelled P₁₁-12 and FITC- β A were synthesised as described for FITC-labelled P₁₁-8 in Scheme 5.1 then purified under the same conditions and the detailed analytical HPLC traces, purity and mass spectrometry results can be found in Appendix A.6 (A.6.1). The

results for mass spectrometry and purity of synthesised FITC-labelled peptides are summarised in Table 5.2.

Table 5.2: Table summarising the analysis results for synthesised FITC-labelled peptides showing the expected molecular mass, mass acquired by mass spectrometry and purity acquired by HPLC.

Peptide	Expected $[M+nH]^{n+}$	LC-MS	Accurate Mass	Purity (%)
FITC-P₁₁-8-NH₂	3+ (662.2923)	3+ (662.3)	3+ (662.2930)	96.7
FITC-P₁₁-12-NH₂	3+ (607.5903)	3+ (607.4)	3+ (607.5927)	64.6
FITC-βA-NH₂	1+ (478.1067)	1+ (478.4)	1+ (478.1074)	71.9

5.4 Click Chemistry

Click chemistry was popularised by Sharpless in 2001 and it describes the modular synthesis of new materials through various robust, reliable and selective reactions by bringing two molecules together in small and large scales²³⁰. Since then, this new powerful approach has been intensively employed and improved in many applications including bioconjugation and peptide chemistry²³¹⁻²³³.

5.4.1 Copper Catalysed Azide-alkyne Click Chemistry

One click reaction that was developed by Meldal and co-workers is the azide-alkyne copper catalysed cycloaddition, which is commonly used due to its biocompatibility, reliability and specificity^{231,234}. This reaction can be carried out for peptide synthesis and functionalisation under physiological mild conditions at room temperatures with high yields^{233,235}. The reaction involves reacting two molecules, one having an azide group and the other an alkyne group at the termini, in the presence of copper catalyst as demonstrated in Figure 5.3.

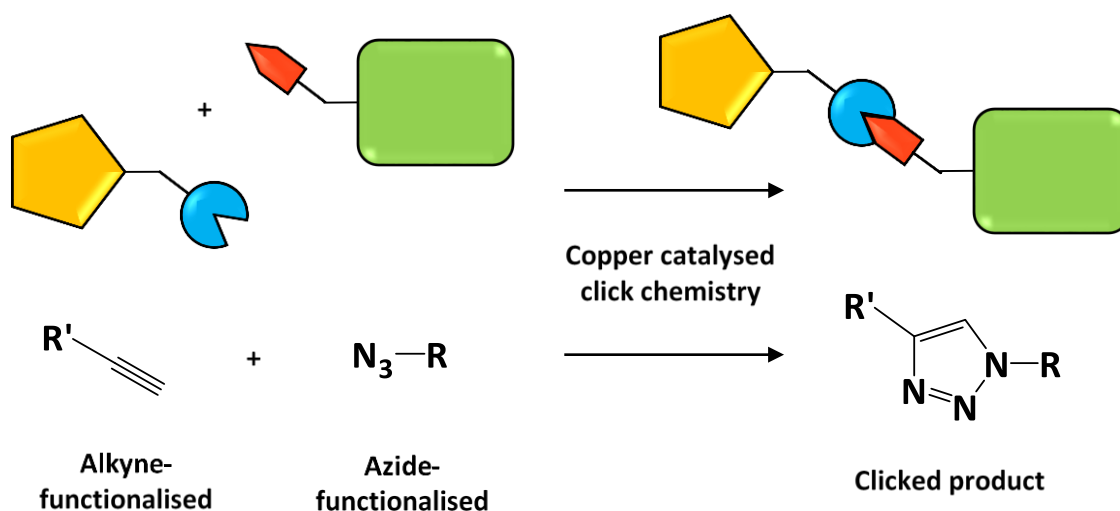


Figure 5.3: General copper catalysed azide-alkyne click chemistry model. Two molecules (green and yellow) one with an azide-functional group (red) and the other with an alkyne-functional group (blue) are brought together through this reaction in the presence of a copper catalyst.

5.4.2 Peptides Functionalised with Cell Attachment Motifs Synthesis

Modular synthesis using click chemistry of peptides functionalised with cell attachment motifs was preferred over conventional linear SPPS because of the longer chain of desired peptide and because synthesis of eight different peptide chains was required which was time-consuming. Therefore by using the copper catalysed azide-alkyne click chemistry, only six shorter peptide chains will be needed; the P₁₁ peptides (P₁₁-4 and P₁₁-8) functionalised with an azide group at the N-terminus and the cell attachment motifs (GRGDS, GRDGS, YIGSR and YIRSG) functionalised with an alkyne group at the C-terminus (Figure 5.4).

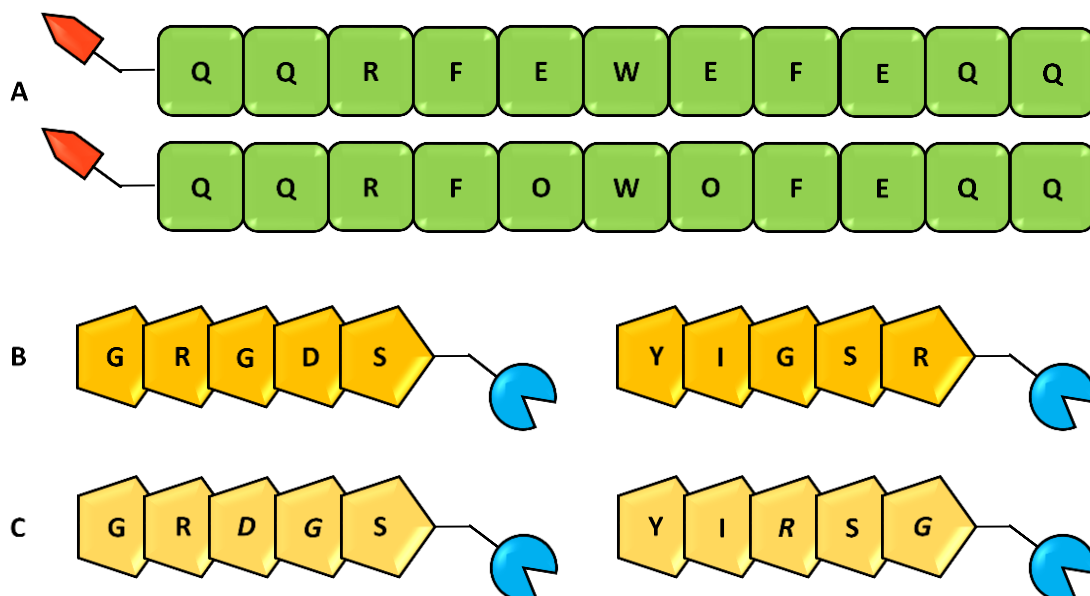


Figure 5.4: Schematic diagram showing the peptide chains required for P_{11} peptide functionalisation with cell attachment motifs through copper catalysed azide-alkyne click chemistry. A) Azide-functionalised P_{11} base peptides (top: P_{11-4} , bottom: P_{11-8}). Alkyne-functionalised: B) cell attachment motifs (left: GRGDS, right: YIGSR) and C) the corresponding scrambled controls.

For the synthesis of functionalised peptides, the four shorter peptide chains (cell attachment motifs) were synthesised by Fmoc SPPS, while the longer base P_{11} peptides were purchased. Consequently, the functionalisation process combined the two methods, starting with the synthesis of bioactive motifs through Fmoc SPPS then followed by functionalisation of the P_{11} peptides via click chemistry.

5.4.2.1 Linear Synthesis of Alkyne-functionalised Cell Motifs using SPPS

Cell attachment motifs, GRGDS and YIGSR, and corresponding scrambled controls, GRDGS and YIRSG, were synthesised (Figure 5.5) as described in Section 2.2.8.2. For the synthesis of alkyne-functionalised GRGDS, the peptide chain was assembled onto the resin starting with propargylglycine containing the alkyne group for the click chemistry followed by $(\text{PEG})_2$ to act as a spacer between the P_{11} peptide and the cell attachment motif after click chemistry. The amino acids S, D, G, R then G were assembled onto the resin followed by acetylation of the N-terminus. Finally, the peptide was cleaved from the resin. The peptide assembly and cleavage procedure is summarised in Scheme 5.2. Peptides were then purified using a reversed-phase HPLC column with UV detection as

described in Section 2.2.8.5. Following synthesis, analysis was carried as described for FITC-P₁₁-8 in Section 5.3.1.

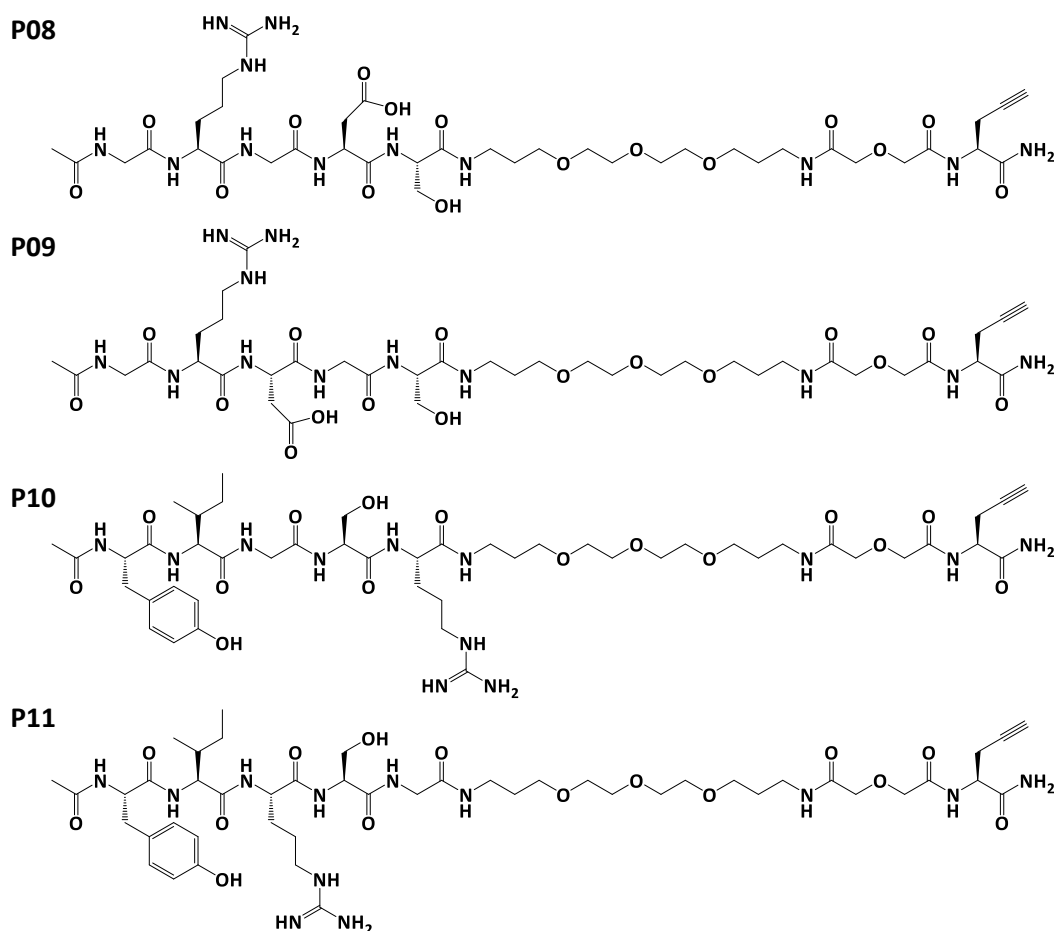
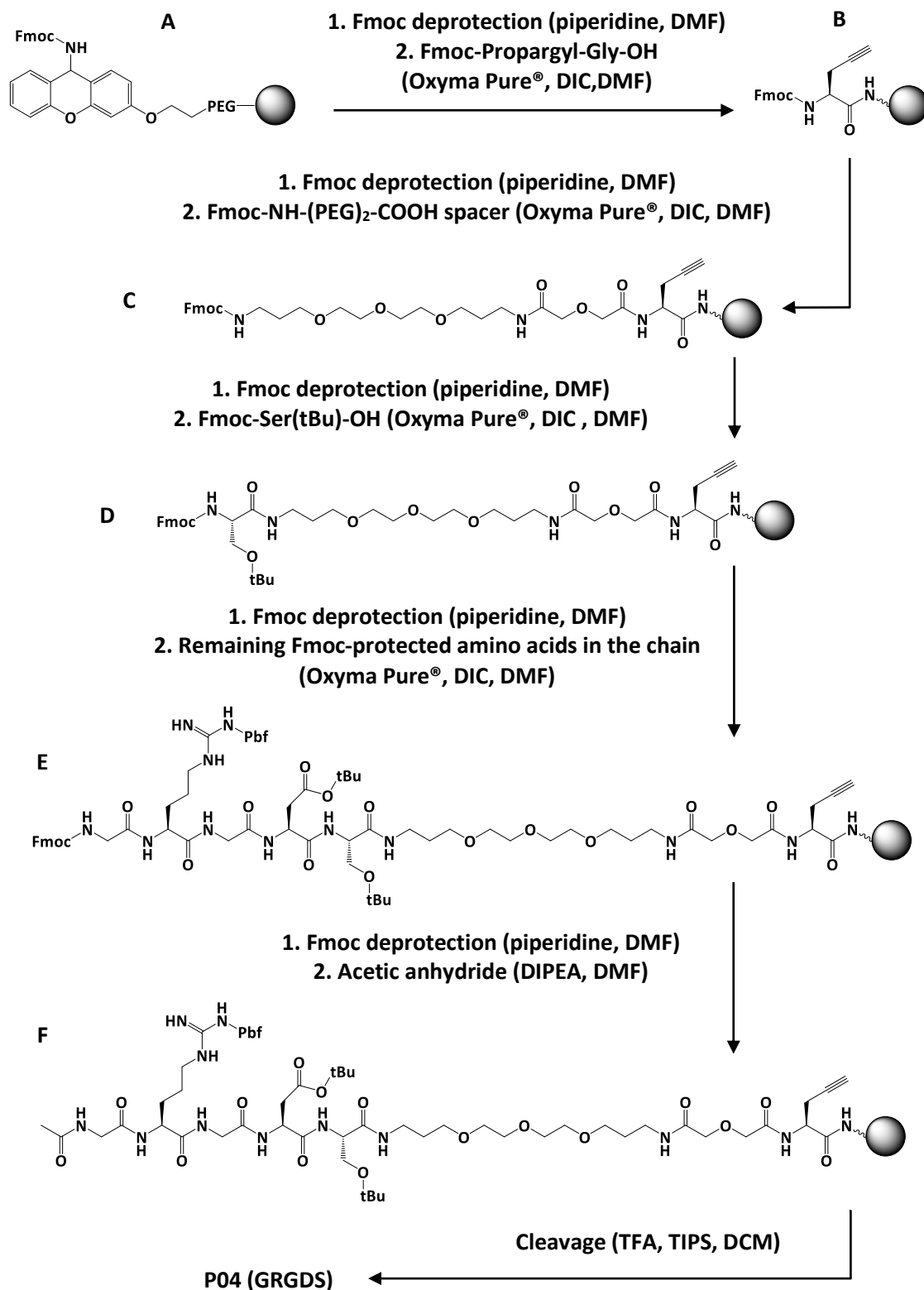


Figure 5.5: Structures of alkyne-functionalised cell attachment motifs and the corresponding scrambled controls (for click chemistry). *GRGDS (P08), corresponding scrambled control GRDGS (P09), YIGSR (P10) and corresponding scrambled control YIRSG (P11).*

Alkyne-functionalised GRGDS, YIGSR, and YIRSG were synthesised as described for GRGDS in Scheme 5.2 then purified under the same conditions. The detailed analytical HPLC traces, purity and mass spectrometry results of cell attachment motifs can be found in Appendix A.6 (A.6.2). The results for mass spectrometry and purity of synthesised cell attachment motifs and scrambled controls are summarised in Table 5.3.



Scheme 5.2: Linear synthesis of cell attachment motifs using Fmoc SPPS. A) NovaSyn[®] TG Sieber resin. B) Loading of alkyne-functionalised amino acid. C) Coupling of (PEG)₂ spacer. D) Coupling of first amino acid. E) Coupling of remaining amino acids in the chain. F) Acetylation of the N-terminus of the peptide chain. Cleavage of F from resin producing P04.

Table 5.3: Table summarising the analysis results for synthesised cell attachment motifs showing the expected molecular mass, mass acquired by mass spectrometry and purity acquired by HPLC (Ac - acetyl group CH₃CO).

Peptide	Expected [M+nH] ⁿ⁺	LC-MS	Accurate Mass	Purity (%)
Ac-GRGDS-NH ₂	1+ (945.4636)	1+ (945.5)	1+ (945.4655)	97.7
Ac-GRDGS-NH ₂	1+ (945.4636)	1+ (945.8)	1+ (945.4655)	89.7
Ac-YIGSR-NH ₂	1+ (1049.5626)	1+ (1049.6)	1+ (1049.5644)	96.6
Ac-YIRSG-NH ₂	1+ (1049.5626)	1+ (1049.6)	1+ (1049.5653)	95.3

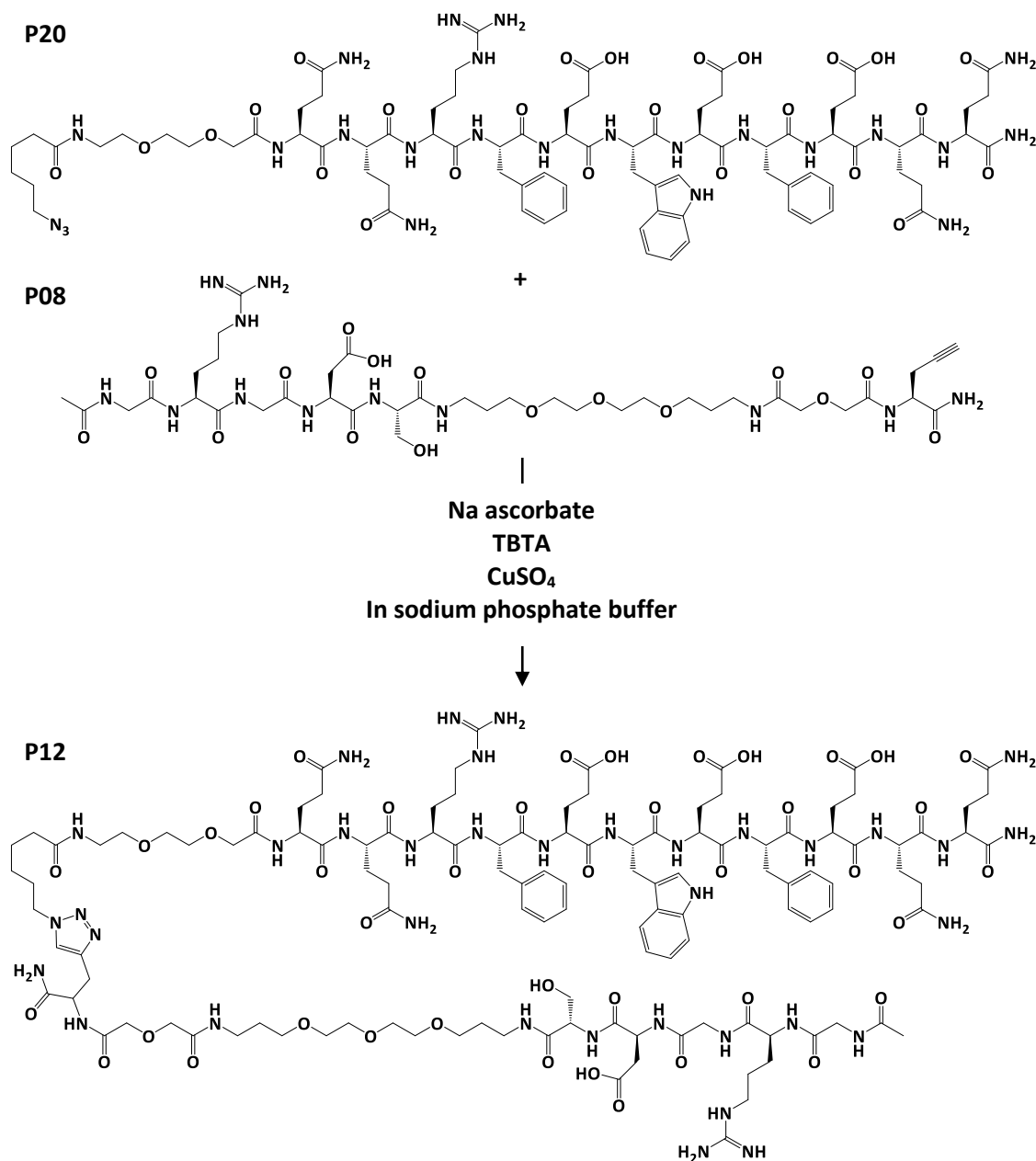
5.4.2.2 Modular Synthesis of Functionalised Peptides using Click Chemistry

P₁₁-4 and P₁₁-8 were functionalised with cell attachment motifs and corresponding scrambled controls using copper catalysed click chemistry between an azide group on the N-terminus of the P₁₁ peptide structure and an alkyne group on the C-terminus of the cell attachment motifs. An initial trial click reaction was carried out with three different conditions displayed in Table 5.4. Solutions were mixed in sodium phosphate buffer (final buffer concentration of 50 mM at pH 7.4) and left to react on a magnetic stirrer in the dark at 40 °C for one hour.

Table 5.4: Different conditions used for the click chemistry reaction. Numbers represent the working concentration of reagents. Peptides and TBTA were solubilised in DMSO whilst CuSO₄, TCEP and sodium ascorbate were dissolved in water.

Condition	Alkyne-functionalised Peptide	Azide-functionalised Peptide	Catalyst	Reducing Reagent	Stabilising Ligand	Yield (%)
1	GRGDS GRDGS YIGSR YIRSG (1 mM)	P ₁₁ -4 P ₁₁ -8 (1 mM)	CuSO ₄ (1 mM)	TCEP (1 mM)	TBTA (1 mM)	0
2			CuSO ₄ (1 mM)	Na ascorbate (10 mM)	-	0
3			CuSO ₄ (1 mM)	Na ascorbate (1 mM)	TBTA (1 mM)	53

The third condition was the most efficient one, hence was followed for subsequent larger scale peptide synthesis for 48 hours as described in Section 2.2.8.3. Functionalisation of P₁₁-4 with GRGDS is summarised in Scheme 5.3.



Scheme 5.3: Modular synthesis of P₁₁ peptide functionalised with cell attachment motifs using copper catalysed azide-alkyne click chemistry. Azide-functionalised P₁₁₋₄ (P20) and alkyne-functionalised GRGDS (P08) were brought together through copper catalysed click chemistry using sodium ascorbate and TBTA in sodium phosphate buffer making P₁₁₋₄ functionalised with GRGDS cell attachment motif (GRGDS-P₁₁₋₄, P12).

The resulting functionalised peptide was dissolved in excess of water with either ammonia (P₁₁₋₄ peptides) or acetic acid (P₁₁₋₈ peptides) to monomerise the peptides. This solution was lyophilised and the residue dissolved in water/DMSO for purification. Peptides were purified using a reversed-phase HPLC column with UV detection as described in Section 2.2.8.5 then analysed as described for FITC-P₁₁₋₈ in Section 5.3.1.

P₁₁-4 functionalisation with GRDGD, YIGSR and YIRSG, and P₁₁-8 functionalisation with GRGDS, GRDGD, YIGSR and YIRSG were performed as described for GRGDS-functionalised P₁₁-4 (Scheme 5.3) then purified under the same conditions. The detailed analytical HPLC traces, purity and mass spectrometry results of bioactive peptides can be found in Appendix A.6 (A.6.3). The results for mass spectrometry and purity of cell attachment functionalised peptides are summarised in Table 5.5.

Table 5.5: Table summarising the analysis results for bioactive (cell attachment functionalised) peptide showing the expected molecular mass, mass acquired by mass spectrometry and purity acquired by HPLC (Ac - acetyl group CH₃CO).

Peptide	Expected [M+nH] ⁿ⁺	LC-MS	Accurate Mass	Purity (%)
Ac-GRGDS-P ₁₁ -4-NH ₂	2+ (1392.1640)	2+ (1392.1)	2+ (1392.1589)	100
Ac-GRDGS-P ₁₁ -4-NH ₂		2+ (1392.3)	2+ (1392.1583)	100
Ac-YIGSR-P ₁₁ -4-NH ₂	2+ (1444.2135)	2+ (1444.1)	2+ (1444.2115)	100
Ac-YIRSG-P ₁₁ -4-NH ₂		2+ (1444.7)	2+ (1444.2092)	96.2
Ac-GRGDS-P ₁₁ -8-NH ₂	3+ (1033.1820)	4+ (775.4)	3+ (1033.1821)	100
Ac-GRDGS-P ₁₁ -8-NH ₂	4+ (775.1387)	4+ (775.2)	3+ (1033.1825)	100
Ac-YIGSR-P ₁₁ -8-NH ₂	3+ (1067.8817)	4+ (801.3)	3+ (1067.8804)	100
Ac-YIRSG-P ₁₁ -8-NH ₂		3+ (1067.9)	3+ (1067.8830)	100

5.5 Discussion

The aim of this chapter was to synthesise FITC-labelled and cell attachment functionalised P₁₁ peptides by Fmoc SPPS and copper catalysed azide-alkyne click chemistry, respectively for studies within acellular artery tissue. A summary of the sequences and net charges at pH 7.4 of the synthesised peptides can be found in Appendix A.2.

In SPPS, a Kaiser colour test was carried out for the initial monitoring of SPPS ensuring all sites on resin were occupied. This was carried out after adding the first amino acid in the peptide chain to ensure complete coupling. An incomplete coupling was indicated by a blue colour because of the presence of free primary amines that were not coupled to added amino acids^{236,237}.

The N-termini of amino acid building blocks used in SPPS were protected by base-labile Fmoc protecting group, whereas the side-chains of amino acids used were protected by acid-labile protecting groups to prevent undesired couplings. The Fmoc protecting groups were deprotected before addition of the following amino acid in the peptide chain by piperidine washes exposing the N-terminus for a coupling reaction without disturbing the side-chain protecting groups, whilst the side-chain protecting groups were removed by the end of the synthesis process simultaneously with peptide cleavage using TFA ²³⁸.

Fmoc SPPS has allowed easier modification of the N and C-termini of the synthesised peptides. The N-terminus of cell attachment motifs was acetylated, while this was not the case for FITC-labelled peptides due to the presence of the fluorescent dye at the terminus. The C-terminus of both FITC-labelled peptides and cell attachment motifs was amidated. Acetylation and amidation were carried out to prevent charging at the termini, hence prevent any unwanted interaction between charged groups at the termini ²³⁸. In addition, such modification is important in peptides used in biological applications as it was shown to increase peptide stability to proteases ²³⁹⁻²⁴¹.

FITC-labelled peptides with purities of approximately: 97 % (FITC-P₁₁-8); 65 % (FITC-P₁₁-12); and 72 % (FITC-βA control) were obtained. The purities of these peptides should not have a significant effect on the results for the purpose of this study. This is because molar ratios of 1:150 of the FITC-labelled peptides to the non-labelled peptide were used, just enough to generate a sufficient fluorescent signal for visualisation under the microscope. These were used to investigate self-assembly of peptides within acellular arteries as will be discussed in Chapter 6.

The widely investigated technique azide-alkyne copper catalysed cycloaddition click chemistry was used for functionalisation of the base P₁₁ peptide with GRGDS and YIGSR cell attachment motifs. This was achieved by introduction of a peptide with an alkyne group to the C-terminus that was separated by (PEG)₂ linker from the cell attachment motifs and an azide-group to the N-terminus of the base peptide.

Functionalisation of P₁₁ peptides with different cell attachment motifs through azide-alkyne copper catalysed click chemistry was achieved with very high purities of 100 %, except for YIRSG-P₁₁-4 (scrambled control) with approximately 96 % purity, due to the

high selectivity of the click reaction even with lower purities of the cell attachment motifs synthesised by Fmoc SPPS. The effect of the use of 1:50 molar ratio of these functionalised peptides to non-functionalised peptides on cell attachment onto acellular artery tissue will be discussed in Chapter 7.

The copper catalysed azide-alkyne click chemistry has been widely applied to biological applications. From the literature, a number of studies have been carried out to investigate the bioconjugation of RGD cell attachment motif in particular to various substrates using this technique under mild conditions with high yield products ²⁴². One study investigated the production of PEG-RGD containing biodegradable hydrogels through click chemistry as biocompatible carriers for cell delivery. It was shown that PEG-RGD hydrogels improved the attachment and proliferation of human dermal fibroblasts when compared to non-RGD hydrogels, hence were suggested as useful biodegradable scaffolds for cell delivery in tissue regeneration ²⁴³. Hydrogels conjugated with RGD and bone morphogenetic protein-2 through click chemistry have provided bone marrow stromal cells with the binding sites for adhesion and mineralisation, respectively and were shown to be non-cytotoxic to cells ²⁴⁴. Another study also demonstrated the functionalisation of multi-layered PEG films with RGD via click chemistry and was shown to improve attachment and growth of epithelial cells ²⁴⁵. The functionalisation of azide-functionalised self-assembled monolayers with alkyne-functionalised RGD-containing peptide through copper catalysed click chemistry using TBTA and sodium ascorbate was shown to support attachment and spreading of stem cells to the substrate ²⁴⁶. From these previous studies, it was shown that various click chemistry products were biocompatible *in vitro* with different cell lines.

At the current stage and for the purpose of this study to test the effectiveness of peptide functionalisation on cell attachment/retention, peptides functionalised with cell attachment motifs synthesised in this chapter were not assessed for *in vitro* biocompatibility. However, this might be of interest in future investigations using these bioactive peptides.

6 Peptide Self-assembly within Acellular Arteries

6.1 Introduction

In this chapter, P₁₁₋₄, P₁₁₋₈ and P₁₁₋₁₂ were tested for effect on thrombus formation and within the acellular artery tissue as surface coatings. For the peptide coating behaviour, it was important to identify different structures within the ECM in order to distinguish different structural components such as collagen and elastin from each other and from peptide fibrillar networks using a combination of microscopic techniques. This was achieved by visualisation of uncoated and peptide coated acellular artery samples under field emission gun scanning electron microscopy (FEGSEM), fluorescent microscopy and multiphoton laser scanning microscopy (MPLSM). For this reason and because both elastin and collagen form fibres, the ECM will be discussed briefly in this chapter and this will help in the identification of the different fibrillar structures when visualised. The efficiency and extent of peptides coating the ECM components at the luminal surface will also help in selecting the better suited peptides for functionalisation with cell attachment motifs as will be discussed in Chapter 7.

6.1.1 The Extracellular Matrix (ECM) – Structural Proteins

The ECM is the non-cellular composition of tissue providing it with structural, mechanical and biological properties, and is tissue-specific²⁴⁷. In blood vessels, the ECM consists mainly of two structural fibrous proteins, collagen and elastin⁷. Other components such as laminin, fibronectin and glycosaminoglycans (GAGs) are also present in blood vessels. The presence of these different components is important to provide blood vessels with strength, elasticity and other functions required for cell-ECM interactions, consequently allowing for structural integrity and normal functioning of vessels^{248,249}.

6.1.1.1 Collagen

Collagen is a stiff protein that provides the blood vessel with tensile strength and exists in many types with collagen fibrils having a triple helix structure^{7,249}. Collagen fibres (bundles) are formed by tightly packed collagen fibrils with a characteristic banding structure^{250,251} (Figure 6.1). Different types of tissues comprise different collagen types

depending on their structure and function. Fibrillar collagen types I and III are the most abundant in blood vessels representing 60 % and 30 % of collagen, respectively ^{7,248}. These display identical banding structures but collagen type I forms thicker fibres ²⁵². Other collagen types including collagen type V (fibrillar collagen), XII, XIV, VI, IV (basement membrane collagen) and VII represent the remaining 10 % ²⁴⁸. Collagen type IV found in the basement membrane in blood vessels forms thin sheets (40 - 50 nm) consisting of fine interconnecting networks with significant branching in structure and does not form organised fibrillar structures like collagen types I and III ^{252,253}. The tunica media collagen fibres are coiled with preferentially circumferential orientation but have smaller diameters than the adventitial collagen fibres that are also coiled with circumferential and random orientations ^{254,255}.

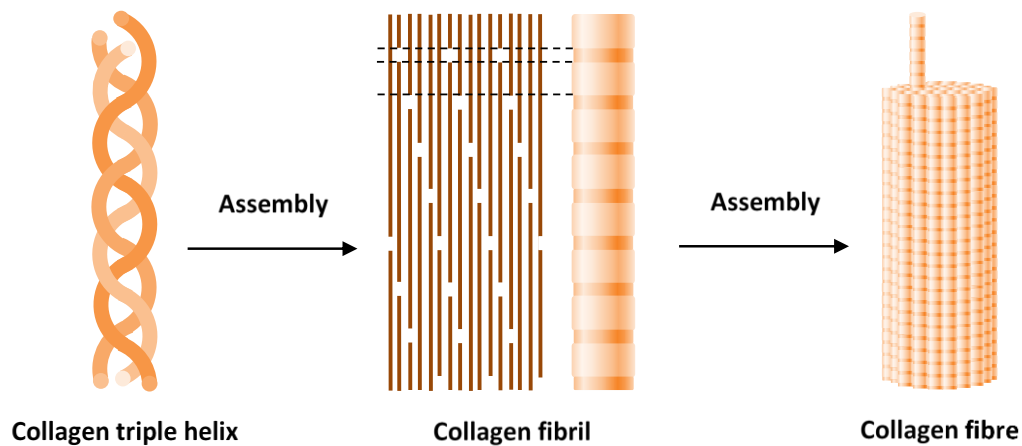


Figure 6.1: Schematic diagram showing the formation of collagen fibres. *The collagen triple helix assembles as presented in the collagen fibril by the lines forming the fibrils. The fibrils assemble together forming the collagen fibre.*

6.1.1.2 Elastin

Elastin represents 90 % of elastic fibres which are also composed of microfibrils and contributes to the elasticity of blood vessels ^{248,249}. Elastin allows for repetitive extension and recovery of vascular tissue under pulsatile blood flow ²¹² (Figure 6.2). It is found mainly in the internal and external elastic membranes as a continuous fenestrated sheet ^{248,249}. Elastin is also present throughout the tunica media layer arranged circumferentially as continuous fenestrated sheets composed of fibrous elastin between collagen fibres and is interconnected in a three-dimensional network by protruding elastin fibres that run circumferentially and radially forming a cage-like

mesh around smooth muscle cells. These elastic sheets are more predominant in elastic arteries ^{250,255,256}.

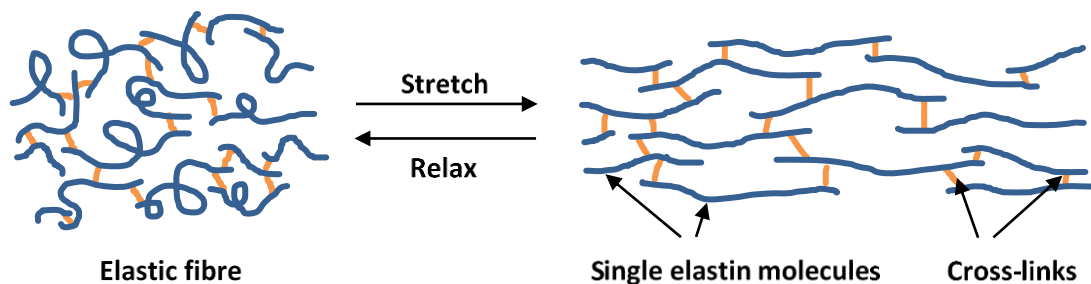


Figure 6.2: Schematic diagram showing the stretching and relaxation of elastic fibres.

6.1.2 Thrombogenicity Evaluation

For the development of biomaterials as vascular grafts, thrombus formation can be evaluated *in vitro* using human/animal blood for laboratory testing with the ability to control model conditions such as blood flow rates relevant to the application. However, this cannot reflect the actual relationship between the patient and clinical use, requiring *in vivo* future studies ^{83,87}. *In vitro* models will therefore allow for evaluation of specific variables that need testing without changing other parameters. Systems that can be used for assessment of platelet adhesion, activation and aggregation include flat-plate flow chambers and parallel/cone-plate viscometers ⁸⁷. However, these are non-tubular systems and for evaluation of thrombogenicity other closed tubular models with blood rotation/movement can be employed. For example, Chandler loop, roller pump and haemobile models, in which the first two are the most extensively employed, are used as *in vitro* models for thrombi evaluation ^{87,257}.

The Chandler loop model allows for repetitive circulation of blood in a closed tubing system partially filled with air, but is limited to low flow rates and may also introduce artefacts to blood components and activate the coagulation cascade due to the air-blood interface ^{82,257}. The roller pump model has no air-blood interface achieved by the use of blood reservoir that circulates blood through the closed tubing system, but blood damage induced by the pump limits its effectiveness to short circulation times limiting exposure of biomaterial ^{82,87,257}. The haemobile model uses a ball valve placed in the

closed tubing system with no air-blood interface and no blood damage, but is limited to semi-circular movements ²⁵⁷.

The roller pump and haemobile models can achieve high flow rates, when compared to a Chandler loop model, which is limited to lower flow rates but can be loaded with a number of loops for faster screening. In small-diameter blood vessels, the blood flow rate is slower than large vessels, making the Chandler loop better suited for evaluation of small-diameter vascular grafts ²⁵⁷. Likewise, Chandler loop models can also be used to assess the anti-thrombogenic properties of certain drugs/agents ²⁵⁸. Microscopic evaluations such as confocal microscopy and SEM may be useful for assessment of composition, morphology and structure of thrombi.

6.2 Aims and Objectives

The aim of this chapter was to investigate self-assembly of P₁₁₋₄, P₁₁₋₈ and P₁₁₋₁₂ within acellular arteries as suitable candidates for anti-thrombogenic surface coatings.

The specific objectives were:

- To investigate the effect of the presence of monomeric peptides in blood on thrombus formation using a Chandler loop model;
- To investigate coating of the acellular artery surface by peptides using field emission gun scanning electron microscopy (FEGSEM);
- To investigate self-assembly of peptides within acellular artery tissue using fluorescent microscopy and multiphoton laser scanning microscopy (MPLSM);
- To select suitable peptide candidates for functionalisation with cell attachment motifs.

6.3 Methods

6.3.1 Effect of Peptides on Thrombus Formation in Blood Using a Chandler Loop Thrombosis Model

Background

The effect of peptides on thrombus formation in blood was investigated using the Chandler Loop model. Chandler developed the model to create a thrombus *in vitro* that resembled an *in vivo* thrombus. In his model, 0.9 mL of fresh blood was rotated in a mounted polyvinyl chloride (PVC) loop at 28 rpm in a 37 °C water bath. This allowed comparison between thrombus formation *in vitro* and *in vivo*. The model also helped in investigation of thrombus structure and formation mechanism ²⁵⁹.

The model was used to investigate the effect of treating blood with the peptides P₁₁₋₄, P₁₁₋₈ and P₁₁₋₁₂ in their monomeric and self-assembled forms on thrombus formation. Thrombi formed were compared to a positive control, blood treated with α -thrombin, which is a clotting agent that promotes thrombus formation and a negative control lacking this clotting agent. Peptides can have: anti-thrombogenic properties if the thrombi formed are significantly smaller than that of a negative control; no effect on thrombus formation if the thrombi formed are not significantly different from the negative control; and thrombogenic properties if the thrombi formed are significantly larger/comparable to that of the positive control.

Method

Peptides were tested for their effect on thrombus weight in their monomeric (0.3 mM) and self-assembled (3 mM) forms in a Chandler loop model as described in Section 2.2.10. Six replicates were tested for each peptide at each concentration (three loops per rotator). Citrated blood was used and was tested for its clotting behaviour before carrying out the tests. The weight of thrombus formed in peptide treated blood mixtures and controls was analysed using one-way ANOVA and post-hoc Tukey's test ($p < 0.05$; Section 2.3).

6.3.2 Visualisation of Peptide Coated Acellular Artery Tissue by FEGSEM (Dry Sample)

Background

SEM works by generating and accelerating electrons through a high voltage producing a thin electron beam that scans the surface of a sample. This produces different signals from the sample including secondary electrons and backscattered electrons and each is detected by a specific detector. The secondary electrons are of importance in obtaining high resolution images of the surface due to the interaction of sample with the electron beam. This signal will be of particular interest for investigating the acellular artery surface coating with the self-assembled peptides.

Method

Acellular artery sections, 1 cm², were fixed in NBF to help maintain the ECM structures preventing them from collapsing upon drying for SEM imaging. P₁₁₋₄, P₁₁₋₈ and P₁₁₋₁₂ were prepared in deionised water at 20 mg.ml⁻¹, self-assembled within the tissue then samples were processed for SEM imaging as described in Section 2.2.11.1. Images of the luminal (internal) and abluminal (external) surfaces of uncoated and peptide coated acellular tissue were acquired using the secondary electrons signal.

6.3.3 Fluorescent Microscopy Imaging of FITC-labelled Peptide Self-assembled within Acellular Artery Tissue (Cryosections)

Background

Fluorescent microscopy is a widely used technique for investigation of biological samples that auto-fluoresce or can be labelled with fluorescent dyes. Unlike the traditional optical microscopes that use transmitted light, fluorescent microscopes detect light emitted from the sample. In this technique, a light of certain wavelength chosen to selectively excite the target dye/molecule (excitation beam) hits the sample and interacts with the dye/molecule emitting light of a larger wavelength from the sample (emission beam) that is allowed to pass through the beam splitter and detected giving an image of the sample. In addition, it can detect different dyes in the sample using the excitation filter, emission filter and beam splitter with the wavelengths relevant to the target fluorescent dyes (Figure 6.3).

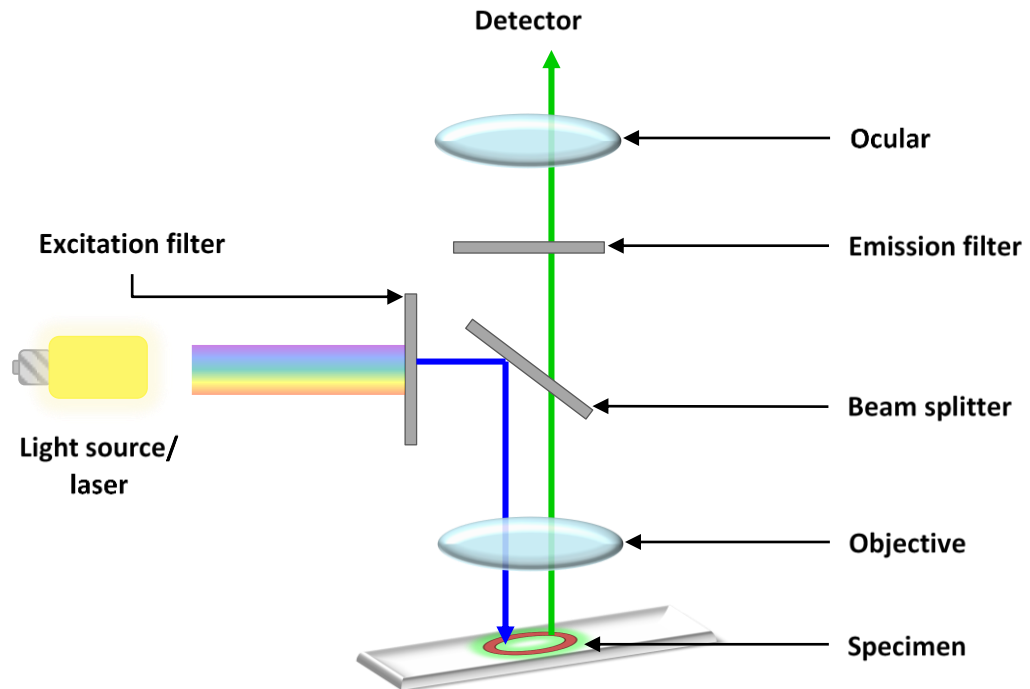


Figure 6.3: Schematic of fluorescent microscopy imaging. *The excitation beam (blue) is passed through a filter of the required wavelength range then reflected onto the sample by a beam splitter. This emits light, emission beam (green), of a specific wavelength longer than the excitation wavelength that is allowed to pass through the beam splitter then a specific range of wavelengths of the fluorescent signal passes through a filter to be detected.*

Method

A fluorescent microscope was used to visualise FITC-labelled peptides to investigate the interaction between self-assembled peptides and acellular tissue using a FITC filter. FITC-labelled P₁₁-4, P₁₁-8 and P₁₁-12 (and FITC-βA control) were prepared in deionised water at 20 mg.ml⁻¹ (molar ratio of 1:150 of the FITC-labelled to the non-FITC-labelled peptides) then self-assembled within acellular tissue segments (0.5 cm). Cryosections of acellular arteries, both coated and uncoated with peptides were prepared for fluorescent microscopy imaging as described in Section 2.2.11.2. Cross-sectional images were acquired using a Zeiss upright microscope with a FITC filter (excitation: 495 nm, emission: 519 nm). Images of the FITC-labelled peptide coated acellular tissue were compared to uncoated, FITC- βA control coated and non-FITC-labelled peptide coated tissue samples.

6.3.4 MPLSM Imaging of FITC-labelled Peptide Coated Acellular Artery Tissue (Wet Sample)

Background

Multiphoton microscopy has many advantages over fluorescent or confocal microscopies. Both confocal and multiphoton microscopies have the ability to produce in-focus z-stacks of the sample, meaning they can image the sample at different depths in a process called optical sectioning without the need of cryosectioning as required for fluorescent microscopy. Multiphoton microscopes work by excitation of the fluorescent dye with the absorption of two-photons simultaneously to emit light. This produces improved z-stack images because excitation occurs at the focal point of the microscope giving a higher resolution signal than the confocal microscope, where a single photon is required for light emission. In a multiphoton microscope, the probability of excitation by simultaneous two-photon absorption is higher at and close to the focal point, so the fluorescent signal detected is only produced from this focal point and there is no need for a pinhole. In a confocal microscope, the fluorescent signal detected is filtered by a pinhole aperture that only allows signal from the focal plane to be detected omitting any other signals from out-of-focus planes. A fluorescent microscope, however detects all fluorescent signals that pass through the emission filter, in-focus and out-of-focus ones, giving blurred images ²⁶⁰. Moreover, less damage to the sample is caused by the laser beam in a multiphoton microscope as photons required for the excitation to produce light of the same wavelength as in the confocal microscope are of a lower energy ²⁶⁰. The schematic diagram shown in Figure 6.4 compares the different ways a fluorescent signal is produced and detected in the three different types of microscope.

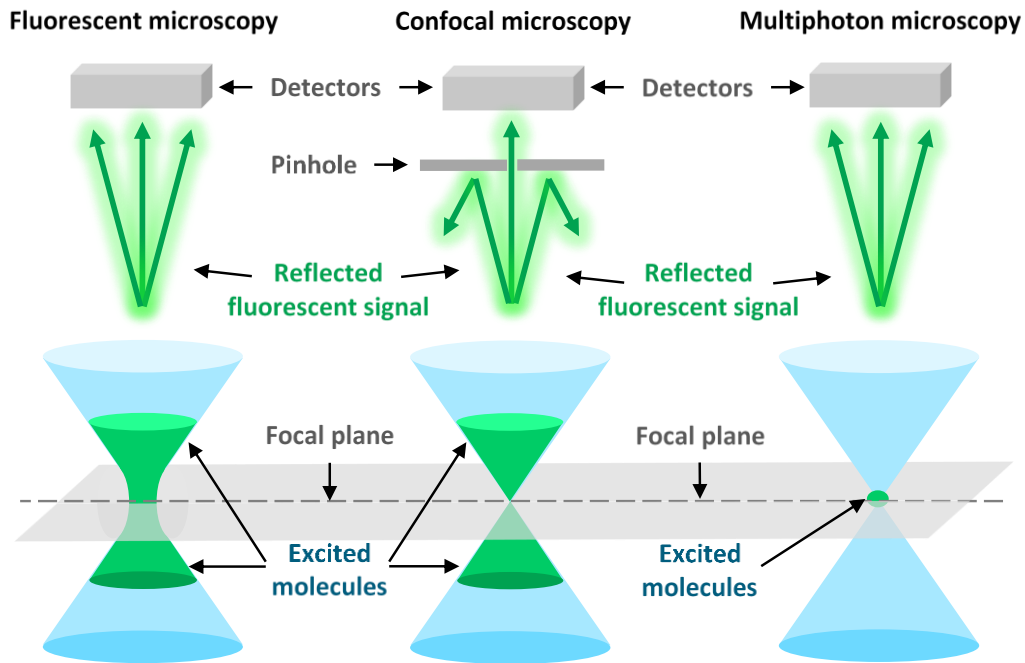


Figure 6.4: A schematic diagram comparing the fluorescent signals detected in fluorescent, confocal and multiphoton microscopes. In a fluorescent microscope a fluorescent signal from the focal plane and the surrounding is detected. A pinhole is used in a confocal microscope that only allows fluorescent signals from the focal plane to be detected. No pinhole is required in a multiphoton microscope due to the fluorescent signal coming from a focal point because of the simultaneous two-photon absorption that produces the signal.

Method

FITC-labelled P₁₁-4, P₁₁-8 and P₁₁-12 (and FITC-βA control) were prepared in deionised water at 20 mg.ml⁻¹ (molar ratio of 1:150 of the FITC-labelled to the non-FITC-labelled peptides) then self-assembled within acellular tissue segments (0.5 cm). Tissue samples were prepared for MPLSM imaging as described in Section 2.2.11.3. Images of near the luminal surface of uncoated and FITC-labelled peptide coated tissue were acquired using x 20 objective air lens and x 63 objective oil lens (unless otherwise stated) and filters for FITC (excitation: 720 nm, detection: 500 - 550 nm), elastin (excitation: 740 nm, detection: 300 - 485 nm) and collagen (excitation: 850 nm, detection: 300 - 485 nm) signals. Z-stacks were acquired near the surface through the first few microns of the tunica media layer and all samples were placed in one direction for imaging (along the artery; Figure 6.5).

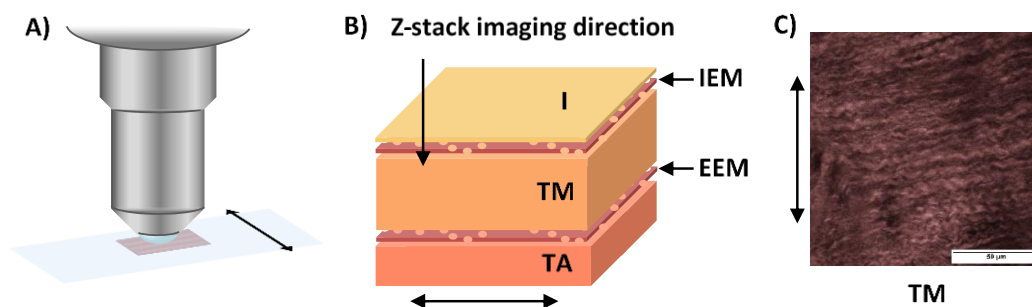


Figure 6.5: Schematic diagram showing MPLSM sample set-up and imaging. A) Artery sample under the microscope lens, in which a coverslip was placed on top and secured with steri-strips to fix tissue in place for imaging. B) Direction of z-stack imaging starting from near the luminal surface into the tunica media. C) Imaged samples showing direction of collagen from left to right i.e. circumferentially when imaging artery in the stated direction. Double-sided arrows represent direction of artery/blood. Starting from the luminal surface: intima (I), internal elastic membrane (IEM), tunica media (TM), external elastic membranes (EEM) and tunica adventitia (TA).

6.4 Results

6.4.1 Effect of Peptides on Thrombus Formation in Blood

Peptides were tested for their effect on thrombus weight in a Chandler loop model at 0.3 and 3 mM concentrations (see corresponding concentrations in $\text{mg}\cdot\text{mL}^{-1}$ in Appendix A.2). The data showed a significant difference between thrombus weight of positive and negative controls (ANOVA; $p < 0.05$). Monomeric peptides P₁₁₋₄ and P₁₁₋₈ at 0.3 mM resulted in significantly reduced thrombus weights when compared to the negative control (ANOVA; $p < 0.05$), while P₁₁₋₁₂ at 0.3 mM had no significant effect on thrombus formation. Self-assembled P₁₁₋₈ and P₁₁₋₁₂ at 3 mM resulted in significantly reduced thrombus weights, while no thrombus was formed with P₁₁₋₄ (ANOVA; $p < 0.05$; Figure 6.6).

P₁₁₋₈ and P₁₁₋₁₂ were solutions in their monomeric form before being added to the blood mixture at both 0.3 mM and 3 mM peptide concentrations since their initial pH was $< \text{pH } 5$. However, P₁₁₋₄ formed a very strong gel at the stock concentration of 49.5 mM because its initial pH was around pH 7 where it self-assembled and this was difficult to pipette, therefore it was mixed with the blood solution. After rotating

samples, no thrombus was formed in blood mixtures treated with 3 mM P₁₁-4 but the blood mixture contained small weak gel-like globules following rotation that prevented blood from sticking to tubing walls (Figure 6.7). This could have been because P₁₁-4 was in its gel state when added to blood as opposed to monomeric solutions of P₁₁-8 and P₁₁-12. This gel was broken down by movement of tubing into smaller globules and mixed within blood mixture.

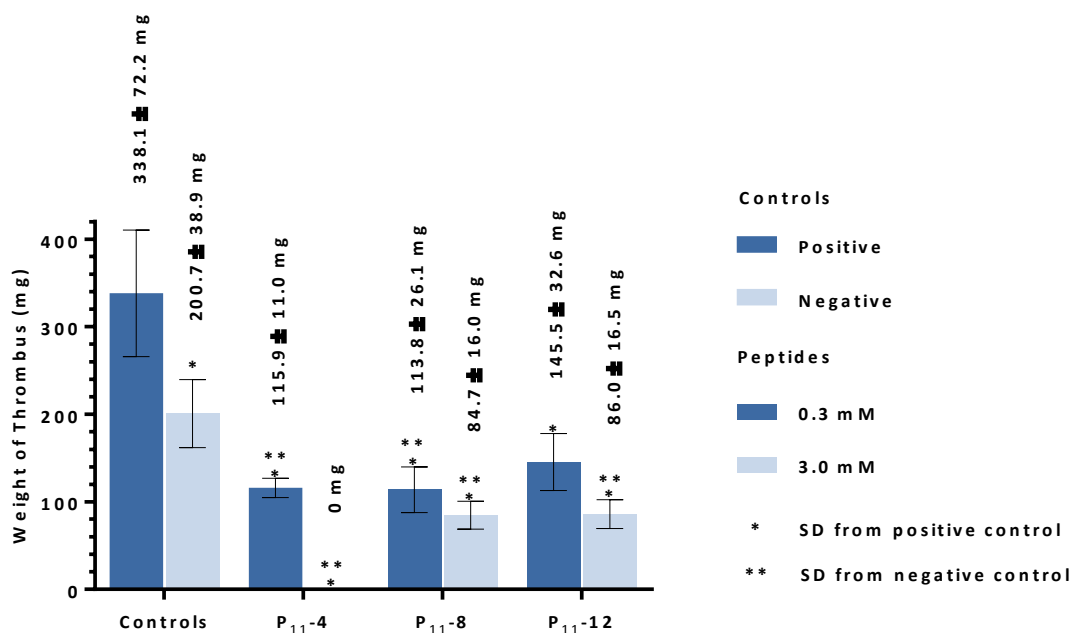


Figure 6.6: Effect of peptides on thrombus weight (mg) using the Chandler loop model. Data represent the means ($n = 6$) \pm 95 % confidence limits. At 0.3 mM, P₁₁-4 and P₁₁-8 significantly reduced thrombus weight. At 3 mM, all peptides significantly reduced thrombus weight with no thrombus formation in P₁₁-4. Significant difference (SD) was determined by one-way ANOVA and post-hoc Tukey's test ($p < 0.05$).



Figure 6.7: Appearance of blood treated with 3.0 mM self-assembled P₁₁-4. The gel-like globules became clear with time and no thrombus was formed.

Thrombi formed in controls and blood mixture with monomeric peptides were cylindrical in shape and consisted of a white head followed by a red tail. In Chandler's study, the aggregates in the leading end of the circulating blood formed a small white head followed by a sudden onset of coagulation of fibrin forming the red tail by trapping red blood cells, which were cylindrical in shape ⁷⁷. Thrombi formed in blood mixture with self-assembled peptides consisted of foamy fragments that could have been due to the presence of peptide gel in the blood because when added to PVC loops, self-assembly was triggered due to pH and ionic strength changes.

6.4.2 FEGSEM Imaging of the Luminal (Internal) Surface of Coated and Uncoated Acellular Artery Tissue

Images of uncoated and 20 mg.mL⁻¹ peptide coated acellular arteries were acquired for the luminal surface (Figure 6.8) and abluminal surface (Appendix A.7). SEM images showed the different surface coating behaviour of each of the tested peptides. In uncoated acellular artery (Figure 6.8 A), the ECM was observed consisting of collagen fibre bundles with similar orientations that were identified by having the characteristic banding structure. Peptides were shown to self-assemble on the tissue surface forming different coating layers. P₁₁₋₄ coated (Figure 6.8 B) and P₁₁₋₈ coated (Figure 6.8 C) acellular arteries showed a dense fibrillar surface coating, which was denser in P₁₁₋₈ treated tissue. This was evident because of loss of the characteristic banding structure of collagen fibres that were rarely exposed in these samples. In addition, these surface coatings consisted of thinner fibrillar networks with random orientations. However, in P₁₁₋₁₂ coated acellular arteries (Figure 6.8 D), a very thin and uniform coating layer was formed, insufficiently coating the surface, as the characteristic banding structure of collagen fibres was observed in large areas of the sample.

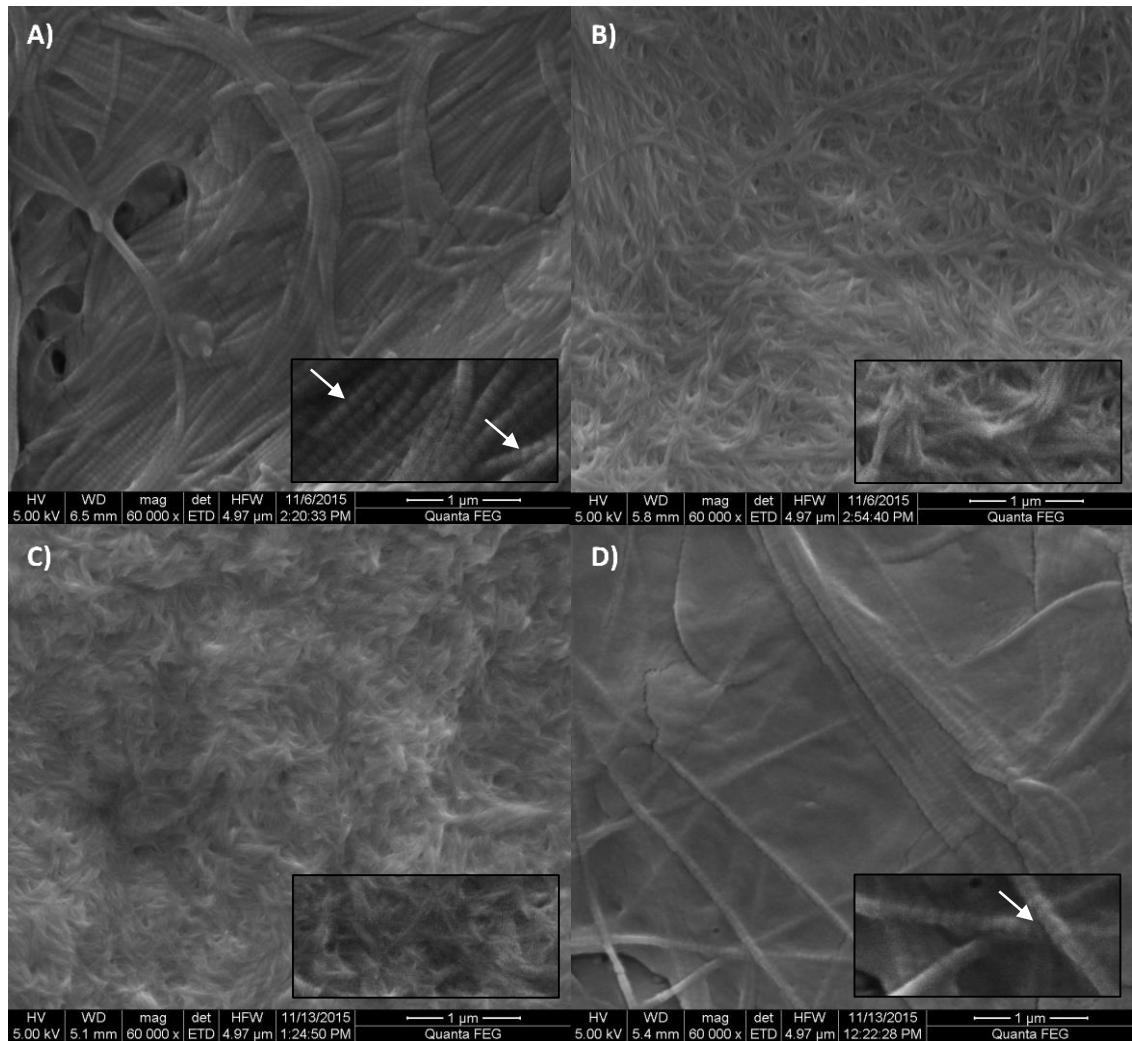


Figure 6.8: FEGSEM images showing self-assembling peptides at 20 mg.mL⁻¹ as surface coatings for the luminal surface of acellular arteries. A) Uncoated acellular artery, B) P₁₁₋₄ coating, C) P₁₁₋₈ coating and D) P₁₁₋₁₂ coating. Arrows point to collagen fibres with a characteristic banding structure. Images were acquired at x 60,000 magnification and scale bars represent 1 μm.

6.4.3 Fluorescent Microscopy Imaging of FITC-labelled Peptide Self-assembled within Acellular Artery Tissue

Cross-sections of FITC-labelled peptides self-assembled within acellular arteries were compared to controls. All FITC-labelled peptides formed yellow gels (solution for FITC-βA control), therefore, FITC incorporated tissue samples were visually distinct from non-FITC incorporated samples by having a yellow colour after leaving overnight. No FITC signal was detected in untreated acellular artery (Figure 6.9 A) and non-FITC-labelled peptide controls (Figure 6.9 B - D). In FITC-βA control solution, penetration

through the ECM was seen and fluorescence was mainly observed in the luminal surface and tunica adventitia (Figure 6.9 E).

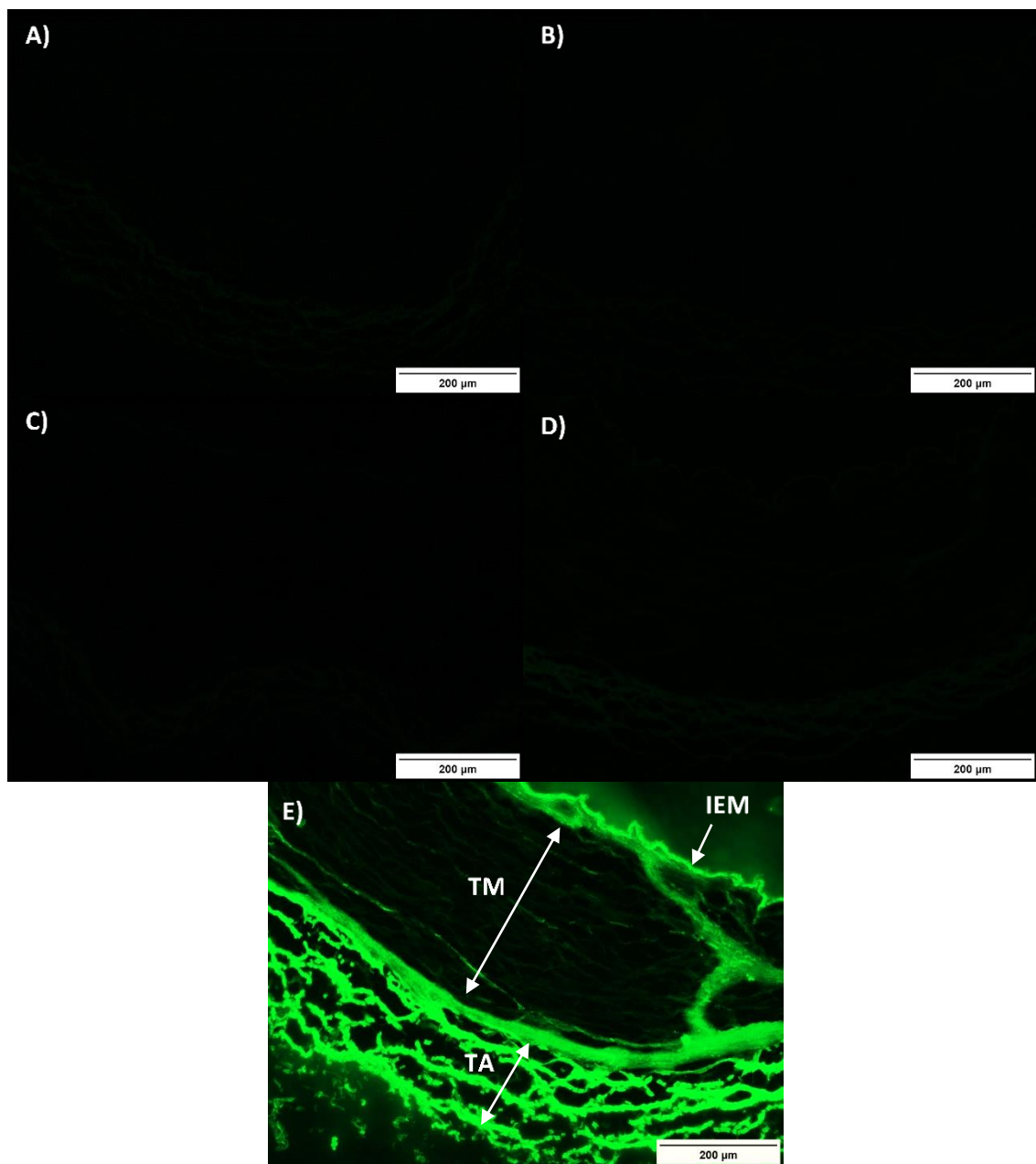


Figure 6.9: Fluorescent microscope cross-sectional images of controls for FITC-labelled peptides self-assembled within acellular artery. Molar ratio of 1:150 of FITC-peptide or FITC- β A control to the non-labelled peptide was used. A) Uncoated acellular artery, non-labelled: B) P_{11-4} , C) P_{11-8} and D) P_{11-12} coated acellular arteries and E) acellular artery immersed in FITC- β A control at a molar ratio equivalent to 1:150 of the control for P_{11} peptides. Internal elastic membrane (IEM), tunica media (TM) and tunica adventitia (TA). Images were acquired using a $\times 10$ objective and scale bars represent 200 μ m.

All FITC-labelled peptides self-assembled within acellular arteries and showed penetration through the ECM. FITC-labelled P₁₁₋₄ (Figure 6.10 A) and P₁₁₋₈ (Figure 6.10 C) showed greater fluorescence in the luminal surface and tunica adventitia but less fluorescence in tunica media. The observed fluorescence in the tunica media appeared to be around elastin (found as elastic sheets between collagen) and around collagen near the luminal surface. The corresponding controls showed similar effects (P₁₁₋₄: Figure 6.10 B, P₁₁₋₈: Figure 6.10 D) with less fluorescence near the luminal surface and around elastic sheets in the tunica media. On the other hand, FITC-labelled P₁₁₋₁₂ (Figure 6.10 E) showed almost uniform fluorescence through the ECM mainly in the internal elastic membrane, tunica media elastic sheets and tunica adventitia. Other structures in the tunica media connecting the ECM structures together were also coated. P₁₁₋₁₂ control had less fluorescence in the tunica media than FITC-labelled P₁₁₋₁₂ (Figure 6.10 F).

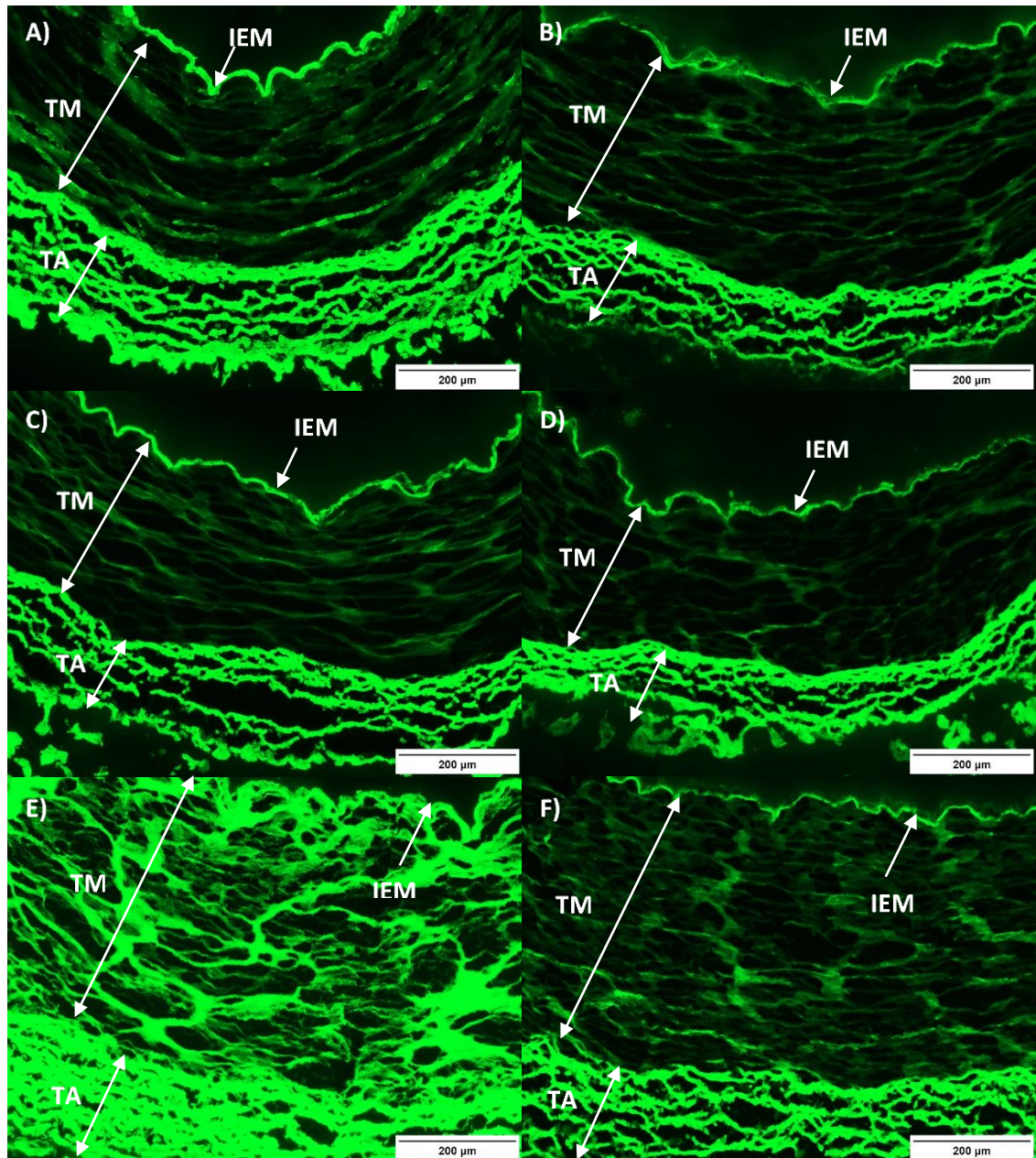


Figure 6.10: Fluorescent microscope cross-sectional images of FITC-labelled peptides self-assembled within acellular artery. Molar ratio of 1:150 of FITC-peptide or FITC- βA control to the non-labelled peptide was used. A) FITC-labelled P_{11-4} , B) FITC- βA + non-labelled P_{11-4} (control), C) FITC-labelled P_{11-8} , D) FITC- βA + non-labelled P_{11-8} (control), E) FITC-labelled P_{11-12} and F) FITC- βA + non-labelled P_{11-12} (control). Internal elastic membrane (IEM), tunica media (TM) and tunica adventitia (TA). Images were acquired using a $\times 10$ objective and scale bars represent 200 μm .

6.4.4 MPLSM Imaging of FITC-labelled Peptide Coated Acellular Artery Tissue

Multiphoton microscopy was utilised to investigate self-assembly of peptides within the acellular artery tissue in the full thickness natural wet form rather than thin cryosections that were investigated using fluorescent microscopy or the surface coating in SEM of the dried coated samples. In addition, high resolution z-stacks of different depths from near the luminal surface of tissue were obtained to test the penetration and coating abilities of the tested peptides using the fact that elastin auto-fluoresce and collagen gives a second harmonic generation signal and both can be distinguished from the FITC signal in peptides.

MPLSM images of samples were taken showing FITC, elastin, collagen and the three combined signals in each sample. Z-stacks of native cellular artery showed that decellularisation did not have a significant effect on the structural composition of the acellular artery (detailed observations can be found in Appendix A.8). In the uncoated acellular artery control (Figure 6.11), a FITC signal was not detected, both elastin (forming the fenestrated internal elastic membrane) and collagen found under this membrane having a characteristic coiled fibre appearance were detected. Collagen fibres appeared to be oriented in one direction in the tunica media (circumferentially). A z-stack of this sample can be found in Appendix A.8 showing the structure of acellular arteries near the luminal surface at low and high magnifications which were compared to cellular arteries.

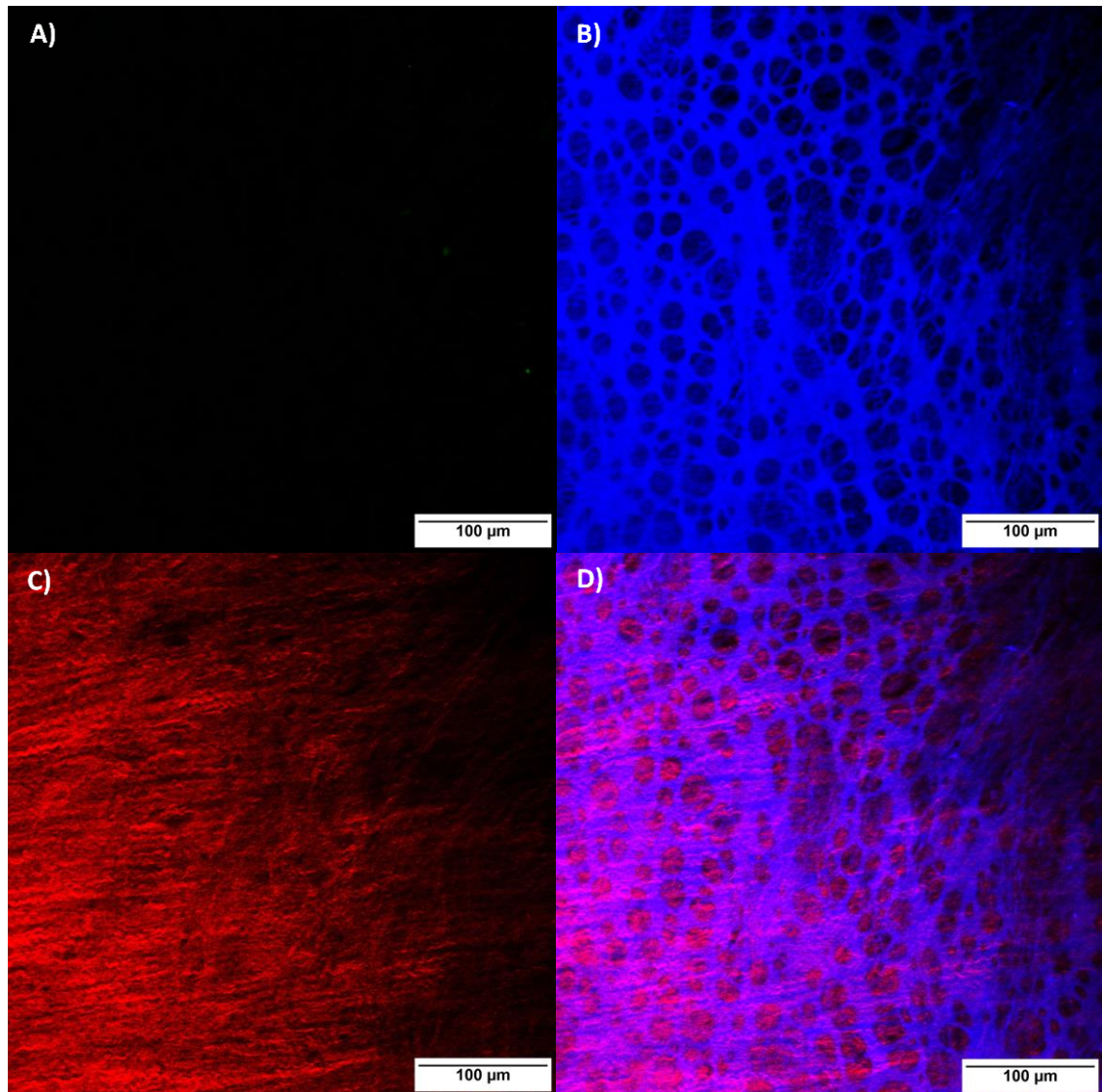


Figure 6.11: Multiphoton images of uncoated acellular artery. FITC (A), elastin (B), collagen (C) and combined (D) signals. Images were acquired using a $\times 20$ objective and scale bars represent $100\ \mu\text{m}$.

In FITC-labelled P₁₁₋₄ coated acellular arteries (Figure 6.12), ECM structures were shown to have been coated by the self-assembled peptide. The peptide mainly coated the fenestrated internal elastic membrane shown by having an intense FITC signal. Collagen fibres were also coated by the peptide but not thoroughly. The peptide also appeared to have filled some of the gaps within the structure and possibly coated other ECM structures where the FITC signal was intense.

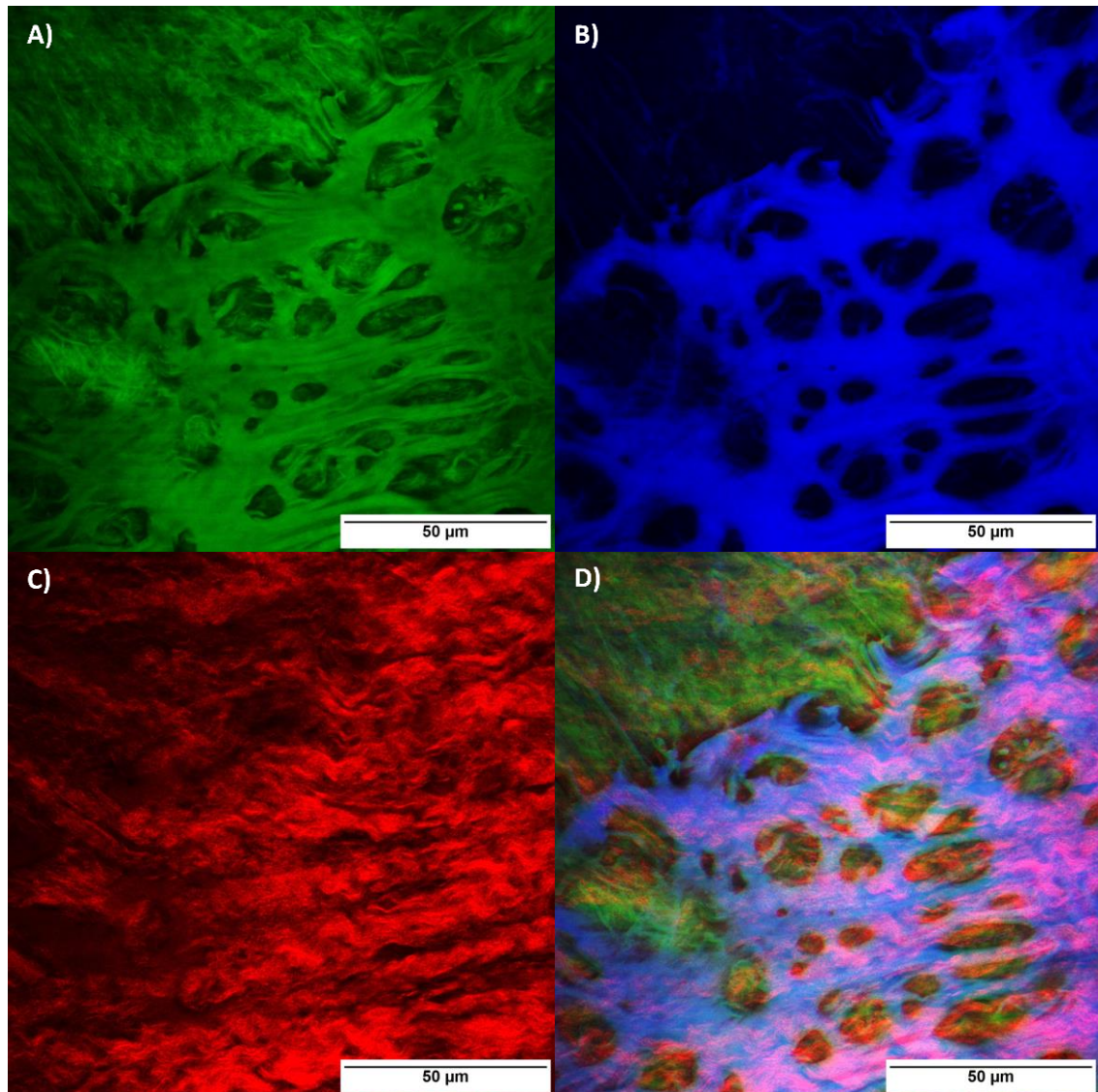


Figure 6.12: Multiphoton images of acellular arteries coated with 20 mg.mL^{-1} FITC-labelled P_{11-4} at a molar ratio of 1:150 of the FITC-labelled to the non-labelled peptides. FITC (A), elastin (B), collagen (C) and combined (D) signals. Images were acquired using a x 63 objective and scale bars represent $50 \mu\text{m}$.

In FITC-labelled P_{11-8} coated acellular arteries (Figure 6.13), ECM structures were shown to have been coated by the self-assembled peptide. Similar to P_{11-4} , the peptide mainly coated the fenestrated internal elastic membrane shown by having an intense FITC signal. Collagen fibres were also coated by the peptide but again not thoroughly. Unlike P_{11-4} , P_{11-8} did not seem to have filled the gaps within the ECM as the combined signal showed almost no FITC signal where the elastin and collagen signals were not detected.

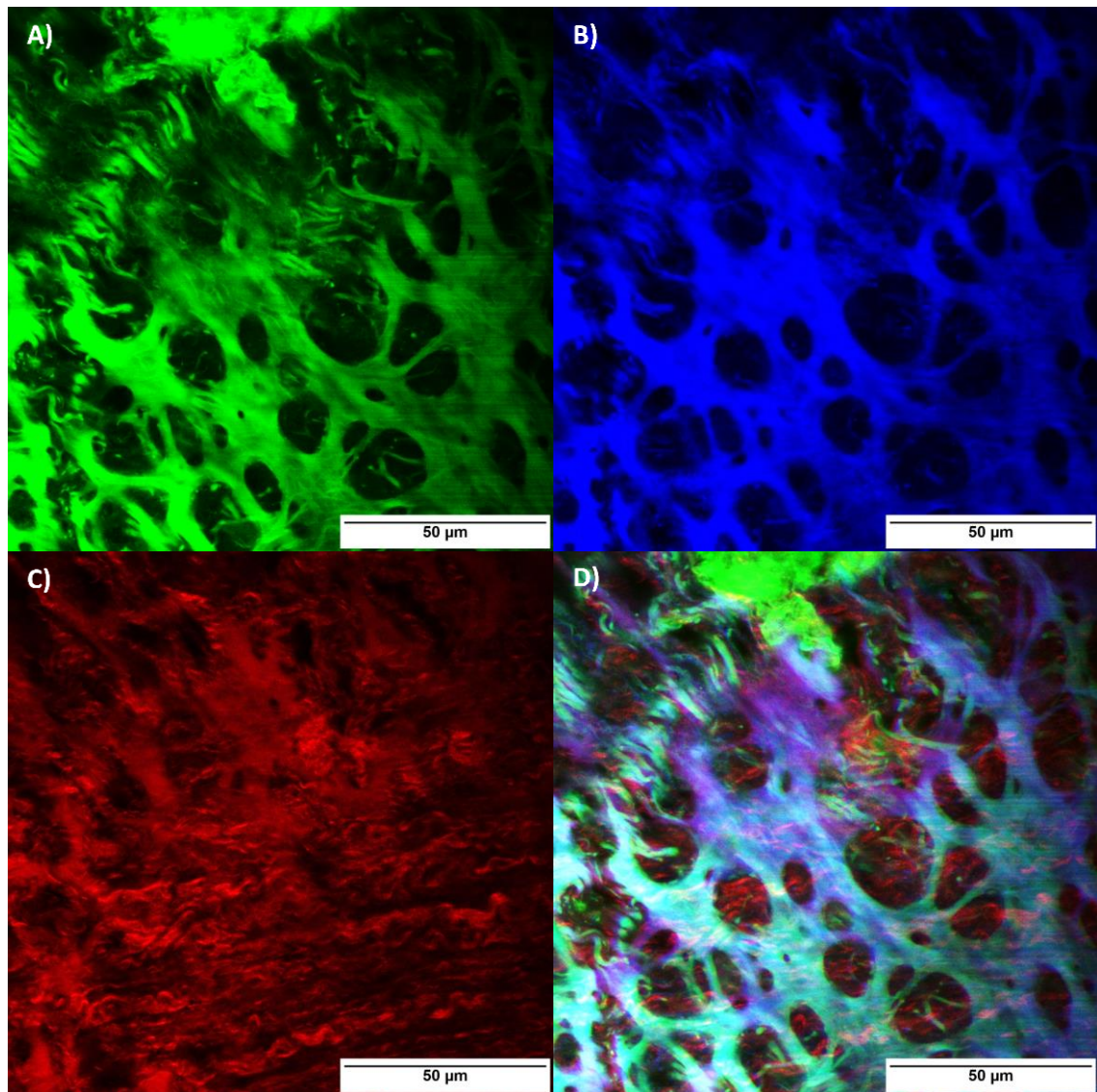


Figure 6.13: Multiphoton images of acellular arteries coated with 20 mg.mL^{-1} FITC-labelled P_{11-8} at a molar ratio of 1:150 of the FITC-labelled to the non-labelled peptides. FITC (A), elastin (B), collagen (C) and combined (D) signals. Images were acquired using a $\times 63$ objective and scale bars represent $50 \mu\text{m}$.

In FITC-labelled P_{11-12} coated acellular arteries (Figure 6.14), ECM structures were shown to have been coated by the self-assembled peptide. This peptide appeared to have coated the fenestrated internal elastic membrane and collagen fibres uniformly. The structure of the internal elastic membrane was less defined in FITC signal than in the images of tissue coated with P_{11-4} and P_{11-8} . This could possibly be due to self-assembly of the peptide through the pores as the FITC signal was detected in pores as seen in the combined signal image. The peptide also appeared to have filled some of

the gaps within the structure and possibly coated other ECM structures where the FITC signal was intense.

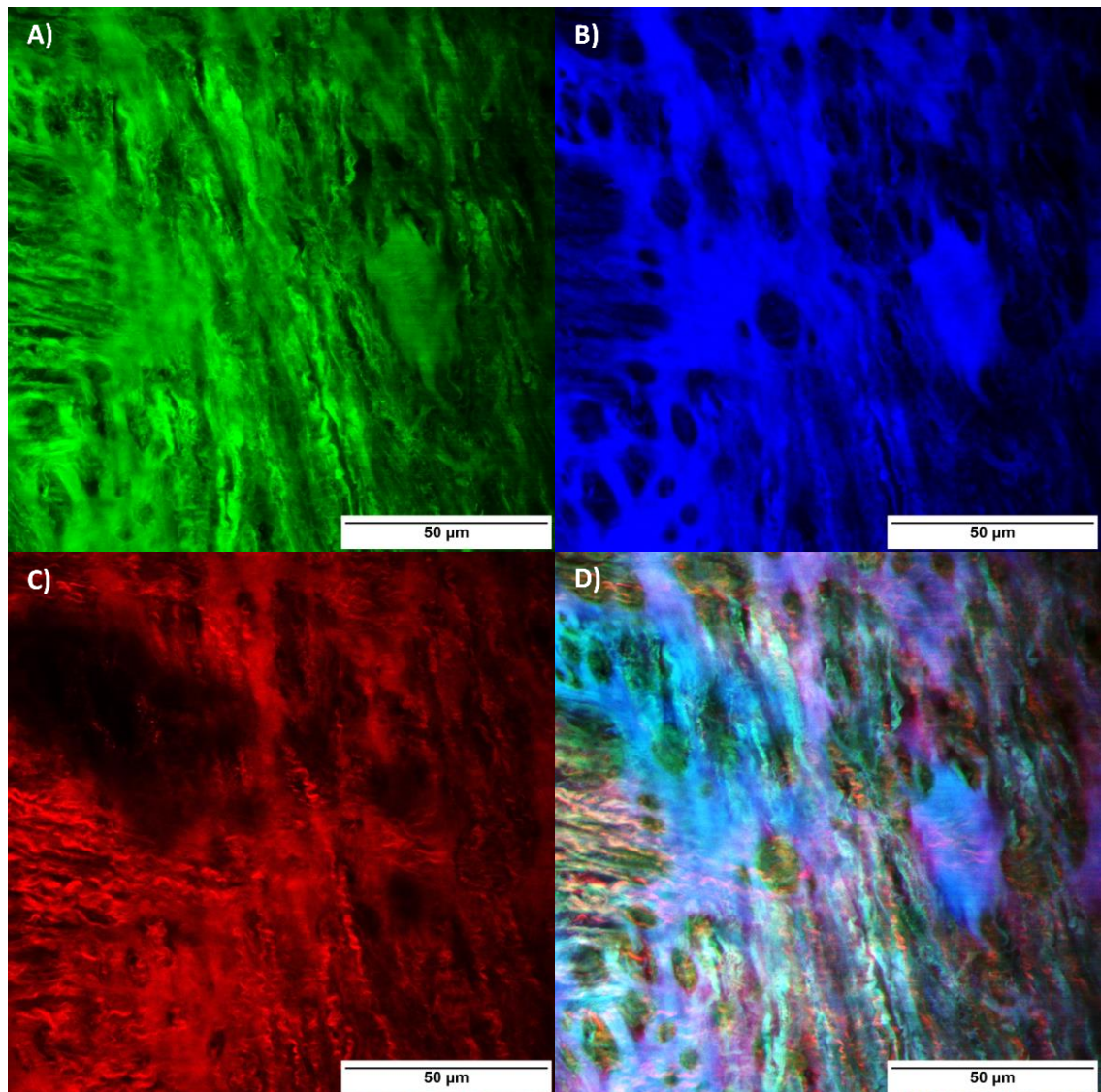


Figure 6.14: Multiphoton images of acellular arteries coated with $20 \text{ mg}\cdot\text{mL}^{-1}$ FITC-labelled P_{11-12} at a molar ratio of 1:150 of the FITC-labelled to the non-labelled peptide. FITC (A), elastin (B), collagen (C) and combined (D) signals. Images were acquired using a x 63 objective and scale bars represent $50 \mu\text{m}$.

Z-stack images of Figure 6.12, Figure 6.13 and Figure 6.14 with all three and combined signals in addition to images of acellular artery immersed in the FITC- βA control can be found in Appendix A.9.

Z-stack images of FITC-labelled peptides were taken at a lower magnification to observe the overall self-assembly of peptides within the ECM structure near the luminal surface

using the FITC signal (Figure 6.15). In FITC-labelled P_{11-4} and P_{11-8} coated samples, high intensity FITC signals were observed on the surface with random structures and these were possibly clumps of gel, which were deposited on the surface and filled some surface gaps. In tissues coated with P_{11-12} , the FITC signal was more uniform on the surface and through the structure. P_{11-8} seemed to have filled the gaps less than P_{11-4} and P_{11-12} , which was mainly near the surface and this was evident by the more defined structure of the internal elastic membrane. P_{11-8} also showed less coating of the collagen fibres suggested by less intense FITC signal observed in the tunica media layer.

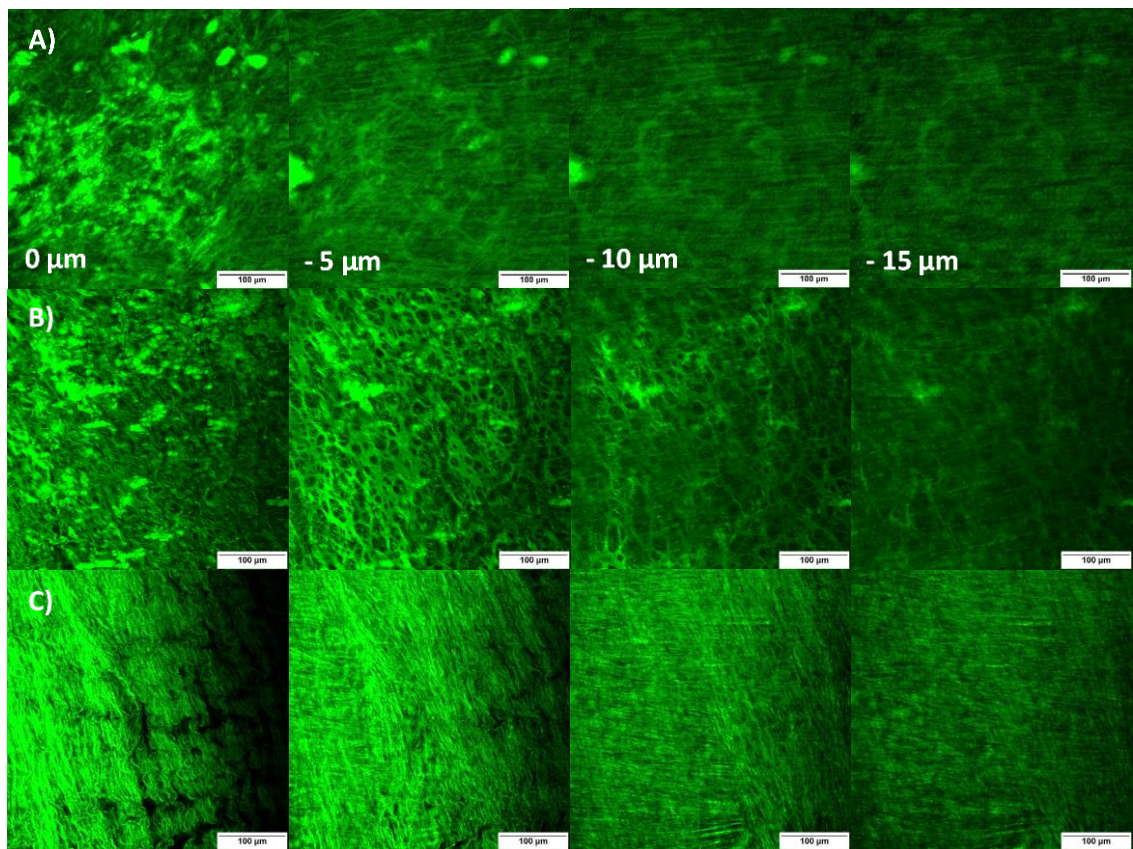


Figure 6.15: Low magnification multiphoton z-stack images of acellular arteries coated with 20 mg.mL^{-1} FITC-labelled peptides at a molar ratio of 1:150 of the FITC to the non-labelled peptides. FITC-labelled: P_{11-4} (A); P_{11-8} (B); and P_{11-12} (C) showing the FITC signal with $5 \mu\text{m}$ intervals from the luminal surface into the tunica media ($15 \mu\text{m}$ depth). Images were acquired using a $\times 20$ objective and scale bars represent $100 \mu\text{m}$.

These observations were more apparent in the higher magnification z-stacks with fewer intervals between slices (Figure 6.16). P_{11-4} and P_{11-8} had intense defined FITC signals,

while P₁₁₋₁₂ had a more uniformly dispersed signal. All peptides seem to have coated the ECM structures near the luminal surface.

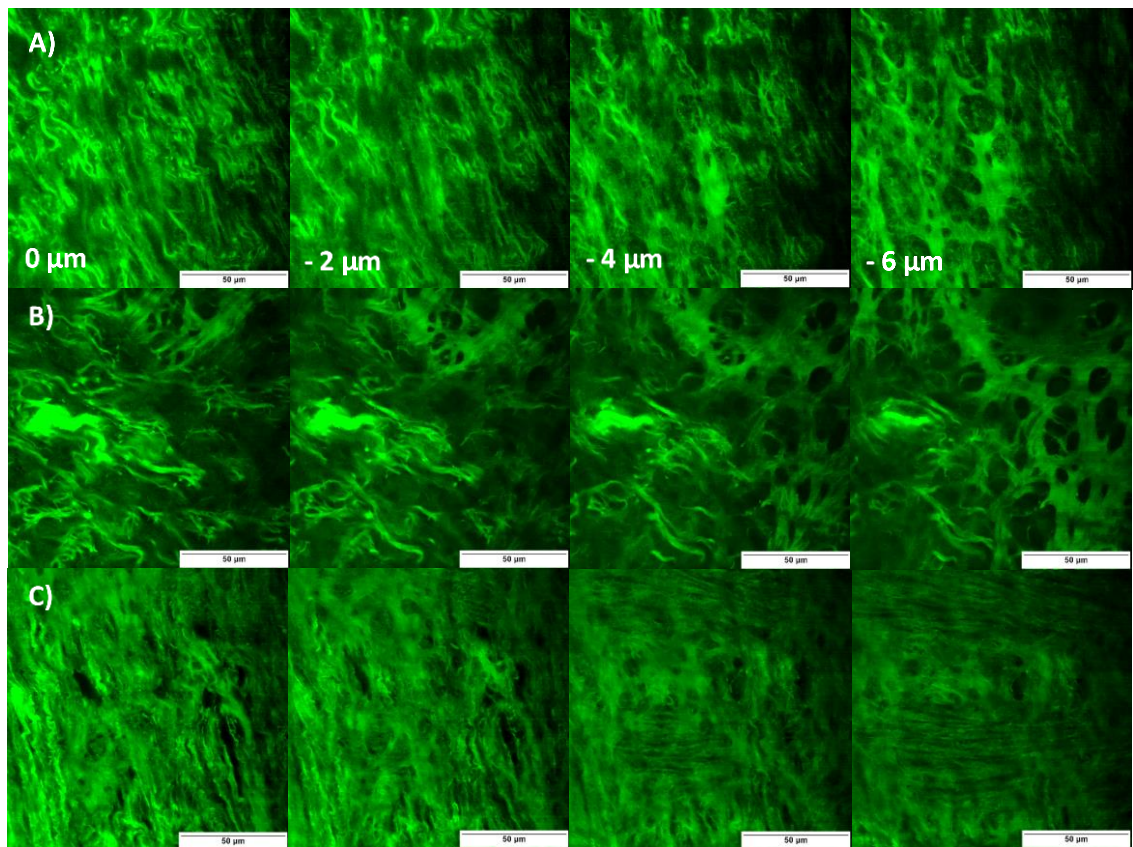


Figure 6.16: High magnification multiphoton z-stack images of acellular arteries coated with $20 \text{ mg}\cdot\text{mL}^{-1}$ FITC-labelled peptides at a molar ratio of 1:150 of the FITC-labelled to the non-labelled peptides. Images of FITC-labelled: P₁₁₋₄ (A); P₁₁₋₈ (B); and P₁₁₋₁₂ (C) showing the FITC signal with $2 \mu\text{m}$ intervals from the luminal surface into the tunica media ($6 \mu\text{m}$ depth). Images were acquired using a $\times 63$ objective and scale bars represent $50 \mu\text{m}$.

The results were compared to FITC- β A treated samples, in which the FITC penetrated through the ECM structure staining different structures (Appendix A.9). It was shown that the FITC signals defined the ECM structures with no gap filling unlike P₁₁₋₄ and P₁₁₋₁₂ and more resemblance to P₁₁₋₈ confirming the self-assembly of these two peptides through the gaps to different extents in the ECM.

6.5 Discussion

6.5.1 Anti-thrombogenic Properties of P₁₁ Peptides

Previous *in vivo* studies have reported that decellularised small-diameter vascular grafts primarily fail due to thrombus formation^{54,58,88,261,262}. Therefore, it was hypothesised that incorporation of self-assembled peptides will prevent thrombosis and facilitate endothelial cell attachment. Consequently, peptides were introduced to blood at 0.3 mM in a Chandler loop model for evaluating the effect of presence of these peptides in the blood on thrombus formation. The peptides were tested in their monomeric form at a concentration below their critical concentration at which self-assembly occurs. This was because when self-assembled within tissue these peptides will always have a proportion in the monomeric state which will enter the circulating blood due to being exposed to excess fluid¹⁷². It was shown that P₁₁-4 and P₁₁-8 reduced thrombus weight significantly compared to the negative control, while P₁₁-12 had no effect on thrombus formation. This can help in reduction of thrombus formation when peptide is removed by the system by acting as an anti-thrombogenic agent. P₁₁-4 and P₁₁-8 are both glutamine based peptides having net charges of - 2 and + 2 at physiological pH, respectively with comparable molecular weights that are higher than P₁₁-12. On the other hand, P₁₁-12 is a serine based peptide having a + 2 net charge at physiological pH. In addition, P₁₁-4 and P₁₁-8 have comparable critical concentrations of self-assembly that are much lower than P₁₁-12, meaning that the two peptides will start to form unstable self-assembled fibrils alongside the stable monomeric peptides at lower concentrations until a stable nucleus is formed at the critical concentration^{172,221}. These unstable structures may have either inhibited or slowed the aggregation of thrombus component. P₁₁-12 had more monomeric random coils than the other two peptides, which may not have interacted with thrombus components, hence was not significantly different from the negative control. The results suggested that in a monomeric form, the size of peptide or the presence of unstable self-assembled fibrils rather than charge contributed more to the interactions causing thrombus formation.

When tested in their self-assembled form at 3 mM in a Chandler loop model, P₁₁-8 and P₁₁-12 resulted in a very significant reduction in thrombus weight compared to the negative control. P₁₁-4 However, did not form a thrombus and blood contained small

gel-like globules afterwards. It is believed that this will not result in thrombosis when applied to vascular grafts as the self-assembled peptide would act as a surface coating and will only be present as a monomeric solution in the bloodstream, so no further investigations were needed. In the self-assembled form, the net charge of peptide or method of introduction might have contributed more to thrombus formation. This is because P₁₁₋₈ and P₁₁₋₁₂ both having a + 2 net charge at physiological pH were introduced to blood in their monomeric form when compared to P₁₁₋₄ with a - 2 net charge at physiological pH that was introduced in its self-assembled form. However, direct comparison was difficult due to the different peptide forms introduced to the blood mixture, which may have affected the kinetics of thrombus formation, implying the importance of optimisation of introduction methods for target application. For applications requiring the use of peptides at high concentration, peptides will be either injected/applied *in situ* in their monomeric form allowing for uniform self-assembly due to pH/ionic strength changes at the site of application or self-assembled on the surface.

The biological response to vascular grafts such as protein adsorption and platelet adhesion is affected by the biomaterial surface properties such as surface chemistry, topography and wettability^{82,85}. In general, hydrophobic surfaces adsorb more proteins than hydrophilic surfaces. These surfaces affect the wettability of material because water molecules are strongly bound to hydrophilic surfaces making it difficult to be displaced by adsorbed proteins as opposed to hydrophobic surfaces⁸⁵. Under high shear conditions, hydrophilic surfaces are believed to have less platelet accumulation than hydrophobic surfaces^{82,263}. This is because it has been reported that platelets adhering to the hydrophilic surface appeared to be more spherical, hence inactivated when compared to extended platelets with stronger contact to the hydrophobic surface, making them easier to detach under high shear forces^{82,101,264}. Conflicting results on the effect of biomaterial surface roughness on thrombus formation were reported in the literature and it is believed that a combination of surface characteristics contribute to the thrombogenicity of material⁸². Surface chemistry was reported to influence fibrinogen and fibrin formation with negatively charged surfaces having the least formation when compared to the positively charged surfaces²⁶⁵. Positively charged surfaces having amine groups may form hydrogen bonding with adsorbed proteins surfaces compared to less protein interactions with negatively charged surfaces⁸⁵.

Endothelial cells in a healthy blood vessel express negatively charged glycoproteins that repel platelets and leukocytes⁹⁴. Negatively charged surfaces provide anti-thrombogenic properties as they repel the negatively charged blood cells⁸². Helmus *et al.* tested the effect of surface charge on thrombus formation and it was reported that unionised surfaces increased thrombus formation when compared to the ionised (negatively charged) surface that was anti-thrombogenic²⁶⁶. This could imply that P₁₁₋₄ will have better anti-thrombogenic properties when used as a surface coating, but this needs further investigation possibly in a Chandler loop model with a coated acellular artery forming part of the tubing as many other factors contribute to thrombus formation and stability including thrombin, platelets and coagulation factors²⁶. In a previous study using P₁₁₋₄, P₁₁₋₈ and P₁₁₋₁₂ as coatings for acellular porcine carotid arteries at 30 mg.mL⁻¹, it has been reported that the peptides lowered the levels of thrombogenesis with P₁₁₋₁₂ having the most significant effect¹⁷⁸.

6.5.2 P₁₁ Peptides as Surface Coatings for Vascular Grafts

The ECM structures of cellular and acellular arteries were studied before coating with peptides to identify different structures and evaluate structural loss following decellularisation. MPLSM images of arteries were obtained from near the luminal surface into the first few micrometres of the media (Appendix A.8). Native cellular arteries were shown to have an internal elastic membrane, a solid sheet-like structure, with small regular fenestrations consisting of thin fibrous elastic fibres above the tunica media, in which tightly packed parallel coiled collagen fibres were found interspersed with elastin fibres circumferentially. Following decellularisation, the internal elastic membrane was shown to have larger fenestration with less packed coiled collagen fibres in the media. These observations match with the previously mentioned results from the literature, suggesting minimal ECM disruption. Similar observations have been reported in the literature of native cellular rat abdominal aorta, porcine thoracic aorta and mouse ascending aorta using SEM, multiphoton and confocal laser scanning microscopies^{250,254,255,267}.

The structure of the ECM and the interaction between collagen and elastin fibres are crucial for functioning arteries, which play a key role in balancing the mechanical load throughout the artery and biological properties^{251,254}. For example, collagen in the

intima mediates endothelial cell growth, while in the tunica media it provides the blood vessel with mechanical support and tensile strength for rupture resistance ²⁵¹. Preservation of the ECM structure is therefore important in vascular graft applications to provide the graft with the appropriate biomechanical and biological properties. A number of studies have shown that the acellular scaffold preserves its biomechanical properties and major ECM structures following decellularisation ^{54,262,268}. In this study, although the ECM structures were minimally affected as observed in multiphoton images, it cannot be concluded that the biomechanical properties were retained and further studies are needed. Having mentioned that, previous studies of decellularised human femoral arteries following methods developed at the University of Leeds have reported minimal loss of the ECM proteins and biomechanical properties ²⁵.

One of the important aspects of vascular grafts is surface coating to completely cover the ECM structures at the luminal surface in order to create a barrier between blood and the ECM structures such as collagen, which can promote thrombus formation ²⁶.

Peptide coated acellular arteries were investigated using a combination of microscopies for better understanding of the self-assembly behaviour within the tissue. SEM images of the luminal surface have shown that P₁₁₋₄ and P₁₁₋₈ formed sufficient surface coatings with almost complete coverage of the ECM structures at the luminal surface, whereas P₁₁₋₁₂ was shown to form a very thin insufficient coating layer leaving collagen fibres exposed. The characteristic banding in organised collagen fibres facilitated the differentiation from thinner randomly oriented peptide fibrils/fibres and it matched the structure reported in the literature ^{250,251}. Cross-sectional fluorescent microscopy images have shown that P₁₁₋₄, P₁₁₋₈ and P₁₁₋₁₂ were able to penetrate throughout the arterial structure but have variable penetration abilities with P₁₁₋₁₂ having the best almost uniform penetration shown by the very intense FITC signal. MPLSM images have shown that all peptides coated different structures of the ECM with varying extents. P₁₁₋₄ and P₁₁₋₈ were shown to deposit on the surface as gel clumps coating the internal elastic membrane and penetrating into the tunica media coating collagen fibres and other structures. P₁₁₋₁₂ was shown to coat the internal elastic membrane without forming deposits on the surface and collagen in the tunica media almost uniformly, filling the gaps better than P₁₁₋₄, hence was shown to have better penetration ability.

The penetration of peptides throughout the artery was possibly facilitated by the porous ECM, which increased the porosity of acellular artery by removal of cells and other components. In general, peptides were shown to form better coatings for: the internal elastic membrane and subendothelium; elastin structures within the tunica media attributed to the interconnection between the elastic sheets throughout the media when compared to closely packed collagen fibre layers; collagen/elastin fibres close to the layered elastin sheets possibly due to the fenestration that allowed peptide infiltration; and collagen/elastin fibres in the adventitia because these are not closely packed and of larger diameters. The first and last regions/structures had the best coatings because these were close to the luminal/abluminal surface of artery and were easily and rapidly accessed by the peptide fibrils.

Peptide self-assembly and gelation properties also contributed to the different coating and penetration behaviour. This is because the results in Chapter 4 have shown that P₁₁₋₄ and P₁₁₋₈ at 20 mg.mL⁻¹ formed gels almost instantaneously following triggering self-assembly as opposed to P₁₁₋₁₂ that formed a gel consisting of thinner fibrils at a slower rate, which was easily disrupted by gentle agitation (pipetting or vortexing). The poor P₁₁₋₁₂ surface coating and better penetration can be attributed to thinner fibrillar networks insufficiently covering the ECM structures. However, this alongside the slower gelation rate has allowed better penetration. In contrast, P₁₁₋₄ and P₁₁₋₈ densely coated the surface due to the faster gelation rates that resulted in poorer penetration. Additionally, it has been reported that increasing the concentration of P₁₁₋₄ increased the thickness of peptide coating the surface of acellular porcine carotid artery confirmed by the disappearance of the characteristic banding structure of collagen at 10 mg.mL⁻¹ in SEM images. However, this has also been reported to decrease the peptide penetration through the tunica media due to the hierarchical self-assembly of the peptide. This means larger/longer structures obtained at high concentrations were unable to penetrate through the artery as opposed to smaller/shorter structures at the lower concentrations. In the same study, self-assembly of P₁₁₋₄ at 30 mg.mL⁻¹ within the tissue was confirmed by FTIR¹⁷⁸.

6.6 Summary of Peptide Self-assembly within Acellular Tissue

P₁₁₋₄ and P₁₁₋₈ peptides were shown to have; superior anti-thrombogenic properties compared to P₁₁₋₁₂ when present in bloodstream; and better surface coating for acellular arteries. This will potentially help in thrombus formation reduction when peptides exist in their monomeric form, while separating the ECM structures from contacting blood in their self-assembled form. P₁₁₋₁₂ however, was shown to have more penetration that was almost uniform through the ECM of acellular arteries. On this basis, P₁₁₋₄ and P₁₁₋₈ were selected as potential candidates for further studies to test for the effect of functionalisation with bioactive (cell attachment) motifs to enhance re-endothelialisation, gradually forming the natural anti-thrombogenic surface. The results obtained in this chapter are summarised in Table 6.1.

Table 6.1: Peptide self-assembly within acellular tissue for anti-thrombogenic surface coating.

Peptide	Effect on Thrombus (Monomeric Form)	Luminal Surface Coating	Penetration and Interaction
P ₁₁₋₄	Significant reduction from negative control	Excellent: coated collagen almost completely	Good: penetrated through the ECM mainly coating the internal elastic membrane and adventitia. Largely deposited as gel clumps on the luminal surface, moderately filling the gaps within ECM, coating elastin, collagen and other ECM structures
P ₁₁₋₈	Significant reduction from negative control	Excellent: coated collagen almost completely	Good: penetrated through the ECM mainly coating the internal elastic membrane and adventitia. Largely deposited as gel clumps on the luminal surface, slightly filling the gaps near the surface resulting in a more defined internal elastic membrane structure (than P ₁₁₋₄ and P ₁₁₋₁₂), coating elastin, collagen and other ECM structures
P ₁₁₋₁₂	No effect when compared to negative control	Poor: insufficient coating of the collagen fibres	Excellent: penetrated through the ECM almost uniformly. No deposition of peptide on the luminal surface, filling the gaps within ECM resulting in less defined internal elastic membrane structure (than P ₁₁₋₄ and P ₁₁₋₈), coating elastin, collagen and other ECM structures

7 Effect of Peptide Functionalisation on Cell Attachment to Peptide Coated Acellular Artery

7.1 Introduction

In Chapter 6, P₁₁₋₄ and P₁₁₋₈ were deemed suitable for use as vascular graft coatings. These peptide coatings could be further improved for better performance in small-diameter vascular grafts by having bioactive functions such as cell attachment motifs. In nature, cell binding to the ECM is facilitated by protein components of the ECM. For example, fibronectin and laminin bind cells commonly through RGD and YIGSR amino acid sequences, respectively ^{269,270}. These two peptide sequences can be recognised by integrins, which are a family of cell adhesion receptors that are known to facilitate cell-ECM binding and are found in many cell types including endothelial cells ²⁷⁰⁻²⁷². Therefore, it was hypothesised that functionalisation of self-assembling peptides with cell attachment motifs would aid rapid endothelialisation of the acellular tissue through facilitating cell binding to the ECM.

P₁₁₋₄ and P₁₁₋₈ were functionalised with the two different commonly investigated cell attachment motifs, GRGDS and YIGSR, separated from the self-assembling domain by a spacer (Chapter 5). In this chapter, the functionalised peptides were tested for enhancement of cell binding. These motifs were compared to: scrambled controls GRDGS and YIRSG that are not known and have not been reported to have cell attachment properties; non-functionalised peptide controls; and untreated acellular tissue for the effect of peptide surface coating on cell attachment to be determined.

7.1.1 Cell Adhesion Molecules

Cell adhesion receptors are transmembrane glycoproteins that mediate many biological processes in addition to cell binding including; cellular growth and differentiation, inflammatory response, wound healing and thrombosis ^{273,274}. There are four major cell adhesion receptor families: immunoglobulin superfamily, cadherin, selectin and integrin. The first three families mainly mediate cell-cell interactions, while integrins mediate cell-ECM adhesion ²⁷⁴. Therefore, this family was of the most interest in this study due to the aim of binding cells to the acellular artery ECM.

Integrins are heterodimers consisting of α and β subunits that are non-covalently associated (Figure 7.1). Each subunit has a short cytoplasmic C-terminal tail and a large extracellular N-terminal head. The extracellular domains of α and β subunits contribute to the formation of ligand binding site which can bind to different proteins including collagen and laminin in the basement membrane and fibronectin in the basement membrane and connective tissue ²⁷³⁻²⁷⁵. The cytoplasmic domains contribute to the interaction between the extracellular environment and intercellular structures such as those involved in cytoskeletal organisation ²⁷⁴. The β subunit has four cysteine-rich repeating units and disulphide bonds between cysteine residues near the N-terminus of the subunit and those within the four repeating units which stabilise the loop of the head region. The α subunits contain divalent cation binding regions in the extracellular domain and disulphide bonds connecting light and heavy chains of the extracellular domain. The cations are essential for the function of integrins whose specificity as well as affinity can be affected by the nature of the cation ^{273,276}. Interaction of integrins with target ligands on the ECM requires the presence of both subunits ²⁷³.

In humans, 24 functional integrins are known to be formed from the identified 18 α and 8 β subunits ^{275,277}. Consequently, the ligand specificity results from the combination of α and β subunits and a single integrin can recognise several different proteins ²⁷⁴. In addition, integrins recognise specific short peptide sequences in their ligands. RGD is one of the most common sequences that is found in many proteins including fibronectin and laminin and is recognised by more than half of the known integrins ^{273,278}. Integrins are expressed on the surface of many cell types and cells can express different integrins on their surface offering a great versatility in cell attachment ²⁷⁶. For example, $\alpha_{IIb}\beta_3$ and $\alpha_v\beta_5$ integrins are involved in various important physiological process and recognise RGD sequences. The $\alpha_{IIb}\beta_3$ is a platelet-specific integrin for RGD and is important for the process of thrombosis initiated by aggregation of platelets ^{276,279}. The $\alpha_v\beta_3$ integrins are selectively expressed on endothelial cells that can bind to various RGD forms and are involved in angiogenesis ²⁷⁸. Other integrin subfamilies have been identified to be expressed by endothelial cells including $\alpha_1\beta_1$, $\alpha_2\beta_1$, $\alpha_3\beta_1$, $\alpha_4\beta_1$, $\alpha_5\beta_1$, $\alpha_6\beta_1$, $\alpha_v\beta_1$ and $\alpha_v\beta_5$ ^{122,280}. YIGSR is another cell attachment sequence found in laminin and is thought to mediate cell binding through $\alpha_3\beta_1$, $\alpha_4\beta_1$ and $\alpha_6\beta_1$ integrins, although there are conflicting suggestions regarding YIGSR from the literature that YIGSR mediates cell

attachment through a non-integrin surface receptor (67 kDa laminin receptor, 67LR)
272,281,282.

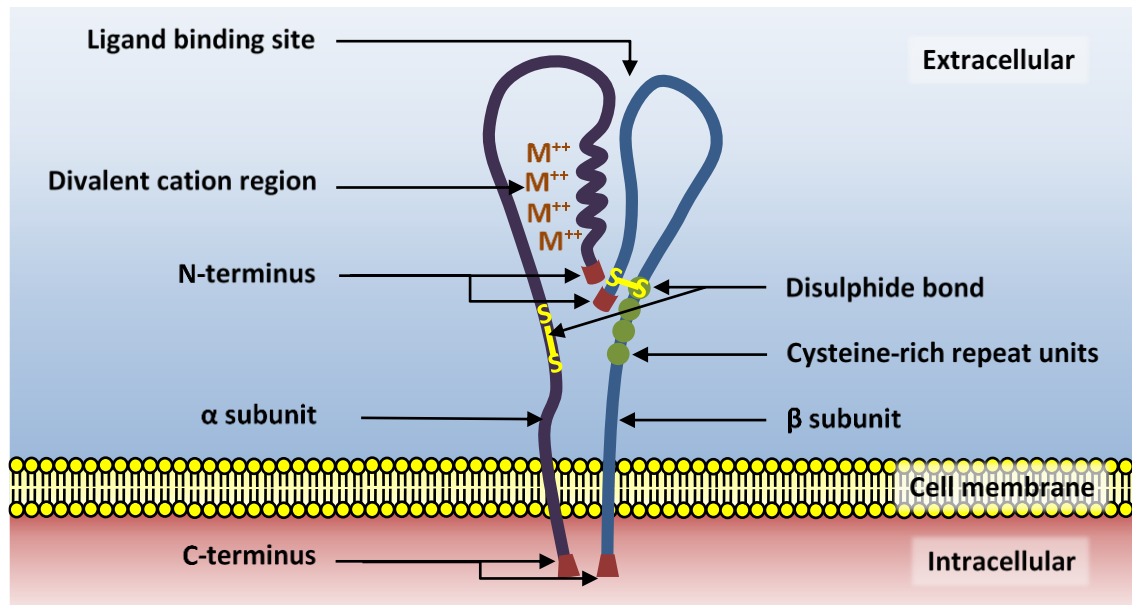


Figure 7.1: Schematic diagram of integrin cell adhesion receptor showing the main features of α and β subunits. *Integrin mediates cell-ECM adhesion.*

Integrin-mediated cell adhesion occurs through four partially overlapping events. The process starts with cell attachment by ligand binding, allowing the cell to withstand gentle shear force. The cell then starts to flatten and spread over the surface. Cytoskeletal organisation then occurs followed by focal adhesion formation, which links the actin cytoskeleton to the ECM, leading to survival and proliferation of cells ²⁸¹.

7.1.2 Design of Synthetic Bioactive Peptides – Cell Attachment Motifs

Peptides can be designed to have certain amino acid sequences derived from nature mimicking the recognition sites on ligands for integrins and potentially improving cellular attachment and proliferation. These can be employed in many biomedical applications such as tissue engineering. Here, interest is in the improvement of vascular grafts by surface coating with bioactive functions to enhance rapid endothelial cell attachment to the graft forming an anti-thrombogenic endothelial layer. Many cell attachment motifs found in nature that are recognised by endothelial cells have been discovered and investigated such as RGD, YIGSR, CAG and REDV ²⁸³. In this study, several

criteria from the literature were followed for the design of efficient cell attachment motif functionalised peptides.

Firstly, specificity of the selected motifs for the target cell. For the design of bioactive peptides for vascular grafts, it was essential to take into consideration that the cell attachment motif had a strong binding affinity for the desired cell type but lower affinity for other cell types that might promote thrombus formation or inflammation, hence specific-cell binding was favourable¹²². Among the sequences known to bind endothelial cells, RGD and YIGSR are the most investigated motifs^{14,113,284,285}. RGD is one of the first discovered peptide sequences that is found in various different ECM proteins and used as a cell attachment motif in many studies^{281,286}, hence was selected. However, because RGD has been reported to promote platelet adhesion contributing to thrombus formation, the YIGRS peptide sequence was also selected because it has been reported to selectively enhance endothelial cell attachment with no platelet adhesion²⁷¹. The integrin $\alpha_4\beta_1$ is expressed by endothelial cells but not platelets and recognises the YIGSR sequence^{272,281}. In addition, to evaluate the bioactivity of the selected cell attachment motifs as well as their integrin selective binding, scrambled controls GRDGS and YIRSG were also synthesised.

Secondly, spacer length and flexibility. The spacer should extend from the surface of the graft so that it is long enough to interact with the binding sites on integrins; but not be too short such that cell attachment motifs cannot enter the binding site and not too long such that cell attachment and spreading is still promoted. An ideal spacer length fits the integrin dimensions²⁸⁷. A number of studies have been carried out to investigate the effect of spacer length and flexibility on the activity of cell attachment motifs. Separation of the base peptides by varying glycine residues (1, 3 and 5) from RGDS was shown to result in better cell spreading and proliferation with increasing spacer length. Longer spacers have also been suggested by Sur *et al.* to overcome the steric barriers that may interfere with cell binding in the crowded environment of nanofibers²⁸⁸. Moreover, the nature of the spacer, rigid or flexible, has been shown to have no significant effect on the morphology of cells, hence the spacer length contributed more to the bioactivity of peptide²⁸⁸. Flexible forms of RGD have also been reported to be preferable for the $\alpha_v\beta_3$ integrins (expressed by endothelial cells) over rigid forms²⁷⁸, possibly because flexibility facilitates access to target integrins. In another study by Lee

et al., it was reported that a minimum of four glycine residues was required to enhance fibroblast integrin binding to G_n RGDSP peptides with varying lengths of glycine residues from 0 to 20 used as a spacer for tissue engineering applications²⁸⁹. The attachment and growth rates of the cells were increased with increasing spacer length possibly due to enhanced accessibility, which levelled off with more than 12 glycine residues²⁸⁹. A less stressful environment has been reported for cells in G_4 RGDSP and G_{12} RGDSP peptides (compared to RGDSP control) reducing apoptosis with higher viabilities in the latter peptide²⁸⁹. As discussed in the previous section, RGD can be recognised by more than half of the known integrins including the $\alpha_{IIb}\beta_3$ subfamily which are the most abundant integrins on platelets playing an important role in platelet aggregation. One study investigated the effect of platelet adhesion through varying lengths of RGD peptide (G_n RGDF). It has been reported that an increase in length by inserting more glycine residues decreased the peptide potency. The study suggested that the majority of $\alpha_{IIb}\beta_3$ integrin sites can be reached between 11 - 32 Å (G_3 RGDF and G_9 RGDF) assuming that each glycine residue is 3.5 Å. In addition, no significant platelet aggregation was observed with $> G_{13}$ RGDF i.e. 46 Å from the surface²⁸⁷. Here, the choice of spacer lengths equivalent to ≥ 13 glycine residues was based on the different findings from the literature in an attempt to enhance the attachment of endothelial cells and potentially reduce platelet aggregation through the RGD sequence. Since no significant effect has been reported regarding the flexibility of spacer, the designed peptide in this study was based mainly on PEG.

The third criterion was choice of peptide sequence because the structure and conformation of peptide influences the binding to different integrin subfamilies²⁸¹. The sequence GRGDS was chosen for this study since the $\alpha_v\beta_3$ integrins expressed by endothelial cells show preference for serine and alanine residues after the RGD sequence²⁷⁸. In one study of RGD X peptides ($X = S, T$ and V) with different cell lines, it was reported that the cell attachment to RGD X peptides was more effective than RGD peptide, out of which RGDS had the most notable cell attachment activity. Also, the peptide sequence in fibronectin contains a serine residue following the RGD sequence (-GRGDS-) ²⁹⁰. Having a serine residue after the RGD was shown to inhibit cell attachment to fibronectin more effectively than other tested residues by competing for the cell binding site even at lower concentrations compared to RGD alone²⁹¹. However,

for YIGSR the same sequence was selected in this study to allow for comparison with GRGDS and because this sequence has been investigated in many previous studies. In addition, fewer studies have been reported in the literature regarding YIGSR with varying residues after/before the sequence, therefore no modifications on the YIGSR sequence were carried out.

The final criterion was *in vivo* stability of the peptide. It is important to consider the design of peptides with prolonged *in vivo* stability and low degradation rates such as the cyclisation of the cell attachment motifs making them more resistant to proteolysis¹²². Amidation and acetylation are commonly used in peptide synthesis for biological applications to increase the stability of peptides against proteolysis though cyclic peptides are much more stable forms than linear peptides²⁸¹. Cyclic peptides may interfere with the self-assembly of peptides especially if used at higher molar ratios because of the bulky structure. Furthermore, these peptide forms are more complex to synthesise than the linear forms. The peptides designed for this study contained amidated C-termini and acetylated N-termini. As discussed in Chapter 4, P₁₁₋₄ and P₁₁₋₈ are thought to be stable under flow conditions due to their critical low self-assembly concentrations, meaning these peptides will always have a monomeric form equivalent to this concentrations in order to establish equilibrium. This would potentially allow for the steady removal of peptide diffused into the bloodstream from the acellular tissue surface.

To summarise, the bioactive peptides (GRGDS and YIGSR functionalised P₁₁ peptides) designed in this study had long spacer lengths which were flexible in order to facilitate the accessibility to integrins. These peptides were designed in the linear form due to the complexity of cyclisation.

7.1.3 Endothelial Cells – Identification and Isolation

Endothelial cells are bound to the basement membrane forming the continuous lining of the luminal surface of blood vessels and play an important role in vascular function such as vessel permeability as well as physiological and pathological responses²⁹². The function of the endothelium was discussed in more detail in Chapter 1 (Section 1.2).

Endothelial cells highly express certain markers such as platelet endothelial cell adhesion molecule (CD31) and von Willebrand factor (vWF). These are membrane-

bound or cytoplasmic molecules that can enable identification of endothelial cells from other cell types. CD31 is a transmembrane glycoprotein of the immunoglobulin superfamily that is expressed on early and mature vascular endothelial cells, while vWF is a glycoprotein produced by endothelial cells and can be found in Weibel-Palade bodies in the cytoplasm and is crucial for haemostasis following vascular injury ²⁹². Different vascular and local environments elicit heterogeneous phenotypes of endothelial cells depending on local needs ²⁹³.

Endothelial cells have been isolated from various tissue types such as umbilical cord veins, horse carotid arteries, bovine pulmonary arteries, sheep bronchial arteries and murine lungs by collagenase digestion under sterile conditions to detach the cells from the basement membrane followed by selective isolation of the required cells by successive passaging, flow cytometry or use of antibody-tagged magnetic beads. These cells are primarily identified morphologically and behaviourally by growing as a monolayer of polygonal-shaped cells in culture with a cobblestone appearance at confluence when compared with fibroblasts and smooth muscle cells that form monolayers of elongated spindle-shaped cells ²⁹⁴⁻²⁹⁹. In addition, freshly isolated microvessel endothelial cells have been reported to form small discrete colonies that grow over time and merge at confluence ³⁰⁰. Because these endothelial cells have been isolated from different tissue types compared to the femoral artery endothelial cells used in this study, they may have slight variations in appearance and behaviour. It has been shown that endothelial cells isolated from murine blood vessels can be maintained in culture by addition of endothelial cell growth supplement (ECGS) and heparin to cell culture medium to promote endothelial cells growth and inhibit smooth muscle cells growth, respectively ³⁰¹. Other than morphology, endothelial cells can be identified by their expression of glycoproteins vWF and CD31.

7.2 Aims and Objectives

The aim of this chapter was to investigate the effect of functionalised self-assembling peptides on cell attachment of ovine arterial endothelial cells to acellular porcine external iliac arteries.

The specific objectives were:

- To isolate and characterise ovine femoral endothelial cells;
- To assess the *in vitro* biocompatibility of acellular porcine external iliac artery tissue with the isolated cells using a contact cytotoxicity assay;
- To assess the effect of different functionalised self-assembled peptides coating the acellular tissue on endothelial cell attachment.

7.3 Methods

7.3.1 Isolation, Maintenance and Characterisation of Endothelial Cells

Ovine femoral endothelial cells were isolated as described in Section 2.2.12.1. Following isolation, cells were maintained in T-25 tissue culture flasks at 37 °C and 5 % (v/v) CO₂ in air. Endothelial cells were isolated from femoral arteries, so other cells including smooth muscle cells and possibly fibroblasts were also present. This heterogeneous cell population was purified by successive passaging with three-minute trypsin/EDTA treatment for cell detachment in an attempt to deplete fibroblasts and smooth muscle cells as described in Section 2.2.12.2. Before each passage, cells in tissue culture flasks were viewed under phase contrast microscopy to observe cell growth and morphology over time, cells were subsequently passaged into T-75 tissue culture flasks at 37 °C and 5 % (v/v) CO₂ in air. After each passage, cells were cryopreserved for future experiments (Section 2.2.12.3). Cells were resurrected and then passaged after reaching 80 % confluency at least once before use. The phenotype of isolated cells was assessed by immunofluorescence as described in Section 2.2.12.4 at different passages using antibodies against vWF, α -actin, myosin and 5B5 (n = 3). Labelled cells were viewed under a Zeiss upright microscope using DAPI (excitation: 353 nm, emission: 465 nm) and FITC (excitation: 495 nm, emission: 519 nm) filters. Three images of DAPI and FITC-labelled antibody were acquired randomly from each antibody/isotype.

7.3.2 Biocompatibility – Contact Cytotoxicity Assay

The *in vitro* biocompatibility of acellular arteries (produced and quality assured as described in Chapter 3) was confirmed with each batch of isolated endothelial cells (n = 4) at different passages after the phenotype of the cells was determined. Cells were passaged as described in Section 2.2.12.2, a contact cytotoxicity assay was carried out as described in Section 2.2.6.1 using the isolated endothelial cells at a concentration of 250,000 cells.mL⁻¹ (2 mL per well i.e. 500,000 cells per well) in M-199 endothelial cell culture medium.

7.3.3 Seeding Method Optimisation

7.3.3.1 Effect of Tissue Preconditioning on Cell Attachment to Uncoated Acellular Tissue

Acellular tissue samples were tested for the effect of tissue preconditioning on cell attachment. Acellular tissue was preconditioned for 0, 4 and 24 hours (n = 3) using supplemented M-199 cell culture medium without ECGS following the same procedure described in Section 2.2.13.1 without the additional washes prior to cell seeding. Cells were seeded for four hours (Section 2.2.13.2), live/dead[®] stained (Section 2.2.13.3) then imaged and analysed by counting live and dead cells as described in Section 7.3.3.5.

7.3.3.2 Cell Densities in Uncoated Acellular Tissue Over Time

The effect of time on cell attachment to acellular tissue without preconditioning was then tested at different time points (n = 3) as described in Section 2.2.13.1 without the additional washes prior to seeding. Cells were seeded for 1, 4, 24, 72 and 120 hours (Section 2.2.13.2), live/dead[®] stained (Section 2.2.13.3) then imaged and analysed by counting live and dead cells as described in Section 7.3.3.5.

7.3.3.3 Effect of Different P₁₁₋₄ Peptides Coatings on Cell Attachment without Tissue Preconditioning

Functionalised P₁₁₋₄ peptides (20 mg.mL⁻¹, molar ratio 1:50) were coated onto acellular tissue (n = 3) as described in Section 2.2.13.1 without the additional washes prior to cell seeding and without tissue preconditioning. Cells were seeded for 4 and 72 hours (Section 2.2.13.2), live/dead[®] stained (Section 2.2.13.3) then imaged and analysed by counting live and dead cells as described in Section 7.3.3.5.

7.3.3.4 Effect of Tissue Preconditioning on Cell Attachment to Non-functionalised Peptide Coated Acellular Tissue

Uncoated, 20 mg.mL⁻¹ P₁₁₋₄ coated and 20 mg.mL⁻¹ P₁₁₋₈ coated acellular tissue samples (n = 3) were prepared with preconditioning of tissue and washing of excess gel as described in Section 2.2.13.1 Cells were then seeded for 4 and 72 hours (Section 2.2.13.2), live/dead[®] stained (Section 2.2.13.3) then imaged and analysed by counting live and dead cells as described in Section 7.3.3.5. This optimised method was carried out for future cell studies within this chapter.

7.3.3.5 Imaging and Data Analysis

Cells were viewed under a Zeiss upright microscope using calcein AM (excitation: 494 nm, emission: 514 nm) and ethidium homodimer-1 (excitation: 350 nm, emission: 617 nm) filters as described in Section 2.2.13.4. Five images were acquired, then percentages of viable cells and cell densities were determined and data plotted as means (n = 3) ± 95 % confidence limits. Data were analysed using two-way ANOVA and post-hoc Tukey's test (p < 0.05; Section 2.3).

7.3.4 Effect of Functionalised Peptides on Attachment and Growth of Endothelial Cells to Acellular Arteries

The ability of endothelial cells to attach to the luminal surface of acellular arteries, uncoated and coated with peptides, was determined using live/dead[®] staining over 72 hours. Samples of acellular artery 12 mm in diameter were coated with 20 mg.mL⁻¹ peptides; (P₁₁₋₄ and P₁₁₋₈ non-functionalised controls, GRGDS and YIGSR functionalised P₁₁₋₄ and P₁₁₋₈ and scrambled controls at a molar ratio of 1:50 of functionalised to non-functionalised peptides). Three replicates for each peptide coated tissue and tissue control were prepared and placed in wells of 12-well plates; each sample and its control were placed in a single plate, so two plates were prepared for the two-time points. Samples were gently washed with 1 mL of preconditioning medium to remove excess gel from the tissue surface then medium was aspirated. Seeding rings with 8 mm internal diameter were placed on each sample and tissue preconditioned with 300 µL endothelial cell culture medium without ECGS overnight at 37 °C and 5 % (v/v) CO₂ in air as described in Section 2.2.13.1. After incubation and aspiration of the cell culture medium, tissue was seeded with 200 µL cell suspension (25,000 cells.mL⁻¹) and

incubated for four hours at 37 °C 5 % (v/v) CO₂ in air. After aspirating medium and removing the seeding rings, samples were washed with 1 mL PBS for one minute. PTFE rings were then placed on the tissue and 200 µL of endothelial cell culture medium was added and replaced every 48 hours as described in Section 2.2.13.2. After four and 72 hours, samples were removed and washed with 1 mL sterile PBS then stained with 1 mL of PBS containing 1 µM calcein AM and 2 µM ethidium homodimer-1 and incubated for one hour at 37 °C, which was removed before washing samples with 1 mL sterile PBS (Section 2.2.13.3). Cells were imaged and analysed as described in Section 7.3.3.5.

7.4 Results

Isolated ovine endothelial cells were observed in culture from passage zero to ten. Cell phenotype was determined using immunofluorescence, the *in vitro* biocompatibility of the acellular porcine external iliac artery tissue for the endothelial cells was determined using a contact cytotoxicity assay before the cells were seeded onto uncoated and peptide coated acellular arteries (n = 4).

7.4.1 Endothelial Cells in Culture

The morphology of isolated cells was observed using phase contrast microscopy through multiple passages before (Figure 7.2) and after (Figure 7.3) confirmation of the presence of endothelial cells and absence of smooth muscle cells and fibroblasts from the cell culture by phenotype assessment using immunofluorescence.

Discrete colonies of cells were observed (Figure 7.2 C), which were characteristic of endothelial cells. Cells had attached to the tissue culture flask forming a monolayer with normal morphologies of polygonal shapes with cobblestone appearance at confluence which was characteristics of endothelial cells (Figure 7.2 and Figure 7.3). However, before confirmation of the absence of other cells by phenotype assessment, a minority of cells with non-endothelial cell morphologies of elongated and single cells attached were also observed (Figure 7.2 A and Figure 7.2 C). These cells with non-endothelial cell appearance were not observed after separation of other non-endothelial cells by successive passaging with three-minute trypsin/EDTA treatments. There were no apparent visual differences in cells at confluency before and after confirmation of the absence of smooth muscle cells and fibroblasts because the majority of cells were

identified as endothelial cells before purification by successive passaging with trypsin/EDTA three-minute treatments.

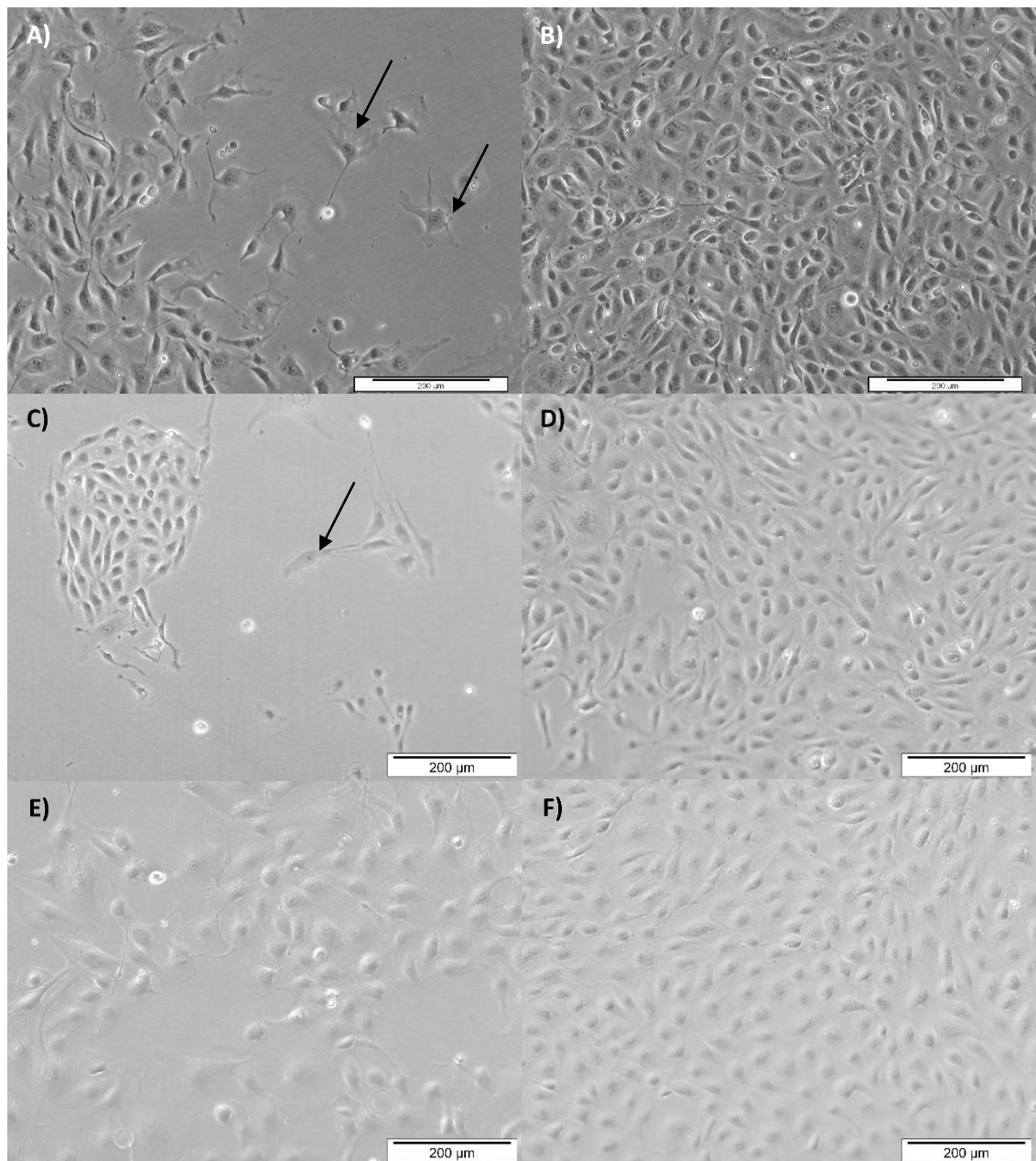


Figure 7.2: Isolated ovine femoral endothelial cells in culture at early passages before purification through successive passaging with three-minute trypsin/EDTA treatments. Freshly isolated cells at passage zero (A - B), passage one (C - D) and passage two (E - F). Arrows point to cells with non-endothelial cell morphologies. Images acquired before (left) and after (right) reaching confluency using $\times 10$ objective and scale bar represents $200\ \mu\text{m}$.

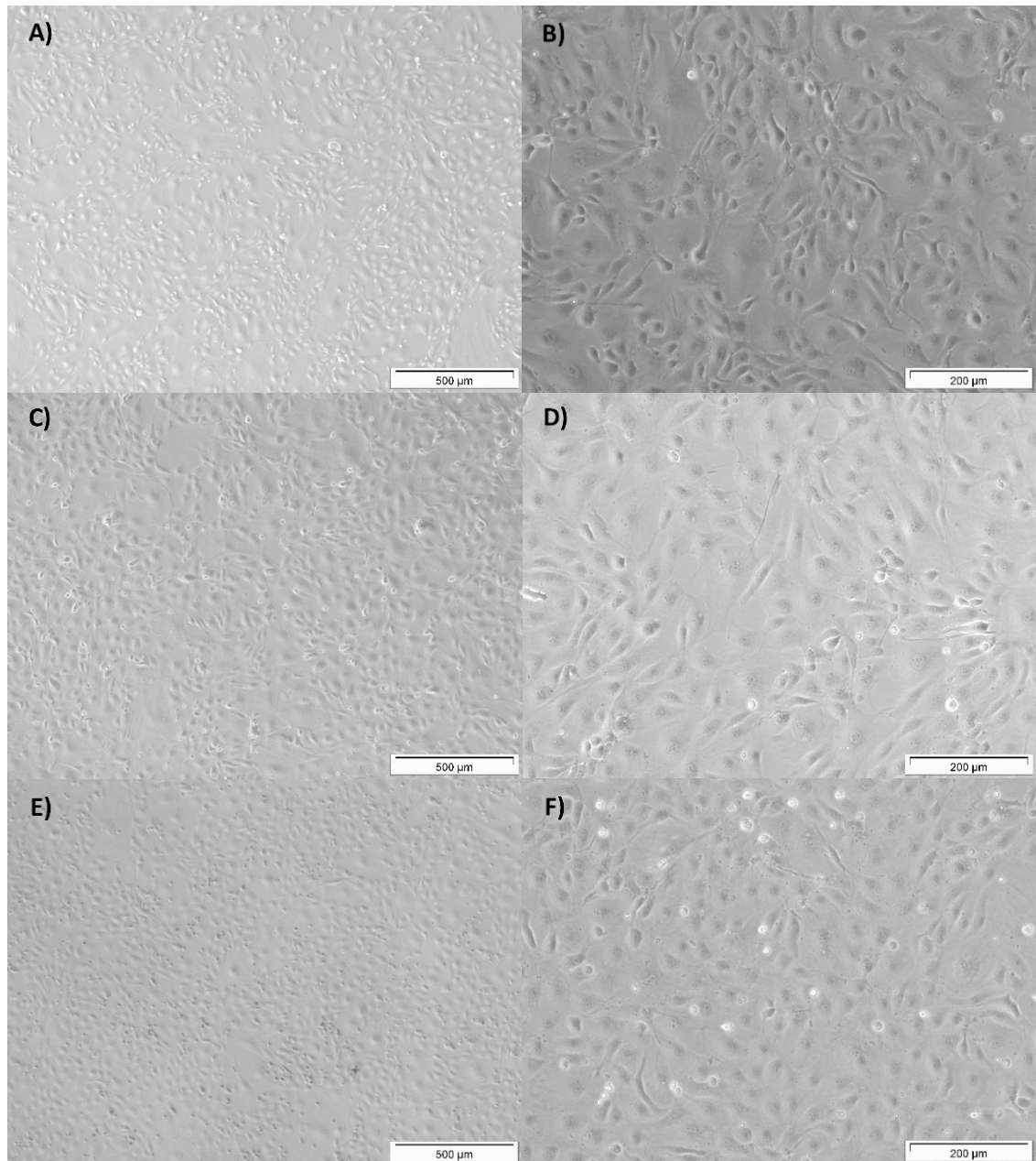


Figure 7.3: Isolated ovine femoral endothelial cells in culture at different passages after purification through successive passaging with three-minute trypsin/EDTA treatments. *Cells at passages: four (A - B), six (C - D) and eight (E - F). Images acquired using: x 4 objective (left) and scale bar represents 500 μm; and x 10 objective (right) and scale bar represents 200 μm.*

7.4.2 Phenotype of Endothelial Cells - Immunofluorescence

The isolated ovine endothelial cells were characterised by antibody labelling of specific cell proteins. Primary antibodies used were: anti-vWF (endothelial cells), anti- α -actin and anti-myosin (smooth muscle cells) and anti-5B5 (fibroblasts). Staining with DAPI was used to confirm presence of cell nuclei.

A cell culture with a mixed population of endothelial cells, smooth muscle cells and fibroblasts was used as a positive control for the labelling of vWF, α -actin, myosin and 5B5. At passage two, the majority of cells present were identified as endothelial cells confirmed by expressing vWF (Figure 7.4 A - B). At this passage, no fibroblasts were present confirmed by cells not expressing 5B5 (Figure 7.4 C - D). A minority of smooth muscle cells was also present and confirmed by expressing α -actin (Figure 7.4 E - F) and myosin heavy chain (Figure 7.4 G - H). Data not presented for antibody isotype controls where only DAPI stained cell nuclei were shown. Further purification was required for isolation of endothelial cells from the culture by successive passaging and treatment with trypsin/EDTA for three minutes.

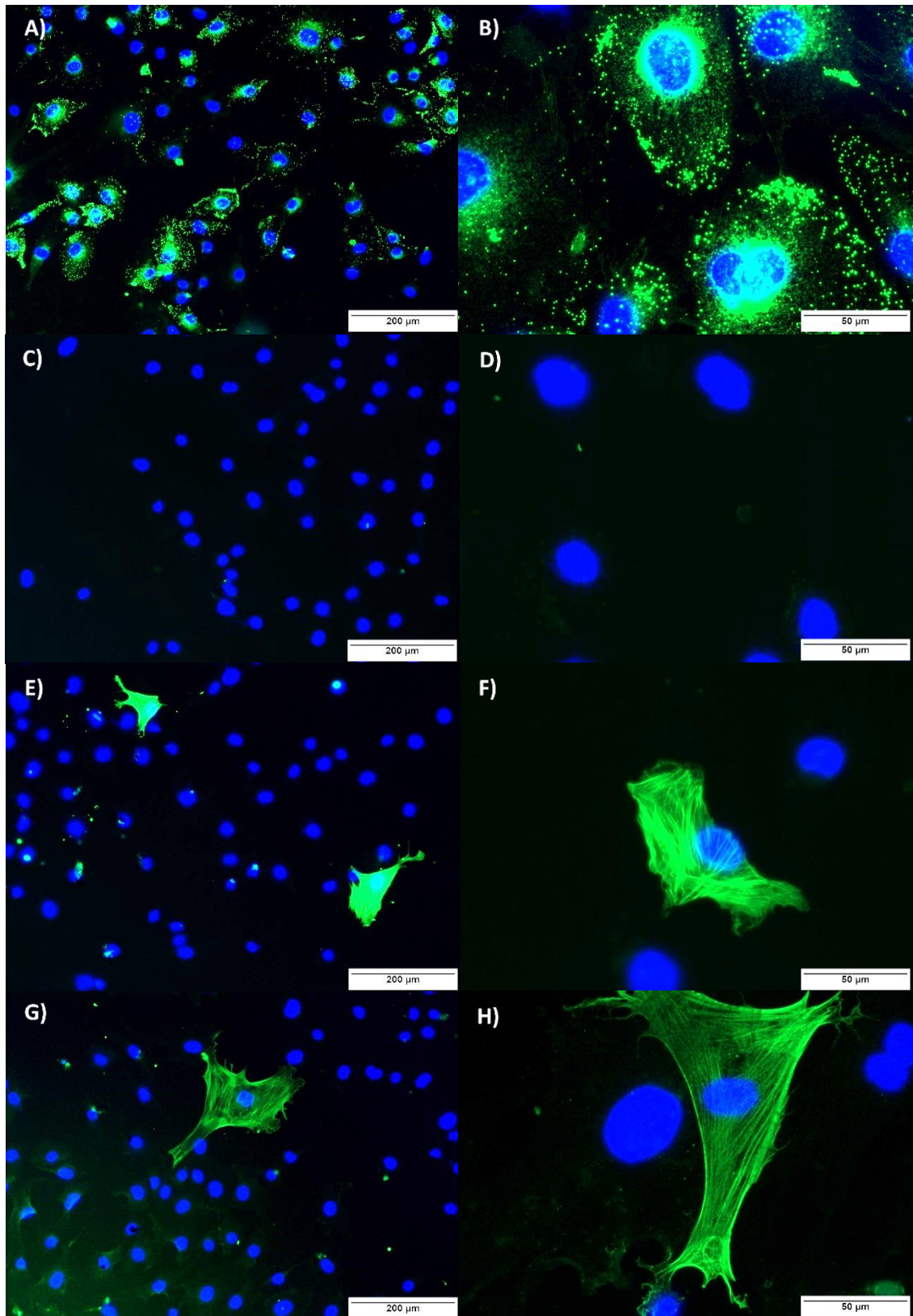


Figure 7.4: Antibody-labelling of impure isolated ovine femoral endothelial cells at passage two. A - B) Anti-vWF, C - D) anti-5B5, E - F) anti-myosin heavy chain and G - H) anti- α -actin with DAPI staining. Images were acquired using: x 10 (left) and x 40 (right) objectives, scale bars represent 200 μ m and 50 μ m respectively.

At passage four, all isolated cell batches were shown to only express vWF (Figure 7.5). The cells did not express fibroblast-5B5 or α -actin and myosin heavy chain confirming an absence of cells with a fibroblast or smooth muscle cell phenotype. Images of purified cell cultures at passage four stained with antibodies and corresponding isotypes are presented in Figure 7.5 and Figure 7.6, respectively. Using cell counting and image analysis it was found that the percentage of staining for vWF was over 70 % of imaged cells, meaning the majority were endothelial cells at this passage.

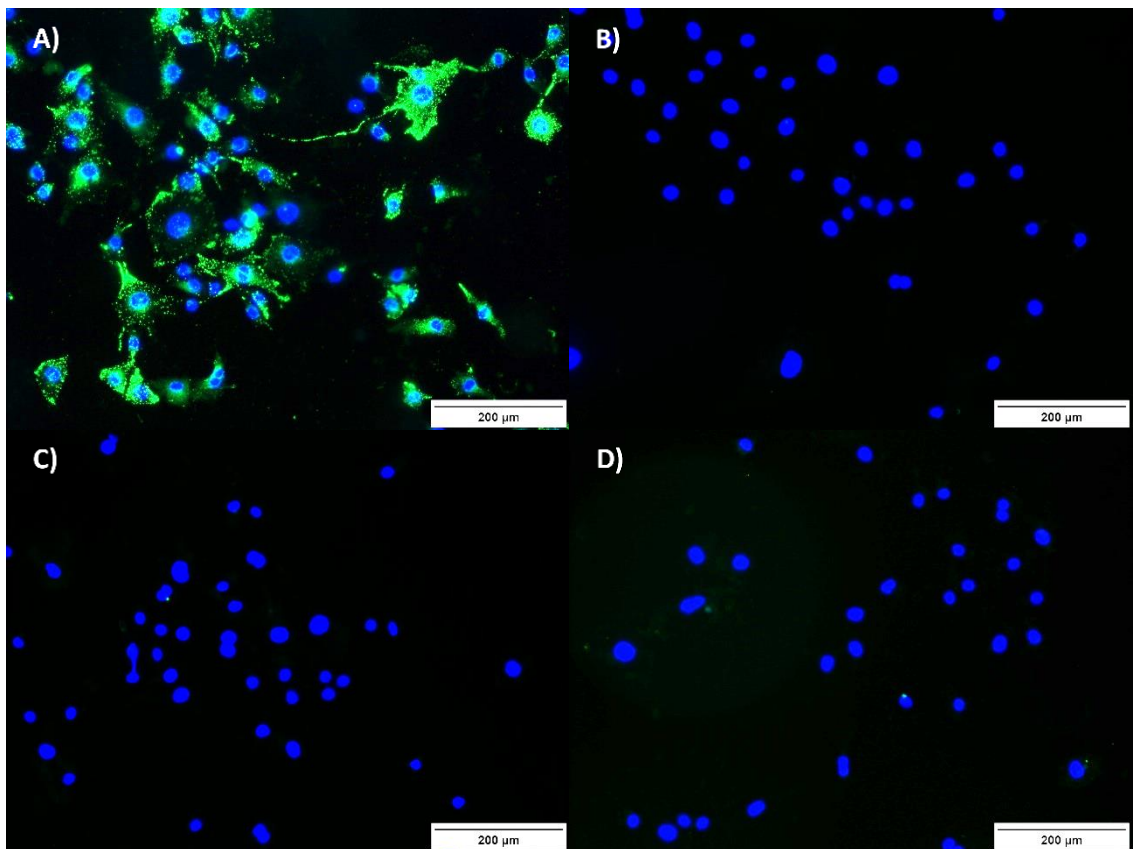


Figure 7.5: Antibody-labelling of isolated ovine femoral endothelial cells at passage four (antibodies). A) Anti-vWF, B) anti-5B5, C) anti- α -actin and D) anti-myosin heavy chain with DAPI staining. Cells were positive for vWF (endothelial cell marker). Cells were negative for: 5B5 (fibroblast marker); α -actin and myosin heavy chain (smooth muscle cell markers). Images were acquired using x 10 objective and scale bar represents 200 μ m.

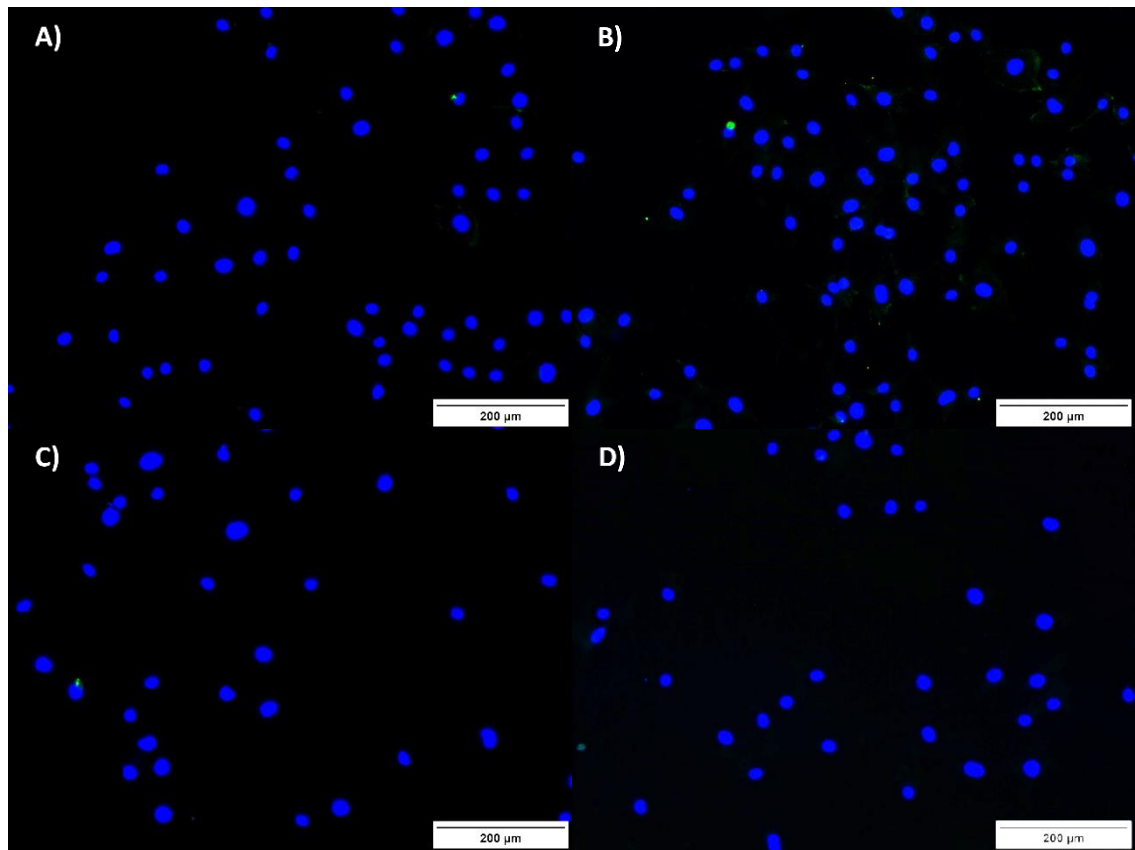


Figure 7.6: Antibody-labelling of isolated ovine femoral endothelial cells at passage four (antibody isotype controls). *A) No antibody-labelled control, B) anti-vWF isotype control, C) anti-5B5 and anti- α -actin isotype control and D) anti-myosin heavy chain isotype control with DAPI staining. Images were acquired using x 10 objective and scale bar represents 200 μ m.*

7.4.3 Biocompatibility of Acellular Arteries with Endothelial Cells

Acellular tissue from all batches used in cell studies was shown to be non-cytotoxic to isolated ovine endothelial cells (Figure 7.7). Following staining with Giemsa, ovine endothelial cells were observed growing up to and in contact with samples of acellular porcine arteries (Figure 7.7 D). Ovine endothelial cells grew up to and in contact with the negative control (steri-strips) and there was no growth of cells in wells with the positive control, cyanoacrylate contact adhesive (superglue). In addition, normal morphologies of cobblestone polygonally-shaped cells were displayed in cells cultured with samples of acellular arteries which compared to cells alone and cells cultured with steri-strips (Figure 7.7).

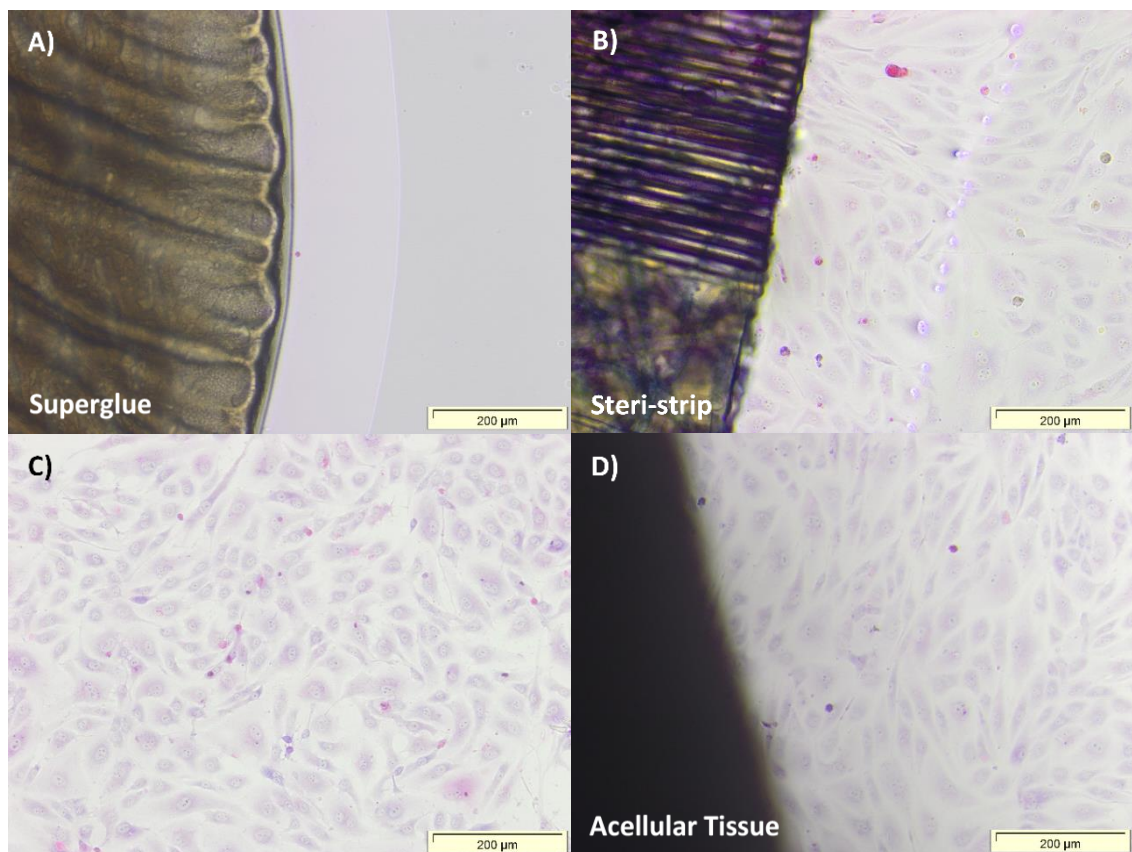


Figure 7.7: Contact cytotoxicity of isolated ovine femoral endothelial cells with acellular arteries. Cells cultured with A) Superglue (positive control), B) steri-strips (negative control) or D) samples of acellular artery for 48 hours and stained using Giemsa stain. C) Cells only control. Endothelial cells were found to grow up to and in contact with the acellular tissue and steri-strips with normal morphologies (as observed in cells cultured alone) indicating no cytotoxicity when compared to positive controls where no cells were present due to the cytotoxic effect of superglue. Images were acquired using x 10 objective and scale bars represents 200 µm.

7.4.4 Seeding Method Optimisation

7.4.4.1 Effect of Tissue Preconditioning on Cell Attachment to Uncoated Acellular Tissue

The effect of tissue preconditioning on cell attachment after 4 hours was assessed first with uncoated acellular arteries by checking the cell density. Cell viability is defined as the percentage of living cells counted, while cell density is the number of living cells per mm^2 of tissue. There was no significant difference in cell viability of tissue with different preconditioning times. There was no significant difference between 0 and 4 hours, however, with 24 hours of preconditioning there was a significant reduction in the cell density from 4 hours (Figure 7.8, ANOVA; $p < 0.05$). No preconditioning of the acellular artery tissue was selected for further investigations.

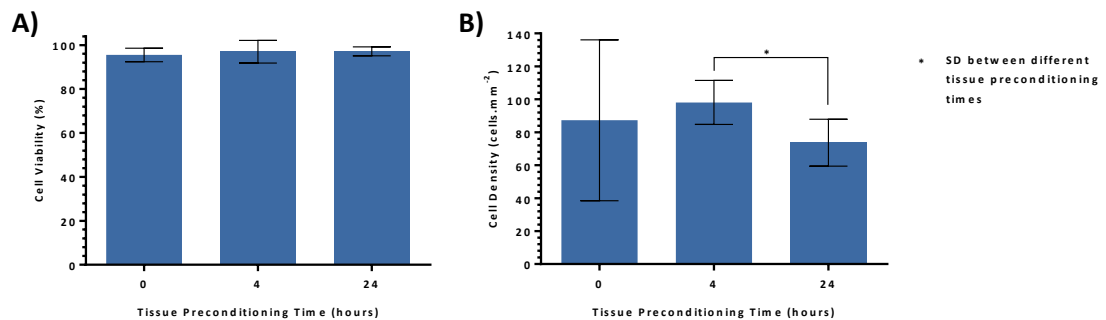


Figure 7.8: A) Viable cells counted (%) and B) number of live cells counted per mm^2 in uncoated acellular artery samples without preconditioning, with 4 and 24 hours of preconditioning. Data represent the means ($n = 3$) \pm 95 % confidence limits. There was no significant difference in cell viability between the different preconditioning times. Tissue preconditioned for 24 hours was shown to have a significant reduction in number of cells per mm^2 from 4 hours. Significant difference (SD) was determined by two-way ANOVA and post-hoc Tukey's test ($p < 0.05$).

7.4.4.2 Cell Densities in Uncoated Acellular Tissue Over Time

Cell densities on uncoated acellular arteries were assessed over time without tissue preconditioning. There was no significant difference in cell viability between different time points. The cell densities after 72 and 120 hours were significantly lower than cell densities after 1, 4 and 24 hours of seeding (Figure 7.9, ANOVA; $p < 0.05$). Therefore, 4 and 72 hours were taken forward for future cell attachment time studies.

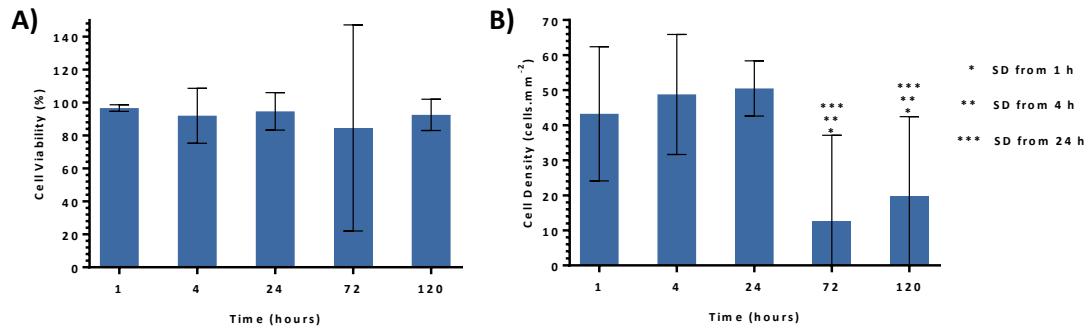


Figure 7.9: A) Viable cells counted (%) and B) number of live cells counted per mm² in uncoated acellular artery sample without preconditioning over time. Data represent the means ($n = 3$) \pm 95 % confidence limits. There was no significant difference in cell viability at different time points. After 72 and 120 hours, cell densities were significantly reduced from 1, 4 and 24 hours. Significant difference (SD) was determined by two-way ANOVA and post-hoc Tukey's test ($p < 0.05$).

7.4.4.3 Effect of Different P₁₁₋₄ Peptides Coatings on Cell Attachment without Tissue Preconditioning

The effect of functionalisation of P₁₁₋₄ peptides without tissue preconditioning on cell attachment onto acellular tissue was assessed. Functionalised P₁₁₋₄ peptides were shown to have no significant effect on cell viabilities after 4 and 72 hours. However, cell densities in uncoated acellular tissue control were significantly higher than all other peptide treatments; P₁₁₋₄ alone, GRGDS-P₁₁₋₄, YIGSR-P₁₁₋₄ and their corresponding scrambled controls. After 72 hours, cell densities were not significantly different from 4 hours and no significant differences were observed between the different treatments with very large variations within some groups (Figure 7.10, ANOVA; $p < 0.05$). Because of the very large variation in data, further optimisation of the method was carried out.

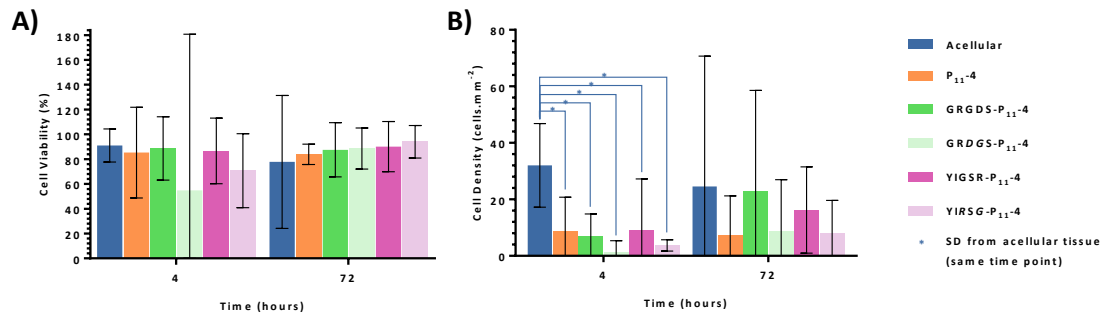


Figure 7.10: A) Viable cells counted (%) and B) number of live cells counted per mm² in acellular artery samples coated with different P₁₁₋₄ peptides without tissue preconditioning after 4 and 72 hours. Data represent the means ($n = 3$) \pm 95 % confidence limits. There was no significant difference between the viability of cells in tissue treated with different peptides at the same time point and between the same treatments at different time points. After 4 hours cell densities of all peptide treated acellular tissue were significantly lower than uncoated acellular tissue but there was no significant difference after 72 hours. Significant difference (SD) was determined by two-way ANOVA and post-hoc Tukey's test ($p < 0.05$).

7.4.4.4 Effect of Tissue Preconditioning on Cell Attachment to Non-Functionalised Peptide Coated Acellular Tissue

Optimisation of the seeding method involved preconditioning of tissue and washing of tissue samples prior to cell seeding to ensure removal of excess gel on the surface. Uncoated, P₁₁₋₄ coated and P₁₁₋₈ coated acellular arteries after 4 and 72 hours following cell seeding (Figure 7.11) showed no significant difference in cell viability. Acellular artery tissue coated with P₁₁₋₄ had significantly higher cell densities than the acellular tissue control at both time points, while coating the tissue with P₁₁₋₈ did not have an effect on cell attachment after four hours and the cell density was significantly lower than the cell density on the acellular tissue control after 72 hours (Figure 7.11, ANOVA; $p < 0.05$). Consequently, these two modifications in seeding method were implemented out for subsequent investigations.

The percentage of cells attached (Table 7.1) were calculated as described in Section 2.2.13.4.

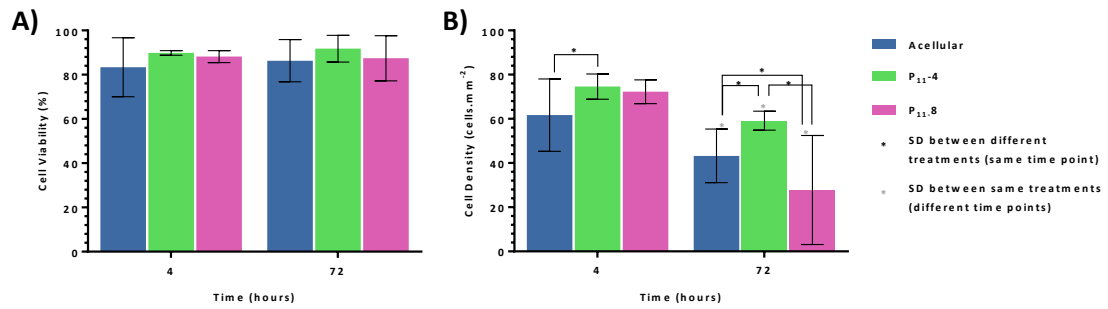


Figure 7.11: A) Viable cells counted (%) and B) number of live cells counted per mm² in acellular artery samples coated with non-functionalised peptides with tissue preconditioning after 4 and 72 hours. Data represent the means ($n = 3$) \pm 95 % confidence limits. There was no significant difference between the viability of cells in tissue treated with different peptides and uncoated tissue at the same time point and between same treatments at different time points. After 4 hours cell density in uncoated tissue was significantly lower than P₁₁₋₄ coated. After 72 hours, cell density in P₁₁₋₄ coated acellular tissue was significantly higher than uncoated and P₁₁₋₈ coated acellular tissue. Significant difference (SD) was determined by two-way ANOVA and post-hoc Tukey's test ($p < 0.05$).

Table 7.1: Percentages of cells attached to non-functionalised peptide coated tissue with preconditioning after 4 and 72 hours. Cell attachment was calculated from the number of seeded cells (as counted from live/dead stained images) and the initial number of seeded cells. Data represent means ($n = 3$) \pm 95 % confidence limits.

Sample	Uncoated Tissue	P ₁₁₋₄ Coated Tissue	P ₁₁₋₈ Coated Tissue
Cells Attached (%; 4 h)	62.0 \pm 16.5	75.0 \pm 5.7	72.7 \pm 5.4
Cells Attached (%; 72 h)	43.5 \pm 12.2	59.5 \pm 4.3	27.9 \pm 24.8

7.4.5 Effect of Functionalised Peptides on Attachment and Growth of Endothelial Cells to Acellular Arteries

Attachment of cells to acellular artery samples coated with different peptides was investigated after 4 and 72 hours of seeding. Ovine endothelial cells were seeded at a density of 5,000 cells.mL⁻¹ (approximately 100 cells.mm⁻²) onto the luminal surface of acellular artery samples. The number of live and dead cells were recorded and analysed for P₁₁₋₄ and P₁₁₋₈ functionalised with cell attachment motifs coating acellular artery samples and were compared with corresponding scrambled controls, non-functionalised peptides and acellular tissue controls. All data were presented as cell viability (%) and density (cells.mm⁻²) against time. The percentage of viable cells attached from the initial number of seeded cells was also determined after 4 and 72 hours.

In acellular artery tissues coated with P₁₁₋₄ (Figure 7.12), all samples/controls were shown to have high cell viabilities at each time point (Figure 7.13). In addition, acellular arteries coated with functionalised peptides had high cell densities with more than 60 % of cells attached after four hours, which was significantly higher than the uncoated sample control. After 72 hours, cell densities dropped but functionalised peptide coated samples had more than 45 % of cells attached, which was significantly higher than the uncoated samples. Cell densities were also significantly higher in acellular artery tissue coated with functionalised peptides when compared to the acellular artery tissue coated with the corresponding scrambled controls (Figure 7.14, ANOVA; $p < 0.05$).

The results for cell attachment to the acellular artery tissue coated with functionalised P₁₁₋₄ peptides showed the ability of these peptides to retain cells after 72 hours of seeding when compared to uncoated acellular artery samples and cell attachment results are summarised Table 7.2.

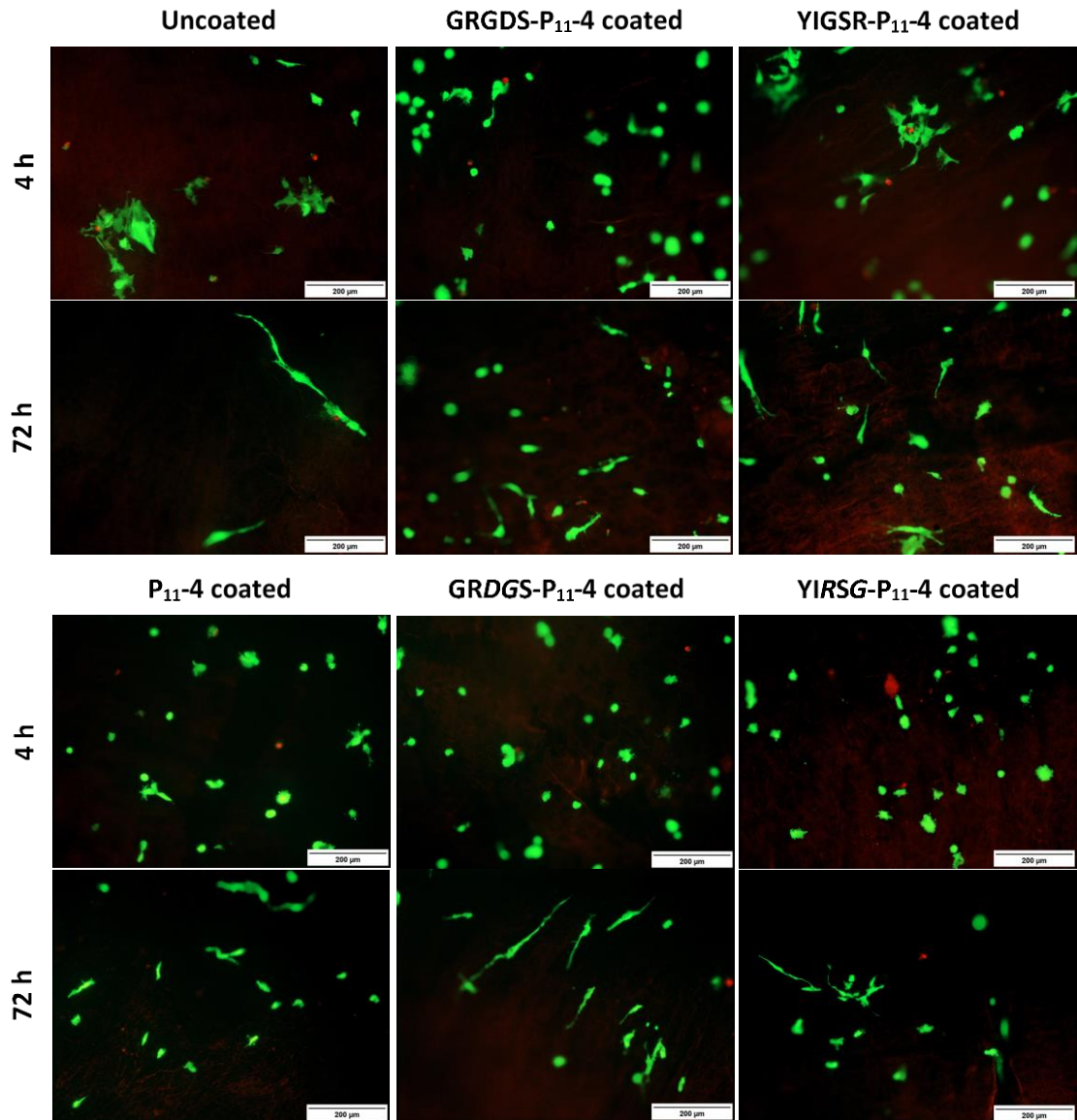


Figure 7.12: Live/dead stained images of non-functionalised and functionalised P₁₁-4 coated acellular artery samples. Images showing live cells (green) and dead cells (red) in uncoated (control), P₁₁-4 coated (non-functionalised control), GRGDS-P₁₁-4 coated, GRDGS-P₁₁-4 coated (scrambled control), YIGSR-P₁₁-4 coated and YIRSG-P₁₁-4 coated (scrambled control) acellular artery tissue samples after 4 and 72 hours of seeding. Images were acquired using x 10 objective and scale bars represent 200 µm.

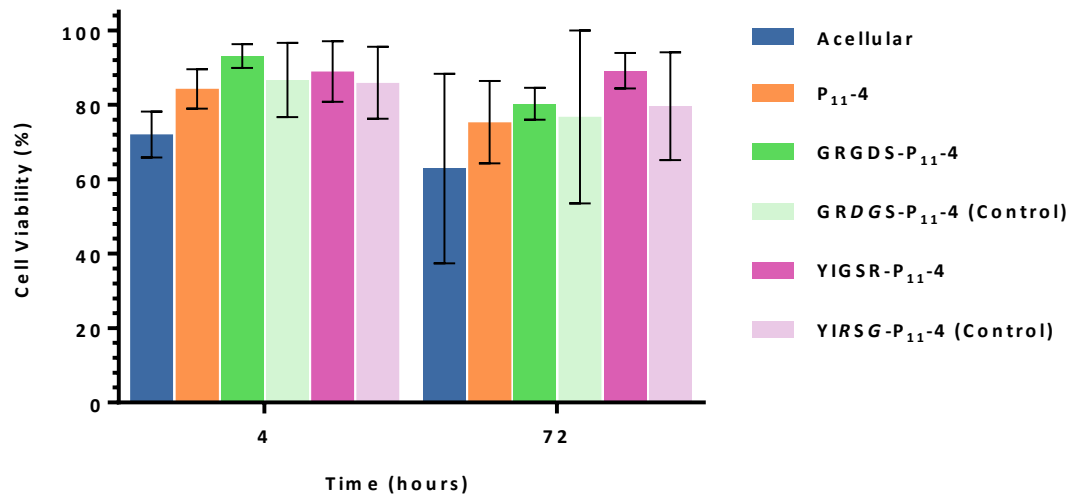


Figure 7.13: Viable cells counted (%) in preconditioned acellular artery samples coated with different P₁₁₋₄ peptides after 4 and 72 hours. Data represent the means ($n = 3$) \pm 95 % confidence limits. There was no significant difference between the viability of cells present on the acellular arteries coated with different peptides at the same time point and between same treatments at different time points as determined by two-way ANOVA and post-hoc Tukey's test ($p < 0.05$).

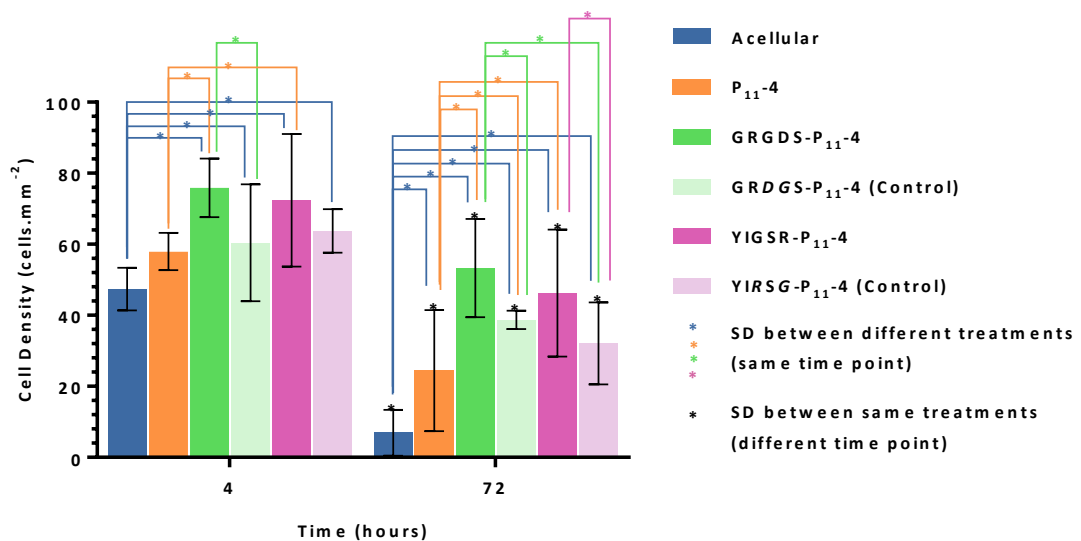


Figure 7.14: Number of live cells counted per mm² in preconditioned acellular artery samples coated with different P₁₁₋₄ peptides after 4 and 72 hours. Data represent the means ($n = 3$) \pm 95 % confidence limits. All acellular artery samples coated with different functionalised peptides showed significantly higher cell densities after 4 hours than the uncoated tissue. All controls/samples coated with the same peptide showed a significant reduction in the number of cells after 72 hours. Significance difference (SD) was determined by two-way ANOVA and post-hoc Tukey's test ($p < 0.05$).

In experiments with acellular artery samples coated with P₁₁₋₈ peptides (Figure 7.15), all samples/controls were shown to have high cell viabilities at the two tested time points (Figure 7.16). After four hours, scrambled control peptides coating acellular tissue were shown to have significantly lower cell attachment than their corresponding functionalised peptide coated, P₁₁₋₈ coated and uncoated samples. In addition, the GRGDS-P₁₁₋₈ coated acellular artery tissue was shown to have significantly higher cell attachment than all other peptide coatings of approximately 95 % cells attached. After 72 hours, all samples/controls were not significantly different from four hours except for GRGDS-P₁₁₋₈ coating acellular artery tissue which had reduced from 95% to approximately 55 %. Nevertheless, the samples coated with GRGDS-P₁₁₋₈ had significantly higher cell densities than samples coated with all the other peptides except for YIRSG-P₁₁₋₈ (scrambled control). Moreover, all the peptide coated samples were not significantly different from uncoated tissue but GRDGS-P₁₁₋₈ (scrambled control) coated acellular artery tissue was significantly lower (Figure 7.17, ANOVA; $p < 0.05$).

It was very difficult to determine the effect of P₁₁₋₈ functionalisation with cell attachment motifs on cell attachment onto acellular artery tissue from the data generated because of the large variation in cell densities within tested samples. The cell attachment results for the different P₁₁₋₈ peptide coatings are summarised in Table 7.2.

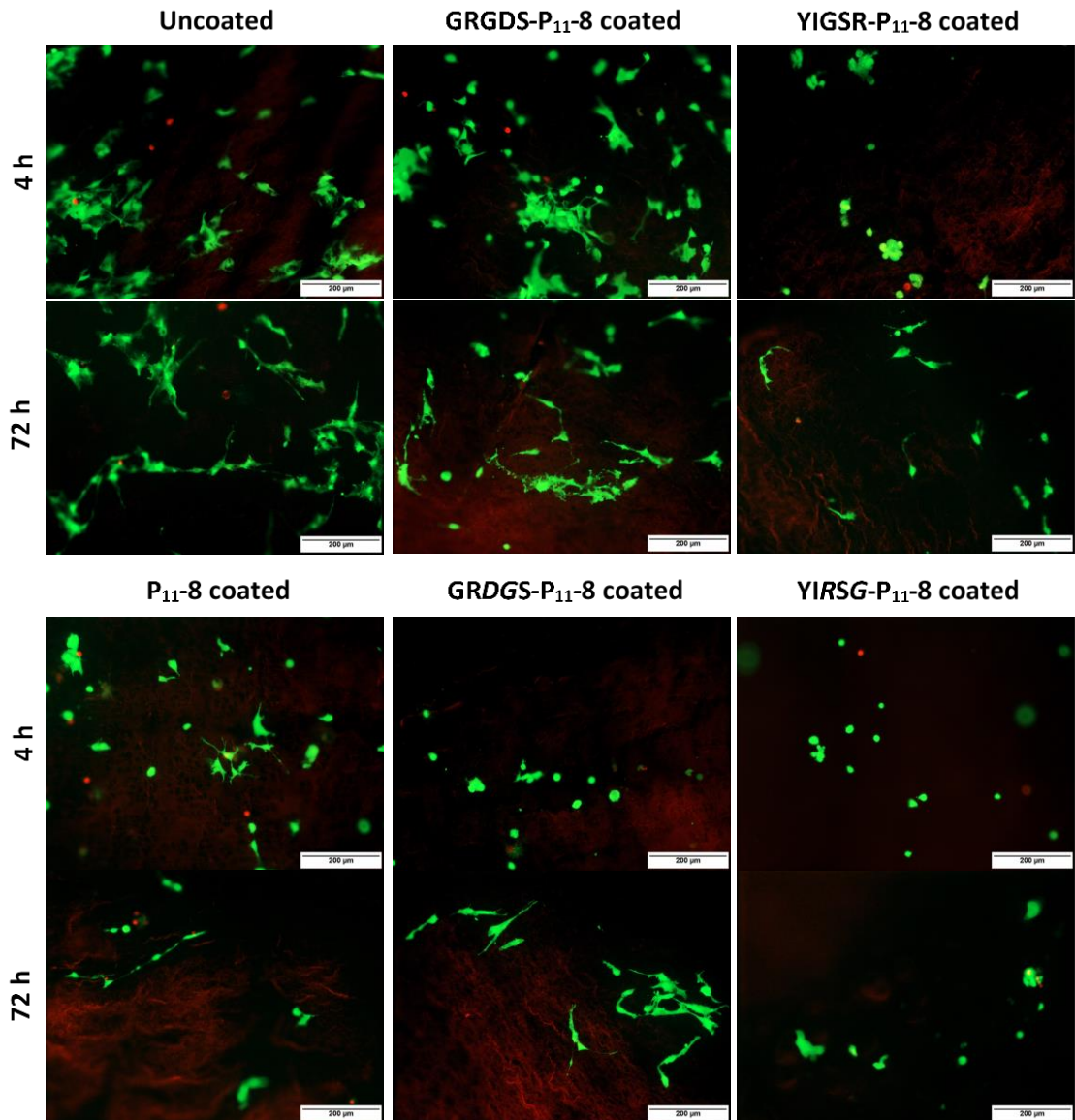


Figure 7.15: Live/dead stained images of non-functionalised and functionalised P₁₁₋₈ coated acellular artery samples. Images showing live cells (green) and dead cells (red) in uncoated (control), P₁₁₋₈ coated (non-functionalised control), GRGDS-P₁₁₋₈ coated, GRDGS-P₁₁₋₈ coated (scrambled control), YIGSR-P₁₁₋₈ coated and YIRSG-P₁₁₋₈ coated (scrambled control) acellular artery tissue samples after 4 and 72 hours of seeding. Images were acquired using x 10 objective and scale bars represent 200 μm.

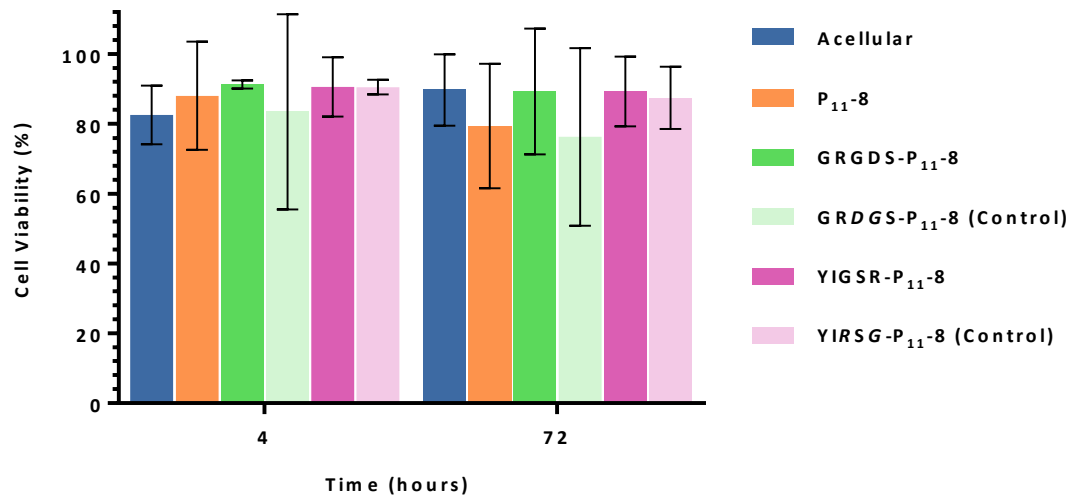


Figure 7.16: Viable cells counted (%) in preconditioned acellular artery samples coated with different P₁₁₋₈ peptides after 4 and 72 hours. Data represent the means ($n = 3$) \pm 95 % confidence limits. There was no significant difference between the viability of cells present on the acellular arteries coated with different peptides at the same time point and between the same treatments at different time points as determined by two-way ANOVA and post-hoc Tukey's test ($p < 0.05$).

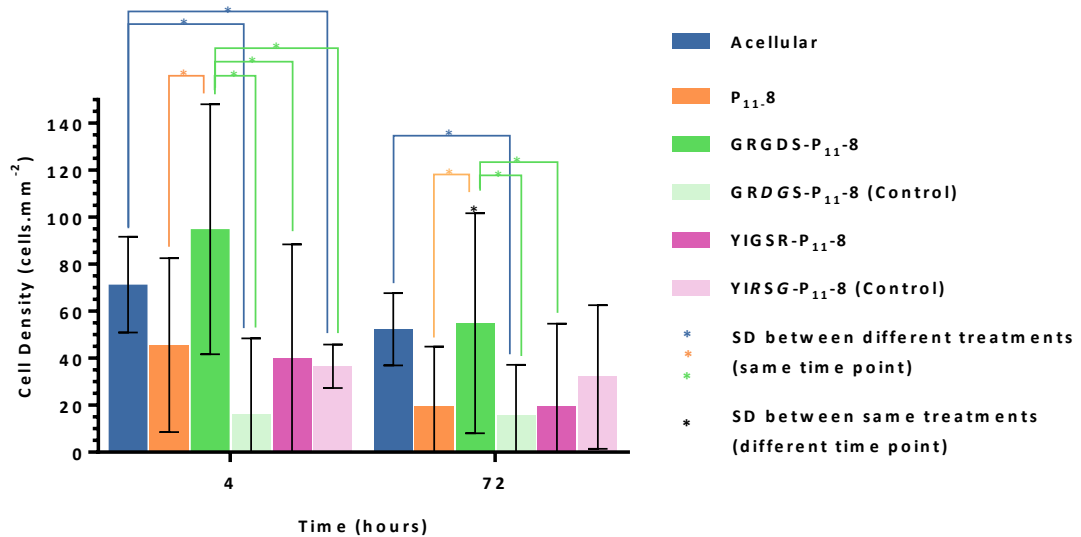


Figure 7.17: Number of live cells counted per mm² in preconditioned acellular artery samples coated with different P₁₁₋₈ peptides after 4 and 72 hours. Data represent the means ($n = 3$) \pm 95 % confidence limits. Acellular artery samples coated with scrambled controls showed significantly lower cell densities after 4 hours than the uncoated tissue. All controls/samples coated with the same peptide showed a significant reduction in the number of cells after 72 hours. Significance difference (SD) was determined by two-way ANOVA and post-hoc Tukey's test.

Table 7.2: Percentages of cells attached to non-functionalised/functionalised P₁₁₋₄ and P₁₁₋₈ peptide coated tissue with preconditioning after 4 and 72 hours. Cell attachment was calculated from the number of seeded cells (as counted from live/dead stained images) and the initial number of seeded cells. Data represent means (n = 3) ± 95 % confidence limits.

Peptide	P ₁₁₋₄		P ₁₁₋₈	
Peptide Coated Acellular Tissue	Cells Attached (%)			
	4 h	72 h	4 h	72 h
Uncoated	47.6 ± 6.0	7.0 ± 6.5	71.7 ± 20.5	52.6 ± 15.5
Non-functionalised	58.3 ± 5.3	24.6 ± 17.2	45.8 ± 37.2	19.9 ± 25.3
GRGDS-functionalised	76.3 ± 8.3	53.5 ± 13.9	95.4 ± 53.4	55.2 ± 47.0
GRDGS-functionalised	60.7 ± 16.5	38.9 ± 2.6	16.0 ± 32.6	15.6 ± 21.8
YIGSR-functionalised	72.8 ± 18.8	46.5 ± 18.0	40.0 ± 48.9	19.6 ± 35.4
YIRSG-functionalised	64.1 ± 6.1	32.2 ± 11.6	36.7 ± 9.3	32.2 ± 30.7

7.5 Discussion

7.5.1 Isolation and Characterisation of Endothelial Cells

Endothelial cells were isolated from ovine femoral arteries through collagenase type II digestion. Endothelial cells were shown to form discrete small colonies that grew in size and merged over time forming a monolayer of polygonal cells with a cobblestone appearance at confluence, a typical behaviour for endothelial cells. Endothelial cell phenotype was confirmed using markers for endothelial cells (vWF) smooth muscle cells (α -actin and myosin heavy chain) and fibroblast (5B5). The staining after passage four indicated the isolated cells largely to be vWF positive cells with an absence of smooth muscle cells and fibroblasts. The vWF staining appeared as granules mainly dispersed through the cytoplasm corresponding to observations in the literature, suggesting presence of vWF within cell organelles namely Weibel-Palade bodies^{302,303}.

Separation of endothelial cells from smooth muscle cells and fibroblasts was achieved by successive passaging of cells by treatment with trypsin/EDTA for no longer than three minutes. It has been previously reported that small polygonal endothelial cells detached before large flat smooth muscle cells after treatment with trypsin/EDTA for three minutes suggesting the use of two - three minute treatment^{295,296}. In addition,

endothelial cells have been reported to reattach to the surface before other cells, hence aspiration of the cell culture medium after attachment allowed for removal of detached cells. However, loss of cell functional characteristics was likely to occur with repeated trypsin exposure ²⁹⁵. The isolated endothelial cells in this study were also characterised by immunofluorescence at passage eight and it was found that cells expressed vWF and were shown to have normal morphology and behaviour until passage ten.

To overcome the issue of endothelial cell functional loss that may result from culturing and subculturing of the cells, other techniques can be used for the direct isolation of endothelial cells from a heterogeneous cell mixture by utilising the phenotypic characteristics of the cell including fluorescence activated, magnetic separation or high speed flow cytometry cell sorting. This can be achieved through endothelial cell-specific antibody-labelling such as CD31 ³⁰⁴.

7.5.2 Seeding Method Optimisation

It was initially thought that preconditioning of the acellular artery tissue was not appropriate for this study as this could have diluted the peptide gel and affected the outcomes of the experiments. Therefore, acellular artery tissue samples were seeded with endothelial cells with and without preconditioning. The cell densities were not significantly different between the non-preconditioned and 24 hours preconditioned tissue, hence acellular artery samples were subsequently tested for the effects of coating with peptides on cell attachment over time without preconditioning. However, investigations of cell adhesion to acellular artery tissue coated with functionalised P₁₁₋₄ peptides without preconditioning showed highly variable and inconclusive results, which were all significantly lower than the uncoated control after 4 hours. This was thought to be because of the excess gel on the acellular tissue surface in which cells settled and were washed away with each washing/aspirating step in the procedure.

Subsequently, non-functionalised peptides coating acellular artery tissues were tested following the optimised method with tissue preconditioning and an additional washing step before seeding and lower variations in cell densities were observed, possibly because of removal of excess gel. Preconditioning was introduced to the preparation procedure because tissue treated with different peptides was processed separately for pH adjustment in order to monomerise the peptide, change the pH to 7.4 then trigger

self-assembly by addition of 10X strength Ringer's solution. The precise pH adjustment to 7.4 was difficult to achieve due to the use of pH test paper that changed in colour according to the peptide pH. As a result, tissue preconditioning may have helped in stabilising and unifying the pH of the tissue samples, stabilising the temperature of tissue and seeding rings and provided tissue with the appropriate nutrients for cells to avoid depletion prior to seeding. The issue of excess peptide on the tissue surface was partially tackled by introducing an additional washing step after placing the tissue in wells and before the addition of seeding rings.

7.5.3 Peptide Functionalisation for Cell Attachment of Endothelial Cells to Acellular Arteries

Acellular arteries lack the natural anti-thrombogenic endothelium and for use in vascular graft applications, it was proposed to replace it with a new layer of functioning endothelial cells to prevent thrombus formation. It was hypothesised that functionalisation of peptides with cell attachment motifs would enhance cell attachment to acellular artery tissue. GRGDS-P₁₁₋₄ and YIGSR-P₁₁₋₄ coatings were shown to enhance the initial cell attachment after 4 hours and cell retention after 72 hours when compared to non-functionalised P₁₁₋₄ coated and uncoated acellular arteries. In addition, the coating of the artery tissue with corresponding scrambled controls for both bioactive P₁₁₋₄ peptides was shown to result in significantly lower cell densities after 72 hours, implying the effectiveness of the GRGDS and YIGSR bioactivities and potential use in tissue engineering applications. However, acellular arteries coated with different P₁₁₋₈ peptides showed much larger variations within the data with less consistency than P₁₁₋₄ peptide coatings, hence it was difficult to draw conclusions. Further investigations are required with functionalised P₁₁₋₈ peptides to determine their effectiveness in enhancing cell attachment onto tissue.

The use of scrambled controls in this study confirmed that cell attachment occurs through specific integrins recognising the bioactive function, which has been reported in previous studies. Jung *et al.* studied the effect of functionalising Q11 peptide based on a glutamine residue with various bioactive functions with a triglycine spacer and two glycine residues at the N-terminus including RGDS and YIGSR and their scrambled controls RDGS and RYGS_I, respectively. These peptides self-assemble into fibrillar gel

networks. RGDS peptide was shown to have the highest endothelial cell growth rate compared to other peptides and corresponding scrambled control ²⁸⁵. Many other previous studies have also reported that RGD peptides displayed higher cell attachment than YIGSR peptides ^{269,290}, which was an observation in this study though it was not significant. This is possibly because RGD mainly mediates cell-ECM binding through the various ECM proteins ^{284,305}. In addition, RGD is known to be recognised by more than half of the known integrins, giving cells higher chances of interaction through RGD sequences than YIGSR.

Although a general initial attachment of cells was observed after 4 hours in bioactive peptide coated tissue, there was a general decrease in cell densities after 72 hours. Therefore, more extensive work is required to characterise the behaviour and assess the bioactivity of peptides synthesised in this work as will be discussed later in this section. A number of factors should also be taken into consideration when carrying out future investigations including accessibility of the bioactive motif, concentration, use of a combination of bioactive peptides, stability of attached cells and effect of integrin binding affinity on cell attachment for the target application.

Accessibility of the bioactive motif is one of the major factors for successful application, which can be affected by dimensions of target surface cell receptor, peptide conformation and length/flexibility of spacer separating the bioactive motif from the surface that may be influenced by peptide form (cyclic/linear or amino acids before/after the main sequence). One study using PEG-conjugates containing RGD that self-assemble into β -sheet structures at sufficiently high concentrations had reported poor cell attachment to low attachment surfaces treated with the conjugate despite the presence of RGD. This was attributed to the hindered access of cell surface receptors to the RGD motifs shielded by PEG crystallisation ³⁰⁶. Another study by Wang *et al.* screened RGD functionalised RADA16-I peptides that self-assembled into β -sheet structures forming gels for angiogenesis promotion in transplants. The peptides were shown to form long nanofibers when mixing functionalised with non-functionalised peptides, while no/short nanofibers were formed in self-assembly of functionalised peptides alone due to steric hindrance. The RGD functionalised peptide was shown to significantly increase endothelial cell attachment and survival when seeded into two-dimensional peptide gels. In contrast, other functionalised peptides containing valine

residues did not improve cell attachment. The presence of hydrophobic residues had negatively impacted self-assembly due to inhibition of water solubility causing different spatial peptide configurations, suggesting that conformation, mobility and orientation of the function is important for accessibility³⁰⁷.

Consequently, it is important to characterise self-assembly behaviour, secondary structures and gelation of the new bioactive peptides developed in this study through spectroscopic and microscopic techniques. This can also be carried out at different concentrations also to determine the optimal concentration for each peptide because concentration was shown to have an effect on the bioactivity of peptides.

In this study, functionalised to non-functionalise peptides were used at a molar ratio of 1:50 (< 4 %; w/w of the total concentration) and this may have had contributed to the different degrees of cell attachment onto acellular tissue. The bioactivity of motifs has been reported to be affected significantly by concentrations/surface densities and generally higher concentrations enhanced cell attachment, spreading or growth^{269,281}. One of the early studies using RGD for $\alpha_v\beta_3$ integrin-mediated cell attachment at different concentrations showed that at low concentrations cell spreading was achieved, while a 10-fold increase in concentration was required to achieve focal contact and stress fibre formation requiring 140 nm and 440 nm spacing between peptides, respectively³⁰⁸. Q11 peptides separately functionalised with RGDS, YIGSR and IKVAV showed an increase in endothelial cell growth with increasing concentration of bioactive peptide from 0 % to 100 % of the functionalised peptide. All bioactive peptides were shown to support optimal cell growth at 20 % (1:5 ratio)²⁸⁵. However, the different bioactive motifs RGDS, YIGSR and IKVAV covalently incorporated into hydrogels separately were shown to display enhanced cell attachment at different optimal concentrations, with RGD requiring the highest concentration³⁰⁹. Chemical surface modification of a silicone membrane was previously studied by covalently binding the synthetic peptides RGD and YIGSR. It was reported that increasing the concentration of the synthetic peptide resulted in an increase in cell attachment to the surface. However, at the highest tested concentration cell attachment was insignificantly different/comparable to the corresponding native protein controls of fibronectin (RGD) and laminin (YIGSR). In addition, morphological changes were observed in myocytes cultured with synthetic peptide treated surfaces as well as

reduced expression of focal adhesion kinase protein and these alterations were attributed to the absence of other native protein domains²⁶⁹. For applications using acellular tissue, native proteins such as laminin and fibronectin have been reported to be present in tissue following decellularisation^{25,205}. This could minimally affect morphological changes and gene expression if coated with the P₁₁ bioactive peptides due to presence of the native proteins to some extent.

Therefore, it is also important for any future work using the bioactive peptides developed in this thesis to observe the morphology and function of cells cultured with functionalised peptide treated surfaces/samples. Nevertheless, additional studies are required in this area to better understand such interactions. It is also clear from the literature that different cell types respond differently to varying bioactive peptide concentrations. These differences may also have been contributed to by the different peptides used and different methods employed for the cell study preparation, whether cells were seeded directly onto gels or onto immobilised/coated on a surface.

A combination of different cell attachment motifs is thought to maximise the bioactivity of peptides by providing multiple active sites for the cell surface receptors, mimicking the natural ECM *in vivo* which contains various interactive adhesive proteins (e.g. collagen, laminin and fibronectin) that regulate cell attachment, spreading, focal contact formation, organisation of cells within the ECM and differentiation^{113,118,273,284,305}. This effect was evident in several previous studies^{113,272,284,288}. The three laminin-derived peptides RGD, YIGSR and IKVAV have been reported to have different functionalities in vessel self-assembly and tubule stability by encapsulating human umbilical vein endothelial cells into hydrogels of PEG-laminin-derived peptides. Hydrogels containing a combination of RGDS and YIGSR have been shown to be the most efficient in terms of vessel stability and density *in vitro* and *in vivo* when compared to using them individually. The study had suggested that the cell response can be tuned by using a different combination of bioactive peptides²⁸⁴. Another study evaluated the effect of inclusion of RGD and YIGSR to PEG hydrogels on growth and spreading of endothelial and smooth muscle cells. It was shown that a combination of both cell attachment motifs resulted in enhanced cell growth¹¹³.

Future studies using a combination of the YIGSR and RGD functionalised peptides developed in this study may be of interest to determine whether the use of different

cell attachment motifs affects the bioactivity of the surface coating, potentially enhancing re-endothelialisation in shorter periods with better stability.

For a functional vascular graft, it is essential that the attached cells are stable and not affected by blood perfusion. This can be achieved by successful formation of focal adhesions provided via stable linking of the bioactive peptide to the surface, improving cell attachment²⁸¹. The effect of coating ePTFE graft with an RGD containing synthetic peptide on endothelial cell attachment and retention was assessed previously by Walluschek *et al*¹³¹. It has been reported that coupling of this synthetic peptide to the graft surface increased cell retention significantly following artificial flow conditions when compared to uncoated and fibronectin coated ePTFE grafts. It has been suggested that bonding of the RGD containing peptide to the vascular graft improves cell attachment and retention due to tighter connection to the surface¹³¹. Future studies to evaluate the stability of attached cells through bioactive peptides with flow will be important to optimise the surface coating. It has been reported that 30 mg.mL⁻¹ of P₁₁₋₄ coating acellular porcine carotid artery was stable under flow conditions that modelled the situation in a small-diameter vessel over 14 days. The use of cyclic RGD-P₁₁₋₄ (1:50 molar ratio) as a coating at the same concentration has been reported to enhance cell attachment at 4 hours and improved cell proliferation after 72 hours compared to uncoated tissue that had no cells attached after 72 hours¹⁷⁸. It is also important to note that this bioactive peptide was designed with a shorter spacer (aminohexanoic acid, ahx) that might have allowed for formation of the focal contacts required for proliferation when compared to the new bioactive peptides in this study, requiring further investigation. This might mean that the longer spacer used in this study might have affected the accessibility of the recognition sites as discussed earlier, by being too long to allow for the cytoskeletal organisation required for successful proliferation.

Moreover, cell binding should be specific to target cells by having high affinities of surface cell receptors to the selected bioactive function. The enhanced endothelialisation of an artificial vascular graft has been reported using collagen and mussel adhesive protein fused with RGD immobilised on the luminal surface. In addition, rounded morphologies of platelets were observed on the surface indicative of non-activated platelets and were suggested to mitigate thrombus formation³¹⁰. RGD immobilised on vascular grafts may not necessarily lead to activated platelet adhesion

through $\alpha_{IIb}\beta_3$ possibly due to the complex events and interactions affecting the activation state of integrins *in vivo* and contributing to cell attachment that involves interactions between different cells and/or different ECM components ²⁸¹. In the literature, there are some conflicting reports regarding RGD binding to platelets. Some studies have reported that the RGD can not only support and enhance the attachment of endothelial cells when used as a surface coating, but can act as an anti-thrombogenic agent. This is because it was believed that RGD inhibits the binding of platelets to fibronectin in its soluble form, which is part of the thrombus formation initiation process ^{270,281,311}. Therefore, it can be anticipated that the functionalised peptides in this study may exhibit both functionalities of selectively promoting attachment of endothelial cells that highly express $\alpha_v\beta_3$ integrin when self-assembled on the surface of acellular artery and anti-thrombogenic properties when present as a monomeric peptide in blood by inhibiting platelet adhesion through $\alpha_{IIb}\beta_3$ integrin ²⁷⁸, but this needs to be further investigated. As mentioned previously, changing the peptide form/sequence can result in the peptide having varying affinities for different cells. For example, Hao *et al.* recently reported a disulphide cyclic peptide (cGRGDdvc; LXW7) which had a strong affinity towards primary endothelial progenitor cells and endothelial cells but not platelets or monocytes ¹²². In contrast to RGD, YIGSR has been shown to selectively enhance the attachment, spreading and proliferation of endothelial cells to tissue culture plates treated with the self-assembled peptide amphiphiles, while not supporting platelet or leukocyte adhesion ²⁷¹. This is important for vascular graft applications because aggregation of platelets and leucocytes are both important in biomaterial-induced thrombosis (Chapter 1, Section 1.6). Many other different peptide sequences have also been shown to support attachment and growth of endothelial cells as discussed in Chapter 1 (Section 1.7.4). For example, REDV peptide sequence that was shown to improve attachment of endothelial cells to REDV surface modified polyurethanes ³¹². A REDV-modified hydrogel was reported by Wang *et al.* to have selective endothelial cell adhesion through $\alpha_4\beta_1$ integrin for angiogenesis promotion by forming higher blood vessel densities after 28 days compared to other peptides ³¹³.

Further investigations are required to assess the anti-thrombogenic properties of bioactive peptides when present in blood compared to non-functionalised peptides and effect on platelet adhesion when coating the tissue in the self-assembled form. This is

necessary to confirm which of the two bioactive peptides (GRGDS and YIGSR) have higher affinities for endothelial cells but lower affinities to platelets and leukocytes, ensuring that the endothelial layer is recovered sufficiently, while aggregation of platelets is minimally reduced, hence reducing thrombus formation.

The bioactive peptides developed in this work can be employed in other tissue engineering applications to improve tissue compatibility when immobilised on the surface or as insoluble gel matrices, requiring the attachment of different cell types including smooth muscle cells, stem cells and neural cells^{113,272,278,309,314}. Some studies have reported that the selection of the bioactive peptide affected differentiation of human mesenchymal stem cells due to specific integrin-ligand interaction that resulted in different morphologies and spreading²⁷². On the other hand, the use of soluble forms of the bioactive peptides has been shown to be effective as drugs for certain diseases by inhibiting/reducing the attachment of cells to natural adhesive proteins caused by competing with binding sites on the ECM proteins²⁷⁸.

The biocompatibility of arterial scaffolds and the presence of an anti-thrombogenic coating are important criteria for the development of successful small-diameter vascular grafts²⁸³. Therefore, for use of acellular arteries as the biological scaffold, the luminal surface should have the ability to re-cellularise rapidly forming a stable and functional endothelium to reduce thrombosis. The use of bioactive functionalised peptides as surface coatings for these biological scaffolds was shown to support cell retention after 72 hours as opposed to non-functionalised peptide. Preliminary experiments using GRGDS-P₁₁-4 and YIGSR-P₁₁-4 were shown to be promising for improving cellular retention and eventually lining the luminal surface with endothelial cells. This shows the importance of peptide functionalisation with bioactive motifs in clinical applications requiring enhanced cellularisation to improve the long-term compatibility of biomaterial, while being removed from the system by degradation.

8 Conclusions

8.1 Summary

Thrombogenesis is one of the major issues resulting in failure of novel small-diameter vascular grafts. Decellularised xenogeneic small-diameter arteries have been developed which have the potential for clinical translation, however the use of decellularised arteries can potentially cause thrombus formation due to the absence of the natural anti-thrombogenic endothelium lining the luminal surface. Therefore, the aim of this study was to develop a series of bioactive functionalised self-assembling peptides as coatings for acellular arteries that can act as a scaffold to enhance the process of re-endothelialisation. There were five areas of interest in this study.

In Chapter 3, the biological artery scaffold was produced by decellularisation of porcine external iliac arteries following established methods which were shown to be reproducible. Acellular arteries produced were also shown to be biocompatible *in vitro* with a cell-free preserved ECM and reduced DNA content of > 97 % (wet weight).

In Chapter 4, three self-assembling peptides P₁₁₋₄, P₁₁₋₈ and P₁₁₋₁₂ were screened under physiological conditions (1X strength Ringer's solution, pH 7.4) at three different concentrations for self-assembly behaviour, gelation and morphology. At 20 mg.mL⁻¹, all three peptides formed gels with high β -sheet content (> 70 % after one day of triggering self-assembly). However, P₁₁₋₄ and P₁₁₋₈ were found to form stronger self-supporting gels than P₁₁₋₁₂ consisting of thicker fibrils/fibres with a lower proportion of peptide being in the monomeric state. The results suggested that both peptides have the potential to be used in *in vivo* applications with higher stability than P₁₁₋₁₂.

In Chapter 5, it was shown that functionalisation of self-assembling peptides (azide-functionalised N-terminus) with bioactive motifs (alkyne-functionalised C-terminus) using copper catalysed azide-alkyne click chemistry produced peptides with very high purities due to the selectivity of the reaction.

In Chapter 6, it was shown that monomeric forms of P₁₁₋₄ and P₁₁₋₈ reduced thrombus weight significantly compared to the negative control. Self-assembly of the three candidates within acellular artery tissue showed that P₁₁₋₄ and P₁₁₋₈ displayed excellent coating of the ECM structures at the surface, while P₁₁₋₁₂ displayed poorer surface

coating despite its better penetration through the ECM. The results implied that both P₁₁₋₄ and P₁₁₋₈ could act as surface coatings to separate blood from contacting the ECM, whilst having anti-thrombogenic properties when diffused into the bloodstream.

In Chapter 7, GRGDS-P₁₁₋₄ and YIGSR-P₁₁₋₄ coating acellular artery tissue at a molar ratio of 1:50 of the functionalised to the non-functionalised peptides were shown to have higher endothelial cell attachment (4 hours) and retention (72 hours) when compared to the corresponding scrambled control coatings, non-functionalised coatings and uncoated acellular arteries. The enhanced cell attachment/retention was attributed to the specific ligand binding through the RGD and YIGSR sequences, since higher cell densities were observed with the bioactive peptides when compared to the corresponding scrambled controls. The results provided evidence that functionalisation of self-assembling peptides with bioactive motifs could potentially enhance the re-endothelialisation of acellular arteries.

8.2 Future Work

Although a preliminary study was carried out to evaluate the effect of coating acellular tissue with functionalised self-assembled peptides on cell attachment to acellular artery to meet the main aim of this study, more future work is required in different areas of this study to establish a better understanding of implications and findings of this study.

In Chapter 4, peptide stability under flow conditions could have been carried out in order to confirm the suggestion that, in an environment with excess fluid, peptides with higher monomeric proportion might be removed faster by de-assembly. This could help in selecting the correct peptide (as well as concentration) for the required application, whether it is preferable to have a short or long lasting scaffold in the system. Here, it is thought that peptides are required to be present on the acellular artery luminal surface providing it with a scaffold for cellular growth until the artery is fully re-cellularised. This can be achieved by testing the different peptide concentrations under flow when self-assembled on the acellular artery surface. Longer term study of peptides under physiological conditions could also help in understanding the behaviour of these peptides for various biological applications, requiring longer lasting peptide gels.

In Chapter 5, for the initial cell studies in this thesis, functionalised peptides were not sterilised because these were produced in a clean environment and formed no more than 4 % (w/w) of the whole weight of peptide used to make the gels and they were stored at - 20 °C until use. Therefore, sterilisation of the synthesised bioactive peptides by gamma irradiation should be investigated for *in vivo* and *in vitro* studies to confirm whether sterilisation causes degradation of the bioactive peptides or has any other effects on their behaviour. This could be done by comparing mass spectrometry results and characterisation of peptides at the macroscopic, microscopic and molecular levels to check for peptide structure modifications, gelation behaviour, morphological or self-assembly changes, respectively.

In Chapter 6, the effect of coating acellular porcine external iliac arteries with self-assembled peptides on thrombus formation could have been assessed in a Chandler loop model. This might have provided the acellular vascular graft with anti-thrombogenic properties in addition to being a scaffold for cellular support. If P₁₁₋₁₂ is shown to have anti-thrombogenic properties it may be taken forward for functionalisation with bioactive motifs for further cell studies also because it may not introduce issues such as the excess surface gel that may have an effect on cell attachment to tissue. The method used for sample preparation for SEM imaging could be improved or environmental SEM could be used in conjunction with SEM to better understand the surface coating behaviour of the peptides. In this study, the tissue was fixed with NBF for imaging, while the peptide was not, possibly leading to collapsing of peptide fibrillar networks upon drying. This could in turn have resulted in images that were not representative of the actual behaviour, particularly for P₁₁₋₁₂ which could have possibly coated the ECM fibres efficiently but collapsed into the structure upon drying more than P₁₁₋₄ and P₁₁₋₈ due to its thinner fibrils. It would also be helpful to understand the interaction of self-assembled peptides with the ECM structures at higher magnifications than those achieved by multiphoton microscopy. For example, by using TEM or SEM to visualise layers other than the surfaces.

The effect of self-assembly within the acellular artery on the migration of cells from neighbouring tissue can be tested by incubating a section of an acellular porcine uncoated tissue and peptide coated tissue with a native cellular porcine tissue (for allografts) or a native cellular sheep tissue (for xenografts). Comparison between re-

cellularisation of the different peptide coatings to the uncoated acellular tissue control can then be carried out at different time points. This can be achieved; qualitatively by immunohistochemistry to selectively test for endothelial cells, smooth muscle cells and fibroblasts that reside different arterial layers or histology using H & E staining for an overview of re-cellularisation, and quantitatively by live/dead[®] staining. This is important to confirm that peptide self-assembly does not slow/prevent cell migration and transport of nutrients through the artery with self-assembled peptides to allow for successful remodelling of the graft following implantation. It can also be used to test for complications that can occur following implantation such as intimal hyperplasia.

In Chapter 7, a number of future studies could be carried out in order to improve and expand on the current work, some of which were discussed briefly in that chapter.

***In vitro* biocompatibility.** Because the bioactive peptides synthesised in this study are novel (GRGDS-P₁₁-4, YIGSR-P₁₁-4, GRGDS-P₁₁-8 and YIGSR-P₁₁-8), it will be important to evaluate the biocompatibility of the bioactive peptides and investigate the viability of cells when cultured in the presence of the bioactive peptides. This could be achieved using contact cytotoxicity assay or ATPlite™ assay. This will help to determine if these new bioactive peptides impose a cytotoxic effect on cells *in vitro*. Confirmation of the biocompatibility of peptides (non-sterilised/sterilised) is crucial because the initial results in Chapter 7 have generally shown a high cell attachment after 4 hours that reduced after 72 hours.

Determination of optimal concentration for cellular growth. An interesting initial experiment would be to test endothelial cell viability at different molar ratios of each of the bioactive peptides and compare them to the corresponding scrambled controls and non-functionalised peptides. As discussed previously in Chapter 7, concentration of peptides can affect cellular behaviour^{269,281,285,308,309}, hence molar ratios that are higher and lower than the 1:50 of the functionalised to non-functionalised peptides could be investigated to determine the optimal concentration for each bioactive peptide that supports cell growth (e.g. 1:5, 1:25, 1:50, 1:100, 1:200).

Optimisation of current seeding method onto acellular porcine external iliac arteries. After establishing the optimal concentration for each bioactive peptide, cell studies with acellular scaffolds could be carried out possibly with two of the optimal

concentrations. However, optimisation of the current seeding methods are required to improve the current methods because in this study, the P₁₁₋₈ peptides were shown to have larger variation than P₁₁₋₄ peptides, which could be caused by P₁₁₋₈ forming denser fibrillar networks on the surface as was found in Chapter 6, although the variation was observed in the majority of peptide coated acellular tissue.

Optimisation of the tissue seeding method is needed to obtain more reliable and accurate results, especially for thin/delicate tissue such as the external iliac artery used here, which was found to easily curl up or fold into itself after addition of cell culture medium. The use of in-house manufactured PTFE support rings may have possibly introduced some errors. Firstly, it was difficult to place the PTFE support rings exactly on the seeded area defined by the seeding ring. Secondly, placing of the PTFE support ring if not done carefully may have caused removal of cells from tissue and this could have resulted in variation of cell densities. Thirdly, placing of the ring required some time and this may have affected the cells if left without medium. Fourthly, aspirating medium from the rings may have scraped some cells from the tissue surface. These issues could be tackled by the use of a PTFE ring which had a larger diameter than the seeding ring (or vice versa), meaning that when placed, the seeded area would be away from the ring's edges and this would have minimal effects on cells with easier application. Moreover, the use of a PTFE ring with a larger diameter would reduce the chance of removing cells while fixing in place or aspirating. However, this could not have been achieved here due to time and tissue limitation. It was not always possible to have tissue sections that were larger than 12 mm (used in this study) in order to accommodate a larger diameter PTFE ring.

Another aspect that requires optimisation is the removal of excess gel from the tissue surface, which was shown to result in large variations in the cell densities. This could be achieved by introducing more washes prior to tissue preconditioning followed by incubation of the tissue in cell culture medium without the seeding ring which may also help in distributing the gel evenly across the tissue rather than clumping it on the seeded area defined by the seeding ring.

Long-term study for the effect of peptide functionalisation with different cell attachment motifs on the growth rate. The initial results presented in Chapter 7 showed that functionalisation of peptides with cell attachment motifs enhanced cell

retention when used as coatings for acellular tissue. However, for the vascular graft to serve its purpose, longer term studies are required in order to provide more evidence for the effect of using bioactive peptides as coatings for acellular arteries on cell attachment, spreading and proliferation in addition to knowledge of the time required to fully re-cellularise a defined area. Therefore, once the seeding method is optimised, cell studies on tissue could be carried out with the optimal concentration of each bioactive peptide and the mixing of both functional groups GRGDS and YIGSR of the same P₁₁ peptide. This is because previous studies have shown enhanced performance of these two motifs when used in combination, possibly due to recognition of the bioactive sequences through different cell surface receptors^{113,118,273,284,305}.

Reproducibility of different bioactive peptides and effect of peptide form and spacer length on cell attachment and proliferation. Comparison of the newly synthesised linear bioactive peptides with those that have been previously studied such as cyclic RGD-P₁₁-4, which has a shorter spacer may also help in assessment of the reproducibility of results with different cells and tissue types (including the previously established method for seeding onto acellular porcine carotid artery). This is because the cell densities in bioactive peptide coated tissues declined after 72 hours, which might have resulted from the inability of attached cells to form focal contacts and proliferate successfully on the surface. Therefore, investigation of bioactive peptides with varying spacer lengths, possibly shorter than the one used in this study, might also be of interest after determining the most favourable bioactive peptide candidate, as previous studies have also shown that the length of spacer separating the functional group from the substrate surface affected cell attachment, spreading and focal contact formation²⁸⁷⁻²⁸⁹. In addition, the behaviour of cells with bioactive motifs is cell-specific and is affected by many factors including the sequence of the bioactive peptide, form of peptide (cyclic/linear) and the method of immobilisation of peptide on the surface (as discussed in Chapter 7).

Stability of the bioactive peptide coating. It is important for the surface coating to be stable under flow conditions ensuring sufficient initial attachment of cells that is stable under flow and will allow for cytoskeletal organisation, hence proliferation and repopulation of the biological acellular scaffold. Therefore, crosslinking the peptide with the acellular artery surface might enhance the stability of the peptide, hence

attachment of cells on the surface as well as proliferation. This can be implemented if the decline in the cell density in this study was caused by unstable self-assembled peptide on the surface rather than seeding method, tissue type or spacer length. In addition, this will allow the peptide to be stable under flow conditions for longer periods possibly sufficient to allow for full coverage of the acellular graft preventing thrombus formation that might be caused by blood contacting the surface that is neither fully re-endothelialised nor peptide coated (i.e. removed by circulating blood). However, tests need to be carried out to ensure that crosslinking does not affect peptide self-assembly.

Specificity of the different bioactive peptides and effect on thrombogenesis.

Attachment and growth of endothelial cells, endothelial progenitor cells, platelet and monocytes can be tested with the bioactive peptides developed in this thesis and cyclic RGD-P₁₁-4. This can help in selecting the best suited bioactive peptides for vascular graft applications and in future work for the design of more specific bioactive peptides to endothelial cells and endothelial progenitor cells as opposed to platelets or monocytes that can trigger thrombus formation or an inflammatory response.

The different bioactive peptides (i.e. functionalised with cyclic RGD, GRGDS and YIGSR) can also be tested for their effect on thrombus formation in a Chandler loop model, in which an acellular artery coated with these peptides make part of the loop. The effect of bioactive coatings can be compared to acellular artery coated with the non-functionalised peptides and uncoated.

Functionality of the endothelium. In order for a vascular graft to be successful, formation of a normal functional layer of endothelial cells on the luminal surface is also required to prevent an adverse host reaction, hence further studies are needed to investigate endothelial cells after re-cellularisation. This could be achieved microscopically by visualisation of native cellular and acellular cell-seeded arteries or by carrying out immunofluorescence tests to check for cellular markers expressed by endothelial cells such as vWF. In addition, use of real-time quantitative reverse transcription polymerase chain reaction (qRT-PCR) could help with the assessment of gene expression of endothelial cells.

8.3 Significance of Work

An ideal vascular graft should mimic the native vessel in both function and structure. Therefore, for successful *in vivo* application, vascular grafts should have: high patency rates, biomechanical properties equivalent to the native vessel, anti-thrombogenic properties, the capacity for re-endothelialisation of the luminal surface and integration with surrounding tissue without displaying an adverse immunological response or other complications.

The work presented in this thesis will positively contribute to the current knowledge of small-diameter vascular grafts, particularly the use of bioactive self-assembled peptide coated acellular arteries to enhance re-endothelialisation of tissue because the results were promising for cell retention after 72 hours.

Furthermore, the functionality of the bioactive P₁₁ peptides developed in this study can be assessed in established and optimised *in vitro* experiments with different types of cells as they may have the potential to be used in other tissue engineering applications.

Finally, more extensive work is required in this area of using bioactive peptides as coatings for acellular arteries for use in small-diameter vascular grafts, from developing an appropriate model for *in vitro* studies, to use in animal models for *in vivo* studies then potentially translated for clinical application.

A Appendix

A.1 Amino Acids

Structures of the 20 naturally occurring amino acids are listed in Figure A.1 (showing the three and one letter codes used throughout the thesis). Ornithine is a non-naturally occurring amino acid that is used throughout the thesis and has a three letter code of Orn and a one letter code of O.

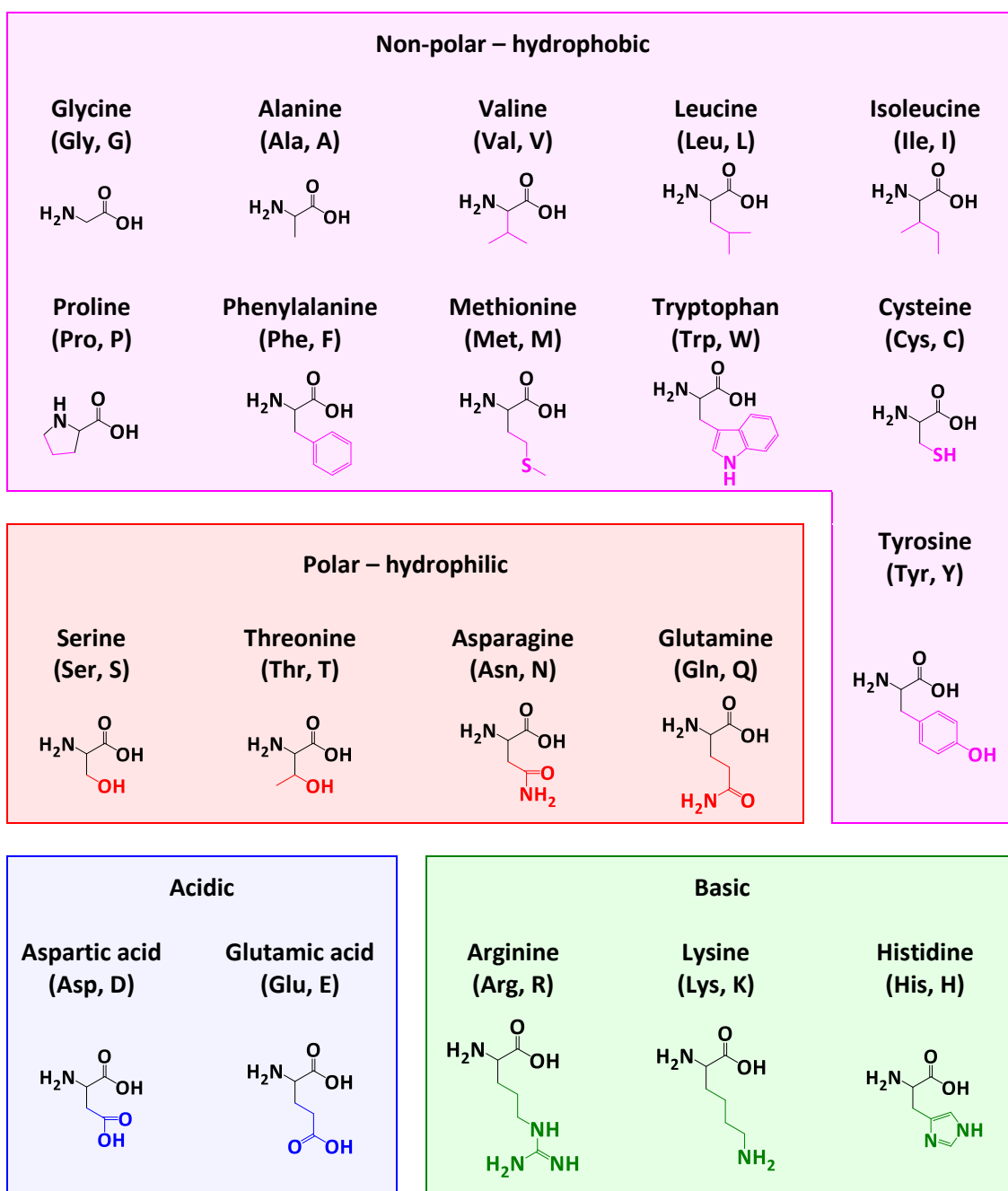


Figure A.1: Categorisation of the twenty naturally occurring amino acids into different groups depending on their side-chain group.

A.2 P₁₁ Peptides

Sequences, molecular weights and net charges at pH 7.4 of peptides used throughout this study are listed in Table A.1. Peptide concentrations used throughout this thesis converted between mg.mL⁻¹ and mM and vice versa are listed in Table A.2.

Table A.1: Sequences, molecular weights and net charges at pH 7.4 of peptides used throughout the study.

Peptide	Sequence	M _w	Net Charge
Non-functionalised P₁₁ Peptides			
P₁₁-4 (P01)	CH ₃ CO-Q-Q-R-F-E-W-E-F-E-Q-Q-NH ₂	1595.7	- 2
P₁₁-8 (P02)	CH ₃ CO-Q-Q-R-F-O-W-O-F-E-Q-Q-NH ₂	1565.7	+ 2
P₁₁-12 (P03)	CH ₃ CO-S-S-R-F-O-W-O-F-E-S-S-NH ₂	1401.5	+ 2
FITC-labelled P₁₁ Peptides			
FITC-P₁₁-4 (P04)	FITC-βA-Q-Q-R-F-E-W-E-F-E-Q-Q-NH ₂	2014.1	- 2
FITC-P₁₁-8 (P05)	FITC-βA-Q-Q-R-F-O-W-O-F-E-Q-Q-NH ₂	1984.2	+ 2
FITC-P₁₁-12 (P06)	FITC-βA-S-S-R-F-O-W-O-F-E-S-S-NH ₂	1820	+ 2
FITC-βA (P07; control)	FITC-βA-NH ₂	477.51	0
Alkyne-functionalised Cell Attachment Motifs			
GRGDS (P08)	CH ₃ CO-G-R-G-D-S-(PEG) ₂ -G(propargyl)-NH ₂	945	0
GRDGS (P09; control)	CH ₃ CO-G-R-D-G-S-(PEG) ₂ -G(propargyl)-NH ₂	945	0
YIGSR (P10)	CH ₃ CO-Y-I-G-S-R-(PEG) ₂ -G(propargyl)-NH ₂	1049	+ 1

Peptide	Sequence	M _w	Net Charge
YIRSG (P11; control)	CH ₃ CO-Y-I-R-S-G-(PEG) ₂ -G(propargyl)-NH ₂	1049	+ 1
Bioactive (Cell Attachment Functionalised) P₁₁ Peptides			
GRGDS-P₁₁-4 (P12)	CH ₃ CO-G-R-G-D-S-(PEG) ₂ -G-(PEG) ₂ -Q-Q-R-F-E-W-E-F-E-Q-Q-NH ₂	2783	- 2
GRDGS-P₁₁-4 (P13; control)	CH ₃ CO-G-R-D-G-S-(PEG) ₂ -G-(PEG) ₂ -Q-Q-R-F-E-W-E-F-E-Q-Q-NH ₂	2783	- 2
YIGSR-P₁₁-4 (P14)	CH ₃ CO-Y-I-G-S-R-(PEG) ₂ -G-(PEG) ₂ -Q-Q-R-F-E-W-E-F-E-Q-Q-NH ₂	2887.1	+ 1
YIRSG-P₁₁-4 (P15; control)	CH ₃ CO-Y-I-R-S-G-(PEG) ₂ -G-(PEG) ₂ -Q-Q-R-F-E-W-E-F-E-Q-Q-NH ₂	2887.1	+ 1
GRGDS-P₁₁-8 (P16)	CH ₃ CO-G-R-G-D-S-(PEG) ₂ -G-K(mca)-(PEG) ₂ -Q-Q-R-F-O-W-O-F-E-Q-Q-NH ₂	3097.4	+ 2
GRDGS-P₁₁-8 (P17; control)	CH ₃ CO-G-R-D-G-S-(PEG) ₂ -G-K(mca)-(PEG) ₂ -Q-Q-R-F-O-W-O-F-E-Q-Q-NH ₂	3097.4	+ 2
YIGSR-P₁₁-8 (P18)	CH ₃ CO-Y-I-G-S-R-(PEG) ₂ -G-K(mca)-(PEG) ₂ -Q-Q-R-F-O-W-O-F-E-Q-Q-NH ₂	3201.6	+ 3
YIRSG-P₁₁-8 (P19; control)	CH ₃ CO-Y-I-R-S-G-(PEG) ₂ -G-K(mca)-(PEG) ₂ -Q-Q-R-F-O-W-O-F-E-Q-Q-NH ₂	3201.6	+ 3

Table A.2: Conversion of peptides concentrations used throughout the study (mg.mL⁻¹ to mM and vice versa).

Peptide	Concentration (mg.mL ⁻¹ to mM)			Concentration (mM to mg.mL ⁻¹)	
	10	20	30	0.3	3
P₁₁-4	6.27	12.53	18.80	0.48	4.79
P₁₁-8	6.39	12.77	19.16	0.47	4.70
P₁₁-12	7.13	14.27	21.41	0.42	4.20

A.3 FTIR Spectra – Other Concentrations

P₁₁-4 FTIR spectra over time at 10 mg.mL⁻¹ (A) and 30 mg.mL⁻¹ (B) are presented in Figure A.2.

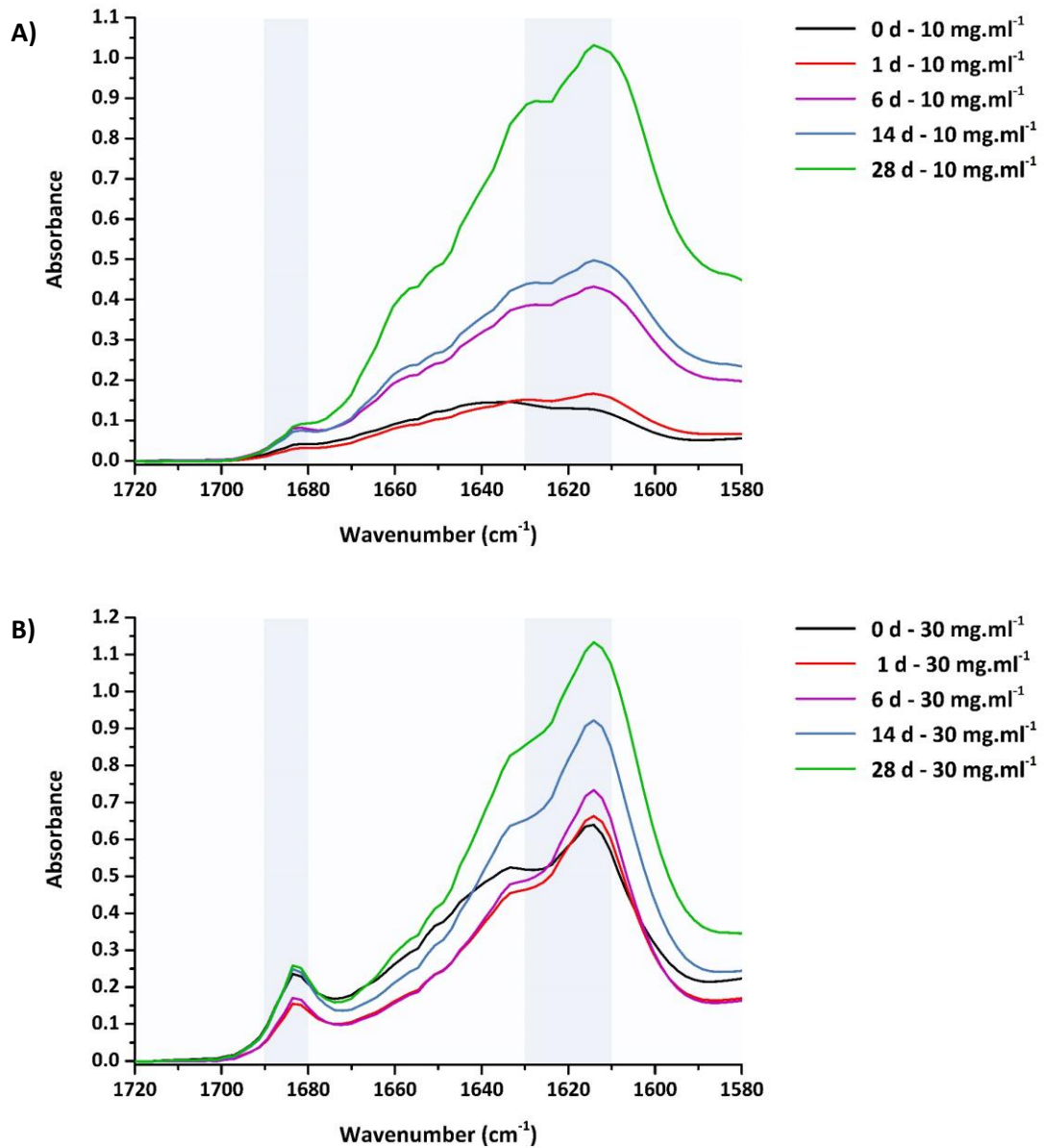


Figure A.2: P₁₁-4 FTIR spectra at 10 mg.mL⁻¹ (A) and 30 mg.mL⁻¹ (B) over time after triggering self-assembly by addition of Ringer's solution. Time: 0 (black), 1 (red), 6 (purple), 14 (blue) and 28 (green) days of incubation at 37 °C. Shaded areas correspond to β-sheet absorptions.

P₁₁₋₈ FTIR spectra over time at 10 mg.mL⁻¹ (A) and 30 mg.mL⁻¹ (B) are presented in Figure A.3.

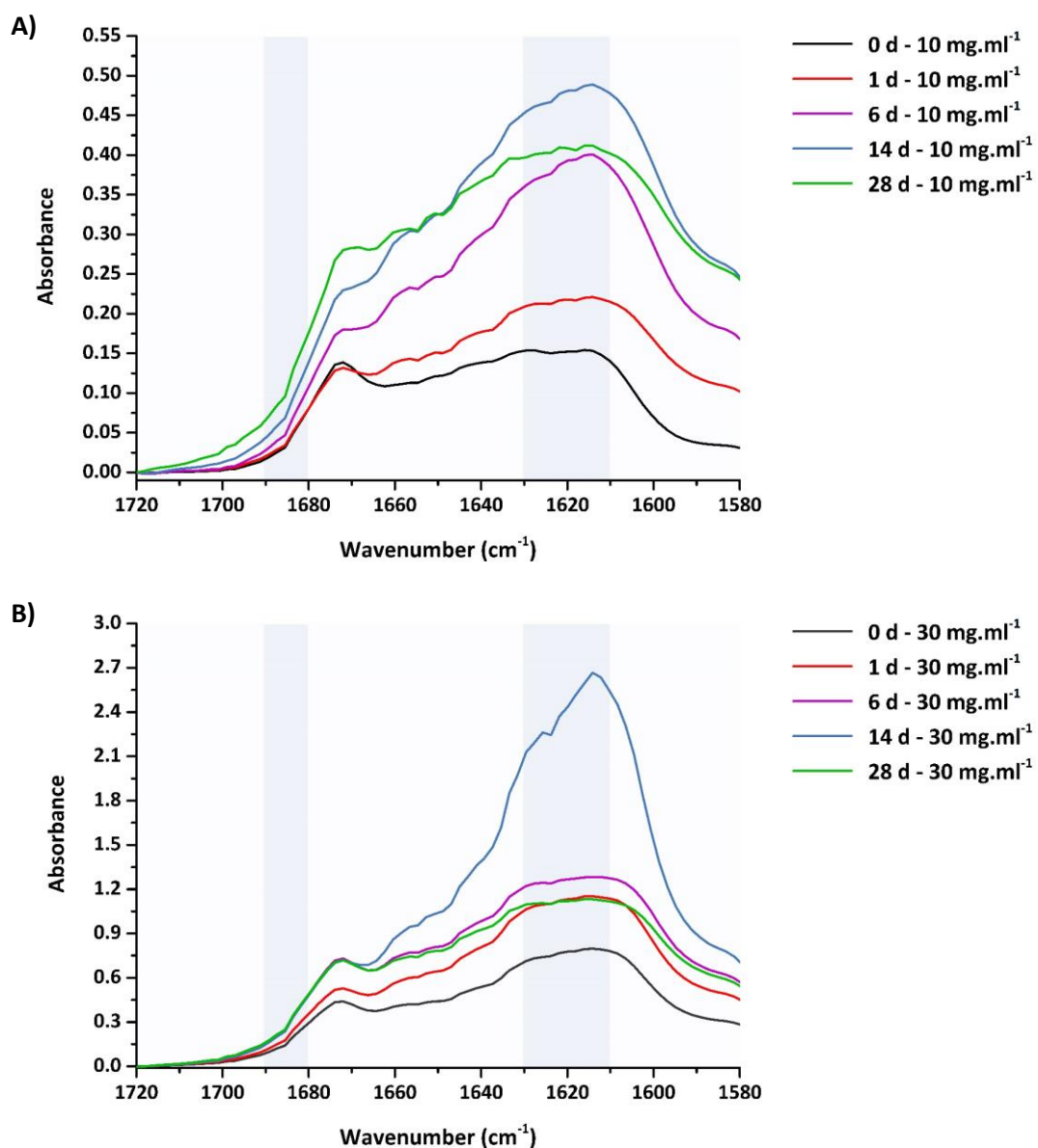


Figure A.3: P₁₁₋₈ FTIR spectra at 10 mg.mL⁻¹ (A) and 30 mg.mL⁻¹ (B) over time after triggering self-assembly by addition of Ringer's solution. Time: 0 (black), 1 (red), 6 (purple), 14 (blue) and 28 (green) days of incubation at 37 °C. Shaded areas correspond to β -sheet absorptions.

P₁₁₋₁₂ FTIR spectra over time at 10 mg.mL⁻¹ (A) and 30 mg.mL⁻¹ (B) are presented in Figure A.4.

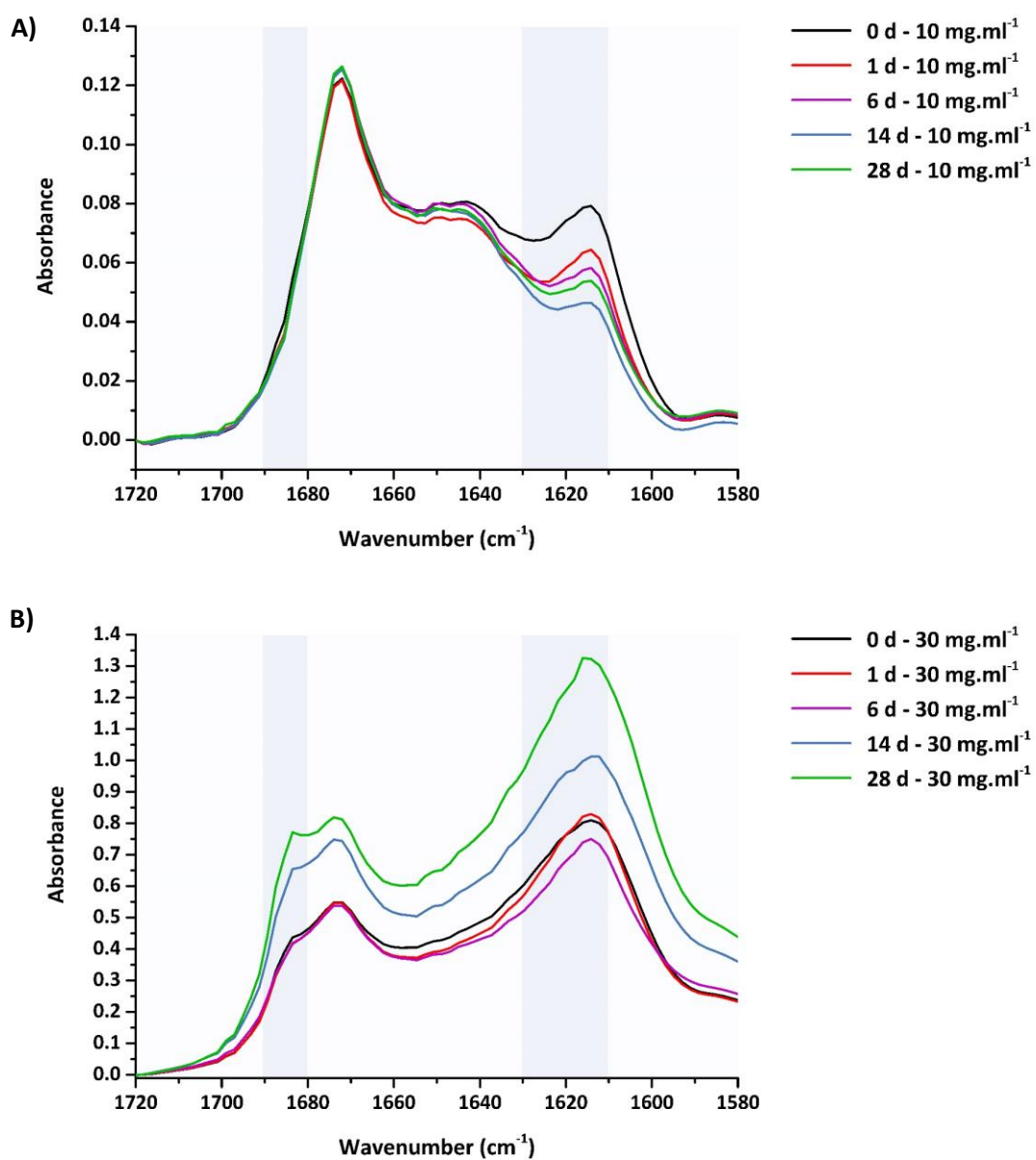


Figure A.4: P₁₁₋₁₂ FTIR spectra at 10 mg.mL⁻¹ (A) and 30 mg.mL⁻¹ (B) over time after triggering self-assembly by addition of Ringer's solution. Time: 0 (black), 1 (red), 6 (purple), 14 (blue) and 28 (green) days of incubation at 37 °C. Shaded areas correspond to β-sheet absorptions.

A.4 P₁₁ Peptides Gelation Over time

P₁₁₋₄, P₁₁₋₈ and P₁₁₋₁₂ were imaged at 10, 20 and 30 mg.mL⁻¹ before triggering self-assembly by addition of Ringer's solution, immediately after and at 0, 1, 6, 14, 28 and 91 days after triggering self-assembly and gelation was observed over time. Detailed observations of the physical state of peptides are listed in Table A.3.

Table A.3: Summary of physical state observations in P₁₁₋₄, P₁₁₋₈ and P₁₁₋₁₂ at different concentrations over time. RS (Ringer's solution).

Peptide	Time (days)	Concentration (mg.mL ⁻¹)		
		10	20	30
P ₁₁₋₄	0 No RS	Clear solution + few white thread-like structures	Clear solution + cloudy gel globules within	Clear solution + more cloudy gel globules within
	0 + RS	Clear solution + small gel globules within. Gets cloudier, more viscous + more small gel globules with time	Cloudy slightly viscous solution + more small gel globules within. Gets cloudier and gels with time	Cloudy slightly viscous solution + more small gel globules within. Gets cloudier and gels with time
	1	Cloudy gel + viscous solution + small cloudy gel globules within	Cloudy gel + more small cloudy gel globules within	Cloudy gel + more small cloudy gel globules within
	6	Cloudy gel + clear viscous solution + small cloudy gel globules within	Cloudy gel + more small cloudy gel globules within	Cloudy gel (strong) + more small cloudy gel globules within
	14	Cloudy gel + small cloudy gel globules within	Cloudy gel (strong) + more small cloudy gel globules within	Cloudy gel (strong) + more small cloudy gel globules within
	28	Cloudy gel + small cloudy gel globules within	Cloudy gel (strong)+ more small cloudy gel globules within	Cloudy gel (strong)+ more small cloudy gel globules within
	91	Milky gel (strong)	Milky gel (strong)	Milky gel (strong)
P ₁₁₋₈	0 No RS	Clear solution + few white thread-like structures	Cloudy viscous solution + small cloudy/milky gel globules within	Cloudy viscous solution + small cloudy/milky gel globules within
	0 + RS	Cloudy solution + small cloudy gel globules within. Gets cloudier, more viscous + more gel globules with time	Milky viscous solution + small milky gel globules within. Gets cloudier and gels with time	Milky viscous solution + more small milky gel globules within. Gets cloudier and gels with time
	1	Cloudy gel + viscous solution + small cloudy gel globules within	Milky gel + more small cloudy gel globules within	Milky gel + more small cloudy gel globules within

Peptide	Time (days)	Concentration (mg.mL ⁻¹)		
		10	20	30
	6	Cloudy gel + clear viscous solution + small cloudy gel globules within	Cloudy gel (strong) + more small cloudy gel globules within	Cloudy gel (strong) + more small cloudy gel globules within
	14	Cloudy gel + cloudy gel globules within	Milky gel (strong) + more small cloudy gel globules within	Milky gel (strong) + more small cloudy gel globules within
	28	milky gel + cloudy gel globules within	Milky gel (strong) + more small cloudy gel globules within	Milky gel (strong) + more small cloudy gel globules within
	91	Milky gel (strong)	Milky gel (strong)	Milky gel (strong)
P ₁₁₋₁₂	0 No RS	Clear solution + clear gel bits within	Clear solution + clear gel bits within	Clear solution + clear gel bits within
	0 + RS	Clear viscous solution + small clear gel bits within. More viscous and gel bits with time	Clear viscous solution + clear and cloudy gel bits within. Gels with time (easily disrupted)	Clear viscous solution + clear and cloudy gel bits within. Gels with time (easily disrupted)
	1	Clear weak gel + viscous solution	Clear gel (easily disrupted) + cloudy gel globules within (strong)	Clear gel (easily disrupted) + more cloudy gel globules within (strong)
	6	Clear gel + viscous solution + small cloudy gel globules within	Clear gel (easily disrupted) + more cloudy gel globules within (strong)	Clear gel (slightly disrupted) + more cloudy gel globules within (strong)
	14	Clear gel + viscous solution + small cloudy gel globules within	Clear gel (slightly disrupted) + more big cloudy gel globules within (strong)	Clear gel (slightly disrupted) + more big cloudy gel globules within (strong)
	28	Clear gel + viscous solution + cloudy gel globules within	Clear gel (slightly disrupted) + more big cloudy gel globules within (strong)	Clear gel (slightly disrupted) + more big cloudy gel globules within (strong)
	91	clear gel + viscous solution	Clear gel (slightly disrupted) + more big cloudy gel globules within (strong)	Clear gel (strong) + more big cloudy gel globules within (strong)

A.5 FTIR – Effect of Temperature on Peptide Self-assembly

The effect of temperature on β -sheet percentage was tested at room temperature and 37 °C in 30 mg.mL⁻¹ P₁₁₋₄, P₁₁₋₈ and P₁₁₋₁₂ over 28 days (Figure A.5). The percentages were similar at both tested temperatures with slight differences ranging between 0 - 3 % in P₁₁₋₄ and P₁₁₋₈ and more variation in P₁₁₋₁₂ ranging between 3 - 10 %. The small variation in β -sheet proportion allowed for carrying further tests using these peptides at room temperature instead of 37 °C.

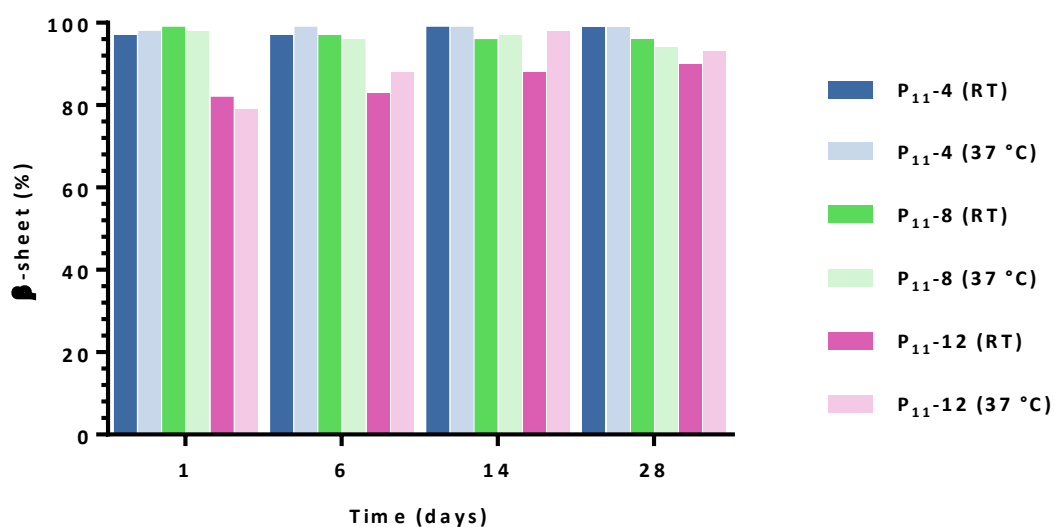


Figure A.5: P₁₁₋₄, P₁₁₋₈ and P₁₁₋₁₂ β -sheet percentages at 30 mg.mL⁻¹ over time at room temperature (RT) and 37 °C.

A.6 Peptide Synthesis Results

A.6.1 FITC-labelled Peptides

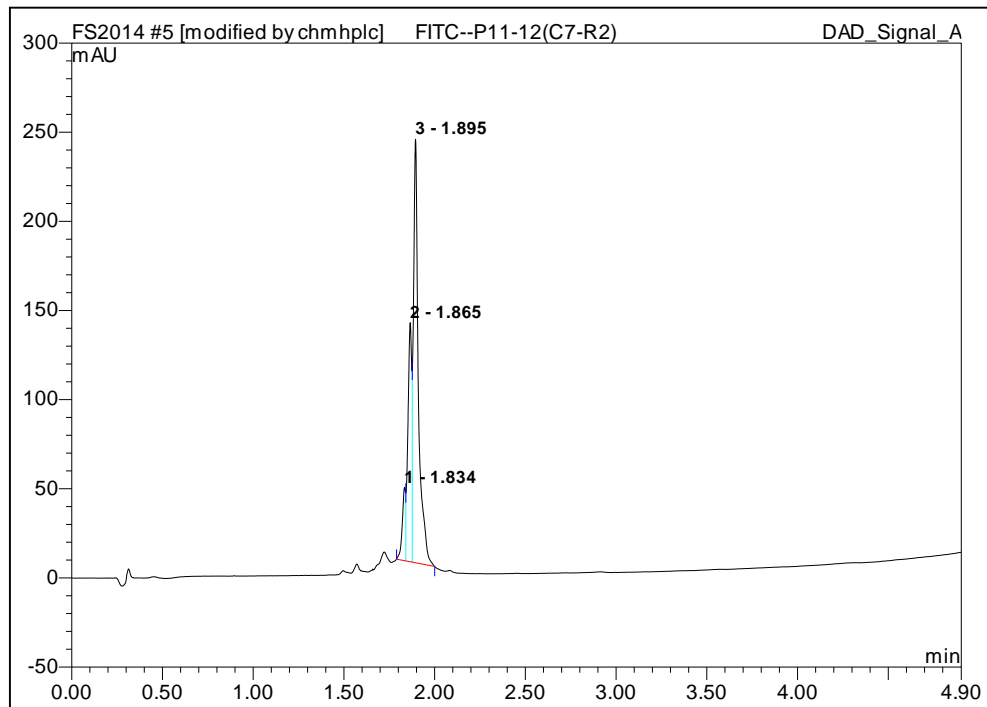
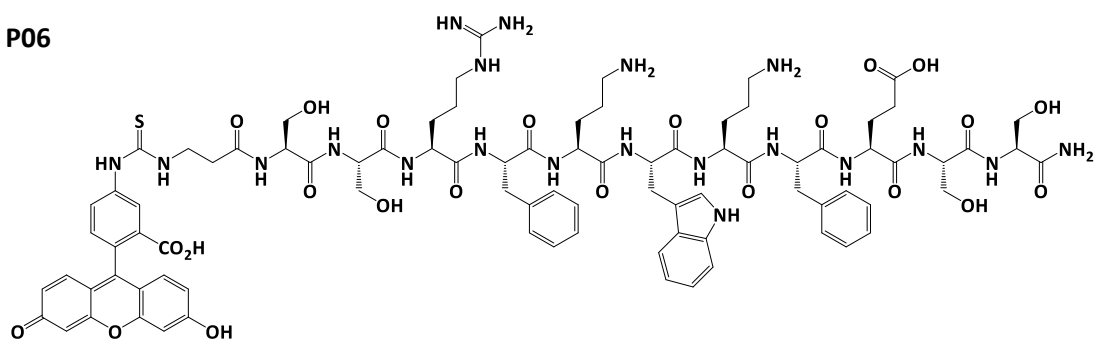
FITC-P₁₁₋₁₂ (P06; M_w 1820)

Analytical HPLC trace: 64.58 % (the sample was run using the Ascentis Express C18 column; acetonitrile/water both with 0.1 % TFA; gradient 5 - 95 % acetonitrile (+ 0.1 % TFA); flow rate 0.5 mL.min⁻¹ over 5 minutes; UV detection at 254 nm);

Accurate MS (ES⁺): *m/z* found [M+3H]³⁺ 607.5927; C₈₆H₁₀₆N₂₀O₂₃S requires 607.5903;

LC-MS (ES⁺): *m/z* found [M+2H]²⁺ 910.9, [M+3H]³⁺ 607.4.

P06



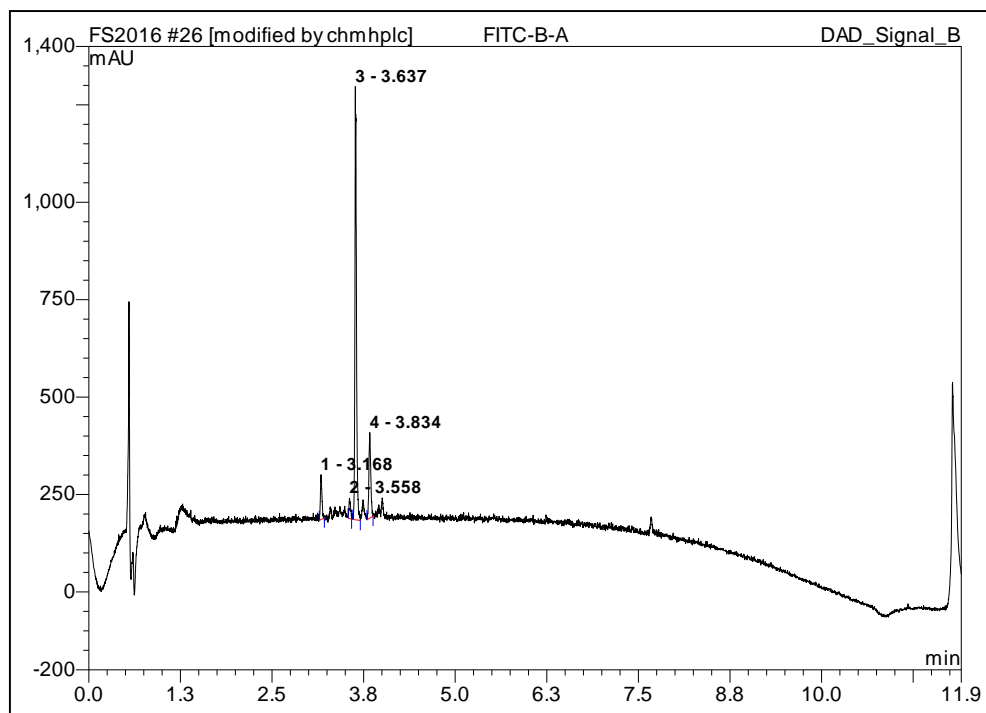
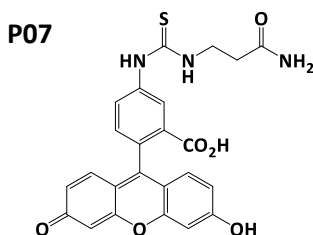
Peak No.	Ret.Time (min)	Height (mAU)	Area (mAU*min)	Rel.Area (%)
1	1.83	41.071	0.870	7.34
2	1.87	134.164	3.327	28.08
3	1.89	237.571	7.652	64.58
Total	-	412.806	11.850	100.00

The Control FITC- β -Ala (P07; M_w 477.5)

Analytical HPLC trace: 71.85 % (the sample was run using the Ascentis Peptide C18 column; MeCN/H₂O both with 0.1 % TFA; gradient 5 - 95 % MeCN (+ 0.1 % TFA); flow rate 0.5 mL.min⁻¹ over 12 minutes; UV detection at 210 nm);

Accurate MS (ES⁺): m/z found [M+H]⁺ 478.1074; C₂₄H₁₉N₃O₆S requires 478.1067;

LC-MS (ES⁺): m/z found [M+H]⁺ 478.4.



Peak No.	Ret.Time (min)	Height (mAU)	Area (mAU*min)	Rel.Area (%)
1	3.17	115.051	2.824	7.49
2	3.56	51.650	1.292	3.42
3	3.64	1111.358	27.107	71.85
4	3.83	219.290	6.505	17.24
Total	-	1497.348	37.728	100.00

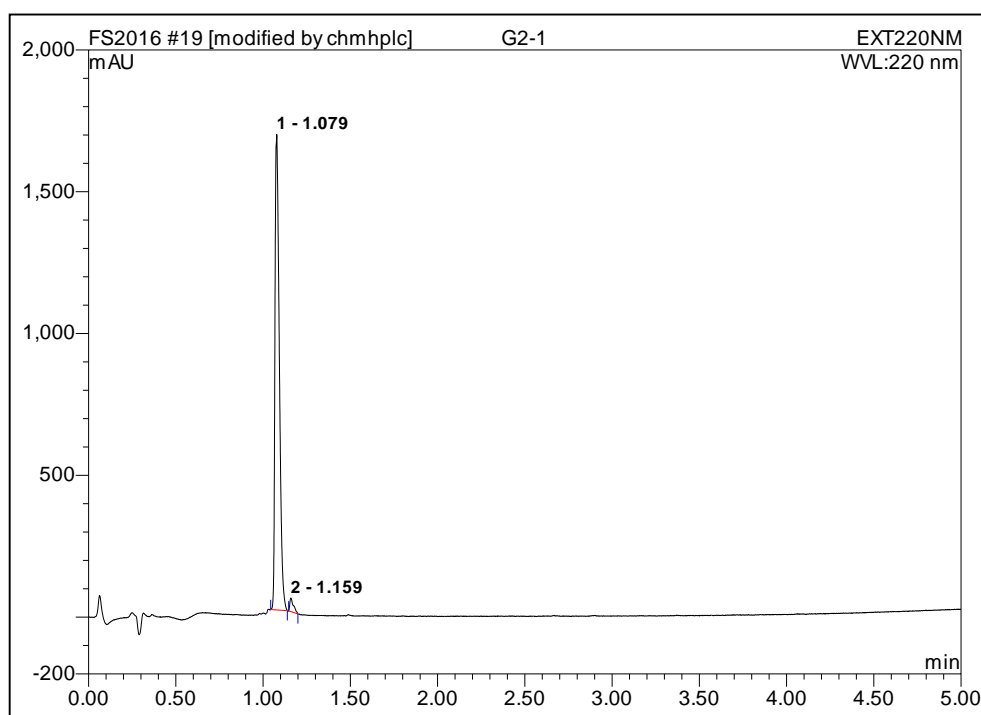
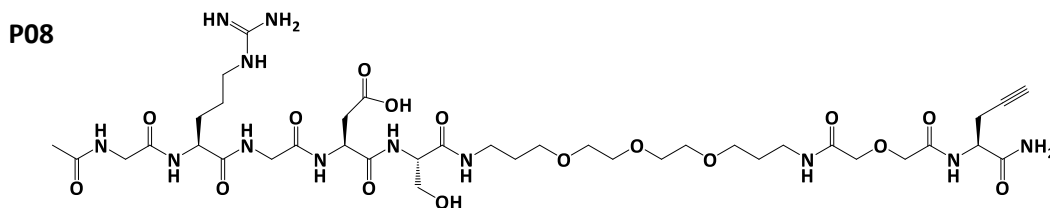
A.6.2 Alkyne-functionalised Cell Attachment Motifs

GRGDS (P08; M_w 945)

Analytical HPLC trace: 97.7 % (the sample was run using the Ascentis Express C18 column; MeCN/H₂O both with 0.1 % TFA; gradient 5 - 95 % MeCN (+ 0.1 % TFA); flow rate 0.5 mL.min⁻¹ over 5 minutes; UV detection at 220 nm);

Accurate MS (ES⁺): *m/z* found [M+H]⁺ 945.4655; C₃₈H₆₄N₁₂O₁₆ requires 945.4636;

LC-MS (ES⁺): *m/z* found [M+H]⁺ 945.5, [M+2H]²⁺ 473.2.



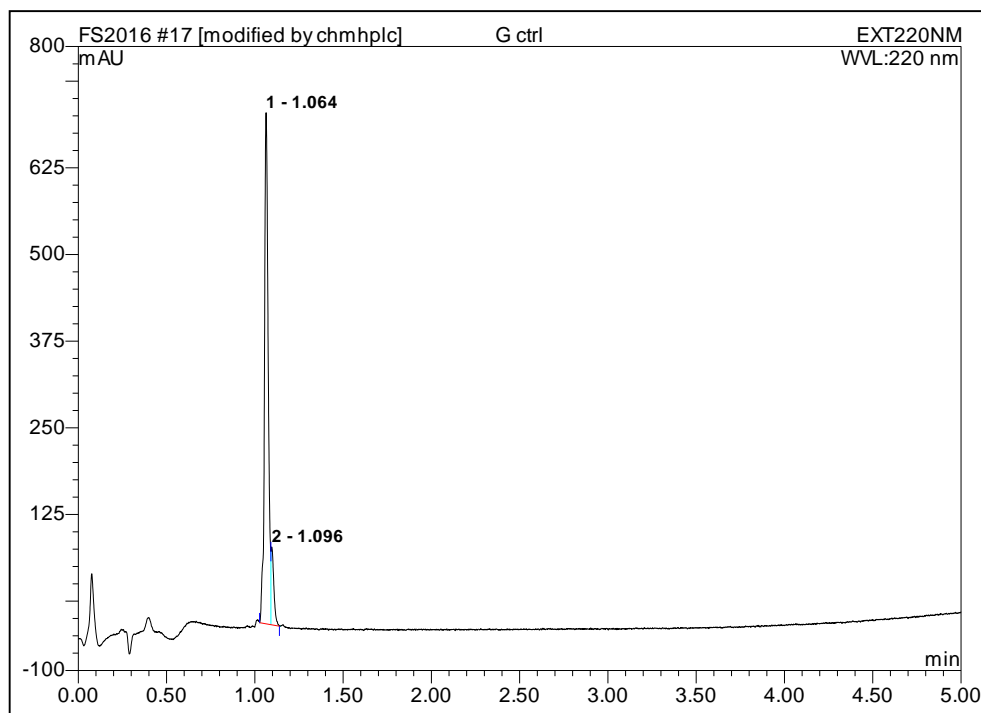
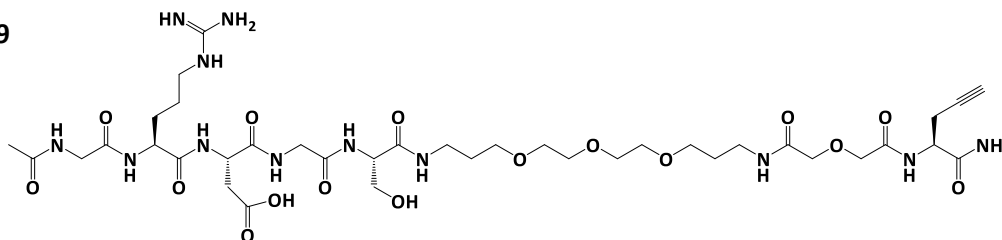
Peak No.	Ret.Time (min)	Height (mAU)	Area (mAU*min)	Rel.Area (%)
1	1.08	1676.550	48.581	97.70
2	1.16	47.819	1.145	2.30
Total	-	1724.369	49.726	100.00

The Scrambled Control GRDGS (P09; M_w 945)

Analytical HPLC trace: 89.68 %; (the sample was run using the Ascentis Express C18 column; MeCN/H₂O both with 0.1 % TFA; gradient 5 - 95 % MeCN (+ 0.1 % TFA); flow rate 0.5 mL.min⁻¹ over 5 minutes; UV detection at 220 nm);

Accurate MS (ES⁺): *m/z* found [M+H]⁺ 945.4655; C₃₈H₆₄N₁₂O₁₆ requires 945.4636;

LC-MS (ES⁺): *m/z* found [M+H]⁺ 945.8.

P09

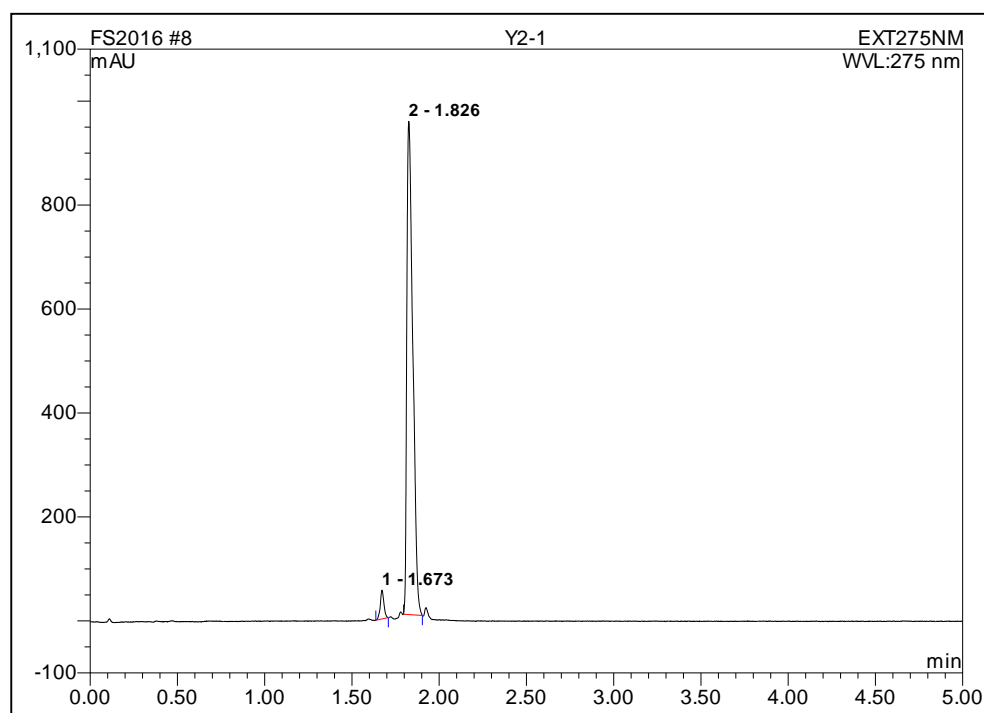
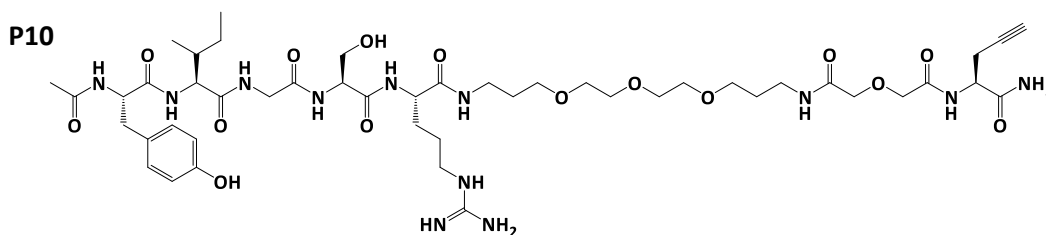
Peak No.	Ret.Time (min)	Height (mAU)	Area (mAU*min)	Rel.Area (%)
1	1.06	737.241	18.078	89.68
2	1.10	112.440	2.081	10.32
Total	-	849.681	20.159	100.00

YIGSR (P10; M_w 1049)

Analytical HPLC trace: 96.59 % (the sample was run using the Ascentis Express C18 column; MeCN/H₂O both with 0.1 % TFA; gradient 5 - 95 % MeCN (+ 0.1 % TFA); flow rate 0.5 mL.min⁻¹ over 5 minutes; UV detection at 275 nm);

Accurate MS (ES⁺): *m/z* found [M+H]⁺ 1049.5644; C₄₇H₇₆N₁₂O₁₅ requires 1049.5626;

LC-MS (ES⁺): *m/z* found [M+H]⁺ 1049.6, [M+2H]²⁺ 525.3.



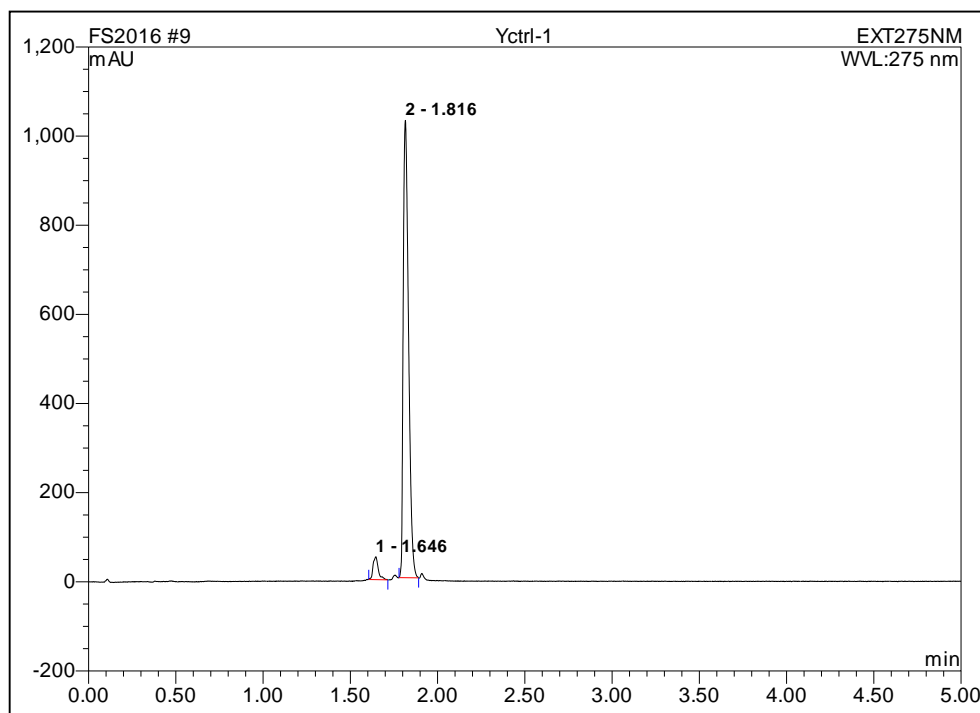
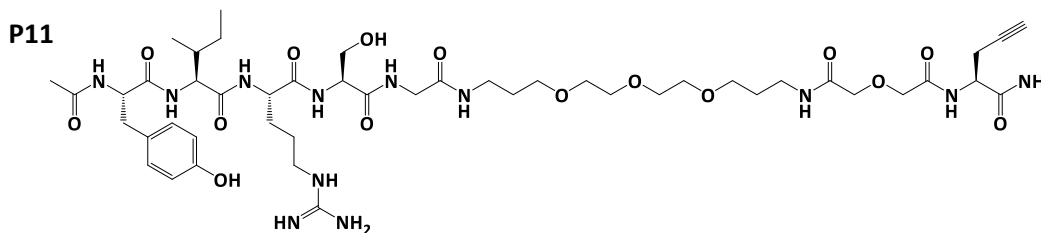
Peak No.	Ret.Time (min)	Height (mAU)	Area (mAU*min)	Rel.Area (%)
1	1.67	55.458	1.331	3.41
2	1.83	949.001	37.661	96.59
Total	-	1004.459	38.992	100.00

The Scrambled Control YIRSG (P11; M_w 1049)

Analytical HPLC trace: 95.33 % (the sample was run using the Ascentis Express C18 column; MeCN/H₂O both with 0.1 % TFA; gradient 5 - 95 % MeCN (+ 0.1 % TFA); flow rate 0.5 mL.min⁻¹ over 5 minutes; UV detection at 275 nm);

Accurate MS (ES⁺): *m/z* found [M+H]⁺ 1049.5653; C₄₇H₇₆N₁₂O₁₅ requires 1049.5626;

LC-MS (ES⁺): *m/z* found [M+H]⁺ 1049.6, [M+2H]²⁺ 525.3.



Peak No.	Ret.Time (min)	Height (mAU)	Area (mAU*min)	Rel.Area (%)
1	1.65	51.387	1.770	4.67
2	1.82	1026.096	36.160	95.33
Total	-	1077.483	37.931	100.00

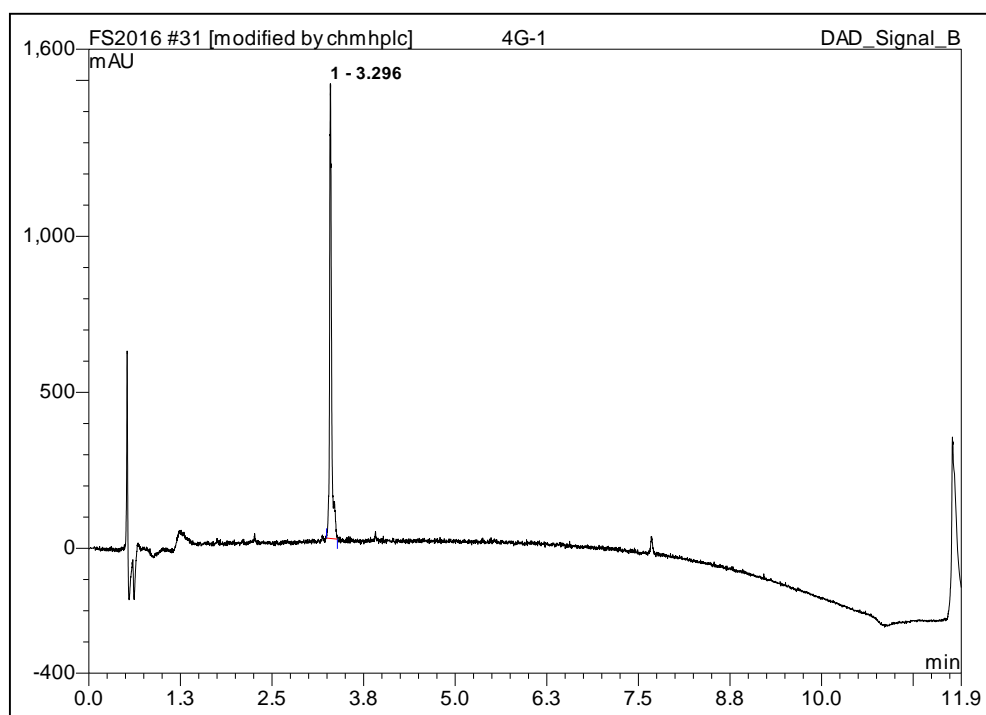
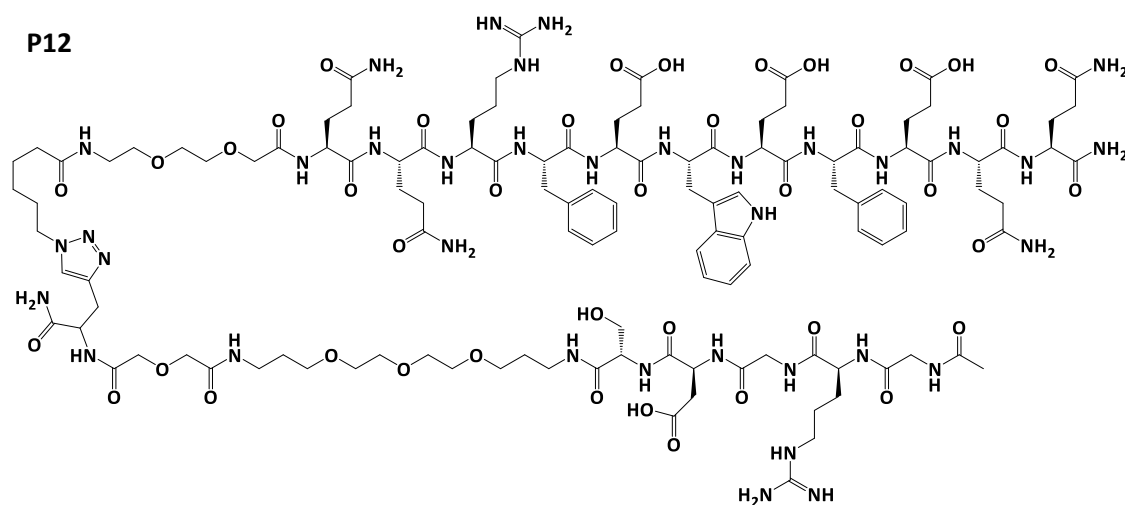
A.6.3 Bioactive (Cell Attachment Functionalised) P₁₁ Peptides

GRGDS-P₁₁-4 (P12; M_w 2783)

Analytical HPLC trace: 100 % (the sample was run using the Ascentis Peptide C18 column; MeCN/H₂O both with 0.1 % TFA; gradient 5 - 95 % MeCN (+ 0.1 % TFA); flow rate 0.5 mL.min⁻¹ over 12 minutes; UV detection at 210 nm);

Accurate MS (ES⁺): *m/z* found [M+2H]²⁺ 1392.1589; C₁₂₀H₁₈₀N₃₆O₄₁ requires 1392.1640;

LC-MS (ES⁺): *m/z* found [M+2H]²⁺ 1392.1, [M+3H]³⁺ 928.4, [M+H]⁴⁺ 696.6.



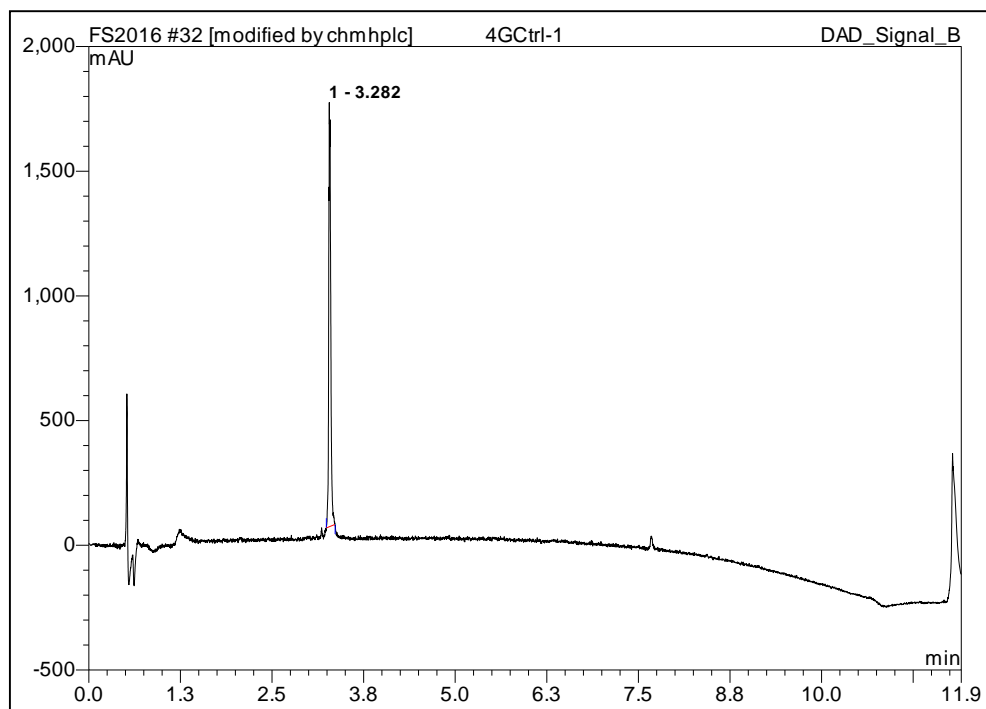
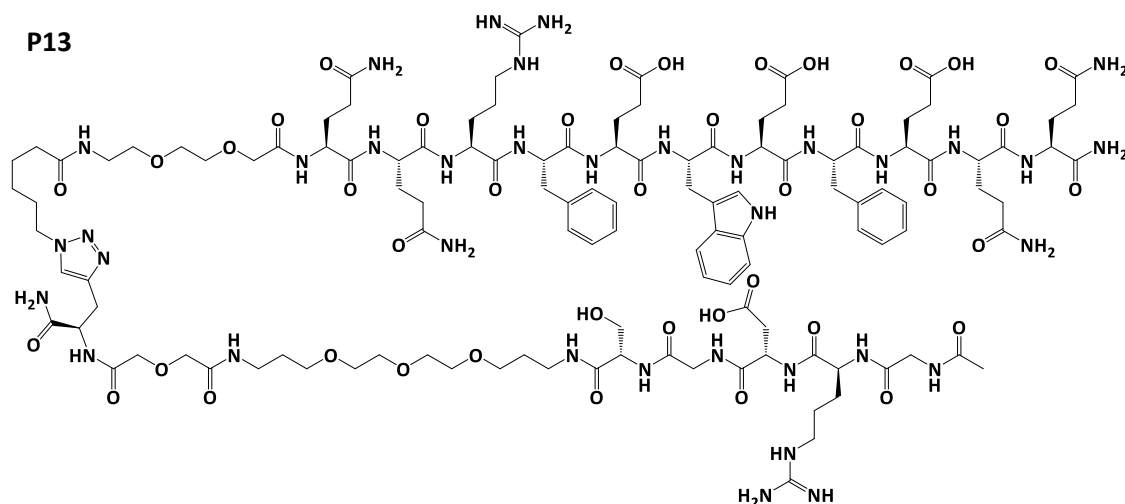
Peak No.	Ret.Time (min)	Height (mAU)	Area (mAU*min)	Rel.Area (%)
1	3.30	1457.087	45.267	100.00
Total	-	1457.087	45.267	100.00

The Scrambled Control GRDGS-P₁₁-4 (P13; M_w 2783)

Analytical HPLC trace: 100 % (the sample was run using the Ascentis Peptide C18 column; MeCN/H₂O both with 0.1 % TFA; gradient 5 - 95 % MeCN (+ 0.1 % TFA); flow rate 0.5 mL.min⁻¹ over 12 minutes; UV detection at 210 nm);

Accurate MS (ES⁺): *m/z* found [M+2H]²⁺ 1392.1583; C₁₂₀H₁₈₀N₃₆O₄₁ requires 1392.1640;

LC-MS (ES⁺): *m/z* found [M+2H]²⁺ 1392.3, [M+3H]³⁺ 928.9.



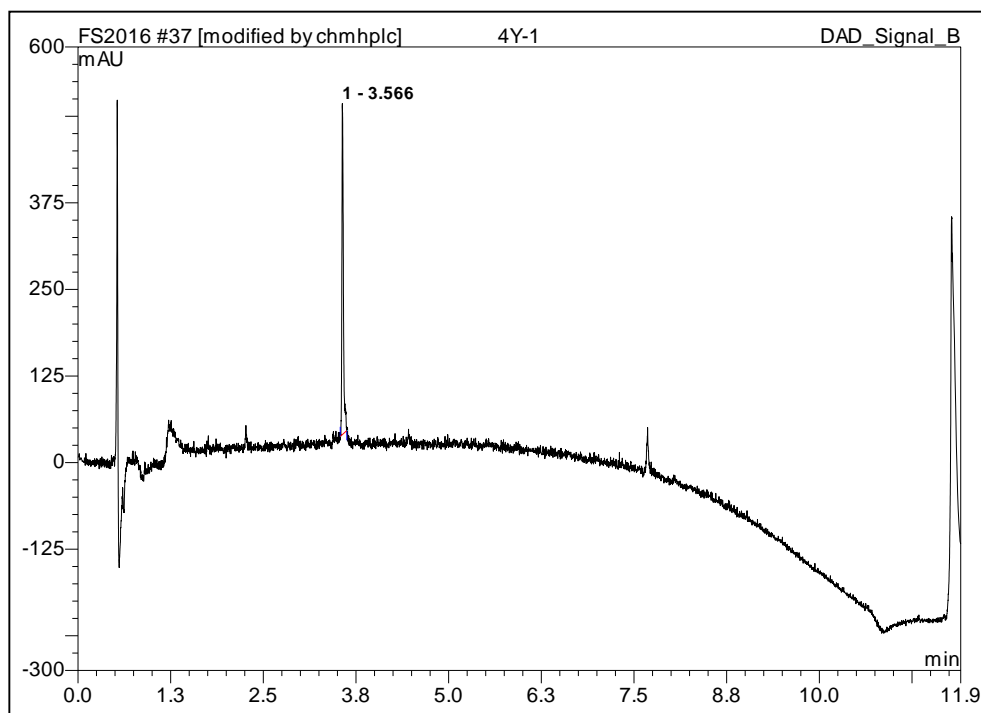
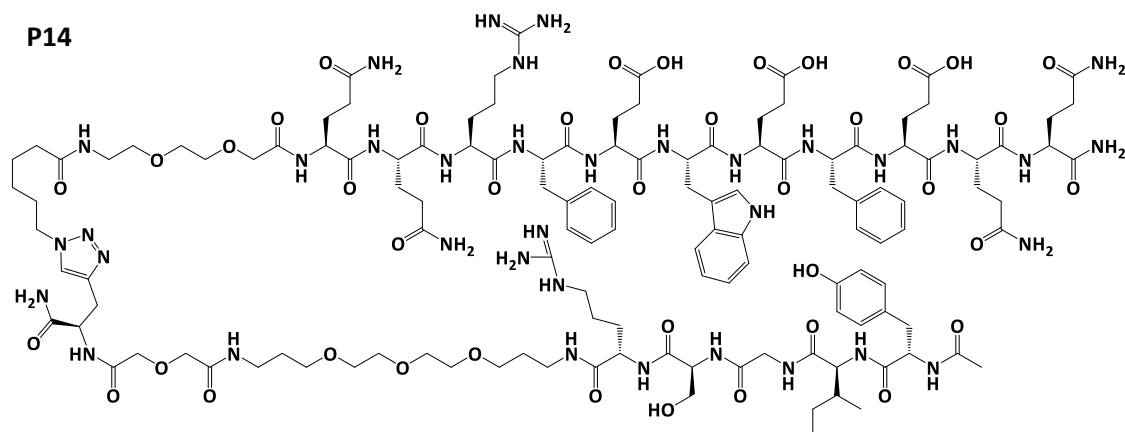
Peak No.	Ret.Time (min)	Height (mAU)	Area (mAU*min)	Rel.Area (%)
1	3.28	1701.010	53.720	100.00
Total	-	1701.010	53.720	100.00

YIGSR-P₁₁-4 (P14; M_w 2887.1)

Analytical HPLC trace: 100 % (the sample was run using the Ascentis Peptide C18 column; MeCN/H₂O both with 0.1 % TFA; gradient 5 - 95 % MeCN (+ 0.1 % TFA); flow rate 0.5 mL.min⁻¹ over 12 minutes; UV detection at 210 nm);

Accurate MS (ES⁺): *m/z* found [M+2H]²⁺ 1444.2115; C₁₂₉H₁₉₂N₃₆O₄₀ requires 1444.2135;

LC-MS (ES⁺): *m/z* found [M+2H]²⁺ 1444.1, [M+3H]³⁺ 963.2, [M+4H]⁴⁺ 722.8.



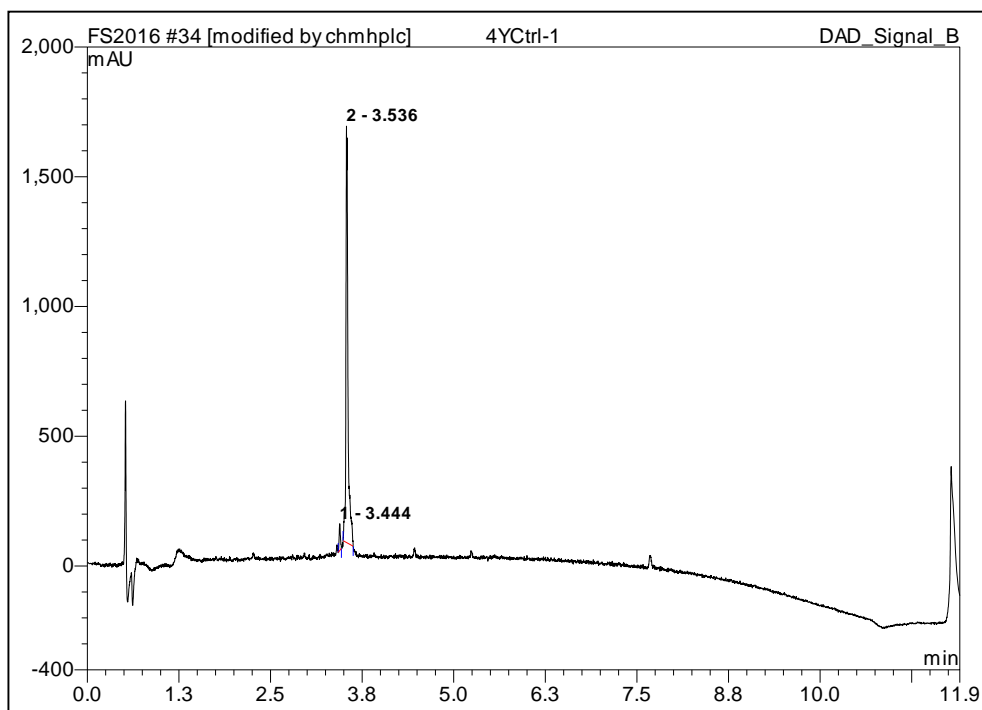
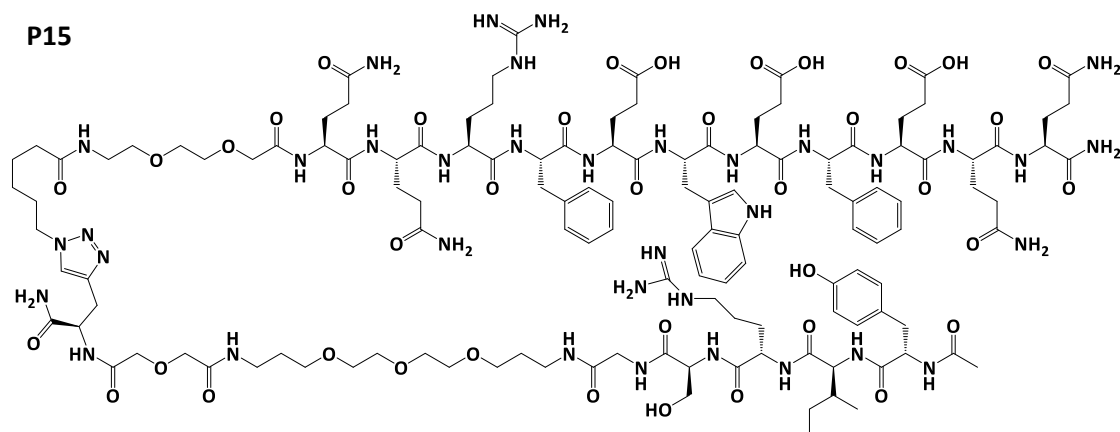
Peak No.	Ret.Time (min)	Height (mAU)	Area (mAU*min)	Rel.Area (%)
1	3.57	477.934	11.280	100.00
Total	-	477.934	11.280	100.00

The Scrambled Control YIRSG-P₁₁-4 (P15; M_w 2887.1)

Analytical HPLC trace: 96.21 % (the sample was run using the Ascentis Peptide C18 column; MeCN/H₂O both with 0.1 % TFA; gradient 5 - 95 % MeCN (+ 0.1 % TFA); flow rate 0.5 mL.min⁻¹ over 12 minutes; UV detection at 210 nm);

Accurate MS (ES⁺): *m/z* found [M+2H]²⁺ 1444.2092; C₁₂₉H₁₉₂N₃₆O₄₀ requires 1444.2135;

LC-MS (ES⁺): *m/z* found [M+2H]²⁺ 1444.7, [M+3H]³⁺ 963.5.



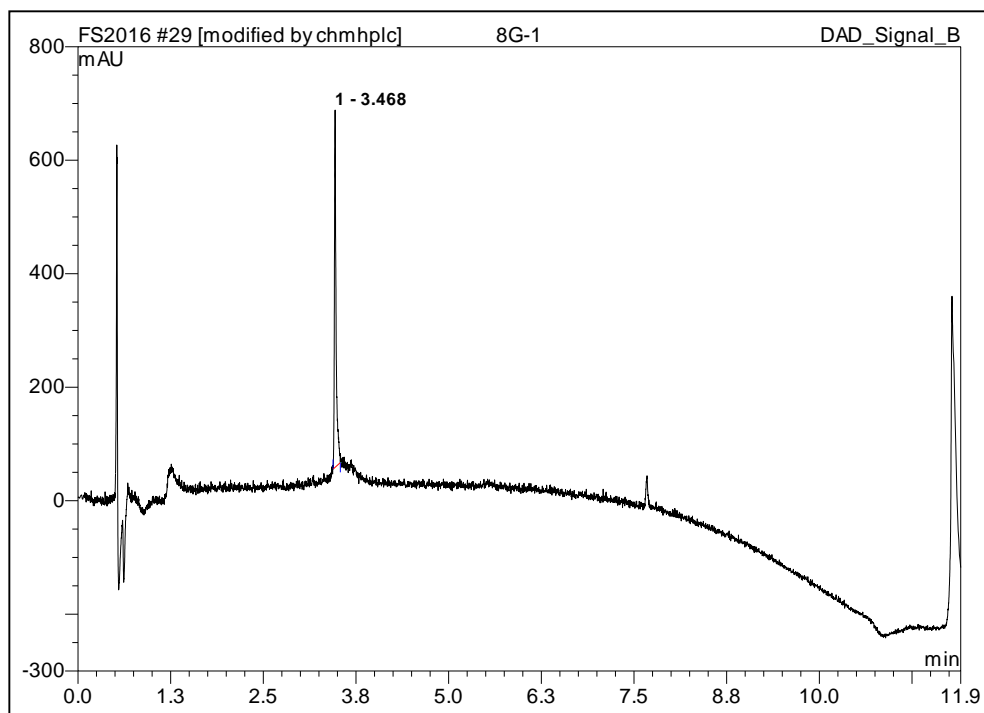
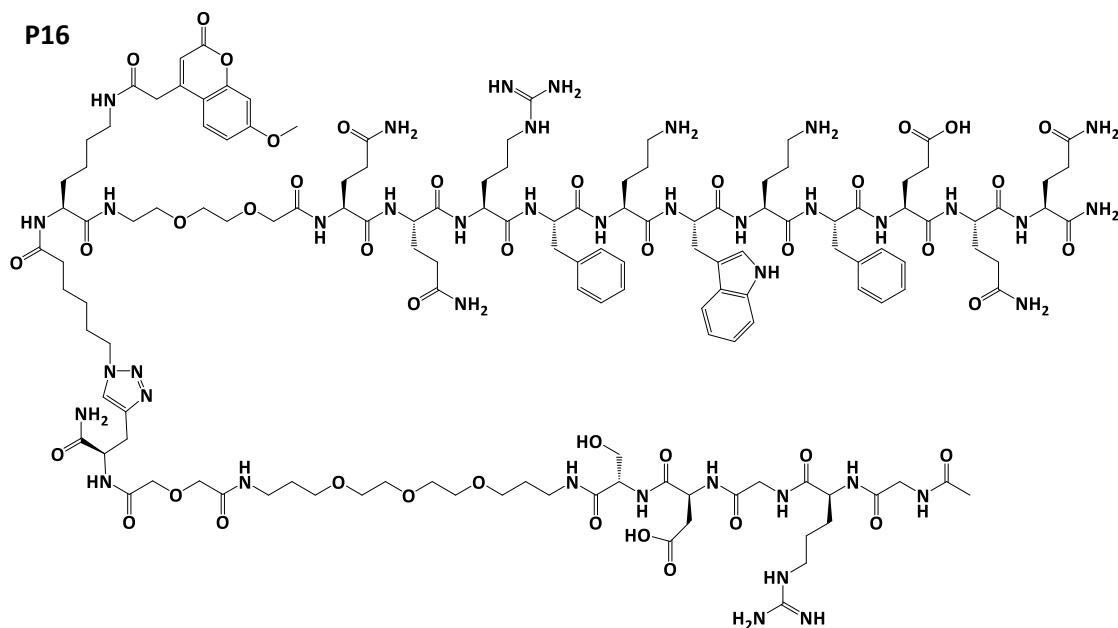
Peak No.	Ret.Time (min)	Height (mAU)	Area (mAU*min)	Rel.Area (%)
1	3.44	103.379	2.054	3.79
2	3.54	1604.399	52.120	96.21
Total	-	1707.779	54.175	100.00

GRGDS-P₁₁-8 (P16; M_w 3097.4)

Analytical HPLC trace: 100 % (the sample was run using the Ascentis Peptide C18 column; MeCN/H₂O both with 0.1 % TFA; gradient 5 - 95 % MeCN (+ 0.1 % TFA); flow rate 0.5 mL.min⁻¹ over 12 minutes; UV detection at 210 nm);

Accurate MS (ES⁺): *m/z* found [M+3H]³⁺ 1033.1821; C₁₃₈H₂₀₆N₄₀O₄₂ requires 1033.1820;

LC-MS (ES⁺): *m/z* found [M+4H]⁴⁺ 775.4.



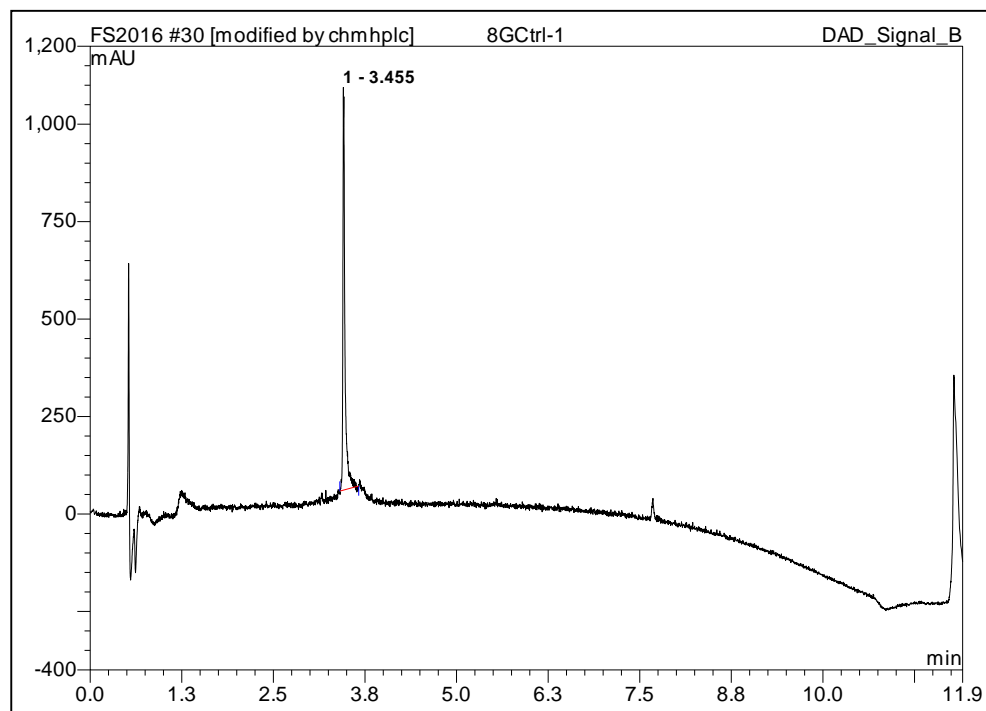
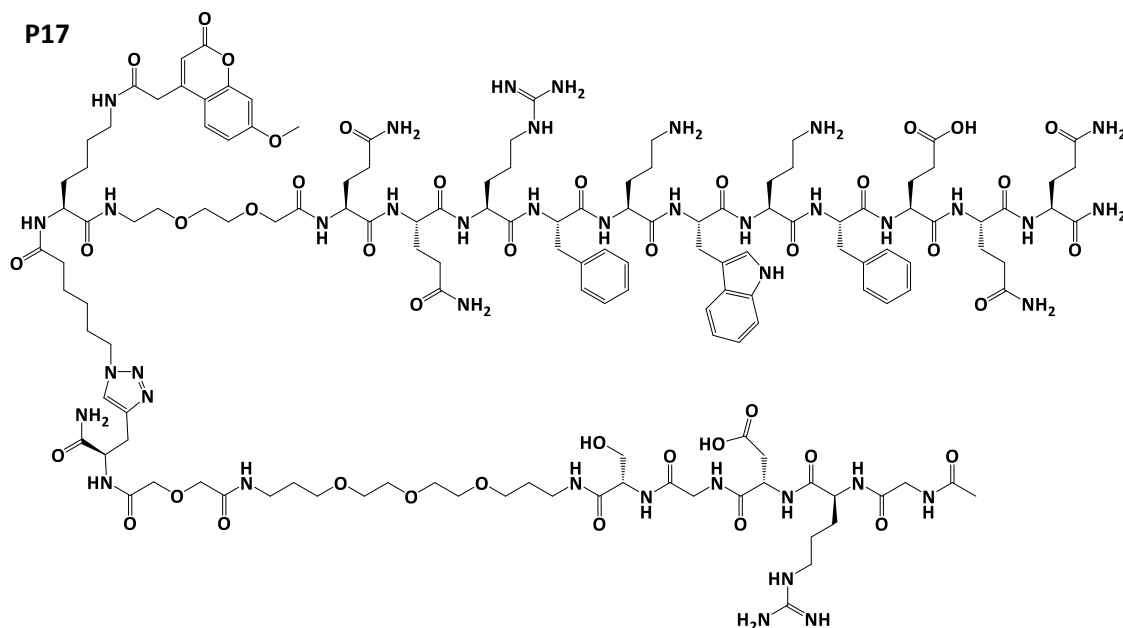
Peak No.	Ret.Time (min)	Height (mAU)	Area (mAU*min)	Rel.Area (%)
1	3.47	629.617	16.048	100.00
Total	-	629.617	16.048	100.00

The Scrambled Control GRDGS-P₁₁-8 (P17; M_w 3097.4)

Analytical HPLC trace: 100 % (the sample was run using the Ascentis Peptide C18 column; MeCN/H₂O both with 0.1 % TFA; gradient 5 - 95 % MeCN (+ 0.1 % TFA); flow rate 0.5 mL.min⁻¹ over 12 minutes; UV detection at 210 nm);

Accurate MS (ES⁺): *m/z* found [M+3H]³⁺ 1033.1825; C₁₃₈H₂₀₆N₄₀O₄₂ requires 1033.1820;

LC-MS (ES⁺): *m/z* found [M+4H]⁴⁺ 775.2.



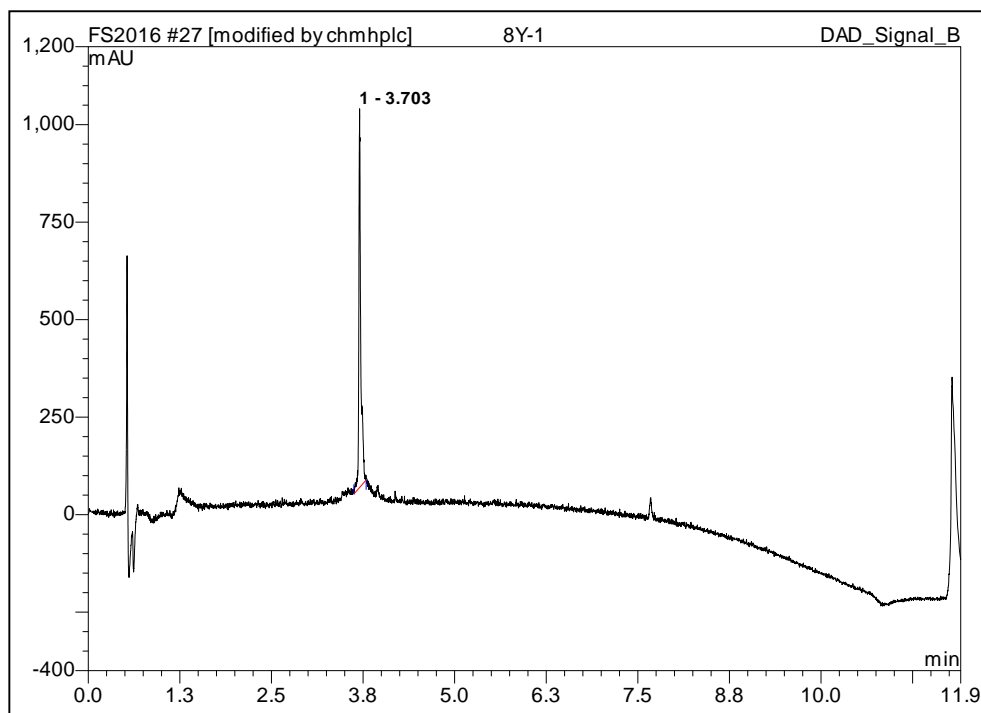
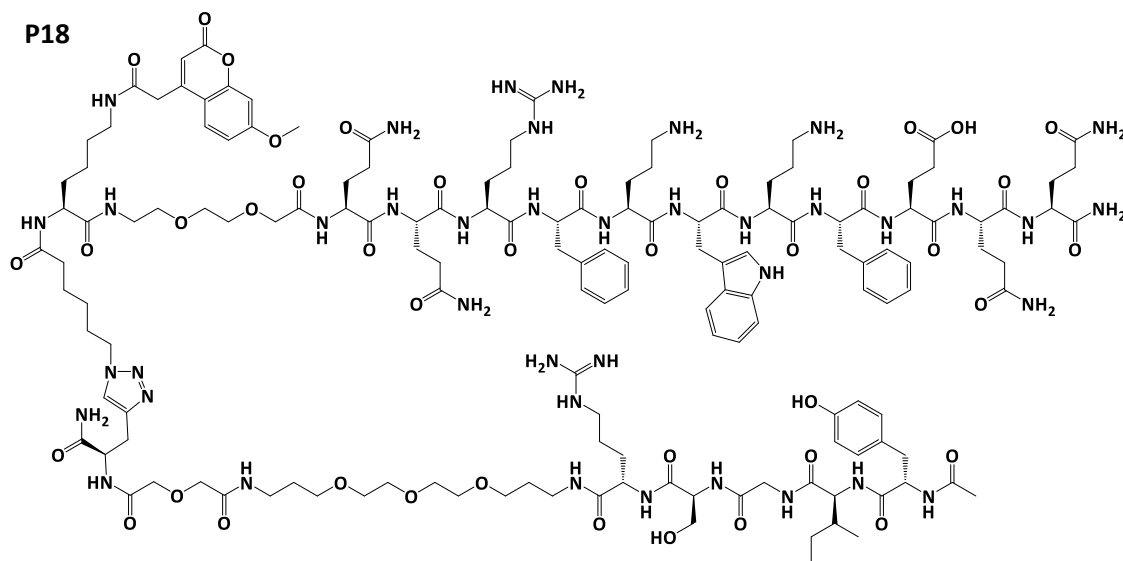
Peak No.	Ret.Time (min)	Height (mAU)	Area (mAU*min)	Rel.Area (%)
1	3.46	1032.936	33.316	100.00
Total	-	1032.936	33.316	100.00

YIGSR-P₁₁-8 (P18; M_w 3201.6)

Analytical HPLC trace: 100 % (the sample was run using the Ascentis Peptide C18 column; MeCN/H₂O both with 0.1 % TFA; gradient 5 - 95 % MeCN (+ 0.1 % TFA); flow rate 0.5 mL.min⁻¹ over 12 minutes; UV detection at 210 nm);

Accurate MS (ES⁺): *m/z* found [M+H]³⁺ 1067.8804; C₁₄₇H₂₁₈N₄₀O₄₁ requires 1067.8817;

LC-MS (ES⁺): *m/z* found [M+4H]⁴⁺ 801.3, [M+5H]⁵⁺ 641.8.



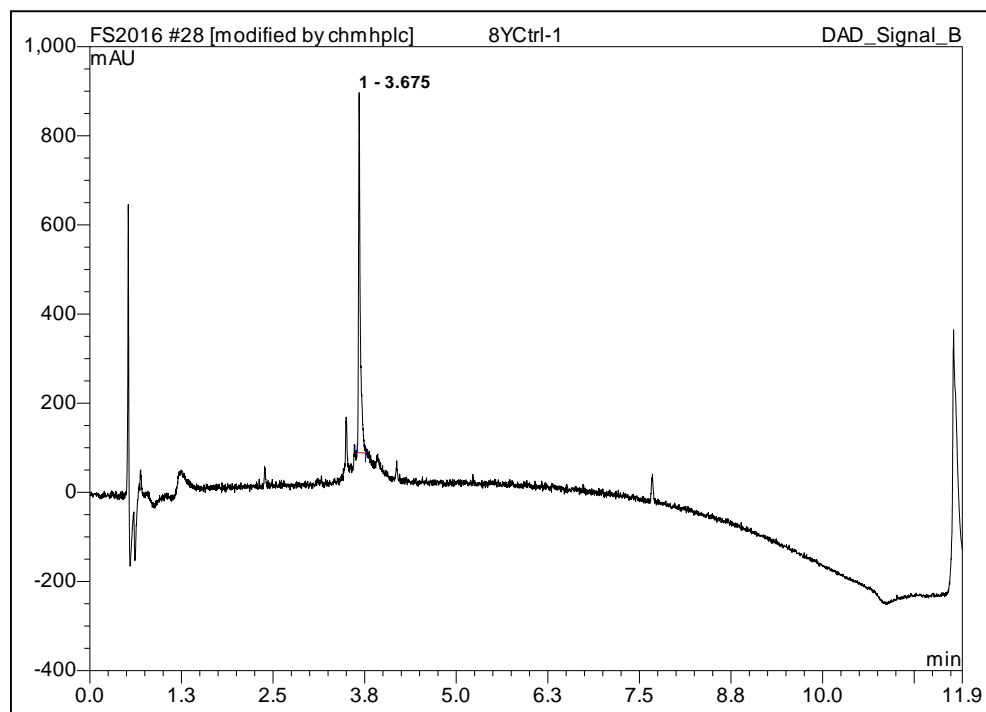
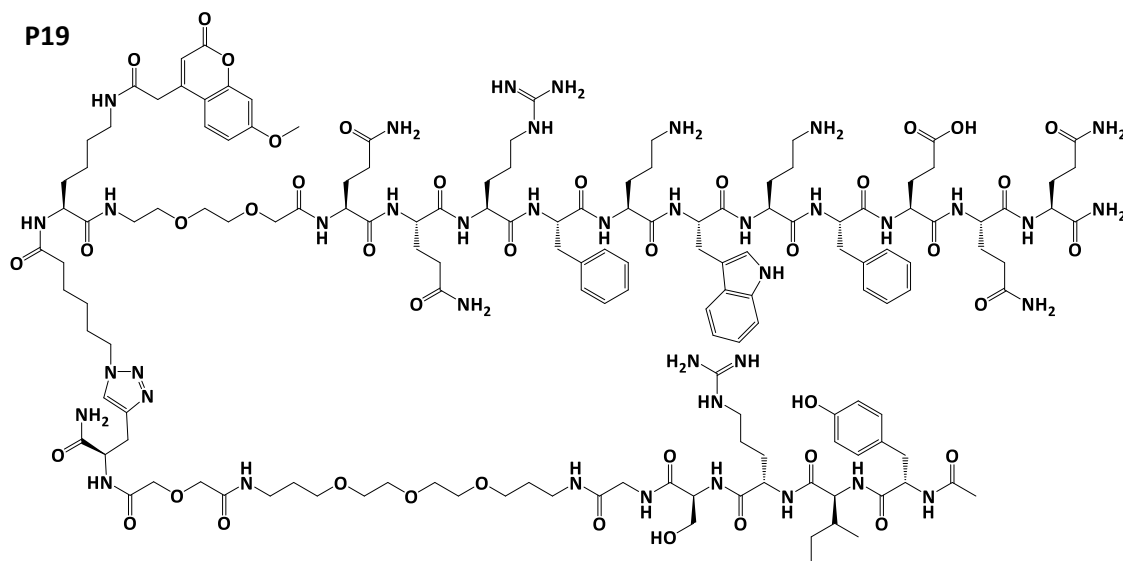
Peak No.	Ret.Time (min)	Height (mAU)	Area (mAU*min)	Rel.Area (%)
1	3.70	970.624	29.893	100.00
Total	-	970.624	29.893	100.00

The Scrambled Control YIRSG-P₁₁-8 (P19; M_w 3201.6)

Analytical HPLC trace: 100 % (the sample was run using the Ascentis Peptide C18 column; MeCN/H₂O both with 0.1 % TFA; gradient 5 - 95 % MeCN (+ 0.1 % TFA); flow rate 0.5 mL.min⁻¹ over 12 minutes; UV detection at 210 nm);

Accurate MS (ES⁺): *m/z* found [M+3H]³⁺ 1067.8830; C₁₄₇H₂₁₈N₄₀O₄₁ requires 1067.8817;

LC-MS (ES⁺): *m/z* found [M+2H]²⁺ 1601.2, [M+3H]³⁺ 1067.9, [M+4H]⁴⁺ 802.3.



Peak No.	Ret.Time (min)	Height (mAU)	Area (mAU*min)	Rel.Area (%)
1	3.68	807.860	22.055	100.00
Total	-	807.860	22.055	100.00

A.7 FEGSEM Images of the Abluminal (External) Surface of Coated and Uncoated Acellular Artery Tissue

The coating of tissue by peptides ($20 \text{ mg}\cdot\text{mL}^{-1}$) was investigated in the abluminal surface of an acellular porcine external iliac artery sections. In uncoated tissue (Figure A.6 A), the characteristic collagen fibre bundles were identified by having the banding structure. P_{11-4} (Figure A.6 B) and P_{11-8} (Figure A.6 C) formed dense fibrillar coatings on the surface identified as thinner fibrils that were randomly oriented, while P_{11-12} (Figure A.6 D) formed a very thin coating that insufficiently coated collagen.

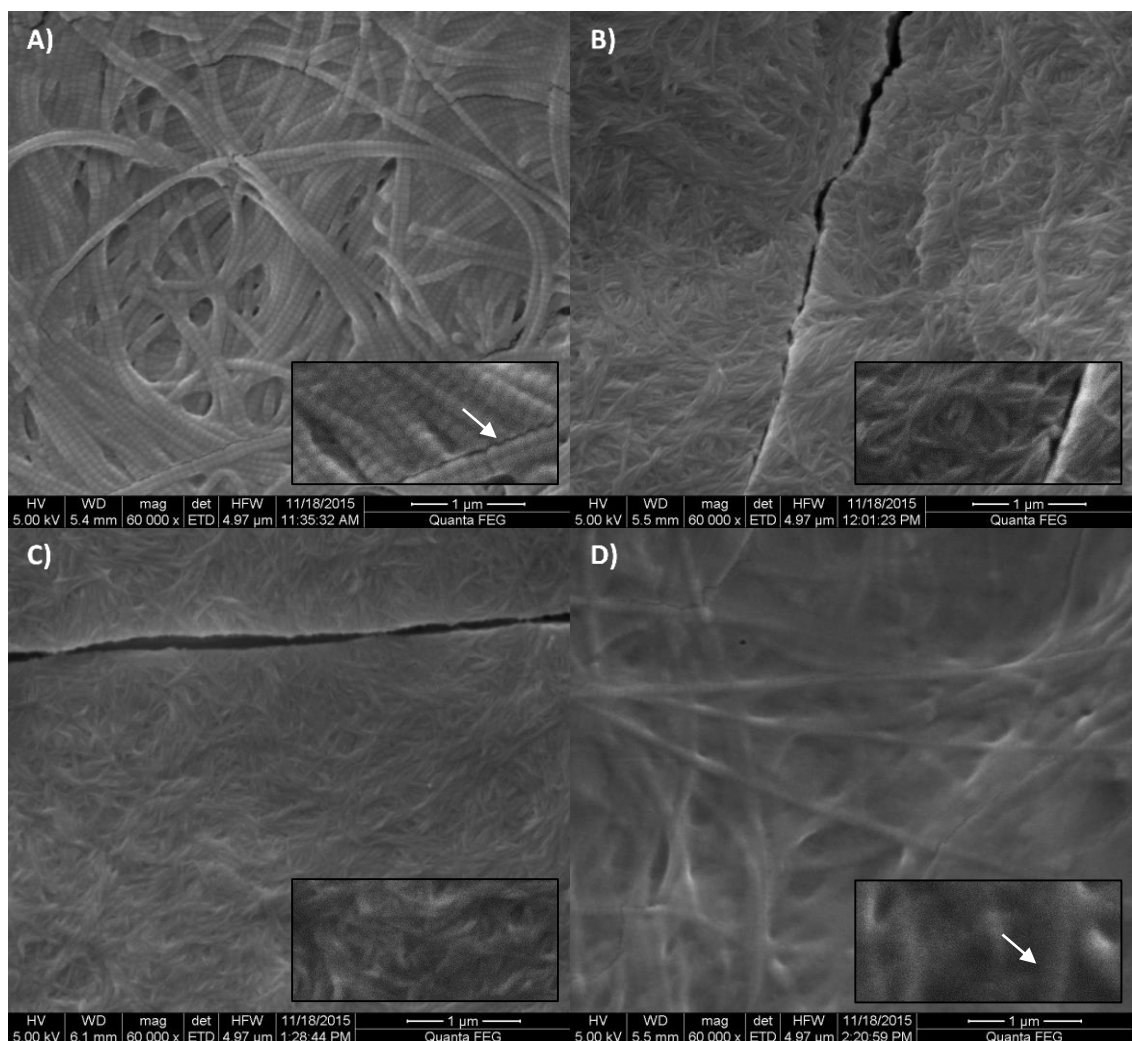


Figure A.6: FEGSEM images showing self-assembling peptides at $20 \text{ mg}\cdot\text{mL}^{-1}$ as surface coatings for the abluminal surface of acellular arteries. A) Uncoated acellular artery, B) P_{11-4} coating, C) P_{11-8} coating and D) P_{11-12} coating. Arrows point to collagen fibres with a characteristic banding structure. Images were acquired at $\times 60,000$ magnification and scale bars represent $1 \mu\text{m}$.

A.8 MPLSM Images of Cellular and Acellular Arteries at the Luminal Surface

In MPLSM images of near the luminal surface of the native cellular porcine external iliac artery into the tunica media, it was found that the internal elastic membrane was a sheet layer that separated the intima from the tunica media. This membrane was fenestrated and consisted mainly of elastin fibres that were packed closely to keep the layer together. The arrangement of the pores was almost consistent through the membrane and the tears might have been caused by dissection, freezing or tissue handling during sample preparation. The tunica media consisted of collagen fibres that were density packed circumferentially in one orientation. The general structure can be seen in the z-stack images of tissue (Figure A.7 A) that were taken at low magnification with 5 μm intervals between each slice. The formation of the internal elastic membrane can be seen clearly in the z-stack images taken at a higher magnification (Figure A.8 A) with 4 μm intervals between slices. These fibres were loosely packed near the surface in random orientations, then were closely packed forming the internal elastic membrane (thick fenestrated sheet). Above the internal elastic membrane in the intima, collagen fibres were also observed. In the tunica media, the densely packed collagen fibres were characterised by having a coiled appearance alongside elastin fibres that were found throughout this layer (as seen previously in histological images of artery cross-sections in Chapter 3).

Following decellularisation, the ECM was slightly disrupted as was evident from images of acellular artery controls taken at low magnification (Figure A.7 B) showing the enlarged pores in the internal elastic membrane and the less packed collagen fibres in the tunica media. The membrane also appeared to be compacted and merged to some extent with the tunica media. At the higher magnification (Figure A.8 B), the formation of the internal elastic membrane by elastic fibres can also be seen. The collagen fibres found above the internal elastic membrane were not always observed in decellularised samples.

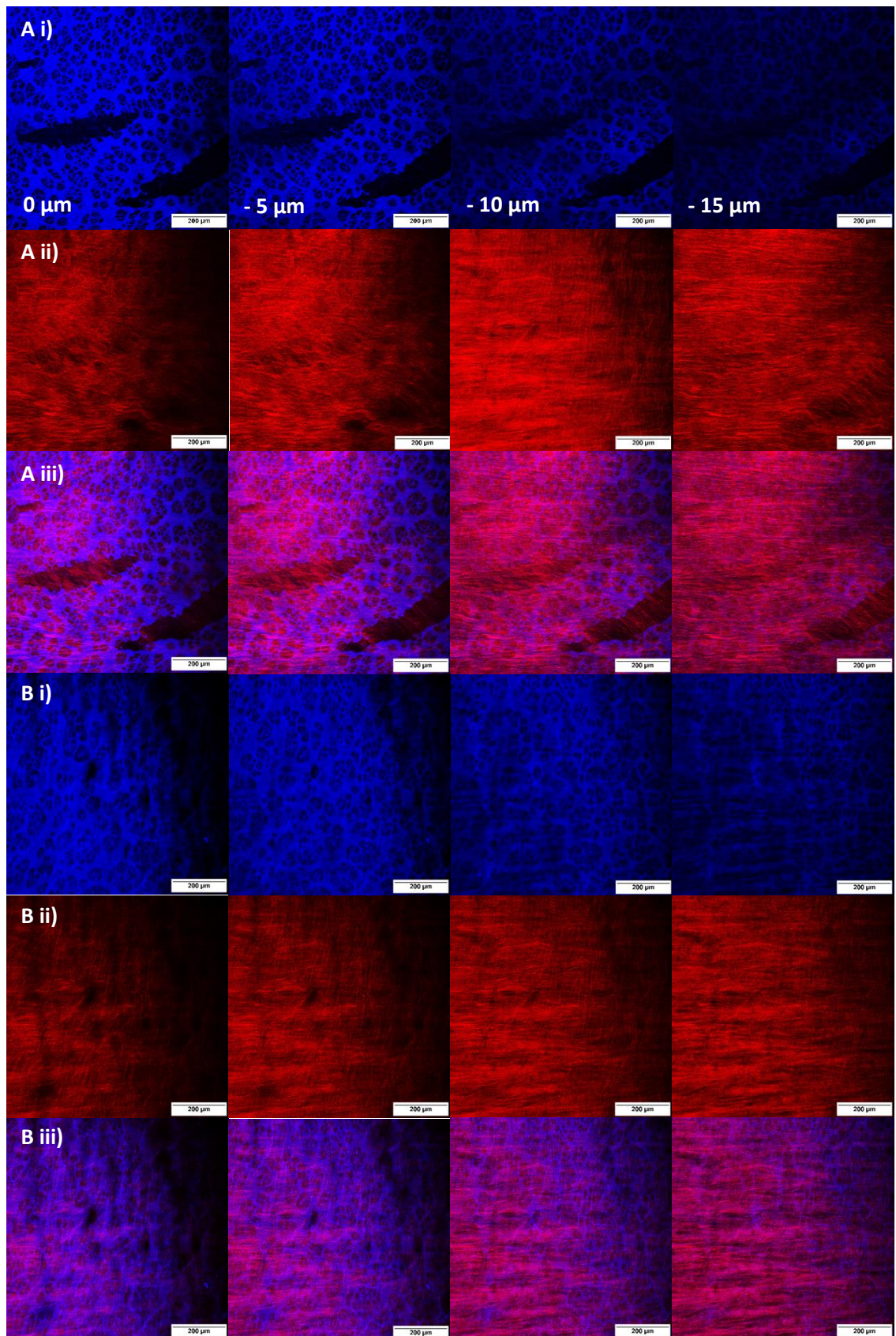


Figure A.7: Multiphoton z-stack images of cellular (A) and acellular (B) arteries with 5 μm intervals near the luminal surface into tunica media. *i) Elastin, ii) collagen and iii) combined signals. Images were acquired using a $\times 10$ objective and scale bars represent 200 μm .*

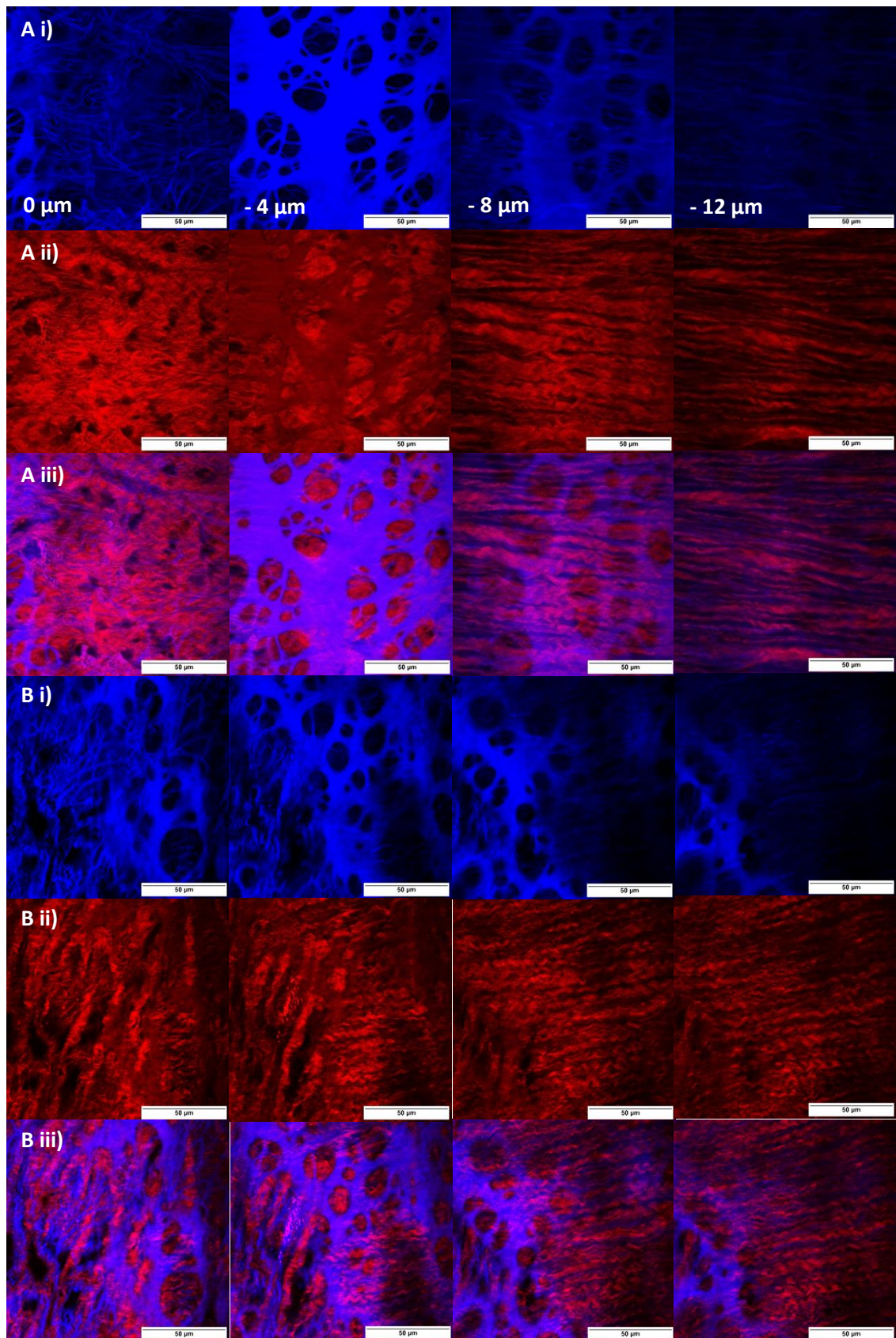


Figure A.8: Multiphoton z-stack images of cellular (A) and acellular (B) arteries with 4 μm intervals near the luminal surface into tunica media. *i) Elastin, ii) collagen and iii) combined signals. Images were acquired using a x 63 objective and scale bar represents 50 μm.*

A.9 MPLSM Images of Peptide Coated Acellular Arteries

Images of FITC- β A control within acellular tissue showing the dispersion of FITC mainly at the surface of the internal elastic membrane and less around collagen in the tunica media (Figure A.9 A). This was more evident in z-stack images in Figure A.9 B.

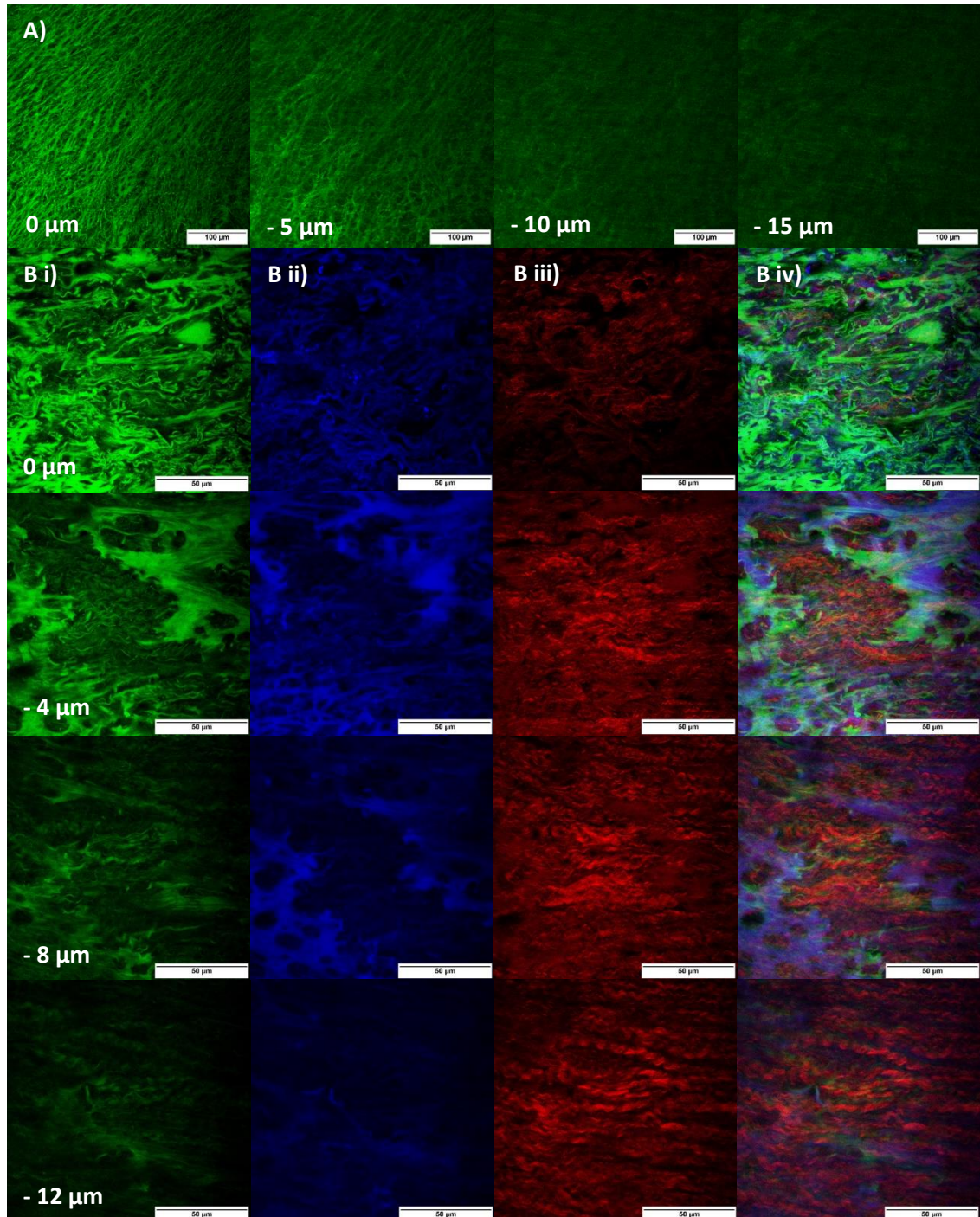


Figure A.9: Multiphoton images of FITC- β A control within acellular artery. Z-stacks with: A) 5 μ m intervals and B) 4 μ m intervals near the luminal surface into the tunica media. i) FITC, ii) elastin, iii) collagen and iv) combined signals. Images were acquired at: A) x 20 objective and scale bar represents 100 μ m and B) using a x 63 objective and scale bar represent 50 μ m.

P_{11-4} was observed as clumps on the surface coating the internal elastic membrane, filling the pores within the ECM structure and also coating collagen in the tunica media (Figure A.10).

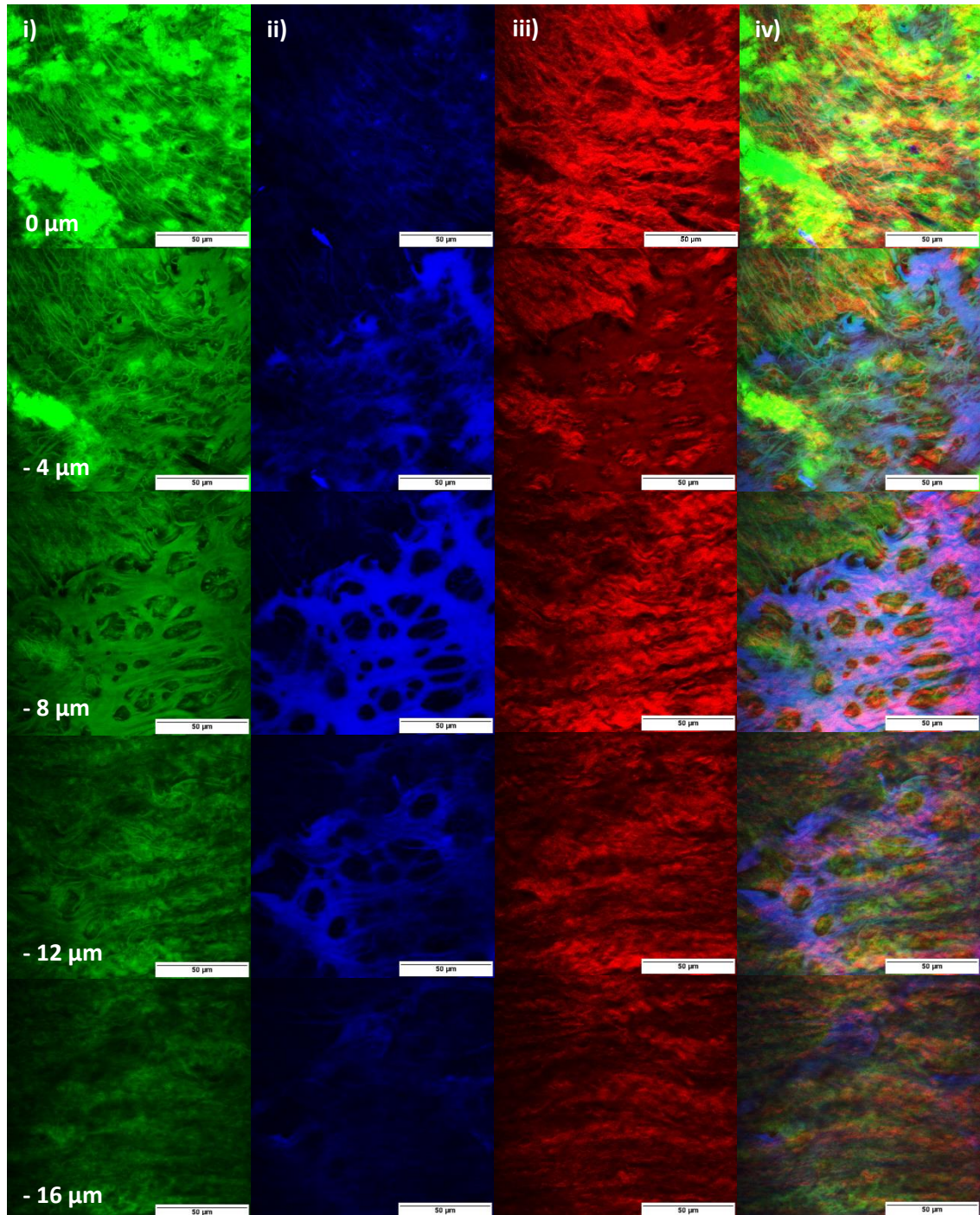


Figure A.10: Multiphoton images of 20 mg.mL^{-1} FITC-labelled P_{11-4} at a molar ratio of 1:150 of the FITC-labelled to the non-labelled peptides within acellular artery. Z-stack with $4 \mu\text{m}$ intervals near the luminal surface into the tunica media. i) FITC, ii) elastin, iii) collagen and iv) combined signals. Images were acquired using a $\times 63$ objective and scale bars represent $50 \mu\text{m}$.

P₁₁-8 was also observed as clumps on the surface coating the internal elastic membrane and coating collagen in the tunica media (Figure A.11).

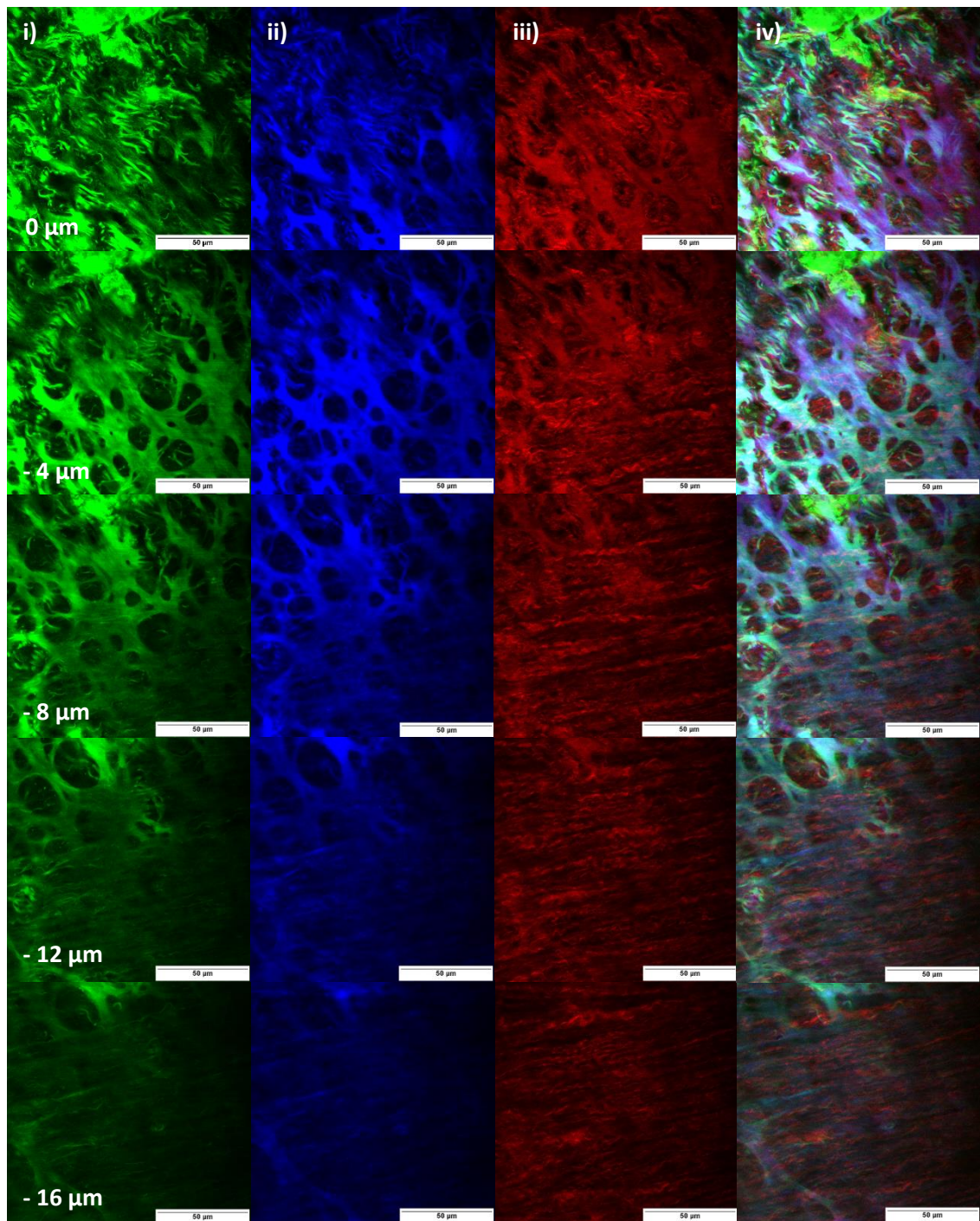


Figure A.11: Multiphoton images of $20 \text{ mg}\cdot\text{mL}^{-1}$ FITC-labelled P₁₁-8 at a molar ratio of 1:150 of the FITC-labelled to the non-labelled peptides within acellular artery. Z-stack with $4 \mu\text{m}$ intervals near the luminal surface into the tunica media. i) FITC, ii) elastin, iii) collagen and iv) combined signals. Images were acquired using a $\times 63$ objective and scale bars represent $50 \mu\text{m}$.

P₁₁-12 coated the ECM structures and filled the pores within the ECM structure without forming clumps on the surface, and it was shown to have more penetration into the tunica media compared to P₁₁-4 and of P₁₁-8 (Figure A.12).

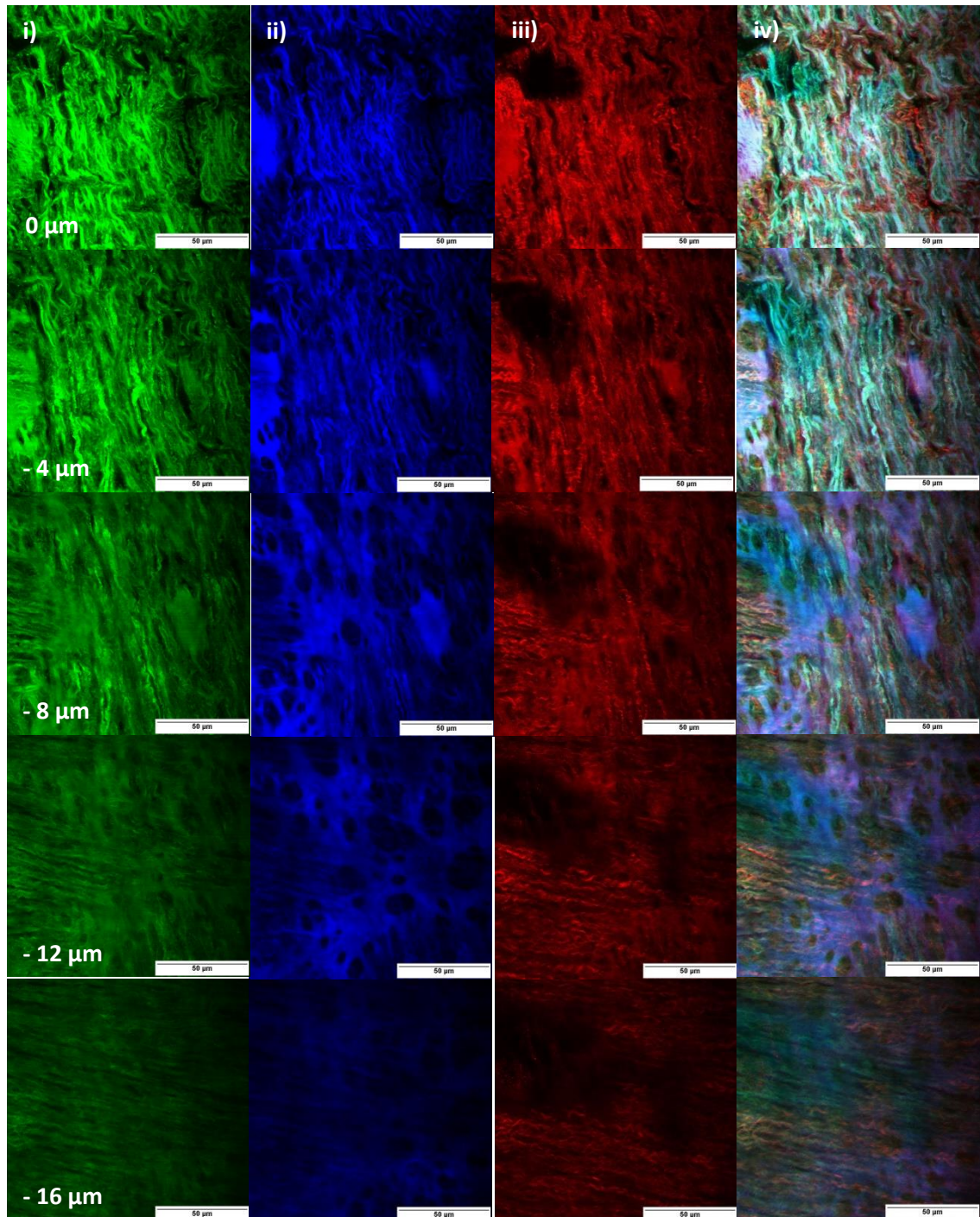


Figure A.12: Multiphoton images of $20 \text{ mg}\cdot\text{mL}^{-1}$ FITC-labelled P₁₁-12 at a molar ratio of 1:150 of the FITC-labelled to the non-labelled peptides within acellular artery. Z-stack with $4 \mu\text{m}$ intervals near the luminal surface into the tunica media. i) FITC, ii) elastin, iii) collagen and iv) combined signals. Images were acquired using a $\times 63$ objective and scale bars represent $50 \mu\text{m}$.

References

1. Bhatnagar, P.; Wickramasinghe, K.; Williams, J.; Rayner, M.; Townsend, N. *Heart* **2015**, *101*, 1182-1189.
2. Scarborough, P.; Bhatnagar, P.; Wickramasinghe, K.; Smolina, K.; Mitchell, C.; Rayner, M. *Coronary heart disease statistics 2010* British Heart Foundation Health Promotion Research Group: Oxford, 2010.
3. Townsend, N.; Wickramasinghe, K.; Bhatnagar, P.; Smolina, K.; Nichols, M.; Leal, J.; Luengo-Fernandez, R.; Rayner, M. *Coronary heart disease statistics 2012*; British Heart Foundation Health Promotion Research Group: Oxford, 2012.
4. Pashneh-Tala, S.; MacNeil, S.; Claeysens, F. *Tissue Engineering Part B: Reviews* **2015**, *22*, 68-100.
5. Zhang, W. J.; Liu, W.; Cui, L.; Cao, Y. *Journal of Cellular and Molecular Medicine* **2007**, *11*, 945-957.
6. Tennant, M.; McGeachie, J. K. *ANZ Journal of Surgery* **1990**, *60*, 747-753.
7. Xu, J.; Shi, G.-P. *Biochimica et Biophysica Acta - Molecular Basis of Disease* **2014**, *1842*, 2106-2119.
8. Londono, R.; Badylak, S. F. *Annals of Biomedical Engineering* **2015**, *43*, 577-592.
9. van Hinsbergh, V. W. *Seminars in Immunopathology* **2012**, *34*, 93-106.
10. Wagenseil, J. E.; Mecham, R. P. *Physiological Reviews* **2009**, *89*, 957-989.
11. Cines, D. B.; Pollak, E. S.; Buck, C. A.; Loscalzo, J.; Zimmerman, G. A.; McEver, R. P.; Pober, J. S.; Wick, T. M.; Konkle, B. A.; Schwartz, B. S. *Blood* **1998**, *91*, 3527-3561.
12. Yousif, L. F.; Di Russo, J.; Sorokin, L. *Cell Adhesion & Migration* **2013**, *7*, 101-110.
13. Hallmann, R.; Horn, N.; Selg, M.; Wendler, O.; Pausch, F.; Sorokin, L. M. *Physiological Reviews* **2005**, *85*, 979-1000.
14. Schnaper, H. W.; Kleinman, H. K.; Grant, D. S. *Kidney International* **1993**, *43*, 20-25.
15. Pankov, R.; Yamada, K. M. *Journal of Cell Science* **2002**, *115*, 3861-3863.
16. Mulvany, M.; Aalkjaer, C. *Physiological Reviews* **1990**, *70*, 921-961.
17. Stewart, J.; Manmathan, G.; Wilkinson, P. *JRSM Cardiovascular Disease* **2017**, *6*, 1-9.
18. Glass, C. K.; Witztum, J. L. *Cell* **2001**, *104*, 503-516.
19. Venkatraman, S.; Boey, F.; Lao, L. L. *Progress in Polymer Science* **2008**, *33*, 853-874.
20. Ross, R. *New England Journal of Medicine* **1999**, *340*, 115-126.
21. Wang, X. W.; Lin, P.; Yao, Q. H.; Chen, C. Y. *World Journal of Surgery* **2007**, *31*, 682-689.

22. Arima, M.; Kanoh, T.; Suzuki, T.; Kuremoto, K.; Tanimoto, K.; Oigawa, T.; Matsuda, S. *Circulation Journal* **2005**, *69*, 896-902.
23. Leask, R. L.; Butany, J.; Johnston, K. W.; Ethier, C. R.; Ojha, M. *Annals of Biomedical Engineering* **2005**, *33*, 301-309.
24. Isenberg, B. C.; Williams, C.; Tranquillo, R. T. *Circulation Research* **2006**, *98*, 25-35.
25. Wilshaw, S. P.; Rooney, P.; Berry, H.; Kearney, J. N.; Homer-Vanniasinkam, S.; Fisher, J.; Ingham, E. *Tissue Engineering Part A* **2012**, *18*, 471-483.
26. Tatterton, M.; Wilshaw, S. P.; Ingham, E.; Homer-Vanniasinkam, S. *Vascular and Endovascular Surgery* **2012**, *46*, 212-222.
27. Callow, A. D. *European Journal of Vascular and Endovascular Surgery* **1996**, *12*, 272-281.
28. Aydin, C.; Ince, V.; Otan, E.; Akbulut, S.; Koc, C.; Kayaalp, C.; Yilmaz, S. *International Surgery* **2013**, *98*, 170-174.
29. Wang, C. C.; Lopez - Valdes, S.; Lin, T. L.; Yap, A.; Yong, C. C.; Li, W. F.; Wang, S. H.; Lin, C. C.; Liu, Y. W.; Lin, T. S. *Liver Transplantation* **2014**, *20*, 173-181.
30. Carpenter, J. P.; Tomaszewski, J. E. *Journal of Vascular Surgery* **1998**, *27*, 492-499.
31. Moran, C. *Theriogenology* **2008**, *70*, 1269-1276.
32. Yow, K. H.; Ingram, J.; Korossis, S. A.; Ingham, E.; Homer-Vanniasinkam, S. *British Journal of Surgery* **2006**, *93*, 652-661.
33. Zilla, P.; Bezuidenhout, D.; Human, P. *Biomaterials* **2007**, *28*, 5009-5027.
34. Ravi, S.; Chaikof, E. L. *Regenerative Medicine* **2010**, *5*, 107.
35. Seifalian, A. M.; Tiwari, A.; Hamilton, G.; Salacinski, H. J. *Artificial Organs* **2002**, *26*, 307-320.
36. Xue, L.; Greisler, H. P. *Journal of Vascular Surgery* **2003**, *37*, 472-480.
37. Kim, B.-S.; Mooney, D. J. *Trends in Biotechnology* **1998**, *16*, 224-230.
38. Bujan, J.; Garcia-Honduvilla, N.; Bellon, J. M. *Biotechnology and Applied Biochemistry* **2004**, *39*, 17-27.
39. Zetrenne, E.; McIntosh, B. C.; McRae, M. H.; Gusberg, R.; Evans, G. R.; Narayan, D. *The Yale Journal of Biology and Medicine* **2007**, *80*, 113-121.
40. Cittadella, G.; Mel, A.; Dee, R.; De Coppi, P.; Seifalian, A. M. *Artificial Organs* **2013**, *37*, 423-434.
41. Cozzi, E.; White, D. J. G. *Nature Medicine* **1995**, *1*, 964-966.
42. Platt, J. L. *Current Opinion in Immunology* **1996**, *8*, 721-728.
43. Sandrin, M. S.; McKenzie, I. F. C. *Current Opinion in Immunology* **1999**, *11*, 527-531.
44. Galili, U. *Immunology Today* **1993**, *14*, 480-482.
45. Badylak, S. F.; Freytes, D. O.; Gilbert, T. W. *Acta Biomaterialia* **2009**, *5*, 1-13.

46. Hasegawa, T.; Okada, K.; Takano, Y.; Hiraishi, Y.; Okita, Y. *The Journal of Thoracic and Cardiovascular Surgery* **2007**, *133*, 1268-1276.
47. Gilbert, T. W.; Sellaro, T. L.; Badylak, S. F. *Biomaterials* **2006**, *27*, 3675-3683.
48. Choi, Y. C.; Choi, J. S.; Kim, B. S.; Kim, J. D.; Yoon, H. I.; Cho, Y. W. *Tissue Engineering Part C: Methods* **2012**, *18*, 866-876.
49. Badylak, S. F. *Seminars in Cell & Developmental Biology* **2002**, *13*, 377-383.
50. Kallenbach, K.; Leyh, R. G.; Lefik, E.; Walles, T.; Wilhelmi, M.; Cebotari, S.; Schmiedl, A.; Haverich, A.; Mertsching, H. *Biomaterials* **2004**, *25*, 3613-3620.
51. Eitan, Y.; Sarig, U.; Dahan, N.; Machluf, M. *Tissue Engineering Part C: Methods* **2009**, *16*, 671-683.
52. Mazza, G.; Al-Akkad, W.; Telese, A.; Longato, L.; Urbani, L.; Robinson, B.; Hall, A.; Kong, K.; Frenguelli, L.; Marrone, G. *Scientific Reports* **2017**, *7*, 5534.
53. Xu, S.; Lu, F.; Cheng, L.; Li, C.; Zhou, X.; Wu, Y.; Chen, H.; Zhang, K.; Wang, L.; Xia, J. *Biomedical Engineering Online* **2017**, *16*, 55.
54. Cho, S.-W.; Lim, S. H.; Kim, I.-K.; Hong, Y. S.; Kim, S.-S.; Yoo, K. J.; Park, H.-Y.; Jang, Y.; Chang, B. C.; Choi, C. Y. *Annals of Surgery* **2005**, *241*, 506-515.
55. Parmaksiz, M.; Dogan, A.; Odabas, S.; Elçin, A. E.; Elçin, Y. M. *Biomedical Materials* **2016**, *11*, 022003.
56. Syedain, Z.; Reimer, J.; Lahti, M.; Berry, J.; Johnson, S.; Bianco, R.; Tranquillo, R. T. *Nature Communications* **2016**, *7*, 12951.
57. Dall'Olmo, L.; Zanusso, I.; Di Liddo, R.; Chioato, T.; Bertalot, T.; Guidi, E.; Conconi, M. T. *BioMed Research International* **2014**, *2014*, 1-9.
58. Borschel, G. H.; Huang, Y.-C.; Calve, S.; Arruda, E. M.; Lynch, J. B.; Dow, D. E.; Kuzon, W. M.; Dennis, R. G.; Brown, D. L. *Tissue Engineering* **2005**, *11*, 778-786.
59. Kim, B. S.; Kim, H.; Gao, G.; Jang, J.; Cho, D.-W. *Biofabrication* **2017**, *9*, 034104.
60. Keane, T. J.; Swinehart, I. T.; Badylak, S. F. *Methods* **2015**, *84*, 25-34.
61. Crapo, P. M.; Gilbert, T. W.; Badylak, S. F. *Biomaterials* **2011**, *32*, 3233-3243.
62. Gilpin, A.; Yang, Y. *BioMed Research International* **2017**, *2017*, 1-13.
63. White, L. J.; Taylor, A. J.; Faulk, D. M.; Keane, T. J.; Saldin, L. T.; Reing, J. E.; Swinehart, I. T.; Turner, N. J.; Ratner, B. D.; Badylak, S. F. *Acta Biomaterialia* **2017**, *50*, 207-219.
64. Vavken, P.; Joshi, S.; Murray, M. M. *Journal of Orthopaedic Research* **2009**, *27*, 1612-1618.
65. Faulk, D. M.; Carruthers, C. A.; Warner, H. J.; Kramer, C. R.; Reing, J. E.; Zhang, L.; D'Amore, A.; Badylak, S. F. *Acta Biomaterialia* **2014**, *10*, 183-193.
66. Tara, S.; Rocco, K. A.; Hibino, N.; Sugiura, T.; Kurobe, H.; Breuer, C. K.; Shinoka, T. *Circulation Journal* **2014**, *78*, 12-19.
67. Badylak, S. F. *Transplant Immunology* **2004**, *12*, 367-377.

68. Grauss, R. W.; Hazekamp, M. G.; Oppenhuizen, F.; van Munsteren, C. J.; Gittenberger-de Groot, A. C.; DeRuiter, M. C. *European Journal of Cardio-Thoracic Surgery* **2005**, *27*, 566-571.
69. Grimes, M.; Pembroke, J. T.; McGloughlin, T. *Bio-medical Materials and Engineering* **2005**, *15*, 65-71.
70. Huang, Q.; Dawson, R. A.; Pegg, D. E.; Kearney, J. N.; Macneil, S. *Wound Repair and Regeneration* **2004**, *12*, 276-287.
71. Luo, J.; Korossis, S. A.; Wilshaw, S.-P.; Jennings, L. M.; Fisher, J.; Ingham, E. *Tissue Engineering Part A* **2014**, *20*, 2963-2974.
72. Davie, E. W. *Journal of Biological Chemistry* **2003**, *278*, 50819-50832.
73. Norris, L. A. *Best Practice & Research: Clinical Obstetrics & Gynaecology* **2003**, *17*, 369-383.
74. Davie, E. W.; Fujikawa, K.; Kisiel, W. *Biochemistry* **1991**, *30*, 10363-10370.
75. Bevers, E. M.; Comfurius, P.; Zwaal, R. F. A. *Blood Reviews* **1991**, *5*, 146-154.
76. Gailani, D.; Renne, T. *Arteriosclerosis, Thrombosis, and Vascular Biology* **2007**, *27*, 2507-2513.
77. Chandler, A. B.; Jacobsen, C. D. *Scandinavian Journal of Clinical & Laboratory Investigation* **1967**, *20*, 129-139.
78. Mackman, N. *Arteriosclerosis, Thrombosis, and Vascular Biology* **2004**, *24*, 1015-1022.
79. Wolberg, A. S. *Blood Reviews* **2007**, *21*, 131-142.
80. Gorbet, M. B.; Sefton, M. V. *Biomaterials* **2004**, *25*, 5681-5703.
81. Hanson, S. R.; Harker, L. A. *Annals of the New York Academy of Sciences* **1987**, *516*, 653-661.
82. van Oeveren, W. *Scientifica* **2013**, *2013*, 1-14.
83. Courtney, J.; Lamba, N.; Sundaram, S.; Forbes, C. *Biomaterials* **1994**, *15*, 737-744.
84. Ekdahl, K. N.; Huang, S.; Nilsson, B.; Teramura, Y. *Seminars in Immunology* **2016**, *28*, 268-277.
85. Xu, L.-C.; Bauer, J. W.; Siedlecki, C. A. *Colloids and Surfaces B: Biointerfaces* **2014**, *124*, 49-68.
86. Tucker, E. I.; Marzec, U. M.; White, T. C.; Hurst, S.; Rugonyi, S.; McCarty, O. J.; Gailani, D.; Gruber, A.; Hanson, S. R. *Blood* **2009**, *113*, 936-944.
87. Sukavaneshvar, S. *Advanced Drug Delivery Reviews* **2017**, *112*, 24-34.
88. Kaushal, S.; Amiel, G. E.; Guleserian, K. J.; Shapira, O. M.; Perry, T.; Sutherland, F. W.; Rabkin, E.; Moran, A. M.; Schoen, F. J.; Atala, A. *Nature Medicine* **2001**, *7*, 1035-1040.
89. Fields, C.; Cassano, A.; Allen, C.; Meyer, A.; Pawlowski, K. J.; Bowlin, G. L.; Rittgers, S. E.; Szycher, M. *Journal of Biomaterials Applications* **2002**, *17*, 45-70.

90. Fields, C.; Cassano, A.; Makhoul, R. G.; Allen, C.; Sims, R.; Bulgrin, J.; Meyer, A.; Bowlin, G. L.; Rittgers, S. E. *Journal of Biomaterials Applications* **2002**, *17*, 135-152.
91. Tiwari, A.; Kidane, A.; Salacinski, H.; Punshon, G.; Hamilton, G.; Seifalian, A. *European Journal of Vascular and Endovascular Surgery* **2003**, *25*, 325-329.
92. Grenier, G.; Rémy-Zolghadri, M.; Guignard, R.; Bergeron, F.; Labbé, R.; Auger, F. A.; Germain, L. *In Vitro Cellular & Developmental Biology - Animal* **2003**, *39*, 131-139.
93. Yoon, Y.-S.; Park, J.-S.; Tkebuchava, T.; Luedeman, C.; Losordo, D. W. *Circulation* **2004**, *109*, 3154-3157.
94. Magin, C. M.; Cooper, S. P.; Brennan, A. B. *Materials Today* **2010**, *13*, 36-44.
95. Krishnan, S.; Weinman, C. J.; Ober, C. K. *Journal of Materials Chemistry* **2008**, *18*, 3405-3413.
96. Ostuni, E.; Chapman, R. G.; Holmlin, R. E.; Takayama, S.; Whitesides, G. M. *Langmuir* **2001**, *17*, 5605-5620.
97. Jeon, S.; Lee, J.; Andrade, J.; De Gennes, P. *Journal of Colloid and Interface Science* **1991**, *142*, 149-158.
98. Larsson, A.; Ekblad, T.; Andersson, O.; Liedberg, B. *Biomacromolecules* **2007**, *8*, 287-295.
99. Lee, J. H.; Jeong, B. J.; Lee, H. B. *Journal of Biomedical Materials Research Part A* **1997**, *34*, 105-114.
100. Ju, H.; McCloskey, B. D.; Sagle, A. C.; Kusuma, V. A.; Freeman, B. D. *Journal of Membrane Science* **2009**, *330*, 180-188.
101. Heo, S.-b.; Jeon, Y.-S.; Kim, S. I.; Kim, S. H.; Kim, J.-H. *Macromolecular Research* **2014**, *22*, 203-209.
102. Hirsh, J.; Anand, S. S.; Halperin, J. L.; Fuster, V. *Arteriosclerosis, Thrombosis, and Vascular Biology* **2001**, *21*, 1094-1096.
103. Mousa, S. A. *Seminars in Thrombosis and Hemostasis* **2007**, *33*, 524-533.
104. Björk, I.; Lindahl, U. *Molecular and Cellular Biochemistry* **1982**, *48*, 161-182.
105. Holmer, E.; Söderberg, K.; Bergqvist, D.; Lindahl, U. *Pathophysiology of Haemostasis and Thrombosis* **1986**, *16*, 1-7.
106. Machovich, R. *Biochimica et Biophysica Acta - Protein Structure* **1975**, *412*, 13-17.
107. Hoshi, R. A.; Van Lith, R.; Jen, M. C.; Allen, J. B.; Lapidus, K. A.; Ameer, G. *Biomaterials* **2013**, *34*, 30-41.
108. Yao, Y.; Wang, J.; Cui, Y.; Xu, R.; Wang, Z.; Zhang, J.; Wang, K.; Li, Y.; Zhao, Q.; Kong, D. *Acta Biomaterialia* **2014**, *10*, 2739-2749.
109. Gong, W.; Lei, D.; Li, S.; Huang, P.; Qi, Q.; Sun, Y.; Zhang, Y.; Wang, Z.; You, Z.; Ye, X. *Biomaterials* **2016**, *76*, 359-370.

110. Zhou, M.; Liu, Z.; Wei, Z.; Liu, C.; Qiao, T.; Ran, F.; Bai, Y.; Jiang, X.; Ding, Y. *Artificial Organs* **2009**, *33*, 230-239.
111. Wang, X. N.; Chen, C. Z.; Yang, M.; Gu, Y. J. *Artificial Organs* **2007**, *31*, 99-104.
112. Knetsch, M. L.; Aldenhoff, Y. B.; Schraven, M.; Koole, L. H. *Journal of Biomedical Materials Research Part A* **2004**, *71*, 615-624.
113. Fittkau, M. H.; Zilla, P.; Bezuidenhout, D.; Lutolf, M. P.; Human, P.; Hubbell, J. A.; Davies, N. *Biomaterials* **2005**, *26*, 167-174.
114. Noel, S.; Hachem, A.; Merhi, Y.; De Crescenzo, G. *Biomacromolecules* **2015**, *16*, 1682-1694.
115. Meyers, S. R.; Grinstaff, M. W. *Chemical Reviews* **2011**, *112*, 1615-1632.
116. Drury, J. L.; Mooney, D. J. *Biomaterials* **2003**, *24*, 4337-4351.
117. Wang, X.; Horii, A.; Zhang, S. *Soft Matter* **2008**, *4*, 2388-2395.
118. Massia, S.; Hubbell, J. *Journal of Biomedical Materials Research Part A* **1991**, *25*, 223-242.
119. Maude, S.; Ingham, E.; Aggeli, A. *Nanomedicine* **2013**, *8*, 823-847.
120. Li, J.; Ding, M.; Fu, Q.; Tan, H.; Xie, X.; Zhong, Y. *Journal of Materials Science: Materials in Medicine* **2008**, *19*, 2595-2603.
121. Zheng, W. T.; Wang, Z. H.; Song, L. J.; Zhao, Q.; Zhang, J.; Li, D.; Wang, S. F.; Han, J. H.; Zheng, X. L.; Yang, Z. M.; Kong, D. L. *Biomaterials* **2012**, *33*, 2880-2891.
122. Hao, D.; Xiao, W.; Liu, R.; Kumar, P.; Li, Y.; Zhou, P.; Guo, F.; Farmer, D. L.; Lam, K. S.; Wang, F. *ACS Chemical Biology* **2017**, *12*, 1075-1086.
123. Ho-Wook, J.; West, J. *Journal of Biomaterials Science, Polymer Edition* **2004**, *15*, 73-94.
124. Gabriel, M.; Niederer, K.; Becker, M.; Raynaud, C. M.; Vahl, C.-F.; Frey, H. *Bioconjugate Chemistry* **2016**, *27*, 1216-1221.
125. Larsen, C. C.; Kligman, F.; Tang, C.; Kottke-Marchant, K.; Marchant, R. E. *Biomaterials* **2007**, *28*, 3537-3548.
126. Meyers, S. R.; Kenan, D. J.; Khoo, X.; Grinstaff, M. W. *Biomacromolecules* **2011**, *12*, 533-539.
127. Li, C.; Hill, A.; Imran, M.; Tio, F. *Hemodialysis International* **2004**, *8*, 360-367.
128. Cooke, M. J.; Phillips, S. R.; Shah, D. S.; Athey, D.; Lakey, J. H.; Przyborski, S. A. *Cytotechnology* **2008**, *56*, 71-79.
129. Hodde, J.; Record, R.; Tullius, R.; Badylak, S. *Biomaterials* **2002**, *23*, 1841-1848.
130. Meinhart, J. G.; Schense, J. C.; Schima, H.; Gorlitzer, M.; Hubbell, J. A.; Deutsch, M.; Zilla, P. *Tissue Engineering* **2005**, *11*, 887-895.
131. Walluscheck, K. P.; Steinhoff, G.; Kelm, S.; Haverich, A. *European Journal of Vascular and Endovascular Surgery* **1996**, *12*, 321-330.
132. Hosseinkhani, H.; Hong, P. D.; Yu, D. S. *Chemical Reviews* **2013**, *113*, 4837-4861.

133. Harrington, D. A.; Cheng, E. Y.; Guler, M. O.; Lee, L. K.; Donovan, J. L.; Claussen, R. C.; Stupp, S. I. *Journal of Biomedical Materials Research Part A* **2006**, *78*, 157-167.
134. Tambralli, A.; Blakeney, B.; Anderson, J.; Kushwaha, M.; Andukuri, A.; Dean, D.; Jun, H.-W. *Biofabrication* **2009**, *1*, 025001.
135. Wang, Z.; Wang, H.; Zheng, W.; Zhang, J.; Zhao, Q.; Wang, S.; Yang, Z.; Kong, D. *Chemical Communications* **2011**, *47*, 8901-8903.
136. Voet, D.; Voet, J. G.; Pratt, C. W. *Principles of Biochemistry*; 4th ed.; Wiley: Singapore, 2012.
137. Whitford, D. *Proteins: Structure and Function*; Wiley: Chichester, 2005.
138. Campbell, M. K.; Farrell, S. O. *Biochemistry*; 6th ed.; Brooks/Cole: Pacific Grove, 2009.
139. Berg, J. M.; Tymoczko, J. L.; Stryer, L. *Biochemistry*; 7th ed.; W. H. Freeman: New York, 2011.
140. Ulijn, R. V.; Smith, A. M. *Chemical Society Reviews* **2008**, *37*, 664-675.
141. Firth, A.; Aggeli, A.; Burke, J. L.; Yang, X.; Kirkham, J. *Nanomedicine* **2006**, *1*, 189-199.
142. Carrick, L. M.; Aggeli, A.; Boden, N.; Fisher, J.; Ingham, E.; Waigh, T. A. *Tetrahedron* **2007**, *63*, 7457-7467.
143. Zhao, X.; Pan, F.; Xu, H.; Yaseen, M.; Shan, H.; Hauser, C. A. E.; Zhang, S.; Lu, J. R. *Chemical Society Reviews* **2010**, *39*, 3480-3498.
144. Stendahl, J. C.; Rao, M. S.; Guler, M. O.; Stupp, S. I. *Advanced Functional Materials* **2006**, *16*, 499-508.
145. Gazit, E. *Chemical Society Reviews* **2007**, *36*, 1263-1269.
146. Aggeli, A.; Bell, M.; Boden, N.; Keen, J. N.; Knowles, P. F.; McLeish, T. C. B.; Pitkeathly, M.; Radford, S. E. *Nature* **1997**, *386*, 259-262.
147. Smulders, M. M. J.; Nieuwenhuizen, M. M. L.; de Greef, T. F. A.; van der Schoot, P.; Schenning, A. P. H. J.; Meijer, E. W. *Chemistry – A European Journal* **2010**, *16*, 362-367.
148. Chen, P. *Colloids and Surfaces A: Physicochemical and Engineering Aspects* **2005**, *261*, 3-24.
149. Aggeli, A.; Bell, M.; Carrick, L. M.; Fishwick, C. W. G.; Harding, R.; Mawer, P. J.; Radford, S. E.; Strong, A. E.; Boden, N. *Journal of the American Chemical Society* **2003**, *125*, 9619-9628.
150. Kyle, S.; Felton, S. H.; McPherson, M. J.; Aggeli, A.; Ingham, E. *Advanced Healthcare Materials* **2012**, *1*, 640-645.
151. Aggeli, A.; Bell, M.; Boden, N.; Carrick, L. M.; Strong, A. E. *Angewandte Chemie International Edition* **2003**, *42*, 5603-5606.
152. Schneider, J. P.; Pochan, D. J.; Ozbas, B.; Rajagopal, K.; Pakstis, L.; Kretsinger, J. *Journal of the American Chemical Society* **2002**, *124*, 15030-15037.

153. Zhang, S.; Gelain, F.; Zhao, X. *Seminars in Cancer Biology* **2005**, *15*, 413-420.
154. Kretsinger, J. K.; Haines, L. A.; Ozbas, B.; Pochan, D. J.; Schneider, J. P. *Biomaterials* **2005**, *26*, 5177-5186.
155. Haines-Butterick, L.; Rajagopal, K.; Branco, M.; Salick, D.; Rughani, R.; Pilarz, M.; Lamm, M. S.; Pochan, D. J.; Schneider, J. P. *Proceedings of the National Academy of Sciences* **2007**, *104*, 7791-7796.
156. Sun, J. E. P.; Stewart, B.; Litan, A.; Lee, S. J.; Schneider, J. P.; Langhans, S. A.; Pochan, D. J. *Biomaterials Science* **2016**, *4*, 839-848.
157. Lindsey, S.; Piatt, J. H.; Worthington, P.; Sönmez, C.; Satheye, S.; Schneider, J. P.; Pochan, D. J.; Langhans, S. A. *Biomacromolecules* **2015**, *16*, 2672-2683.
158. Haines-Butterick, L. A.; Salick, D. A.; Pochan, D. J.; Schneider, J. P. *Biomaterials* **2008**, *29*, 4164-4169.
159. Salick, D. A.; Kretsinger, J. K.; Pochan, D. J.; Schneider, J. P. *Journal of the American Chemical Society* **2007**, *129*, 14793-14799.
160. Zhang, S.; Holmes, T.; Lockshin, C.; Rich, A. *Proceedings of the National Academy of Sciences* **1993**, *90*, 3334-3338.
161. Zhang, S. G.; Lockshin, C.; Cook, R.; Rich, A. *Biopolymers* **1994**, *34*, 663-672.
162. Loo, Y.; Zhang, S.; Hauser, C. A. *Biotechnology advances* **2012**, *30*, 593-603.
163. Luo, Z.; Zhang, S. *Chemical Society Reviews* **2012**, *41*, 4736-4754.
164. Zhang, S.; Zhao, X.; Spirio, L. In *Scaffolding in Tissue Engineering*; CRC Press: Boca Raton, 2005, p 217-238.
165. Davis, M. E.; Motion, J. P. M.; Narmoneva, D. A.; Takahashi, T.; Hakuno, D.; Kamm, R. D.; Zhang, S.; Lee, R. T. *Circulation* **2005**, *111*, 442-450.
166. Cho, H.; Balaji, S.; Sheikh, A. Q.; Hurley, J. R.; Tian, Y. F.; Collier, J. H.; Crombleholme, T. M.; Narmoneva, D. A. *Acta Biomaterialia* **2012**, *8*, 154-164.
167. Hauser, C. A. E.; Zhang, S. *Chemical Society Reviews* **2010**, *39*, 2780-2790.
168. Gelain, F.; Horii, A.; Zhang, S. *Macromolecular Bioscience* **2007**, *7*, 544-551.
169. Holmes, T. C.; de Lacalle, S.; Su, X.; Liu, G.; Rich, A.; Zhang, S. *Proceedings of the National Academy of Sciences* **2000**, *97*, 6728-6733.
170. Genové, E.; Shen, C.; Zhang, S.; Semino, C. E. *Biomaterials* **2005**, *26*, 3341-3351.
171. Aggeli, A.; Bell, M.; Boden, N.; N. Keen, J.; C. B. McLeish, T.; Nyrkova, I.; Radford, S. E.; Semenov, A. *Journal of Materials Chemistry* **1997**, *7*, 1135-1145.
172. Maude, S.; Miles, D. E.; Felton, S. H.; Ingram, J.; Carrick, L. M.; Wilcox, R. K.; Ingham, E.; Aggeli, A. *Soft Matter* **2011**, *7*, 8085-8099.
173. Aggeli, A.; Nyrkova, I. A.; Bell, M.; Harding, R.; Carrick, L.; McLeish, T. C. B.; Semenov, A. N.; Boden, N. *Proceedings of the National Academy of Sciences* **2001**, *98*, 11857-11862.
174. Aggeli, A.; Nyrkova, I. A.; Bell, M.; Carrick, L.; Mcleish, T. C. B.; Semenov, A. N.; Boden, N. In *Self-Assembling Peptide Systems in Biology, Medicine and Engineering*; Springer Netherlands: Dordrecht, 2002, p 1-17.

175. Bowerman, C. J.; Nilsson, B. L. *Journal of the American Chemical Society* **2010**, *132*, 9526-9527.
176. Davies, R. P. W.; Aggeli, A.; Beevers, A. J.; Boden, N.; Carrick, L. M.; Fishwick, C. W. G.; McLeish, T. C. B.; Nyrkova, I.; Semenov, A. N. *Supramolecular Chemistry* **2006**, *18*, 435-443.
177. Wilshaw, S. P.; Aggeli, A.; Fisher, J.; Ingham, E. *Tissue Engineering Part A* **2008**, *14*, 785-785.
178. Guilliatt, R. S. PhD Thesis, University of Leeds, 2013.
179. Brunton, P.; Davies, R.; Burke, J.; Smith, A.; Aggeli, A.; Brookes, S.; Kirkham, J. *British Dental Journal* **2013**, *215*, E6-E6.
180. Alkilzy, M.; Tarabaih, A.; Santamaria, R. M.; Splieth, C. H. *Journal of Dental Research* **2017**, *00*, 1-7.
181. Petka, W. A.; Harden, J. L.; McGrath, K. P.; Wirtz, D.; Tirrell, D. A. *Science* **1998**, *281*, 389-392.
182. Branco, M. C.; Schneider, J. P. *Acta Biomaterialia* **2009**, *5*, 817-831.
183. Sivashanmugam, A.; Arun Kumar, R.; Vishnu Priya, M.; Nair, S. V.; Jayakumar, R. *European Polymer Journal* **2015**, *72*, 543-565.
184. Fan, T.; Yu, X.; Shen, B.; Sun, L. *Journal of Nanomaterials* **2017**, *2017*, 1-16.
185. Sun, L.; Zheng, C.; Webster, T. J. *International Journal of Nanomedicine* **2017**, *12*, 73-86.
186. Li, Y.; Wang, F.; Cui, H. *Bioengineering & Translational Medicine* **2016**, *1*, 306-322.
187. Nisbet, D. R.; Williams, R. J. *Biointerphases* **2012**, *7*, 1-14.
188. Colombo, G.; Soto, P.; Gazit, E. *Trends in Biotechnology* **2007**, *25*, 211-218.
189. Nguyen, M. K.; Alsberg, E. *Progress in Polymer Science* **2014**, *39*, 1236-1265.
190. Ravichandran, R.; Griffith, M.; Phopase, J. *Journal of Materials Chemistry B* **2014**, *2*, 8466-8478.
191. Luo, Z.; Wang, S.; Zhang, S. *Biomaterials* **2011**, *32*, 2013-2020.
192. Song, H.; Zhang, L.; Zhao, X. *Macromolecular Bioscience* **2010**, *10*, 33-39.
193. Saini, A.; Serrano, K.; Koss, K.; Unsworth, L. D. *Acta Biomaterialia* **2016**, *31*, 71-79.
194. Fabian, H.; Mäntele, W. In *Handbook of Vibrational Spectroscopy*; John Wiley & Sons, Ltd: 2006, p 1-27.
195. Susi, H.; Byler, D. M. *Methods in Enzymology* **1986**, *130*, 290-311.
196. Chirgadze, Y. N.; Fedorov, O.; Trushina, N. *Biopolymers* **1975**, *14*, 679-694.
197. Surewicz, W. K.; Mantsch, H. H.; Chapman, D. *Biochemistry* **1993**, *32*, 389-394.
198. Cornish, J.; Callon, K.; Lin, C.-X.; Xiao, C.; Mulvey, T.; Cooper, G.; Reid, I. *American Journal of Physiology - Endocrinology And Metabolism* **1999**, *277*, E779-E783.

199. Chen, Y.; Mehok, A.; Mant, C.; Hodges, R. *Journal of Chromatography A* **2004**, *1043*, 9-18.
200. Kawecki, M.; Łabuś, W.; Klama - Baryla, A.; Kitala, D.; Kraut, M.; Glik, J.; Misiuga, M.; Nowak, M.; Bielecki, T.; Kasperczyk, A. *Journal of Biomedical Materials Research Part B: Applied Biomaterials* **2017**, *2017*, 1-15.
201. Derham, C.; Yow, H.; Ingram, J.; Fisher, J.; Ingham, E.; Korrossis, S. A.; Homer-Vanniasinkam, S. *Tissue Engineering Part A* **2008**, *14*, 1871-1882.
202. Wilshaw, S. P.; Kearney, J. N.; Fisher, J.; Ingham, E. *Tissue Engineering* **2006**, *12*, 2117-2129.
203. Booth, C.; Korossis, S. A.; Wilcox, H. E.; Watterson, K. G.; Kearney, J. N.; Fisher, J.; Ingham, E. *The Journal of Heart Valve Disease* **2002**, *11*, 457-462.
204. Owen, K.; Wilshaw, S. P.; Homer-Vanniasinkam, S.; Bojar, R. A.; Berry, H.; Ingham, E. *European Journal of Vascular and Endovascular Surgery* **2012**, *43*, 573-581.
205. Zilic, L.; Wilshaw, S.-P.; Haycock, J. W. *Biotechnology and Bioengineering* **2016**, *113*, 2041-2053.
206. Levy, M. F. *Proceedings (Baylor University Medical Center)* **2000**, *13*, 3-6.
207. Rashid, S. T.; Salacinski, H. J.; Hamilton, G.; Seifalian, A. M. *Biomaterials* **2004**, *25*, 1627-1637.
208. Paniagua Gutierrez, J. R.; Berry, H.; Korossis, S.; Mirsadraee, S.; Lopes, S. V.; da Costa, F.; Kearney, J.; Watterson, K.; Fisher, J.; Ingham, E. *Tissue Engineering Part A* **2015**, *21*, 332-342.
209. Dunmore-Buyze, J.; Boughner, D. R.; Macris, N.; Vesely, I. *The Journal of Thoracic and Cardiovascular Surgery* **1995**, *110*, 1756-1761.
210. Keane, T. J.; Londono, R.; Turner, N. J.; Badylak, S. F. *Biomaterials* **2012**, *33*, 1771-1781.
211. Brown, B. N.; Badylak, S. F. *Translational Research* **2014**, *163*, 268-285.
212. Muiznieks, L. D.; Keeley, F. W. *Biochimica et Biophysica Acta - Molecular Basis of Disease* **2013**, *1832*, 866-875.
213. Conklin, B. S.; Richter, E. R.; Kreutziger, K. L.; Zhong, D. S.; Chen, C. *Medical Engineering & Physics* **2002**, *24*, 173-183.
214. Kyle, S.; Aggeli, A.; Ingham, E.; McPherson, M. J. *Trends in Biotechnology* **2009**, *27*, 423-433.
215. Pelton, J. T.; McLean, L. R. *Analytical Biochemistry* **2000**, *277*, 167-176.
216. Krimm, S.; Bandekar, J. *Advances in Protein Chemistry* **1986**, *38*, 181-364.
217. Seshadri, S.; Khurana, R.; Fink, A. L. *Methods in Enzymology* **1999**, *309*, 559-576.
218. Zou, Y.; Li, Y.; Hao, W.; Hu, X.; Ma, G. *The Journal of Physical Chemistry B* **2013**, *117*, 4003-4013.
219. Zandomenighi, G.; Krebs, M. R.; McCammon, M. G.; Fändrich, M. *Protein Science* **2004**, *13*, 3314-3321.

220. Miles, D.; Mitchell, E.; Kapur, N.; Beales, P.; Wilcox, R. *Journal of Materials Chemistry B* **2016**, *4*, 3225-3231.
221. Miles, D. E. PhD Thesis, University of Leeds, 2012.
222. Bell, C. J.; Carrick, L. M.; Katta, J.; Jin, Z.; Ingham, E.; Aggeli, A.; Boden, N.; Waigh, T. A.; Fisher, J. *Journal of Biomedical Materials Research Part A* **2006**, *78*, 236-246.
223. Cui, H.; Webber, M. J.; Stupp, S. I. *Peptide Science* **2010**, *94*, 1-18.
224. Ozbas, B.; Kretsinger, J.; Rajagopal, K.; Schneider, J. P.; Pochan, D. J. *Macromolecules* **2004**, *37*, 7331-7337.
225. Merrifield, R. B. *Journal of the American Chemical Society* **1963**, *85*, 2149-2154.
226. Merrifield, R. B. *Journal of the American Chemical Society* **1964**, *86*, 304-305.
227. Wellings, D. A.; Atherton, E. *Methods in Enzymology* **1997**, *289*, 44-67.
228. Guy, C. A.; Fields, G. B. *Methods in Enzymology* **1997**, *289*, 67-83.
229. Jullian, M.; Hernandez, A.; Maurras, A.; Puget, K.; Amblard, M.; Martinez, J.; Subra, G. *Tetrahedron Letters* **2009**, *50*, 260-263.
230. Kolb, H. C.; Finn, M. G.; Sharpless, K. B. *Angewandte Chemie International Edition* **2001**, *40*, 2004-2021.
231. Moses, J. E.; Moorhouse, A. D. *Chemical Society Reviews* **2007**, *36*, 1249-1262.
232. Presolski, S. I.; Hong, V. P.; Finn, M. G. *Current Protocols in Chemical Biology* **2011**, *3*, 153-162.
233. Nwe, K.; Brechbiel, M. W. *Cancer Biotherapy & Radiopharmaceuticals* **2009**, *24*, 289-302.
234. Tornøe, C. W.; Christensen, C.; Meldal, M. *The Journal of Organic Chemistry* **2002**, *67*, 3057-3064.
235. Lutz, J.-F.; Zarafshani, Z. *Advanced Drug Delivery Reviews* **2008**, *60*, 958-970.
236. Sarin, V. K.; Kent, S. B. H.; Tam, J. P.; Merrifield, R. B. *Analytical Biochemistry* **1981**, *117*, 147-157.
237. Kaiser, E.; Colescott, R. L.; Bossinger, C. D.; Cook, P. I. *Analytical Biochemistry* **1970**, *34*, 595-598.
238. Maude, S.; Tai, L. R.; Davies, R. P. W.; Liu, B.; Harris, S. A.; Kocienski, P. J.; Aggeli, A. *Topics in Current Chemistry* **2012**, *310*, 27-69.
239. Maillère, B.; Mourier, G.; Hervé, M.; Ménez, A. *Molecular Immunology* **1995**, *32*, 1377-1385.
240. Di, L. *The AAPS Journal* **2015**, *17*, 134-143.
241. Wang, G. *Current Biotechnology* **2012**, *1*, 72-79.
242. Colombo, M.; Bianchi, A. *Molecules* **2010**, *15*, 178-197.
243. Liu, S. Q.; Rachel Ee, P. L.; Ke, C. Y.; Hedrick, J. L.; Yang, Y. Y. *Biomaterials* **2009**, *30*, 1453-1461.
244. He, X.; Ma, J.; Jabbari, E. *Langmuir* **2008**, *24*, 12508-12516.

245. Kinnane, C. R.; Wark, K.; Such, G. K.; Johnston, A. P.; Caruso, F. *Small* **2009**, *5*, 444-448.
246. Hudalla, G. A.; Murphy, W. L. *Langmuir* **2009**, *25*, 5737-5746.
247. Frantz, C.; Stewart, K. M.; Weaver, V. M. *Journal of Cell Science* **2010**, *123*, 4195-4200.
248. Jacob, M. P.; Badier-Commander, C.; Fontaine, V.; Benazzoug, Y.; Feldman, L.; Michel, J. B. *Pathologie Biologie* **2001**, *49*, 326-332.
249. Rozario, T.; DeSimone, D. W. *Developmental Biology* **2010**, *341*, 126-140.
250. Ushiki, T. *Archives of Histology and Cytology* **2002**, *65*, 109-126.
251. Miranda-Nieves, D.; Chaikof, E. L. *ACS Biomaterials Science & Engineering* **2016**, *3*, 694-711.
252. Bornstein, P.; Sage, H. *Annual Review of Biochemistry* **1980**, *49*, 957-1003.
253. Sherman, V. R.; Yang, W.; Meyers, M. A. *Journal of the Mechanical Behavior of Biomedical Materials* **2015**, *52*, 22-50.
254. Chow, M.-J.; Turcotte, R.; Lin, Charles P.; Zhang, Y. *Biophysical Journal* **2014**, *106*, 2684-2692.
255. O'Connell, M. K.; Murthy, S.; Phan, S.; Xu, C.; Buchanan, J.; Spilker, R.; Dalman, R. L.; Zarins, C. K.; Denk, W.; Taylor, C. A. *Matrix Biology* **2008**, *27*, 171-181.
256. Kusuma, S.; Zhao, S.; Gerecht, S. *The FASEB Journal* **2012**, *26*, 4925-4936.
257. van Oeveren, W.; Tielliu, I. F.; de Hart, J. *International Journal of Biomaterials* **2012**, *2012*, 1-7.
258. Lawson, D. H.; Hutton, M. M.; McNicol, G. *Journal of Clinical Pathology* **1973**, *26*, 452-453.
259. Stary, H. C.; Chandler, A. B.; Dinsmore, R. E.; Fuster, V.; Glagov, S.; Insull, W.; Rosenfeld, M. E.; Schwartz, C. J.; Wagner, W. D.; Wissler, R. W. *Circulation* **1995**, *92*, 1355-1374.
260. Ishikawa-Ankerhold, H. C.; Ankerhold, R.; Drummen, G. P. C. *Molecules* **2012**, *17*, 4047-4132.
261. Huynh, T.; Abraham, G.; Murray, J.; Brockbank, K.; Hagen, P.-O.; Sullivan, S. *Nature Biotechnology* **1999**, *17*, 1083-1086.
262. Quint, C.; Kondo, Y.; Manson, R. J.; Lawson, J. H.; Dardik, A.; Niklason, L. E. *Proceedings of the National Academy of Sciences* **2011**, *108*, 9214-9219.
263. Spijker, H.; Graaff, R.; Boonstra, P.; Busscher, H.; van Oeveren, W. *Biomaterials* **2003**, *24*, 4717-4727.
264. Jen, C. J.; Li, H.; Wang, J.-S.; Chen, H.; Usami, S. *American Journal of Physiology - Heart and Circulatory Physiology* **1996**, *270*, H160-H166.
265. Wang, H.; Ratner, B. D.; Sage, E. H.; Jiang, S. *The Journal of Physical Chemistry C* **2007**, *111*, 8504-8508.
266. Helmus, M. N.; Gibbons, D. F.; Jones, R. D. *Journal of Biomedical Materials Research Part A* **1984**, *18*, 165-183.

267. López-Guimet, J.; Andilla, J.; Loza-Alvarez, P.; Egea, G. *Scientific Reports* **2017**, *7*, 1505.
268. Gui, L.; Muto, A.; Chan, S. A.; Breuer, C. K.; Niklason, L. E. *Tissue Engineering Part A* **2009**, *15*, 2665-2676.
269. Boateng, S. Y.; Lateef, S. S.; Mosley, W.; Hartman, T. J.; Hanley, L.; Russell, B. *American Journal of Physiology - Cell Physiology* **2004**, *288*, C30-C38.
270. D'Souza, S. E.; Ginsberg, M. H.; Plow, E. F. *Trends in Biochemical Sciences* **1991**, *16*, 246-250.
271. Andukuri, A.; Minor, W. P.; Kushwaha, M.; Anderson, J. M.; Jun, H.-W. *Nanomedicine: Nanotechnology, Biology and Medicine* **2010**, *6*, 289-297.
272. Frith, J. E.; Mills, R. J.; Hudson, J. E.; Cooper-White, J. J. *Stem Cells and Development* **2012**, *21*, 2442-2456.
273. Albelda, S. M.; Buck, C. A. *The FASEB Journal* **1990**, *4*, 2868-2880.
274. Aplin, A.; Howe, A.; Alahari, S.; Juliano, R. *Pharmacological Reviews* **1998**, *50*, 197-264.
275. Danen, E. H. Integrins: An overview of structural and functional aspects. *Madame Curie Bioscience Database, Landes Bioscience* [Online]. Published Online: 2000-2013. <https://www.ncbi.nlm.nih.gov/books/NBK6259/> (accessed Sep 03, 2017).
276. Hynes, R. O. *Cell* **1992**, *69*, 11-25.
277. Hynes, R. O. *Cell* **2002**, *110*, 673-687.
278. Ruoslahti, E. *Annual Review of Cell and Developmental Biology* **1996**, *12*, 697-715.
279. Quinn, M. J.; Plow, E. F.; Topol, E. J. *Circulation* **2002**, *106*, 379-385.
280. Short, S. M.; Talbott, G. A.; Juliano, R. L. *Molecular Biology of the Cell* **1998**, *9*, 1969-1980.
281. Hersel, U.; Dahmen, C.; Kessler, H. *Biomaterials* **2003**, *24*, 4385-4415.
282. Maeda, T.; Titani, K.; Sekiguchi, K. *Journal of Biochemistry* **1994**, *115*, 182-189.
283. Ren, X.; Feng, Y.; Guo, J.; Wang, H.; Li, Q.; Yang, J.; Hao, X.; Lv, J.; Ma, N.; Li, W. *Chemical Society Reviews* **2015**, *44*, 5680-5742.
284. Ali, S.; Saik, J. E.; Gould, D. J.; Dickinson, M. E.; West, J. L. *BioResearch Open Access* **2013**, *2*, 241-249.
285. Jung, J. P.; Moyano, J. V.; Collier, J. H. *Integrative Biology* **2011**, *3*, 185-196.
286. Pierschbacher, M. D.; Ruoslahti, E. *Nature* **1984**, *309*, 30-33.
287. Beer, J. H.; Springer, K. T.; Collier, B. S. *Blood* **1992**, *79*, 117-128.
288. Sur, S.; Tantakitti, F.; Matson, J. B.; Stupp, S. I. *Biomaterials Science* **2015**, *3*, 520-532.
289. Lee, J. W.; Park, Y. J.; Lee, S. J.; Lee, S. K.; Lee, K. Y. *Biomaterials* **2010**, *31*, 5545-5551.

290. Hirano, Y.; Okuno, M.; Hayashi, T.; Goto, K.; Nakajima, A. *Journal of Biomaterials Science, Polymer Edition* **1993**, *4*, 235-243.
291. Pierschbacher, M. D.; Ruoslahti, E. *Journal of Biological Chemistry* **1987**, *262*, 17294-17298.
292. Rakocevic, J.; Orlic, D.; Mitrovic-Ajtic, O.; Tomasevic, M.; Dobric, M.; Zlatic, N.; Milasinovic, D.; Stankovic, G.; Ostojić, M.; Labudovic-Borovic, M. *Experimental and Molecular Pathology* **2017**, *102*, 303-313.
293. Rajendran, P.; Rengarajan, T.; Thangavel, J.; Nishigaki, Y.; Sakthisekaran, D.; Sethi, G.; Nishigaki, I. *International Journal of Biological Sciences* **2013**, *9*, 1057-1069.
294. Jaffe, E. A.; Nachman, R. L.; Becker, C. G.; Minick, C. R. *Journal of Clinical Investigation* **1973**, *52*, 2745-2756.
295. Gimbrone, M. A.; Cotran, R. S.; Folkman, J. *The Journal of Cell Biology* **1974**, *60*, 673-684.
296. Ryan, U. S. *Environmental Health Perspectives* **1984**, *56*, 103-114.
297. Dong, Q. G.; Bernasconi, S.; Lostaglio, S.; Wainstok De Calmanovici, R.; Martin-Padura, I.; Breviario, F.; Garlanda, C.; Ramponi, S.; Mantovani, A.; Vecchi, A. *Arteriosclerosis, Thrombosis, and Vascular Biology* **1997**, *17*, 1599-1604.
298. Dietze, K.; Slosarek, I.; Fuhrmann-Selter, T.; Hopperdietzel, C.; Plendl, J.; Kaessmeyer, S. *Clinical Hemorheology and Microcirculation* **2014**, *58*, 127-146.
299. Sanders, S.; Harrison, S.; Lee, W.; Pearse, D.; Wagner, E. *Methods in Cell Science* **1995**, *17*, 33-39.
300. Davison, P. M.; Bensch, K.; Karasek, M. A. *Journal of Investigative Dermatology* **1980**, *75*, 316-321.
301. Choi, S.; Kim, J. A.; Kim, K. C.; Suh, S. H. *The Korean Journal of Physiology and Pharmacology* **2015**, *19*, 35-42.
302. Levenberg, S.; Golub, J. S.; Amit, M.; Itskovitz-Eldor, J.; Langer, R. *Proceedings of the National Academy of Sciences* **2002**, *99*, 4391-4396.
303. Wagner, D. D.; Olmsted, J.; Marder, V. J. *The Journal of Cell Biology* **1982**, *95*, 355-360.
304. Van Beijnum, J. R.; Rousch, M.; Castermans, K.; Van Der Linden, E.; Griffioen, A. W. *Nature Protocols* **2008**, *3*, 1085-1091.
305. Grant, D. S.; Tashiro, K.-I.; Segui-Real, B.; Yamada, Y.; Martin, G. R.; Kleinman, H. K. *Cell* **1989**, *58*, 933-943.
306. Castelletto, V.; Gouveia, R. J.; Connon, C. J.; Hamley, I. W. *European Polymer Journal* **2013**, *49*, 2961-2967.
307. Wang, X.-m.; Lin, Q.; Horii, A. *Progress in Natural Science: Materials International* **2011**, *21*, 111-116.
308. Massia, S. P.; Hubbell, J. A. *The Journal of Cell Biology* **1991**, *114*, 1089-1100.
309. Gunn, J. W.; Turner, S. D.; Mann, B. K. *Journal of Biomedical Materials Research Part A* **2005**, *72A*, 91-97.

310. Kang, T. Y.; Hong, J. M.; Kim, B. J.; Cha, H. J.; Cho, D. W. *Acta Biomaterialia* **2013**, *9*, 4716-4725.
311. Ruoslahti, E.; Pierschbacher, M. D. *Cell* **1986**, *44*, 517-518.
312. Butruk, B.; Bąbik, P.; Marczak, B.; Ciach, T. *Procedia Engineering* **2013**, *59*, 126-132.
313. Wang, W.; Guo, L.; Yu, Y.; Chen, Z.; Zhou, R.; Yuan, Z. *Journal of Biomedical Materials Research Part A* **2015**, *103*, 1703-1712.
314. Liu, X.; Wang, X.; Wang, X.; Ren, H.; He, J.; Qiao, L.; Cui, F.-Z. *Acta Biomaterialia* **2013**, *9*, 6798-6805.